



**T.C.  
ISTANBUL UNIVERSITY-CERRAHPASA  
INSTITUTE OF GRADUATE STUDIES**



**Ph.D. THESIS**

**BEHAVIOR OF COLD FORMED, THIN-WALLED, RACK TYPE FRAMES  
AND THEIR USE IN BUILDING STRUCTURES**

**BASSEL ELKADI**

**SUPERVISOR  
ERDEM DAMCI**

**Department of Civil Engineering  
Civil Engineering Programme**

**ISTANBUL-2019**

This study was accepted on 30/5/2019 as a Ph. D. thesis in Department of Civil Engineering, Civil Engineering Programme by the following Committee.

### **Examining Committee Members**

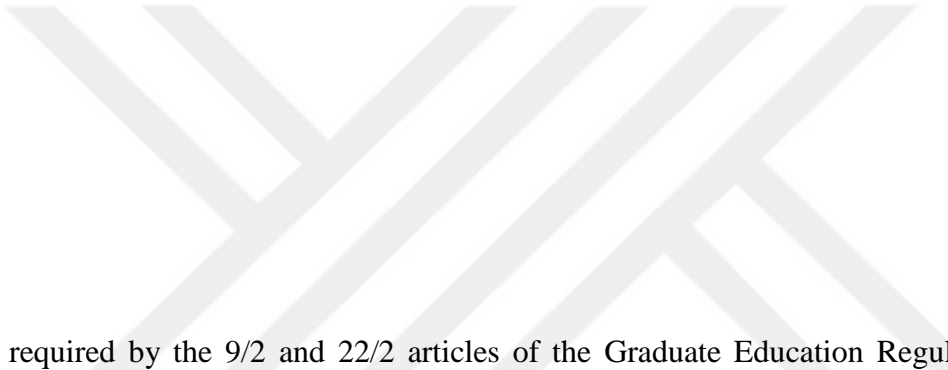
Assist. Prof. Dr. Erdem DAMCI (Supervisor)  
Istanbul University-Cerrahpaşa  
Faculty of Engineering

Prof. Dr. Cenk ALHAN  
Istanbul University-Cerrahpaşa  
Faculty of Engineering

Assoc. Prof. Dr. Gebrail BEKDAŞ  
Istanbul University-Cerrahpaşa  
Faculty of Engineering

Prof. Dr. Tuncer ÇELİK  
Altınbaş University  
Faculty of Engineering and Natural  
Sciences

Prof. Dr. Gülay ALTAY  
Özyeğin University  
Faculty of Engineering



As required by the 9/2 and 22/2 articles of the Graduate Education Regulation which was published in the Official Gazette on 20.04.2016, this graduate thesis is reported as in accordance with criteria determined by the Institute of Graduate Studies by using the plagiarism software to which Istanbul University-Cerrahpasa is a subscriber.

## **FOREWORD**

I express sincere appreciation to Assist. Prof. Dr. Erdem DAMCI for his guidance and insight throughout the research.

Thanks go to the other committee members, Prof. Dr. Tuncer ÇELİK, Prof. Dr. Gülay ALTAY, Prof. Dr. Cenk ALHAN and Assoc. Prof. Dr. Gebrail BEKDAŞ for their valuable suggestions and comments.

I express my thanks and appreciation to my family for their understanding, motivation and patience. Lastly, but in no sense the least, I am thankful to all colleagues and friends for their support and encouragement.

May 2019

Bassel ELKADI

# TABLE OF CONTENTS

	Page
<b>FOREWORD</b> .....	<b>iv</b>
<b>TABLE OF CONTENTS</b> .....	<b>v</b>
<b>LIST OF FIGURES</b> .....	<b>vii</b>
<b>LIST OF TABLES</b> .....	<b>xv</b>
<b>LIST OF SYMBOLS AND ABBREVIATIONS</b> .....	<b>xvi</b>
<b>ÖZET</b> .....	<b>xix</b>
<b>SUMMARY</b> .....	<b>xxi</b>
<b>1. INTRODUCTION</b> .....	<b>1</b>
<b>2. EXPERIMENTAL STUDY</b> .....	<b>26</b>
2.1. DESCRIPTION OF THE TEST SPECIMENS AND THE TEST METHODOLOGY .....	26
2.2. TEST RESULTS.....	33
2.2.1 Cyclic Behavior of the Connections.....	33
2.2.2 Comparison of Test Results.....	35
2.3. PERFORMANCE LEVELS OF RACK FRAMES .....	50
<b>3. SEISMIC PERFORMANCE ASSESMENT</b> .....	<b>52</b>
<b>4. FINITE ELEMENT ANALYSIS</b> .....	<b>57</b>
4.1. CONNECTION MODELLING .....	57
4.2. PINS MODELLING AND CONTACT SURFACES .....	59
4.3. BOUNDARY CONDITIONS AND ASSIGNING OF LOADS.....	59
4.4. MODEL MESHING .....	63
4.5. SUBSTEPS .....	64
4.6. FAILURE MODES.....	65
4.7. MOMENT ROTATION RESULTS .....	66
<b>5. NON-LINEAR STATIC ANALYSIS OF RACK STRUCTURES</b> .....	<b>70</b>
5.1. PUSHOVER ANALYSIS USING SAP2000 .....	70
5.2. EQUIVALENT LATERAL FORCE CALCULATION .....	76
<b>6. USAGE OF RACK MEMBERS IN RESIDENTIAL STRUCTURES</b> .....	<b>79</b>
6.1. CALCULATIONS OF THE AXIAL LOAD CAPACITY OF THE COLUMN.....	86

6.1.1 Flexural, Torsional, or Flexural-Torsional Buckling .....	91
6.1.2 Local Buckling .....	91
6.1.3 Distortional Buckling .....	92
6.2. CALCULATIONS OF THE MOMENT CAPACITY OF THE BEAMS.....	93
6.2.1 Moment Capacity Calculations of the Roof Slab Beams .....	93
6.2.2 Moment Capacity Calculations of the Floor Slab Beams .....	94
6.3. SAP2000 INPUTS AND RESULTS .....	96
6.4. PERFORMANCE BASED DESIGN USING ETABS .....	107
6.4.1 Pushover Analysis in the X Direction .....	109
6.4.2 Pushover Analysis in the Y Direction .....	112
6.5. DESIGN OF 8 STORY RESIDENTIAL BUILDING USING RACK MEMBERS .....	115
6.5.1 Obtaining the Axial Load Capacities of the Columns.....	117
6.5.2 SAP2000 Results .....	120
6.5.3 Non-Linear Pushover Analysis in the X Direction Using ETABS .....	124
6.5.4 Non-Linear Pushover Analysis in the Y Direction Using ETABS .....	127
<b>7. CONCLUSIONS AND FUTURE WORK.....</b>	<b>131</b>
<b>REFERENCES .....</b>	<b>136</b>
<b>CURRICULUM VITAE .....</b>	<b>142</b>

## LIST OF FIGURES

	<b>Page</b>
<b>Figure 1.1:</b> Cold-formed steel rack system (Elkadi, 2015). .....	2
<b>Figure 1.2:</b> Cold-formed steel rack system (URGO racking, 1998).....	3
<b>Figure 1.3:</b> Typical hooked beam-to-column connection in storage rack frames. ....	7
<b>Figure 1.4:</b> Beam-column connection (Elkadi, 2015). .....	7
<b>Figure 1.5:</b> Collapsed rack system in Christchurch earthquake in 2011 (Clifton et al., 2011).....	9
<b>Figure 1.6:</b> Pinching4 model in OpenSees (X. Zhao et al., 2018).....	24
<b>Figure 2.1:</b> Column cross-section dimensions in mm. ....	27
<b>Figure 2.2:</b> Dimensions of the column's and the bracket's perforations in mm. ....	27
<b>Figure 2.3:</b> Dimensions of the beams cross-sections used in the experimental study in mm. ....	28
<b>Figure 2.4:</b> Schematic description of the test specimens.....	29
<b>Figure 2.5:</b> Schematic diagram of the test setup that was developed according to RMI 2012 specification (ANSI MH16.1:2012). ....	30
<b>Figure 2.6:</b> Experimental setup for cyclic testing of rack beam-to-column connections. ....	31
<b>Figure 2.7:</b> Specimen with and without additional bolts (pins). ....	31
<b>Figure 2.8:</b> Cyclic loading curve used in the experimental study. ....	33
<b>Figure 2.9:</b> Moment rotation results for the left side connection of the beam (WB100.40.NP).....	37
<b>Figure 2.10:</b> Moment rotation results for the right side connection of the beam (WB100.40.NP).....	37
<b>Figure 2.11:</b> Moment rotation results for the left side connection of the beam (WB100.40.2P).....	38
<b>Figure 2.12:</b> Moment rotation results for the right side connection of the beam (WB100.40.2P).....	38

<b>Figure 2.13:</b> Moment rotation results for the left side connection of the beam (WB100.40.4P).....	39
<b>Figure 2.14:</b> Moment rotation results for the right side connection of the beam (WB100.40.4P).....	39
<b>Figure 2.15:</b> Moment rotation results for the left side connection of the beam (WB120.40.NP).....	40
<b>Figure 2.16:</b> Moment rotation results for the right side connection of the beam (WB120.40.NP).....	40
<b>Figure 2.17:</b> Moment rotation results for the left side connection of the beam (WB120.40.2P).....	41
<b>Figure 2.18:</b> Moment rotation results for the right side connection of the beam (WB120.40.2P).....	41
<b>Figure 2.19:</b> Moment rotation results for the left side connection of the beam (WB120.40.4P).....	42
<b>Figure 2.20:</b> Moment rotation results for the right side connection of the beam (WB120.40.4P).....	42
<b>Figure 2.21:</b> Moment rotation results for the left side connection of the beam (WB140.40.NP).....	43
<b>Figure 2.22:</b> Moment rotation results for the right side connection of the beam (WB140.40.NP).....	43
<b>Figure 2.23:</b> Moment rotation results for the left side connection of the beam (WB140.40.2P).....	44
<b>Figure 2.24:</b> Moment rotation results for the right side connection of the beam (WB140.40.2P).....	44
<b>Figure 2.25:</b> Moment rotation results for the left side connection of the beam (WB140.40.4P).....	45
<b>Figure 2.26:</b> Moment rotation results for the right side connection of the beam (WB140.40.4P).....	45
<b>Figure 2.27:</b> Peak moment-rotation curves of the connections NP, 2P, and 4P for the beam with the depth of 100 mm.....	46
<b>Figure 2.28:</b> Peak moment-rotation curves of the connections NP, 2P, and 4P for the beam with the depth of 120 mm.....	47
<b>Figure 2.29:</b> Peak moment-rotation curves of the connections NP, 2P, and 4P for the beam with the depth of 140 mm.....	47



<b>Figure 2.30:</b> The peak moment-rotation curves of the NP connection for the different depths of the beams (100,120 and 140).....	48
<b>Figure 2.31:</b> The peak moment-rotation curves of the 2P connection for the different depths of the beams (100,120 and 140).....	49
<b>Figure 2.32:</b> The peak moment-rotation curves of the 4P connection for the different depths of the beams (100,120 and 140).....	49
<b>Figure 2.33:</b> Performance levels of the rack structures. ....	51
<b>Figure 3.1:</b> Analytical model used for the seismic performance assessment of down-aisle frame behavior (Filiatrault et al., 2006). ....	52
<b>Figure 4.1:</b> The column designed in Solidworks.....	58
<b>Figure 4.2:</b> The hooked beam designed in Solidworks. ....	58
<b>Figure 4.3:</b> The beam-to-column connection designed in Solidworks.....	58
<b>Figure 4.4:</b> Pins Modeling using the bonded contact surface between the edges of the perforations of both the bracket and the column. ....	59
<b>Figure 4.5:</b> Fixed support applied to the lower face of the column.....	60
<b>Figure 4.6:</b> Constant 50 kN axial load applied to the top of the column.....	60
<b>Figure 4.7:</b> 5 kN pallet loads applied to the left and right beams.....	61
<b>Figure 4.8:</b> Simplified displacement curve to be used in ANSYS model. ....	62
<b>Figure 4.9:</b> The displacement curve that was used in the final ANSYS model. ....	62
<b>Figure 4.10:</b> The displacement curve that was used in the experimental study. ....	62
<b>Figure 4.11:</b> Displacement applied on the right beam.....	63
<b>Figure 4.12:</b> Body meshing of the column, beam and beam end connector bracket.....	63
<b>Figure 4.13:</b> Body meshing of the hooks of the bracket.....	64
<b>Figure 4.14:</b> The convergence results of the beam to column connection model. ....	64
<b>Figure 4.15:</b> The failure mode of the hooked connection that shows high stress concentrations at the hook. ....	65
<b>Figure 4.16:</b> The column buckling failure mode obtained from the pinned connection. ....	65
<b>Figure 4.17:</b> Moment-displacement curves of the no-pin beam-to-column connection in ANSYS.....	66

<b>Figure 4.18:</b> Moment-displacement curves of the pinned beam-to-column connection in ANSYS.....	66
<b>Figure 4.19:</b> The moment-rotation curves of the beam-to-column connection from ANSYS and experimental test results of the no pin model.....	67
<b>Figure 4.20:</b> The moment-rotation curves of the beam-to-column connection from ANSYS and experimental test results of the pinned model.....	68
<b>Figure 4.21:</b> Comparison between the peak moment-rotation points of each loading step in ANSYS and the experimental test results for the no-pin connection.....	68
<b>Figure 4.22:</b> Comparison between the peak moment-rotation points of each loading step in ANSYS and the experimental test results for the pinned connection.....	69
<b>Figure 4.23:</b> Comparison between the initial stiffness of both the test and ANSYS results.....	69
<b>Figure 5.1:</b> SAP2000 model of the rack system.....	70
<b>Figure 5.2:</b> Defining the column in SAP2000 using section designer menu.....	70
<b>Figure 5.3:</b> Defining the link element to the beam-to-column connection.....	71
<b>Figure 5.4:</b> Pushover analysis result for the rack with the connection of 100.40.4P.....	72
<b>Figure 5.5:</b> Pushover analysis result for the rack with the connection of 120.40.4P.....	72
<b>Figure 5.6:</b> Plastic yield moment compared to the test result for the 100 mm depth beam.....	73
<b>Figure 5.7:</b> Plastic yield moment compared to the test result for the 120 mm depth beam.....	73
<b>Figure 5.8:</b> Plastic yield moment compared to the test result for the 140 mm depth beam.....	74
<b>Figure 5.9:</b> Pushover curves of the racks with beam of 100 mm depth.....	74
<b>Figure 5.10:</b> Pushover curves of the racks with beam of 120 mm depth.....	75
<b>Figure 5.11:</b> Pushover curves of the racks with beam of 140 mm depth.....	75
<b>Figure 5.12:</b> Equivalent lateral force compared to pushover curves of the 100 mm beam racks.....	77
<b>Figure 5.13:</b> Equivalent lateral force compared to pushover curves of the 120 mm beam racks.....	78
<b>Figure 5.14:</b> Equivalent lateral force compared to pushover curves of the 140 mm beam racks.....	78

<b>Figure 6.1:</b> The architectural plan of the residential structure.....	79
<b>Figure 6.2:</b> The architectural elevation of the residential structure.....	80
<b>Figure 6.3:</b> The structural plan of the residential structure. ....	81
<b>Figure 6.4:</b> The structural plan and elevation of the residential structure. ....	82
<b>Figure 6.5:</b> Details of the beam-to column direction in the down-aisle direction.....	83
<b>Figure 6.6:</b> Defining the dimensions of the column using the section designer menu in SAP2000.....	84
<b>Figure 6.7:</b> Defining the moment rotation experimental results to the beam-to-column connection in SAP2000. ....	84
<b>Figure 6.8:</b> SAP2000 model for 5 stories residential building using rack members (3D and X-Z view).....	85
<b>Figure 6.9:</b> SAP2000 model for 5 stories residential building using rack members. (3D and Y-Z view).....	85
<b>Figure 6.10:</b> Input page on CUFSM program. ....	87
<b>Figure 6.11:</b> The signature curve and the plot for the local buckling failure mode in CUFSM.....	87
<b>Figure 6.12:</b> The signature curve and the plot for the distortional buckling failure mode in CUFSM. ....	88
<b>Figure 6.13:</b> The effective unbraced length of the columns in both of group (1) and (2). ....	89
<b>Figure 6.14:</b> CUTWP input and result page with a plot for the flexural-torsional buckling failure mode of the first group of columns.....	90
<b>Figure 6.15:</b> CUTWP input and result page with a plot for the flexural-torsional buckling failure mode of the second group of columns. ....	90
<b>Figure 6.16:</b> Cross-section of the beam and the roof slab (dimensions in mm).....	93
<b>Figure 6.17:</b> Cross-section of the beam and the floor slabs (dimensions in mm). ....	94
<b>Figure 6.18:</b> Response spectrum function definition into SAP2000 model. ....	96
<b>Figure 6.19:</b> The first modal shape of the structure obtained from SAP2000 for the X-Z plan.....	97
<b>Figure 6.20:</b> The second modal shape of the structure obtained from SAP2000 for the Y-Z plan.....	97

<b>Figure 6.21:</b> The third modal shape of the structure obtained from SAP2000 for the X-Y plan. ....	98
<b>Figure 6.22:</b> Maximum Axial load results for the columns from SAP2000 model under dead load, live load and snow load combination.....	99
<b>Figure 6.23:</b> Maximum Axial load result for the columns from SAP2000 model under earthquake load, dead load, live load and snow load combination for the group (1) of columns. ....	99
<b>Figure 6.24:</b> Maximum Axial load result for the columns from SAP2000 model under earthquake load, dead load, live load and snow load combination for group (2) of columns.....	100
<b>Figure 6.25:</b> Maximum M 3-3 moment result for the columns from SAP2000 model.....	100
<b>Figure 6.26:</b> Maximum M 2-2 moment result for the columns from SAP2000 model.....	101
<b>Figure 6.27:</b> Moment results for the beams from SAP2000 model.....	101
<b>Figure 6.28:</b> Maximum deflection of the beams from SAP2000 model. ....	102
<b>Figure 6.29:</b> Maximum roof displacements due to seismic loads for the 5 stories building in the X direction.....	103
<b>Figure 6.30:</b> Maximum roof displacements due to seismic loads for the 5 stories building in the Y direction.....	104
<b>Figure 6.31:</b> The S11 and S22 stress distributions on the walls under the dead load, live load and snow load combination. ....	105
<b>Figure 6.32:</b> The S11 and S22 stress distributions on the walls under the earthquake load in X direction, dead load, live load and snow load combination.....	106
<b>Figure 6.33:</b> The S11 and S22 stress distributions on the walls under the earthquake load in Y direction, dead load, live load and snow load combination.....	106
<b>Figure 6.34:</b> The maximum positive and negative moment rotation values obtained from SAP2000 results due to the earthquake loads compared to the experimental moment rotation results. ....	107
<b>Figure 6.35:</b> 3D views for the residential building modeled in ETABS. ....	108
<b>Figure 6.36:</b> Defining the experimental moment rotation results to the link properties in ETABS. ....	109
<b>Figure 6.37:</b> Stress-strain curve of plywood inserted to ETABS (Yoshihara, 2010). ....	109
<b>Figure 6.38:</b> Pushover curve obtain from ETABS in X direction. ....	110
<b>Figure 6.39:</b> Plastic and fiber hinges formed during the pushover analysis in the X direction at the last step of loading.....	110

<b>Figure 6.40:</b> Target displacement values and the capacity curve in the X direction.....	111
<b>Figure 6.41:</b> No plastic or fiber hinges were formed at the target displacement in X direction.....	112
<b>Figure 6.42:</b> Pushover curve obtain from ETABS in Y direction. ....	113
<b>Figure 6.43:</b> Plastic and fiber hinges formed during the pushover analysis in the Y direction at the last step of loading.....	113
<b>Figure 6.44:</b> Target displacement values and the capacity curve in the Y direction.....	114
<b>Figure 6.45:</b> No plastic or fiber hinges were formed at the target displacement in Y direction.....	115
<b>Figure 6.46:</b> Defining the dimensions of (C1) column using section designer in SAP2000.....	116
<b>Figure 6.47:</b> Defining the dimensions of (C2) column using section designer in SAP2000.....	116
<b>Figure 6.48:</b> Defining the dimensions of (C3) column using section designer in SAP2000.....	116
<b>Figure 6.49:</b> The signature curve for the local buckling failure mode in CUFSM for C2. ....	117
<b>Figure 6.50:</b> CUTWP input and result page with a plot for the flexural-torsional buckling failure mode of the first group of columns for C2 with effective buckling length of 1400 mm.....	118
<b>Figure 6.51:</b> CUTWP input and result page with a plot for the flexural-torsional buckling failure mode of the second group of columns for C2 with effective buckling length of 3000 mm.....	118
<b>Figure 6.52:</b> The stress strain curve of the micro concrete from SAP2000. ....	120
<b>Figure 6.53:</b> Maximum Axial load result for the columns from SAP2000 model under earthquake load, dead load, live load and snow load combination. ....	121
<b>Figure 6.54:</b> Comparison between the interaction diagrams of C1, C2 and C3.....	122
<b>Figure 6.55:</b> Maximum roof displacements due to seismic loads for the 8 stories building in the X and Y directions. ....	122
<b>Figure 6.56:</b> The S11 and S22 stress distributions on the walls under the earthquake load in X direction, dead load, live load and snow load combination.....	123
<b>Figure 6.57:</b> The S11 and S22 stress distributions on the walls under the earthquake load in Y direction, dead load, live load and snow load combination.....	124
<b>Figure 6.58:</b> Pushover curve obtain from ETABS in X direction. ....	125

<b>Figure 6.59:</b> Plastic or fiber hinges formed during the pushover analysis in the X direction at the last step of loading .....	125
<b>Figure 6.60:</b> Target displacement values and the capacity curve in the X direction.....	126
<b>Figure 6.61:</b> No plastic or fiber hinges were formed at the target displacement in X direction.....	127
<b>Figure 6.62:</b> Pushover curve obtain from ETABS in Y direction. ....	128
<b>Figure 6.63:</b> Plastic or fiber hinges formed during the pushover analysis in the Y direction at the last step of loading.....	128
<b>Figure 6.64:</b> Target displacement values and the capacity curve in the Y direction.....	129
<b>Figure 6.65:</b> No palstic or fiber hinges were formed at the target displacement in Y direction.....	130

## LIST OF TABLES

	<b>Page</b>
<b>Table 2.1:</b> Summary of the test program. ....	28
<b>Table 2.2:</b> Loading sequence for rack beam-to-column connections (ANSI MH16.1:201) .....	33
<b>Table 2.3:</b> Collapse behavior of the tested connections (100mm depth beam connection). ....	34
<b>Table 2.4:</b> Collapse behavior of the tested connections (120 mm depth beam connection). ....	34
<b>Table 2.5:</b> Collapse behavior of the tested connections (140 mm depth beam connection). ....	35
<b>Table 2.6:</b> Peak moment values for left and right beam connections. ....	36
<b>Table 2.7:</b> Observations and results obtained from the experimental study. ....	50
<b>Table 3.1:</b> Input and calculated values for a four bay, three story rack frame (140.40.NP). ....	54
<b>Table 3.2:</b> Seismic performance assesment of rack frames with different connection configurations. ....	55
<b>Table 5.1:</b> Importance factors according to RMI (2012). ....	76
<b>Table 5.2:</b> Equivalent lateral force calculated for the different connections. ....	77
<b>Table 6.1:</b> Plastic and fiber hinges results due to pushover load in X direction at the last loading step. ....	111
<b>Table 6.2:</b> Plastic and fiber hinges results due to pushover load in Y direction at the last loading step. ....	114
<b>Table 6.3:</b> Plastic and fiber hinges results due to pushover load in X direction at the last loading step. ....	126
<b>Table 6.4:</b> Plastic and fiber hinges results due to pushover load in Y direction at the last loading step. ....	129

## LIST OF SYMBOLS AND ABBREVIATIONS

<b>Symbol</b>	<b>Explanation</b>
<b>B</b>	: Damping Coefficient
<b>C<sub>s</sub></b>	: Seismic Response Coefficient
<b>D<sub>max</sub></b>	: Maximum Displacement
<b>E</b>	: Youngs Modulus
<b>E<sub>c</sub></b>	: Modulus of Elasticity of Concrete
<b>E<sub>s</sub></b>	: Modulus of Elasticity of Steel
<b>H</b>	: Clear Height Of Upright
<b>h<sub>i</sub></b>	: Height of the Floor
<b>I<sub>b</sub></b>	: Beam Inertia
<b>I<sub>c</sub></b>	: Upright Inertia
<b>I<sub>p</sub></b>	: Importance Factor
<b>I<sub>s</sub></b>	: Moment of Inertia of Steel
<b>k<sub>b</sub></b>	: Minimum Permitted Base Plate Stiffness
<b>k<sub>be</sub></b>	: Beam End Rotational Stiffness
<b>k<sub>c</sub></b>	: Beam-to-Column Connection Stifness
<b>k<sub>c</sub></b>	: Minimum Permitted Connection Stiffness
<b>k<sub>ce</sub></b>	: Upright End Rotational Stiffness
<b>L</b>	: Clear Span of Beams
<b>M<sub>max</sub></b>	: Maximum Moment
<b>N<sub>b</sub></b>	: Number of Base Plate Connections
<b>N<sub>bay</sub></b>	: Number of Bays
<b>N<sub>c</sub></b>	: Number of Beam to Upright Connection
<b>N<sub>cr</sub></b>	: Critical Axial Load of the Columns
<b>N<sub>L</sub></b>	: Number of Levels
<b>N<sub>p</sub></b>	: Design Axial Capacity of the Column
<b>P<sub>crd</sub></b>	: Critical Distortional Column Buckling Load
<b>P<sub>cre</sub></b>	: Critical Flexural Torsional Column Buckling Load
<b>P<sub>crl</sub></b>	: Critical Local Column Buckling Load
<b>P<sub>h</sub></b>	: Pallet Height
<b>P<sub>n1</sub></b>	: Nominal Axial Strength of Column C1



<b><math>P_{n2}</math></b>	: Nominal Axial Strength of Column C2
<b><math>P_{n3}</math></b>	: Nominal Axial Strength of Column C3
<b><math>P_{nd}</math></b>	: Nominal Axial Strength of the Column for Distortional Buckling
<b><math>P_{ne}</math></b>	: Nominal Axial Strength of the Column for Flexural Torsional Buckling
<b><math>P_{nl}</math></b>	: Nominal Axial Strength of the Column for Local Buckling
<b>R</b>	: Reduction Factor
<b><math>S_{M1}</math></b>	: One-Second MCE Accelartion
<b><math>T_1</math></b>	: Fundamental Period
<b>V</b>	: Equivelant Lateral Force
<b><math>W_{pi}</math></b>	: Pallet Weight
<b><math>W_s</math></b>	: Effective Seismic Weight
<b><math>\Delta_i</math></b>	: Maximum Displacement
<b><math>\theta</math></b>	: Rotation
<b><math>\theta_{demand}</math></b>	: Rotational Demand
<b><math>\theta_{max}</math></b>	: Maximum Rotation Capacity
<b><math>\delta</math></b>	: Contribution Factor
<b><math>\lambda</math></b>	: Relative Slenderness
<b><math>\chi</math></b>	: Reduction Factor

<b>Abbreviation</b>	<b>Explanation</b>
<b>2P</b>	: Two Pins Hooked Connection
<b>3D</b>	: Three Dimensional
<b>4P</b>	: Four Pins Hooked Connection
<b>ACW</b>	: Anti-Clockwise
<b>AISI</b>	: American Iron And Steel Institute
<b>CW</b>	: Clockwise
<b>EN</b>	: Eurocode
<b>FE</b>	: Finite Element
<b>FEMA</b>	: Federal Emergency Management Agency
<b>kN</b>	: Kilo Newtons
<b>m</b>	: Meters
<b>MCE</b>	: Maximum Credible Earthquake
<b>mm</b>	: Millimeters
<b>MPa</b>	: Megapascals

<b>N</b>	: Newtons
<b>NP</b>	: No Pins Hooked Only Connection
<b>RMI</b>	: Rack Manufacture Institute
<b>Sec</b>	: Seconds
<b>WB</b>	: Welded Bolted Connection



## ÖZET

### DOKTORA TEZİ

#### SOĞUK ŞEKİLLENDİRİLMİŞ, İNCE CIDARLI RAF TIPI ÇERÇEVELERİNİN DAVRANIŞI VE BINA TÜRÜ YAPILARDA KULLANIMI

**Bassel ELKADI**

**İstanbul Üniversitesi**

**Lisansüstü Eğitim Enstitüsü**

**İnşaat Mühendisliği Anabilim Dalı**

**Danışman : Dr. Öğr. Üyesi Erdem DAMCI**

Bu tez paletli depo raf sistemlerinin koridor doğrultusunda sergiledikleri deprem davranışına odaklanmaktadır. Deneysel çalışmalar ile de gösterildiği üzere, depo raf sistemlerinin koridor doğrultusundaki deprem davranışını, kolon-kiriş birleşimlerinin lineer olmayan davranış önemli ölçüde etkilemektedir. Söz konusu birleşimler koridor doğrultusunda yatay deprem yüklerini moment aktaracak şekilde tasarlanan özel birleşimler ile karşılarlar. Bu birleşimler genellikle cıvatasız kancalı tip birleşimlerdir ve kuvvetli deprem etkileri altında çerçevelerin yatayda büyük yer değiştirmelerine sonuç verecek şekilde önemli düzeyde dönme davranışı sergilerler. Bu tez çalışmasında, tipik kancalı kolon-kiriş birleşimlerinin tersinir çevrimsel moment-dönme ilişkilerini ortaya çıkarmak üzere bir deneysel çalışma gerçekleştirilmiştir. İlave olarak, aynı yükleme koşulları altında içinde kancalar ile birlikte cıvataların da kullanıldığı karma tip birleşimler de deneysel olarak çalışılmıştır. Kancalı depo raf kolon-kiriş birleşimlerine bu şekilde cıvata ilave edilmesinin birleşimin yapısal açıdan güçlendirilmesi ile ilgili pratik bir yöntem olduğu düşünülebilir. Deneyler ile ortaya çıkarılan birleşim davranış özellikleri çevrimsel yükleme protokolü içinde maksimum moment ve dönme kapasiteleri açısından karşılaştırılmıştır. Elde edilen sonuçlar daha sonra ele alınan birleşim tiplerini içeren depo raf çerçevelerinin deprem performans değerlendirilmesinde kullanılmıştır. Söz konusu değerlendirme çerçevelerinin koridor doğrultusunda deprem davranışını tespit etmek üzere kullanılan yer değiştirme tabanlı bir basit analitik yöntemin kullanılmasını kapsamaktadır. Değerlendirme çalışması sonucunda elde edilen sonuçlar incelendiğinde önerilen güçlendirme yönteminin depo raf sistemlerinde kullanılan kancalı birleşimlerin ve dolayısıyla çerçevelerin deprem performansını artırdığına yönelik etkili bir yöntem olduğu tespit edilmiştir. ANSYS

sonlu eleman yazılımını kullanarak kancalı ve civatalı birleşimlerin deprem davranışının benzetimi amacıyla bir kabuk sonlu eleman modeli geliştirilmiştir. ANSYS modelleri kullanılarak elde edilen sonuçlar deney sonuçları ile karşılaştırıldıklarında elastik bölge rijitliği ile ulaşılan maksimum moment değerleri açısından oldukça yakın sonuçlar elde edildiği görülmüştür. SAP2000 yazılımını kullanılarak farklı birleşim tiplerini içeren çerçeve modelleri için lineer olmayan statik itme analizleri gerçekleştirilmiştir. İtme eğrileri önerilen kancalı-civatalı karma birleşim tipinin raf sistemi deprem performansını önemli ölçüde artırdığını göstermektedir. İlave olarak, sonuçlar kullanılarak depo raf sistemleri için performans seviyeleri belirtilmiştir. Önerilen birleşimlerin kullanıldığı çerçeveler için elde edilen olumlu deprem performans sonuçlarından yola çıkılarak söz konusu birleşimlerin konut tipi yapılarda kullanılması ile ilgili ilave bir çalışma gerçekleştirilmiştir. Bu çalışma kapsamında 82.8 m<sup>2</sup> lik taban oturma alanına sahip 5 katlı konut tipi üç boyutlu yapı modelleri SAP2000 ve ETABS programları kullanılarak incelenmiştir. Modellerde, yukarıda bahsedilen deneysel çalışmada kullanılan çelik depo raf elemanları/kesitleri esas alınmıştır ve 5 kata kadar güvenli sonuçlar elde edilebileceği gösterilmiştir. Bunun dışında, ilk iki katta kullanılan ince cidarlı kolon kesitlerini bir adet levha ile kapatarak ve içine beton dökerek yapılabilecek küçük değişikliklerle kat sayısının 8 kata kadar artırılabilceği sonucu elde edilmiştir.

Mayıs 2019, 165 sayfa.

**Anahtar kelimeler:** Çelik depo raf birleşimleri, çevrimsel test, deprem performansı, yapısal iyileştirme, raf elemanlar.

## **SUMMARY**

### **Ph.D. THESIS**

#### **BEHAVIOR OF COLD FORMED, THIN-WALLED, RACK TYPE FRAMES AND THEIR USE IN BUILDING STRUCTURES**

**Bassel ELKADI**

**İstanbul University**

**Institute of Graduate Studies in Science and Engineering**

**Department of Civil Engineering**

**Supervisor : Assist. Prof. Dr. Erdem DAMCI**

This thesis focuses on the seismic performance of pallet-type steel storage rack structures in their down aisle direction. As evidenced by experimental research, the seismic response of storage racks in the down-aisle direction is strongly affected by the nonlinear moment-rotation response of the beam-to-column connections. In their down-aisle direction, rack structures are designed to resist lateral seismic loads with typical moment frames utilizing proprietary beam-to-column moment-resisting connections. These connections are mostly boltless hooked type connections and they exhibit significantly large rotations resulting in large lateral frame displacements when subjected to strong ground motions. In this thesis, typical hooked boltless beam-to-column connections are studied experimentally to obtain their non-linear reversed cyclic moment-rotation response. Additionally, a compound type connection involving the standard hooks and additional bolts were also tested under similar conditions. The simple introduction of the additional bolts within the hooked connection is considered to be a practical way of structural upgrade in the connection. The experimentally evaluated characteristics of the connections are compared in terms of the most important performance indicator which is the maximum moment and rotation capacity within the cyclic loading protocol. The obtained characteristics were used to carry out seismic performance assessment of rack frames incorporating the tested beam-to-column connections. The assessment involves a displacement based approach that utilizes a simple analytical model that captures the seismic behavior of racks in their down-aisle direction. The results of the study indicate that the proposed method of upgrading appears to be a very practical and

effective way of increasing the seismic performance of hooked connections and hence the rack frames in their down-aisle direction. A finite element shell model that simulates the experimental behavior of both the hooked and the pinned connection was developed using ANSYS finite element software. The results from the ANSYS models were very promising with very low error percentage of the peak moment rotation results, and with an initial stiffness that is almost identical to the experimental results. Non-linear static pushover analysis was carried out using SAP2000 software in order to analyze the difference of the behavior of the frames using the different beam-to-column connections. The pushover curves obtained showed how the newly proposed bolted connections enhance the seismic performance of the rack system significantly. Additionally, performance levels for the rack structures were stated based on the experimental results and observations. Finally, the great enhancement in the seismic behavior of the rack beam-to-column connection was a motivation to try to develop a new design for residential buildings using these connections. SAP2000 and ETABS software were used to carry out both of linear and non-linear analysis on a residential building with 82.8 m<sup>2</sup> ground area in order to reach the maximum number of stories using the rack members. It was obtained that a 5 story residential building can be constructed totally using the rack members that were tested in the experimental study. Additionally, with small modifications such as pouring concrete and adding one more plate to close the column cross-section in the first two stories, the number of stories could be increased up to 8 stories.

May 2019, 165 pages.

**Keywords:** Steel storage rack connections, cyclic test, seismic performance, structural upgrade, rack members.

## 1. INTRODUCTION

Steel storage rack systems play a key role in the industrial supply chain by providing efficient storage spaces for industrial products. In today's rapidly developing world of manufacturing, the need for storage rack systems is increasing and in addition to the existing number of storage systems a lot more number of systems is being constructed for use by various industry producers.

In big cities finding an available land for construction is a very hard issue, that leads to the solution of building high rise buildings and structures which minimizes the space for the industrial constructions. One of the main reasons of the high need for the rack structures nowadays, is that rack structures are designed on a very small floor area compared to the number of goods that it can store. The goods are being stored by storing pallets on beams with a minimum spacing and on several number of stories.

As a result of that, during the last fifty years there is significant growth in the number of huge warehouses that uses the rack structures as it is the best solution for large shopping markets and factories for storing enormous number of goods in an optimal area as shown in Figure 1.1.

Rack systems are designed to carry different types of goods, including hazardous materials, that leads to a great concern for the safety of the rack structures, because the hazardous materials can cause fire and can lead to life losses. Several reasons may lead to the instability and collapse for a rack structure, such as; impact of forklifts, over loading and earthquakes. As a result of that a proper design of the rack systems is a must, not only to avoid economical loss due to collapse but also to avoid potential life losses of the people in the area of existence of the rack structures.

If the storage rack systems are not well designed, loaded, installed and maintained they may face a total collapse or overturn during an earthquake, that will result in economic losses due to the damage of the stored goods and it may put the life of the workers or the occupants in danger.



**Figure 1.1:** Cold-formed steel rack system (Elkadi, 2015).

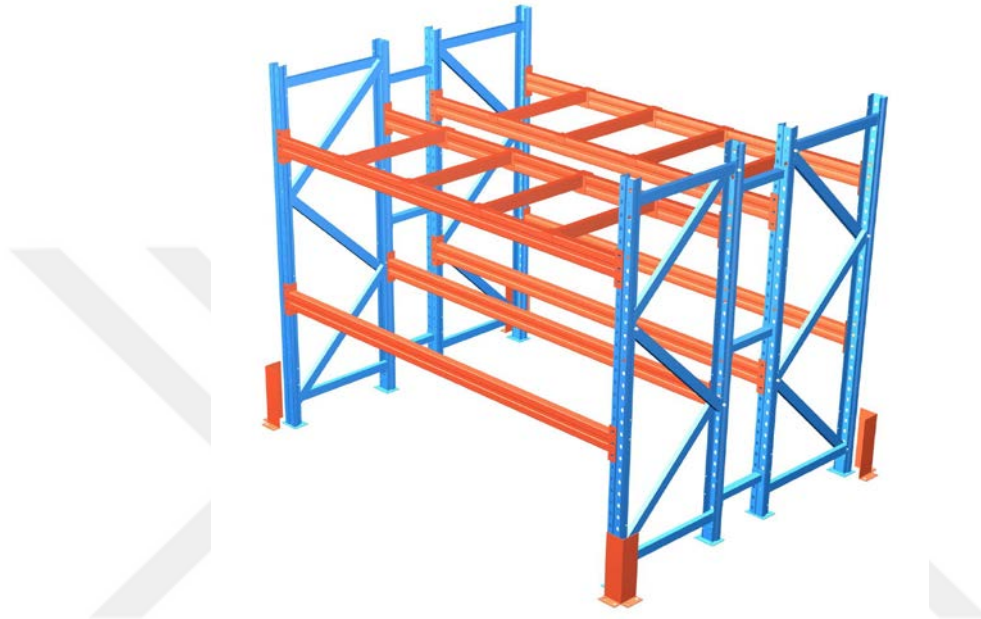
Storage racks may exist outdoors or inside a host building. The performance of the host building during an earthquake affects the performance of the rack structure. Therefore, the life safety is dependent not only on the structural performance of the racks but also it depends on the structure performance of the host building.

Most of the developing countries doesn't have a specific code for the design of rack structures, which makes economical and life losses more crucial.

There are two types of rack systems, the braced and the unbraced frames. The unbraced system is much more preferred to be used than the braced system, as the braced system has bracings both in the transverse and the longitudinal directions which acts as an obstruction for placing the products to the racks. In the unbraced rack frames, bracings exist only in the transverse direction, while the longitudinal direction is remained unbraced, in order to make it easy for the products to be placed to the racks as shown in Figure 1.2. In the unbraced rack systems, the longitudinal direction is called as the down-aisle direction while the transverse direction is called as the cross-aisle direction. In the cross-aisle direction the lateral forces are carried by



the bracings while in the down-aisle direction the lateral loads are resisted by moment frames in which the behavior of the frame depends mostly on the behavior of the beam-to-column connections.



**Figure 1.2:** Cold-formed steel rack system (URGO racking, 1998).

The unbraced storage rack frames consist of cold formed steel elements that are well known of their high strength compared to their light weights which makes them easy to install and uninstall in short periods of time. The behavior of the beam-to-column connections that resists the lateral loads in the down-aisle direction needs to be determined by experimental or numerical tests in order to have a proper design to the rack frame and to predict the behavior of these connections under seismic or lateral loads.

The beam-to-column connection is defined as semi rigid connection, as their behavior cannot be considered as one of the two extreme definitions of rigid or pinned connection. In the rigid connections all the members of the joints are considered to be extremely stiff in which there is no differences in the rotations in the end of the members connected in the joint. In contrast, in the pinned connection is a connection without any stiffness that cannot transfer any moment. The beam-to-column connection of the unbraced rack system behaves in between this two cases. The parameter that transmits the moment to a relative rotation is the rotational stiffness,

which is the difference between the rotations of the two connected members. The connection is considered as a pinned connection if the rotational stiffness is zero or relatively small, while the connection is considered to be rigid connection if the rotational stiffness is infinity or relatively high. For all the intermediate cases between these two cases the connection is considered to be a semi rigid connection and this is the case for the beam to column connection for the rack systems. (Jaspart, 1999).

FEMA 460 presents a simple analytical model for the displacement based seismic design of storage rack systems in the down-aisle direction. Simple equations were used to calculate the base shear, the fundamental period and the top lateral displacement of the rack storage frames in the down-aisle direction, based on the beam-to-column connection characteristics. The most important parameters that describes the behavior of the beam-to-column connection are the rotational stiffness of the connection and the rotational capacity, and these are the main parameters used in the equations.

In order to find the rotational stiffness and the rotational capacity of the beam-to-column connection of the storage rack systems, experimental tests are required. FEMA 460 proposes beam-to-column connection tests in order to obtain the rotational stiffness and the rotational capacity at targeted displacements. In the design of the standard steel structures it easy to design the connections with direct equations, while in the rack cold formed steel structures, it is not that easy to design the beam to column connection, due to the high variety in cross-sections of the used members and the existence of perforations along them. Tests to the beam-to-column connections must be carried out in order to obtain the rotational stiffness and the rotational capacity to have a precise design for the connection.

The test procedures for the beam-to-column connections of the rack structures is described in the Rack Manufacture Institute (RMI, 2008) and EN 15512-2009, however it is so hard to determine the behavior of the beam-to-column connection due to its semi-rigid behavior. Additionally, it is so hard to present a standard test procedure due to the high variation in the connection types.

The main standards that are used nowadays to design the rack storage structures are the American specifications such as (Rack Manufactures Institute Specifications for the Design,

Testing and Utilization of Industrial Steel Storage Rack, RMI 2008) and (Steel Static Storage Systems Adjustable Pallet Racking System-Principles for Structural Design EN15512-2009) in Europe. Since the rack members are being produced in different countries with different cross-sections, a lot of countries do not have their own designing standards for the rack structures including Turkey. This leads to a lot of unsafe designs for the rack structures all over the world that leads to a lot of life and economical losses. Because of that there is an essential need for more research for the design of the members and specially the beam to column connections as the behavior of the rack structures mainly depends on the behavior of the connections in the down-aisle direction.

RMI 2008 and EN 15512-2009 are used with added provisions to design the storage rack structures such as the (National Earthquake Hazards Reduction Program NEHRP). The provisions were added to add an upper limit to the period of rack structures under seismic conditions, and to cause large base shear force in the resulting analysis since the RMI 2008 did not widely explain the behavior of the rack storage structures under seismic conditions.

The results of the period of the rack structures obtained from the current provisions are having a maximum limit of 0.6 seconds while the actual period of a typical rack storage structure in the down-aisle direction varies between 2 to 4 seconds. Additionally, it is well known that the beam to column connection has a very big role in the performance of the rack structure as the moment rotation characteristics of the connection affects the periods and the damping characteristics of the whole rack system, (RMI, 2008).

Significant differences can be found when the rack storage structural systems are compared to the other structural systems. The main three parameters that are taken into consideration while designing any building are; safety, regulations and economy. If the designer gives the same importance for the three parameters so the result will be a perfect highly efficient structural design. For example, designing a residential structure starts by architectural and structural designs according to the known standards and regulations, while caring at the same time for the budget restrictions. However, for the rack storage structures there is no such a procedure due to the lack of information about the behavior of these systems, so mostly the users are caring only

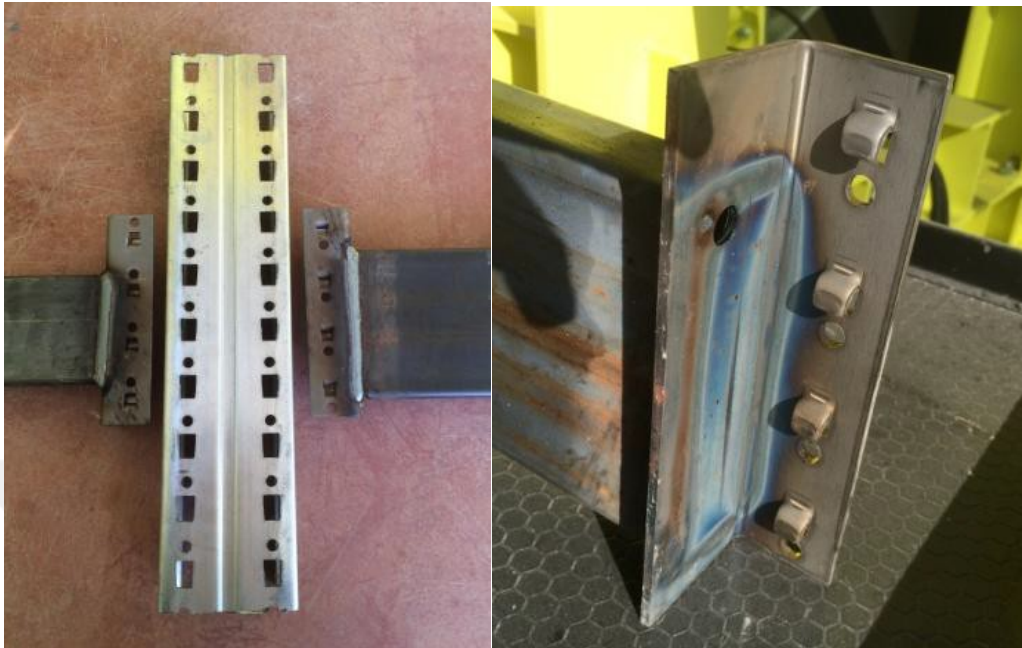
for the economical parameter and they neglect the regulation and safety parameters. This leads to disastrous results in the future.

A lot of research is being performed to understand the behavior of the steel storage rack structures in order to find significant solutions for the problems that are mentioned in the previous sections. Most of the research focuses on finding solutions specially for the safety parameter in the design of the rack structures. In this thesis the aim is to propose different solutions for the three main parameters safety, economy and regulations in the design of the storage rack systems.

The main focus of this thesis is on the behavior of the connections of the rack structures. In the steel storage rack structures, the behavior in the down-aisle direction depends mainly on the behavior of the beam-to-column connection, because no braces are used in this direction to allow the loading and unloading of the pallets.

Considering all the constituent structural elements that make up the structural system, steel storage racks resemble much like the conventional steel frames. However, there are a number of peculiarities that differentiate these systems from conventional steel frames. In steel storage rack systems, all members are thin-walled cold formed steel members, that are manufactured by bending flat sheets of steel into shapes without any form of heating. The main components of a typical rack storage system are; the upright column that has perforations along its height. The pallet beam, which is a horizontal member linking the columns together in the down-aisle direction. The beam-end-connector bracket, which is mostly and L shaped member, welded to the beam and has hooks welded to it in order to be placed into the perforations that exists along the height of the column as shown in Figure 1.3 and Figure 1.4. Bracings, that are used to connect the column in the cross-aisle direction.

Therefore, compared to the conventional steel frames, all these features of steel storage rack frames result in lightweight, flexible and low-redundancy structural systems.



**Figure 1.3:** Typical hooked beam-to-column connection in storage rack frames.



**Figure 1.4:** Beam-column connection (Elkadi, 2015).

The spacing between the columns in the down-aisle direction is generally between 1.5 m to 4 m depending on the type of products that will be stored in the rack structure. The spacing

between the columns in the cross-aisle direction generally varies between 0.5 m to 1.2 m. The existence of the hooks at the beam end connector bracket and the perforations along the height of the column makes it easy for the beams to be placed in the required levels depending on the height of the stored products. The products are usually placed over wooden pallets that transfers the loads to the beam. The wooden pallets can carry loads from 500 kg up to 3000 kg depending on the need of the storing warehouse.

It is hard to find standards or design codes in each country for designing the rack structures, because till now the rack structures are not giving the same importance like other residential structures, although the huge economical and life losses that can occur due to their collapsing. In the countries that codes and standards for rack structures exists, the standards are considered more as a design guide than being a design code. Because of that more research is being performed to understand the behavior of rack structures specially under seismic loads in order to have a clear approach for the design of the rack storage systems.

The regulations and guidelines that are available for the seismic design of rack storage structures are listed below.

- RMI, Rack Manufacturer Institute 2008, Specification for the Design, Testing and Utilization of Industrial Steel Storage Racks.
- FEMA 460, Seismic Considerations for Steel Storage Racks Located in Areas Accessible to the Public.
- AISI S-100, Specification for the Design of Cold-Formed Steel Structural Members.
- AISI S110-07/S1-09 (2012) : AISI Standard for Seismic Design of Cold-Formed Steel Structural Systems.
- FEM 10.2.08, The Seismic Design of Static Steel Pallet Racks.

According to FEMA 460 the life safety and collapse prevention levels in the seismic considerations for steel storage racks located in areas accessible to the public is achieved under specific conditions. Life safety performance level is achieved if the following conditions are met:

- 1) Preventing the failure of any component that may lead to contents shedding or collapse of the rack structure.
- 2) Preventing the risk of overturning of the rack structure.
- 3) Preventing the loss of stored items from rack shelves located 2.5 m or more above the ground level.

Collapse prevention performance in the MCE is achieved if the following conditions are met:

- 1) Preventing the collapse of rack structure.
- 2) Preventing the risk of overturning of the rack structure.

Shedding of contents prevention is not a must for the collapse prevention performance state which can lead to some injuries and even life losses.

Safe storage of products is of vital importance to prevent both economic and possible human life losses. Among various possible reasons that could risk the safety of the systems, one important reason is the earthquake. The above mentioned flexibility and low-redundancy characteristics of the systems may complicate the behavior of rack frames under lateral seismic effects. In particular, the behavior of the hooked beam-to-column connections plays an important role in the seismic behavior of these structures (Figure 1.5).



**Figure 1.5:** Collapsed rack system in Christchurch earthquake in 2011 (Clifton et al., 2011).

Experimental and analytical studies related to the seismic performance of storage racks are limited to warrant a satisfactory basis for seismic design of these systems. On the other hand, due to the great number of types of beam-to-column connectors used in practice as well as the different geometries employed for rack beam and column members, design approaches to evaluate the seismic performance of rack frames are not completely available. Therefore, to understand the seismic behavior of storage rack systems and to fill the gap in design a number of experimental and analytical studies have been carried out.

Prabha et al. (2010) carried out eighteen experiments on boltless column-beam rack connection that are available commercially. The main aim of their experiment study was to evaluate the flexibility of the beam to column joint and to obtain a three parameter model by a Frye-Morris type moment rotation relationship. In order to quantify these values, they varied the most effective parameters on the beam to column connection behavior, such as; the depth of the beam end connector, thickness of the upright and the depth of the beams. Additionally, they have created a finite element shell model using ABAQUS finite element software that is used to simulates the actual behavior of the beam to column connection that was observed during the experimental study.

From this study it was found that the moment rotation characteristics of the beam to column connection does not depend only on the design of the beam end connector, but also it depends on the quality of the other members in the connection, specially the column.

The parametric studies that they carried out show that increasing the number of the hooks in beam to column connection, that are designed to resist the loads applied to the connection, leads to an increase in the strength and the stiffness of the beam end connector. It was proved also that increasing the thickness of the column and the depth of the beam improves the stiffness and the strength of the beam to column connection.

The ABAQUS finite element model obtained a very good fit to the experimental studies behavior, which made it validated to be used for a further parametric studies. They proposed two analytical models, a model based on the Frye-Morris procedure and they called it as the polynomial model, and another model for the boltless cold formed semi-rigid connections that they called as the power model. Using the polynomial Frye-Morris model, the could reach to a



standardization constant  $K$  that takes into consideration the three variable parameters; the depth of the beam end connector, thickness of the upright and the depth of the beams based on the experimental results. It was found that the initial stiffness of the tested beam to column connections could be predicted very well using the polynomial model. On the other hand, the ultimate capacity of the connection can be predicted using the newly proposed power model, that has a close fit with the results obtained from the experimental study.

Saravanan et al. (2014) studied the dynamic characteristics of a 3D two story pallet rack structure with a single bay and a hooked connector by shake table testing. Finite element analysis modelling of the tested system was used to evaluate the dynamic characteristics that was observed in the real tests. The stiffness values used in modeling of the hooked connector were taken from a previous study that was done by Prabha et al. (2010). The results obtained from the analysis were in a good agreement with the results of the experimental study.

Kalavagunta et al. (2012) used push over analysis to investigate the collapse of cold formed storage rack structures subjected to seismic loading. A non-linear static procedure was used according to FEMA 356 specifications to analyze a simple storage rack structure. Good estimations of the base shears, plastic hinges and displacement demands were obtained successfully from the study which let the study to be considered as a useful tool to analyze a simple storage rack structure.

Petrovic et al. (2012) examined the seismic performance of an existing externally braced high-rack steel frame structure and analyzed the consequences of positioning the stored loads asymmetrically that will lead to high mass eccentricities. Both of non-linear static analysis and dynamic analysis were used to analyze the seismic performance of the high-rack structure. It was obtained that the seismic risk may increase due to high stored load eccentricities which can lead to significant instabilities to the rack columns.

Sideris et al. (2010) investigated the seismic behavior of pallet type steel storage racks with palletized merchandise stored on shelves. Additionally, the concept of incorporating slightly inclined shelving was proposed. The newly proposed inclined shelving concept was tested using shake table tests and pull tests. The main aim from the shake table tests was to analyze the dynamic response of the palletized merchandise subjected to earthquake loads at the base of the

rack structures, and to determine experimentally the fragility of the pallet shedding under an ensemble of ground excitations. From the results obtained from the shake table tests, it was found that the concept of inclined shelving is very effective.

Bajoria et al. (2010) analyzed the seismic response of pallet rack structures through three dimensional finite element modeling of pallet rack frames with semi-rigid connections. Stiffness values for the connections were obtained by carrying out conventional cantilever tests on typical rack beam-to-column connections. From the experimental study on connections and finite element modal analysis, a simple analytical model that captures the seismic behavior of storage racks in their down aisle direction was proposed.

Besides the aforementioned latest research on seismic behavior of storage rack systems a number of valuable earlier studies should also be mentioned. Shake table tests were carried out by various researchers both in Europe and the USA. Two full-scale shake-table testing investigations of storage racks fully loaded have been performed in Europe (Castiglioni et al. (2003)) and other three in the United States (Chen et al. (1980), Chen et al. (1981)); Filiatrault et al. (2004)). Shake table tests on different types of rack systems were carried out on both down-aisle and cross-aisle directions. The test results showed that the main factor which affect the seismic behavior of the rack structures in the down-aisle direction is the rotational stiffness of the beam to column connections.

Bernuzzi et al. (2001) performed an experimental study to investigate the behavior of the beam to column connections in the rack systems. Eleven tests on two different types of beam to column connections. They have applied three different types of tests.

The first type is a monotonic test under hogging moment, to understand the behavior of the connection under static loading, which is the usual usage of the rack systems.

The second type is a monotonic test under sagging moment, to understand the behavior of the connection while subjected to an accidental upward movement or moments that may lead to the sway of the frame.

The third type is two cyclic tests under constant symmetrical loading amplitude. Different values of displacements were applied to increase the deterioration of the main parameters that affects the behavior of the connection, such as (stiffness, strength and energy absorption capability).

The monotonic tests showed that a ductile behavior occurs at the nodal zone of the beam to column connection and that collapse never happened in these types of tests.

The cyclic tests showed that the behavior of the joint has a great influence on the behavior of the whole frame. The slippage that occurs during the earthquake which is accompanied with high deformations causes very large sway for the uprights, leading to a significant increase of the second order effects.

The results of the cyclic tests showed a significant reduction in the energy dissipation capacity of the connection with a pinching behavior that appears with the increasing of the number of cycles due to the plastic deformations and the slippage occurs to the connectors.

Quasi-static testing was carried out on 22 different types of beam-to-column subassemblies by Filiatrault et al. (2006). The test data indicated that beam-to-column connections exhibit stable and very ductile behavior, with rotational capacities beyond the values observed during shake-table tests and expected from a design seismic event.

Markazi et al. (1997) performed an experimental study on the semi-rigid boltless connector of the rack industry systems. The aim of his study was to obtain the parameters that leads to an efficient beam to column connection design. Four types of beam to column connections were used. The first type is called as tongue and slot design, in which the term tongue describes the cantilevered hook which is designed out of the bracket. The second type is called as blanking design, in which a blanking operation produces hooks that interlocks perpendicular or parallel to the web of the upright depending on the design of the column. The third type is called stud-incorporated design in which studs replaces the hooks in the tongue and slot design. The fourth type is called as dual integrated tab design, in which the hooks are formed and punched out of the connector so that they remain connected to the bracket at two points. Bending tests were carried out to determine the moment-rotation curves for each connection.

It was found that for a beam to column connection under a combination of axial load and bending moment may face an overall bending of the end plate combined with distortion of the bracket, but this depends on the applied axial load, bending moment and the design of the connection itself. Additionally, it was stated that the characteristic of the moment-rotation behavior of the connection is not only affected by the design of the beam to column connection, but it is also affected by the design of the accompanying elements, specially the upright.

Factors affecting the efficiency of a beam to column connection were determined using the results obtained from the moment rotation curves, the deformation modes and the ultimate loads which are stated below:

- The number of the hooks: increasing the number of the hooks will increase the strength and the stiffness of the beam to column connection. But it should be taken into consideration that the hooks should be designed to participate in resisting the applied loads.
- The details of the geometry of the hooks: stronger hooks should be used to be able to resist the stress concentrations.
- Design of the bracket: the bracket should be designed efficiently to not to face any hook bracket failure.
- The gauge between the bracket and the upright: increasing the gauges of the bracket and the column improve the strength and stiffness of the connection.
- The profile of the column: using a profile of the column with high stiffness will increase the stiffness of the beam to column connection.
- The number of contact planes between the bracket and the column: increasing the number of contact planes will increase the stiffness of the beam to column connection.

Aguirre (2005) carried out an experimental study on a typical beam to column rack connection under both static and cyclic loads. Five monotonic static tests were performed to understand the collapse mechanism and the behavior of the beam to column connection. The tests were kept running until collapse of the connection occurs or until the loading device reaches its maximum displacement. The moment rotation curves from the five tests were obtained.

For a 500 mm displacement stroke double action Sheffer jack was used. Additional transducers were added to measure the displacement of the load application point and the gap of the connection. The loading history was applied as a series of three cycles of equal displacement with 30 mm increment (30 mm, 60 mm and 90 mm, while the test was running till the connection fails in order to reach the maximum displacement.

From the test results it was found that the connection is classified as semi rigid connection, but its behavior is a little different from other types of connections, as the rack connections either bolted or hooked, reaches three times the moment capacity of a typical semi rigid connection, but this happens at much higher deformations, which leads to a small slope of the moment rotation curve.

Besides the experimental study, non-linear frame analysis was carried out in order to understand the behavior of the rack steel frame. The analysis was performed on a two span frame using the Ruaumoko program developed by Carr (1996) using the same structural properties obtained from the test results. It was found that the small stiffness of the frame leads to larger displacements. High moments at the columns were obtained due to the high flexibility of the structure that leads to high lateral displacements.

From the experimental and the nonlinear analysis conducted it was found that, due to the flexibility of the rack beam to column connections, the proper way to analyze the frame is by taking into consideration the nonlinear properties of the connection because the nonlinear displacements reaches twice the predicted displacements from the standard rigid analysis.

It is necessary to carry out more tests to have deeper knowledge about the seismic behavior of the rack structures because there is no enough information about the beam to column connections used in these systems.

The beam to column connections requires a type of locking to be applied to it, that can be obtained by adding a bolt or a safety clip. The clip was considered as the best solution as it is easier and faster to be used, however the easy unlocking on the beam to column connection will let the structure to less resisting to the lateral loads.

As soon as a hook yields, it stops carrying the required loads, leading to a decrease in the redundancy of the beam to column connection. Because of that, redistribution of the bending moment occurs by increasing the moments at the center of the beam span that leads to early failure to the beam.

It was found that the failure mode in the both loading cases of static and cyclic test is so similar, as the failure is totally controlled by the hooks, which means that the failure occurs at the beam, that can be easily replaced, avoiding having column failures.

The connection performs well in resisting the vertical loads, but they are more vulnerable for seismic loads, which makes it necessary to find a better alternative solution to provide more stability under high lateral loads.

Markazi et al. (2001) carried out a finite element analysis of a boltless semi rigid beam to column connection of the storage rack systems. An elastic linear analysis of a three dimensional model of the connection was performed and the results were compared with existing experiments. From the experimental work it was noticed that the behavior of the connection is mainly related to the behavior of the connecting bracket between the beam and the column, as the final failure always occurred at the hooks of the bracket, and this usually occurs after reaching the maximum moment. Because of that, the analysis of the beam to column connection was limited only on the analysis of the beam end connector bracket.

The analysis was performed using the PAFEC-FE program on a three dimensional model of the bracket and the cross-section of the beam. The analysis was a linear analysis with an eight noded, three-dimensional, hexahedron, isoparametric element with three linear displacements,  $u$ ,  $v$  and  $w$  at each corner without any midside degree of freedom. The section of the beam welded to the bracket was called as stub beam. The hardest part of the work was to model the right boundary conditions to simulate the actual behavior on the contact areas and to get the real effect of providing resistance to the rotation of the beam end connector bracket.

Two models were created to obtain the rotation stiffness before the face of the bracket becomes in contact with the web of the column, and two other models to obtain the rotation stiffness

after the bracket is in contact with the web of the column when the initial gap between the bracket and the web of the column has been closed.

From the results of the two sets of models, both the rigid and the semi-rigid connection gave results similar to the results obtained from the experiments. The accuracy of the two types of analyses were approximately the same. However, it is more recommended to use the rigid connection analyses as it gives more conservative rotation stiffness. It was noted that the difference in rotation stiffness that was found between several experiments was in the same order as the differences found between the semi-rigid and rigid connections.

Shah et al. (2016) performed a numerical study through a three dimensional nonlinear finite element model that was compared to existing experimental results. The finite element model took into consideration the main effective parameter of the beam column connection for pallet steel rack systems, such as the geometrical properties, material nonlinearities and large displacements.

Thirty-two tests were carried out, including two different column thicknesses and four different beam depths and the number of hooks in the beam end connector bracket was differing between four or five.

Double cantilever tests were carried out to observe the moment rotation behavior of the beam to column connection. The hooks of the beam end connector bracket were reversely hooked in the column perforation. Additionally, to protect the beam to column connection from any sudden accidental uplift, a locking pin was added to the connection. The test was a displacement control test in which a 50 kN hydraulic actuator was used and controlled by a computer at a rate of 3 mm/mm till the failure of the connection occurs.

During the experimental study and among all the test it was found that only three different failure moods were observed which are; yielding or fracture of the hooks, yielding in the beam end connector bracket or tearing of the upright. The failure of the hooks was the pre-dominating failure mode, in which the top hooks in the compression zone at the two sides were completely ruptured, while the bottom two hooks were deformed and teared the flange of the upright

moving out from the upright perforations. The bracket experienced great deformations during the total failure.

Using ABAQUS software a non-linear 3D model of the beam, upright and the beam end connector bracket were modeled. The hooks of the bracket were modeled using a 4 mm thickness solid element in order to simulate the original test conditions. Modeling the hooks as a structural element made the finite element model more complicated. But this was done in order to simulate the actual system which will help in obtaining the deformation behavior of the hooks.

Nonlinear contact surfaces were defined to the finite element model by inserting the actual interactions between the upright, beam and the beam end brackets. The column and the bracket has a surface-to-surface contact that was modeled as a frictionless tangential contact surface. The surface-to-surface contact between the upright and the hooks are defined in two ways, as a hard normal contact and as a frictionless tangential contact, and this was done to avoid the existence of large movements between the surface of the column and the hook. A beam element was used in order to simulate the welded connection that connects the upright and the beam end connector bracket.

The mapped discretization was used to all the components of the beam end connection in the finite element model in order to enhance the computational accuracy. From the experimental tests it was noticed that in the regions of contact between the hook and the bracket large amount of deformations were taking place, and because of that in these regions a dense mesh was used in order to simulate the deformation with a high precision. The size of the time step and the dense of the mesh in critical regions were decreased to be able to overcome convergence problems that occurred due to the material nonlinearities, contact regions or geometrical properties.

The failure modes obtained from the finite element model was so close to the failure modes observed during the experimental study. Deformation of all the hooks was observed in the specimens however the hooks experienced higher stresses in the tension area that leads to tearing in the perforations of the columns. The finite element model also showed the distortion of the flanges of the upright and the attempts of the hooks to go out of the columns perforations.



However, the distortion occurs at the columns perforations was less intense in the finite element model than what was observed during the experimental study.

The finite element analysis showed that the beam end connector bracket experience large deformations in the tension zone, similar to the results obtained from the experimental tests. The gap between the upright and the beam-end connector bracket was increasing with the gradual increase of the loading that leads to the connection failure.

The finite element model couldn't predict the complete rapture of the top hooks out of the bracket as it was observed during the experimental study. However, the distortion occurred at bottom hooks was so similar to deformations observed during the experimental tests.

The tear occurred in the upright flange perforations was the third failure type noticed from the tests performed in the experimental study. From the finite element solution, it was noticed that the upright was subjected to high stresses based on Mises stress distribution in the tension area of the beam to column connection. Because of that the part of the upright near the compression area experienced lower stress than the part of the column near the tension zone. Additionally, high stresses concentrations were noticed at the part of the upright where the hooks come in contact with the upright's perforations. It was noticed from the experimental study that the hooks in the tension area came out from the columns perforations by tearing the upright. The finite element model predicted successfully the tear of the upright perforations, however the amount of the tears was less than what was noticed during the tests.

The experimental behavior was predicted very well using the finite element model. The stiffness of the finite element model matched very well with the results obtained from the experimental study. The ultimate moment capacity of the beam to column connection from the finite element model was a little bit higher than the ultimate capacity obtained from the experimental tests. The rupture of the top hooks was not noticed by the finite element model, that leads to an increase in the moment capacity obtained from the finite element model.

The finite element model that was validated to the experimental study was used to carry out a parametric analysis. The analyzed parameter are the parameters that affects the behavior of the beam to column connection the most. The parameters are as follows: variation in beam depth,

upright thickness, number of hooks in the beam end connector bracket, variation in the thickness of the beam end connector bracket, variation in the spacing between the hooks while keeping the beam end bracket's depth constant, and variation of the position of the weld between the beams and the beam end connector bracket.

The parametric study showed that by increasing the thickness of column, beam depth and the number of hooks in the beam end connector bracket the intensity of the failure was decreasing. The larger the thickness of the beam end connector bracket the better the performance of the beam to column connection. The results of the parametric analysis showed that an excess welding of the beam leads to non-uniform stresses distributions in the hooks that forces the beam to column connection to an early failure that reduces the performance of the connection. While down-welding of the beam leads to enhances the performance of the connection specially by increasing its stiffness and strength. According to the parametric results, it was found that the best spacing between that hooks in the bracket is to be one fourth the beam end connector bracket's depth.

Zhao et al. (2014) carried out an experimental study to investigate the flexural behavior of the connections of the cold formed steel storage pallet racks. Seventeen different groups of beam to column connections were used with different constructional details, depending on changing the most influencing parameters on the behavior of the beam to column connection, such as; column profile and thickness, the profile of the beams, and the number of hooks in the beam end connector bracket. Three identical specimens for each group were subjected to static, monotonic, hogging loading in a single cantilever test setup. The displacements and strains were measured at the important points of the beam to column connection.

Shahshenas (2015) has carried out monotonic and slow quasi-static reversed cyclic tests on hooked beam to column rack connections. However, the interlocked boltless beam to column connection caused difficulties in measuring the desired data from the tests. New test set up was used to conduct the tests that was verified using a finite element model using SAP2000. Additionally, ANSYS software was used to simulate the test and to model the beam to column connection. ANSYS results showed a good match with the experimental results, comparing the moment-rotation curve results, ultimate strength, initial stiffness and the level of ductility.

In general, the connections with the same profiles and configurations exhibited similar deformation behavior. The upper part of the beam end connector bracket was separated from the column while the lower part of the bracket continued to be in contact with the flange of the column due to the hogging bending moment effects. Because of the stiffening effect the beams provide to the beam end connector bracket, the plate of the bracket attached to the beam rotated as a rigid body. The elements of the connection experienced large deformations with the increasing of the loads. Flexural deformations took place to the beam end connector bracket and the flange of the column.

The failure mode of the columns can be considered as a tearing that occurs at the perforations, this tearing mostly occurs at the topmost hook, due to the effect of the maximum flexural tension. The crack at the perforation keep developing with the increase of the loads which leads to a high increase in the deformations value and a decrease in the load carrying capacity of the connection till the tearing starts to happen, at this point the connection reaches the peak load capacity. This failure mode occurs due to the cross section thickness of the column which is thinner and weaker than the thickness of the hooks. But for the other column with thicker thicknesses it was observed once again that the peak load capacity corresponds to the moment of tearing of the perforation, but in this case the failure was due to the hook that was ruptured from the beam end connector bracket. This mode of failure occurs due to weaker hook strong column design.

In all of these failure modes, the connection becomes ineffective once the crack starts to occur at the perforation of the column, as a redistribution of stresses occurs towards the center of the end connector, and if the test is continued and loading goes on the second hook or the corresponding hook will start a new crack. The second failure mode is always preferred in which the failure occurs in the hook first, which is considered as a beam failure, as it is always better to be away from any failure that may occur at the upright.

The moment rotation curves of the beam to column connection obtained from the experimental tests shows a linear behavior at the beginning, after that a nonlinear behavior starts to occur before the point of peak moment which is the ultimate moment value. This nonlinear behavior can be due to several factors, such as; relative slippage between the column and the beam end

connector bracket, yielding of the hooks, yielding of some points on the bracket or the columns perforations due to the stress concentrations that occurs during the test. There is another possibility that the nonlinear behavior can be due to geometrical nonlinearity. The ultimate moment value or the peak point of the curve always reflect a failure of an element in the connection that occurs during the test, and it can be either a cracking in the perforations of the column or failure in the top hook of the bracket. After the peak moment or the ultimate moment, the load carrying capacity decreases until the start of a second crack in a different hook or column perforation or due to any other failure mode.

From the moment rotation results of all the specimens it was found that the typical failure mode for the beam to column connections is either tearing of the column wall or cracking of the hooks. The relative relation between the thickness of the column and the thickness of the beam end connector bracket determine the failure mode. Because if the thickness of the column is higher than the thickness of the bracket, then the failure will be due to the failure of the hook, while if the thickness of the bracket is higher than the thickness of the column, then the failure will be due to tearing in the column perforation. It was found that the cracking hook failure mode gives worse post peak behavior (ductility) compared to the tearing of the column failure mode.

The depth of the beam, the thickness of the column and the number of the hooks are the main parameters that determines the initial stiffness and the moment capacity of the connections. The thickness of the column and the number of the hooks are having higher influence on the moment capacity of the beam to column connection than the depth of the beam.

The hooks are having a very high effect on the performance of the beam to column connection and their design controls the behavior and the strength of the whole rack storage structure, because of that a proper design of the hooks is a must, and according to the experimental study it was found that a bracket with four hooks give the best performance.

Zhao et al. (2018) carried out an experimental study on sixteen individual cyclic tests on boltless hooked connected beam to column connections. Different column profiles, column thicknesses, beam heights and the number of hooks in the brackets of the connections were used during the experiments in order to investigate the influence of this main parameters on the behavior of the

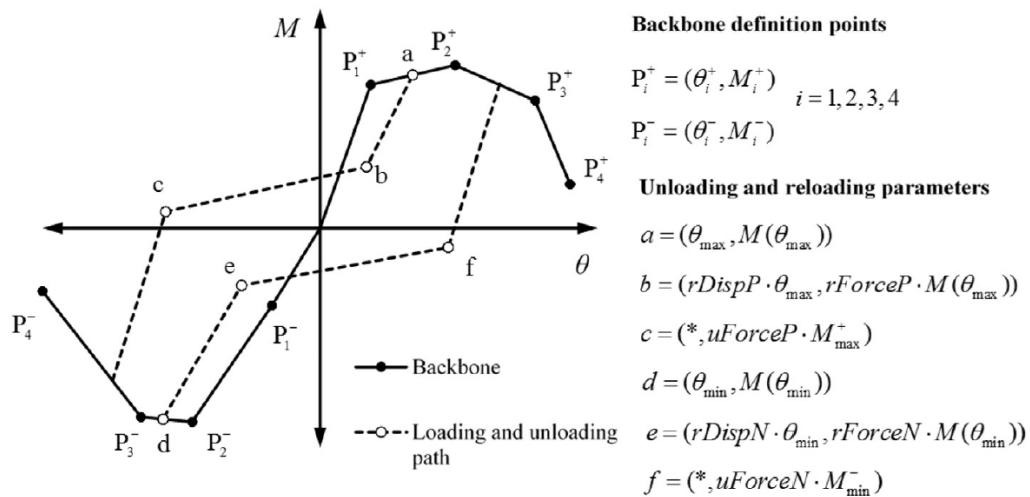
beam to column connection. Additionally, a Pinching4 model is applied to characterize the hysteretic behavior of hooked beam to column connections, in which the parameters used in the model were determined from the test data. In order to apply Direct Design method (DDM) for rack structures, the proposed hysteretic model of the beam to column connections is going to be used during the analysis of seismic performance of steel storage rack structures.

It was observed that the deformation of the connection was mainly occurring in the hooks of the beam end connector bracket, the column walls and the bracket. High values of bending or buckling were not noticed in the beam or the column. The behavior of the beam to column connection was divided to three different stages; linear elastic stage, nonlinear inelastic stage and the softening stage. At the start of the test the hooks were in contact to the perforations of the column, and due to the well design of the hooks that guaranteed a comprehensive contact between the hooks and the edges of the perforations of the column, very little amount of initial looseness was noticed. And this leads to an elastic behavior of the connection at the first stage of the test.

By increasing the load amplitude, a progressive reduction in the stiffness of the connection was observed which indicates the start of the nonlinear inelastic phase. During this phase, plastic deformations start to occur at the outer most hooks or around the perforations of the columns. At the positive peak load a tear in the column wall was noticed, while at the negative peak load cracking of the lower most hook was observed. In the following stage, the crack in the column wall increased till the upper most hook was separate from the column perforation and the lower most hook was totally teared, and that leads to a huge decrease in the loads carried by the beam to column connection.

It was observed that the number of the hooks is the main affecting parameter on the cyclic behavior of a hooked boltless beam to column connection. Changing the hooks numbers has a huge effect on the strength, ductility, stiffness, and energy dissipation capacity. All the connections used in the tests during the experimental study were classified as partial strength semi-rigid connections. The connections showed an average energy dissipation behavior, good ductility and hysteresis loops that were highly pinched.

Depending on the results and the observations obtained from the experimental study, the Pinching4 model is developed to characterize the non-linear cyclic behavior of the hooked beam to column connection as demonstrated in Figure 1.6. The Pinching4 model is formed out of unloading, reloading paths and a backbone curve. The backbone curve is being obtained using four positive and four negative points representing the cyclic response of the connection and its asymmetric nature. The loading and unloading paths consists of six points in which two points are determined for the loading history while the other four points are determined by pinching parameters and the unloading stiffness.



**Figure 1.6:** Pinching4 model in OpenSees (X. Zhao et al., 2018).

The pinching parameters are obtained from the moment rotation results acquired from the experimental study, in order to minimize the predicted error of the energy dissipated per cycle. No initial looseness is observed in the first cycle. However, the second cycle initial reloading path is in the direction of the x-axis, and regains the resistance till the residual rotation of the previous cycle is reached. This occurs because the structure elements such as the hooks and the perforations of the column are not in a perfect contact with one another at the initial stages of loading, and the plastic deformations takes place progressively in the hooks and the beam end connector bracket.

The proposed model results were fitting very well with the results obtained for the experimental study. Therefore, the proposed hysteretic model was considered to be an accurate prediction for

the boltless hooked beam to column connection used in the experimental study. Including the pinching characteristics and the energy dissipation capacity.

In general, findings with regards to the behavior of beam-to-column connections in the down aisle direction revealed that the seismic response of storage racks in the down-aisle direction is strongly affected by the nonlinear moment-rotation response of the beam-to-column connections.

From this viewpoint, in this thesis the main intention is to focus on the cyclic behavior of the hooked beam-to-column connections and investigate possible practical ways to upgrade the strength and energy dissipation characteristics of existing hooked connections. An experimental program was carried out to study typical hooked beam-to-column connections to obtain their non-linear reversed cyclic moment-rotation response.

Additionally, a compound type connection involving the standard hooks and additional bolts were also tested under similar conditions. The simple introduction of the additional bolts within the hooked connection is considered to be a practical way of structural upgrade in the connection. The experimentally evaluated characteristics of the connections are compared in terms of some important performance indicators such as maximum moment and rotation capacity and change in stiffness.

Finally, the obtained characteristics were used to carry out seismic performance assessment of rack frames composed of the tested beam-to-column connections. The assessment involves a displacement based approach that utilizes a simple analytical model that captures the seismic behavior of racks in their down-aisle direction.

## **2. EXPERIMENTAL STUDY**

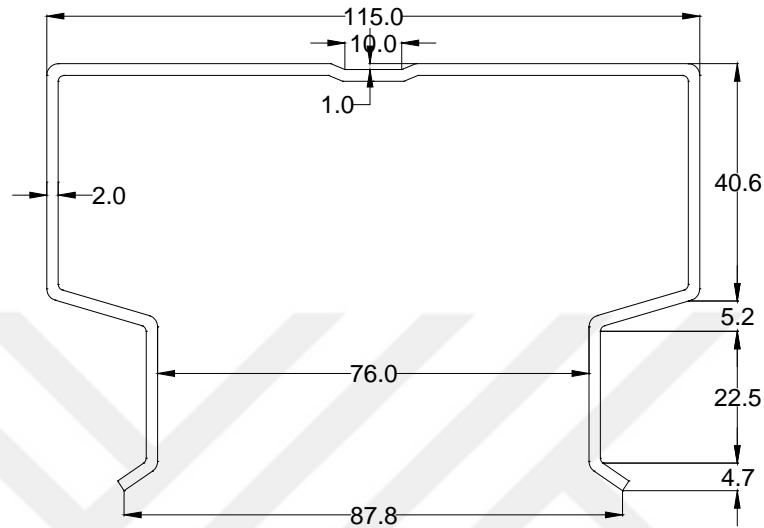
### **2.1. DESCRIPTION OF THE TEST SPECIMENS AND THE TEST METHODOLOGY**

An experimental program was carried out on rack beam to column connections with varying beam depths and methods of connections. Three different beam depths (100 mm, 120 mm and 140 mm box sections). Column member cross-section was kept constant for all tests. Also a constant column length of 500 mm was used and beam lengths were taken as 750 mm. The dimensions of the column, beams and the column to beam connector bracket are given in Figure 2.1, Figure 2.2 and Figure 2.3. Three different connection methods were adopted (Figure 2.4). In total 9 different tests were carried on rack beam-to-column connections under reversed cyclic loading conditions. Table 2.1 presents a summary of the test program. The tests were carried out in 2015 at the Industrial Storage Rack Systems Design and Test Center at Buyukcekmece Campus, which is currently affiliated with Istanbul University-Cerrahpaşa.

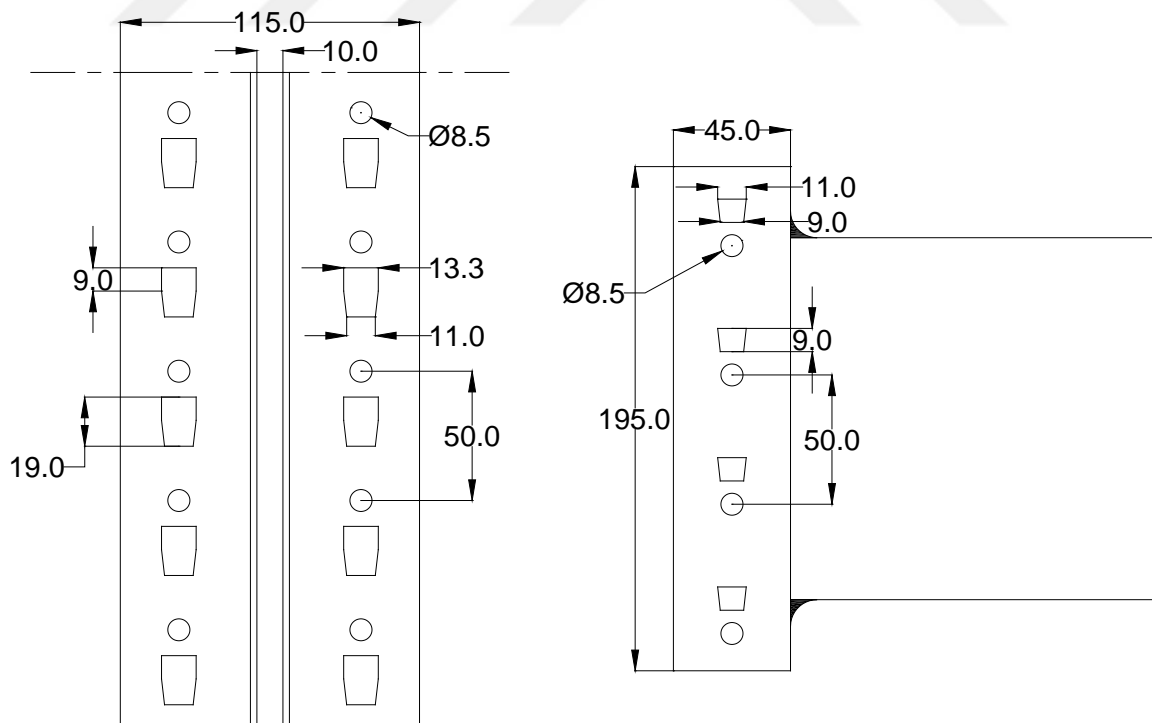
The test apparatus was developed in accordance with RMI 2012 Specification (ANSI MH16.1:2012. Specification for the Design, Testing and Utilization of Industrial Steel Storage Racks, Rack Manufacturers Institute (RMI)), Section 9.6). A schematic diagram of the test apparatus is shown in Figure 2.5, while the test apparatus with a sample installed can be seen in Figure 2.6. The rack column and beams are installed in horizontal orientation for maximum support rigidity. Two servo-hydraulic actuators were utilized to apply the rotation and moment at each beam end. The actuators were controlled in displacement mode for equal rotation at each test cycle. The actuator rod displacements were measured by two linear displacement transducers. The applied loads were measured with two 50 kN precision load cells installed between the actuator rod and beam-end clamp fixture. A constant 50 kN axial compression load was applied on the rack column by a hydraulic cylinder during the test. The applied force was maintained by supplying a constant system pressure that was calculated based on the cylinder piston area. Two small hydraulic cylinders were installed on the beam top surface within 50 mm from the beam connector. A 5 kN force was applied at each side of the beam simulating pallet loads. The hydraulic pressure was supplied by a pressure reducing valve regulating the



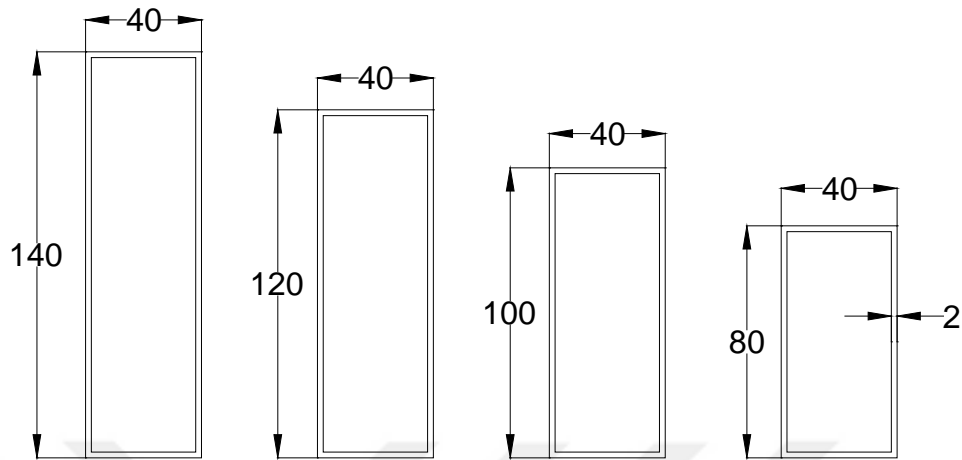
pressure at constant 600 psi, so that the applied force would not change when the beams slightly move up and down during the test.



**Figure 2.1:** Column cross-section dimensions in mm.



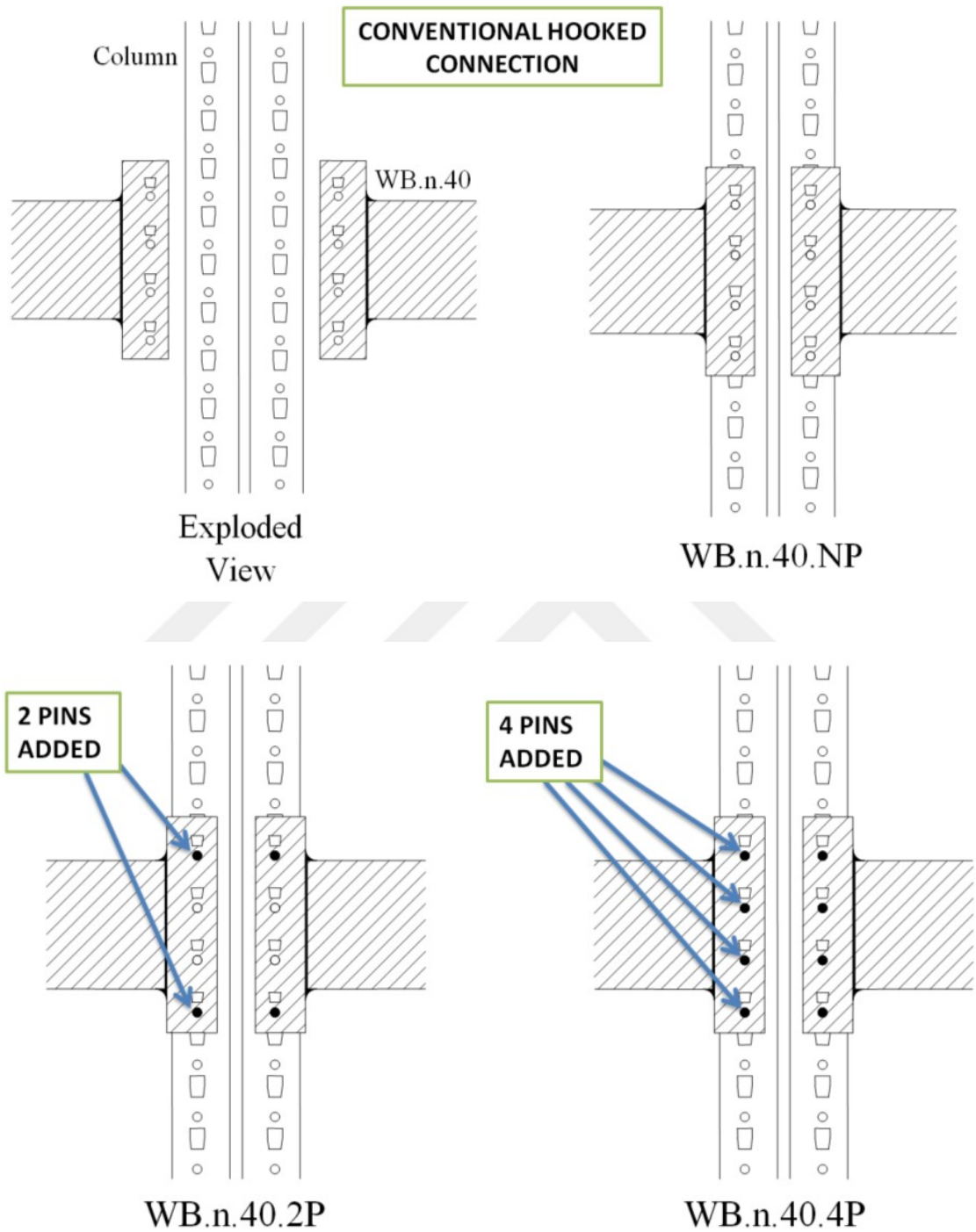
**Figure 2.2:** Dimensions of the column's and the bracket's perforations in mm.



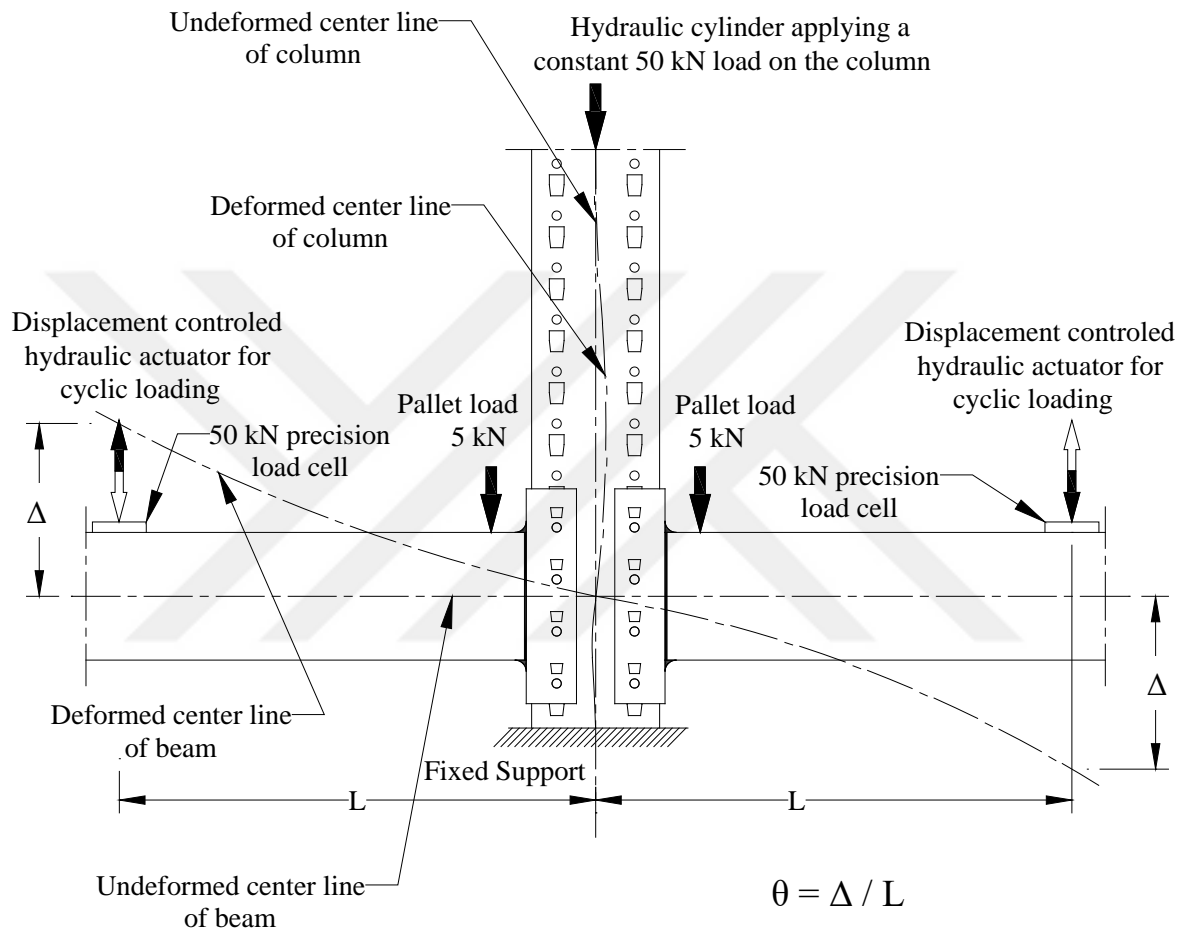
**Figure 2.3:** Dimensions of the beams cross-sections used in the experimental study in mm.

**Table 2.1:** Summary of the test program.

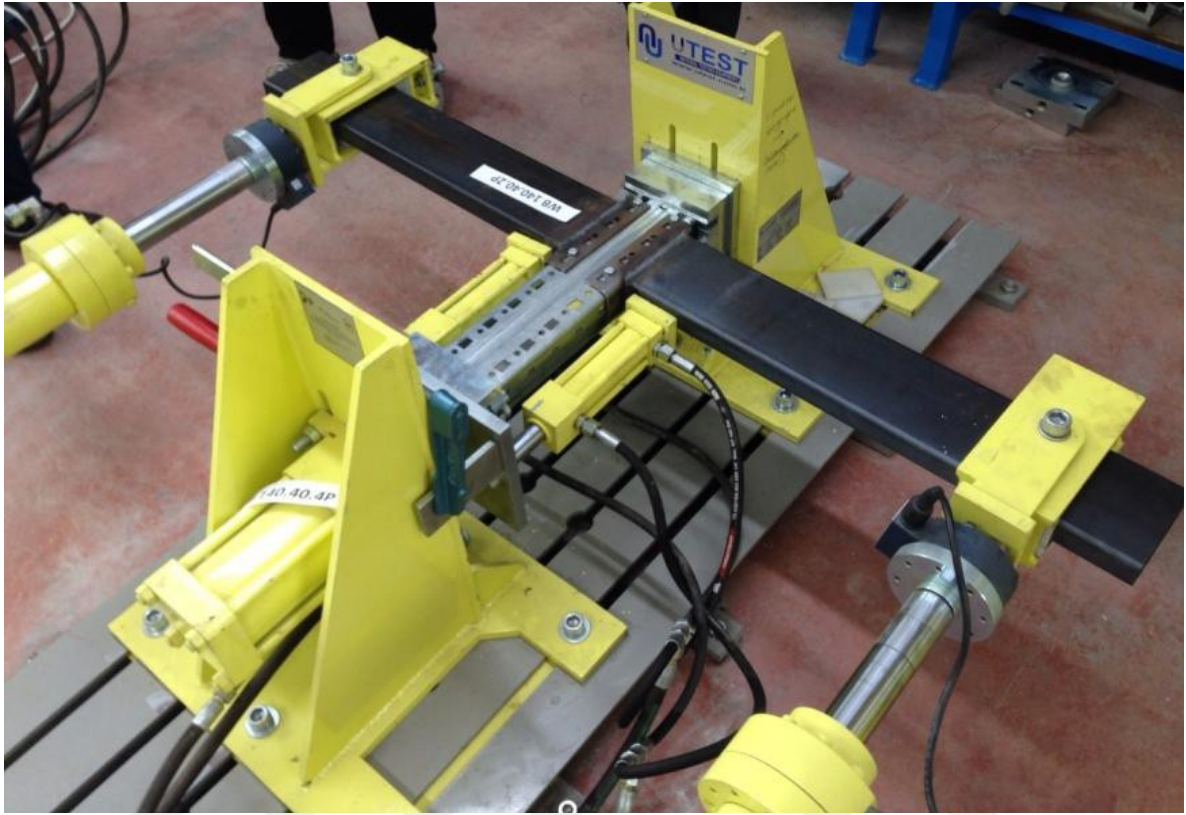
Sample ID	Beam section	Method of connection
WB100.40.NP	Box 100.40.2mm	Hooked
WB100.40.2P	Box 100.40.2mm	2 pins added on both sides
WB100.40.4P	Box 100.40.2mm	4 pins added on both sides
WB120.40.NP	Box 120.40.2mm	Hooked
WB120.40.2P	Box 120.40.2mm	2 pins added on both sides
WB120.40.4P	Box 120.40.2mm	4 pins added on both sides
WB140.40.NP	Box 140.40.2mm	Hooked
WB140.40.2P	Box 140.40.2mm	2 pins added on both sides
WB140.40.4P	Box 140.40.2mm	4 pins added on both sides



**Figure 2.4:** Schematic description of the test specimens.



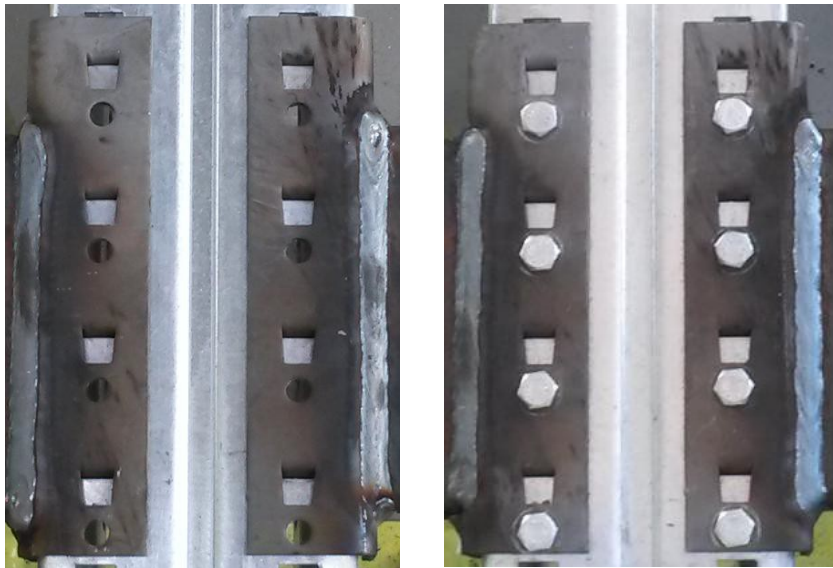
**Figure 2.5:** Schematic diagram of the test setup that was developed according to RMI 2012 specification (ANSI MH16.1:2012).



**Figure 2.6:** Experimental setup for cyclic testing of rack beam-to-column connections.

**With hooks only**

**Hooks + additional bolts**



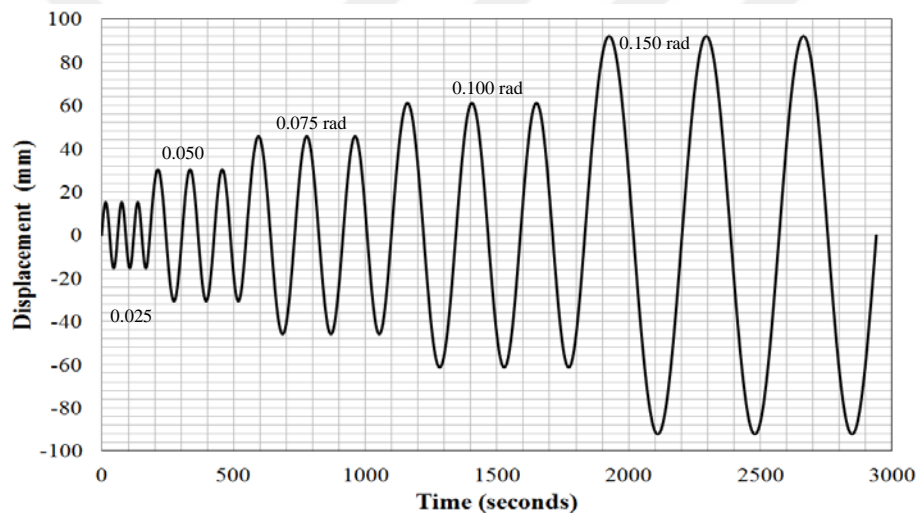
**Figure 2.7:** Specimen with and without additional bolts (pins).

Three different beam cross-section depths were tested with three different connection types as shown in Figure 2.3, Figure 2.4 and Figure 2.7. As previously mentioned, typically, in practice, rack beams are connected to the perforated rack columns by the so called hooked connections (Figure 1.3). Also note that the beam is welded to a steel angle section (usually called a “connector”) on which the hooks are located. In this study, a simple practical idea is tested as a means to upgrade the performance of hooked connections under reversed cyclic effects. As shown in Figure 1.3, in the fabrication stage closely spaced circular holes are provided along the column web. Typically, these holes are used to insert a so called “safety pin” to prevent possible uplift of the beam due to an accidental hitting of a forklift truck. In this thesis, this application is taken a step forward such that similar size bolts (rather than unthreaded pins) are used so as to provide a degree of structural upgrade. In the experimental work, the chosen specimens included four hooks and at most four bolt holes available to connect the beam end connector element onto the column web. Hence it was decided to provide the hooked connections with 2 and 4 additional bolts on the two sides of the column. Schematic description of the test specimens produced in this fashion is presented in Figure 2.4. Also in Figure 2.7, connections with hooks only and hooks and additional bolts are compared for the 4 bolt case. The designation for this specimen in Figure 2.7 is WB140.40.4P and refers to a Welded Beam of cross-section Box 140.40 and connected by hooks and additional 4 bolts or Pins (4P) on both left and right connections. In Table 2.1, specimen designations were given in this format e.g. 2P referring to 2 additional bolts and NP referring to no bolts i.e. only hooked.

Cyclic loading protocol recommended in the relevant chapter of the current Specification for the Design, Testing and Utilization of Industrial Steel Storage Racks (ANSI MH16.1:2012) document was used. Section 9.4 of the ANSI MH16.1:2012 Specification contains a testing protocol in order to evaluate the characteristics of rack beam-to-column connections. Table 2.2 presents the details of the loading sequence whereas Figure 2.8 presents the corresponding loading curve. The tests were performed by controlling the peak drift angle,  $\theta$ , that was applied on the test specimen. For a load application point at 600 mm from the column side along the beam length corresponding beam end displacement values are as given in Table 2.2.

**Table 2.2:** Loading sequence for rack beam-to-column connections (ANSI MH16.1:201)

Test Stage	Number of Cycles	Beam End Displacement(mm)
1	3 cycles at $\theta = 0.025$ radians	15,25
2	3 cycles at $\theta = 0.050$ radians	30,53
3	3 cycles at $\theta = 0.075$ radians	45,84
4	3 cycles at $\theta = 0.100$ radians	61,20
5	2 cycles at $\theta = 0.150$ radians	92,19

**Figure 2.8:** Cyclic loading curve used in the experimental study.

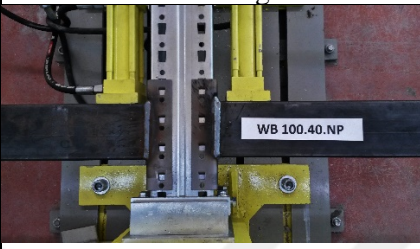
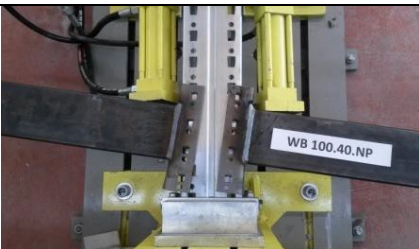
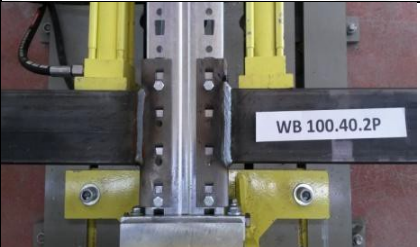



## 2.2. TEST RESULTS

### 2.2.1 Cyclic Behavior of the Connections

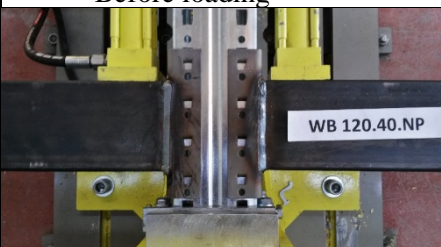
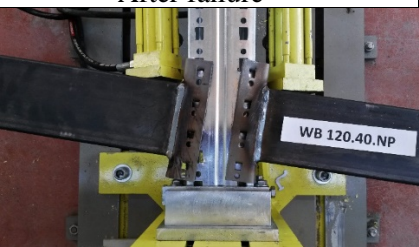
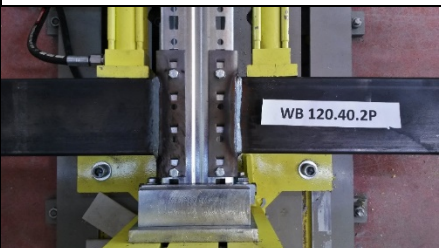
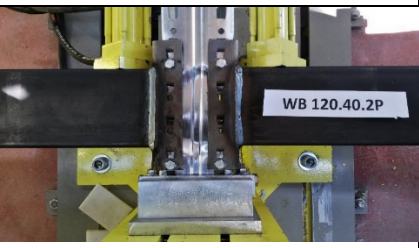
Table 2.3, Table 2.4 and Table 2.5 present photographs of all the specimens before loading and right after failure. As expected for the NP (No Pin but only hooked) connections, failure occurred simply by shearing off the hooks (the weakest link). On the other hand, for connections with additional bolts (2P or 4P), failure was either accumulating over the beam end welds or the column web depending on the stiffness of the beam. For the 100 mm depth beams, both for 2P and 4P cases, failure occurred by tension rupturing of the welds. For the stiffer 120 mm and 140 mm depth beams, welds were stronger and the failure behavior was governed by a

combination of column web buckling and localized rupture failure of the column material around bolt holes and hook perforations.

**Table 2.3:** Collapse behavior of the tested connections (100mm depth beam connection).

Sample ID	Before loading	After failure
WB100.40.NP		
WB100.40.2P		
WB100.40.4P		


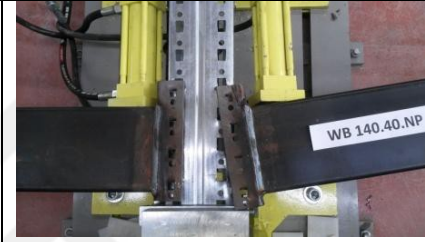


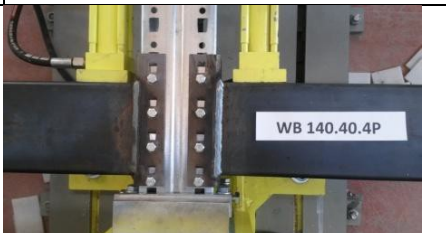

**Table 2.4:** Collapse behavior of the tested connections (120 mm depth beam connection).

Sample ID	Before loading	After failure
WB120.40.NP		
WB120.40.2P		





**Table 2.5:** Collapse behavior of the tested connections (140 mm depth beam connection).

Sample ID	Before loading	After failure
WB140.40.NP		
WB140.40.2P		
WB140.40.4P		

### 2.2.2 Comparison of Test Results

In Table 2.6, peak moment values achieved by left and right beam connections are given. These values are maximum values obtained throughout the test history that includes all 5 cycles. Rotations corresponding to maximum moments were achieved mostly between 3<sup>rd</sup> and 4<sup>th</sup> cycles after which failure started and they varied between 0,075 and 0,100 radians. In the last two columns of Table 2.6, average values of clockwise and anti-clockwise (positive and negative) moments of left and right beam connections are presented. Comparing NP samples with 2P and 4P samples, change in achieved peak moments ranges between 26 % and 47%. Therefore, the

contribution of adding 2 or 4 bolts into an existing hooked connection is significant in terms of maximum moment resistance. Comparing 2P and 4P samples among themselves, change in peak moment values is not as noticeable ranging between 1% and 9% and as expected favoring the 4P cases.

**Table 2.6:** Peak moment values for left and right beam connections.

Sample ID	Left beam		Right beam		Whole joint	
	Clockwise (CW) Moment	Anti-clockwise (ACW) Moment	Clockwise (CW) Moment	Anti-clockwise (ACW) Moment	Average CW Moment	Average ACW Moment
WB100.40.NP	2,9100	3,3042	2,9244	3,4692	2,9172	3,3867
WB100.40.2P	4,3986	4,4712	3,9336	4,2882	4,1661	4,3797
WB100.40.4P	4,2510	4,6524	4,3824	4,1946	4,3167	4,4235
WB120.40.NP	3.3642	3.513	3.1452	3.6012	3.2547	3.5571
WB120.40.2P	3.834	5.2404	4.3248	4.6722	4.0794	4.9563
WB120.40.4P	4.509	4.9206	4.5924	5.3652	4.5507	5.1429
WB140.40.NP	3,9432	3,5034	3,1344	3,9498	3,5388	3,7266
WB140.40.2P	4,8066	4,5810	4,1520	4,9656	4,4793	4,7733
WB140.40.4P	4,2162	5,8044	5,6904	4,3428	4,9533	5,0736

Moment-rotation curves for left and right beam connections of each sample are given in the figures below. In general, for a specific sample, left and right connections exhibit very similar moment-rotation characteristics. A noticeable improvement in cyclic behavior is noted for the upgraded connections achieved by the introduction of additional bolts (2P and 4P). Also, a more stable hysteretic behavior is observed for these connections evidenced by less “pinched” hysteretic behavior which is more observed for the hooked (NP) connections. In general, comparing the average maximum moment values ( $M_{max}$ ) achieved by the 100 mm, 120 mm and 140 mm depth beam connections it is noted that relatively greater maximum moment values were achieved for 140 mm depth specimens and at relatively greater values of corresponding rotation values ( $\theta_{max}$ ).

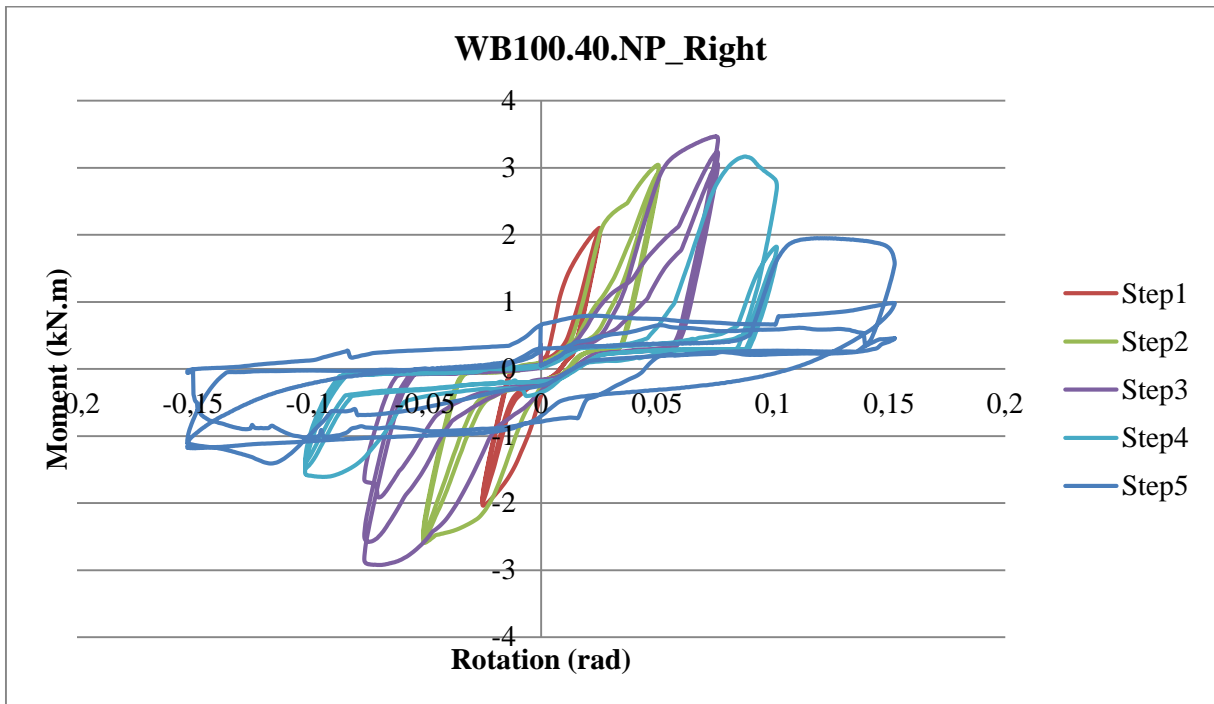


Figure 2.9: Moment rotation results for the left side connection of the beam (WB100.40.NP).

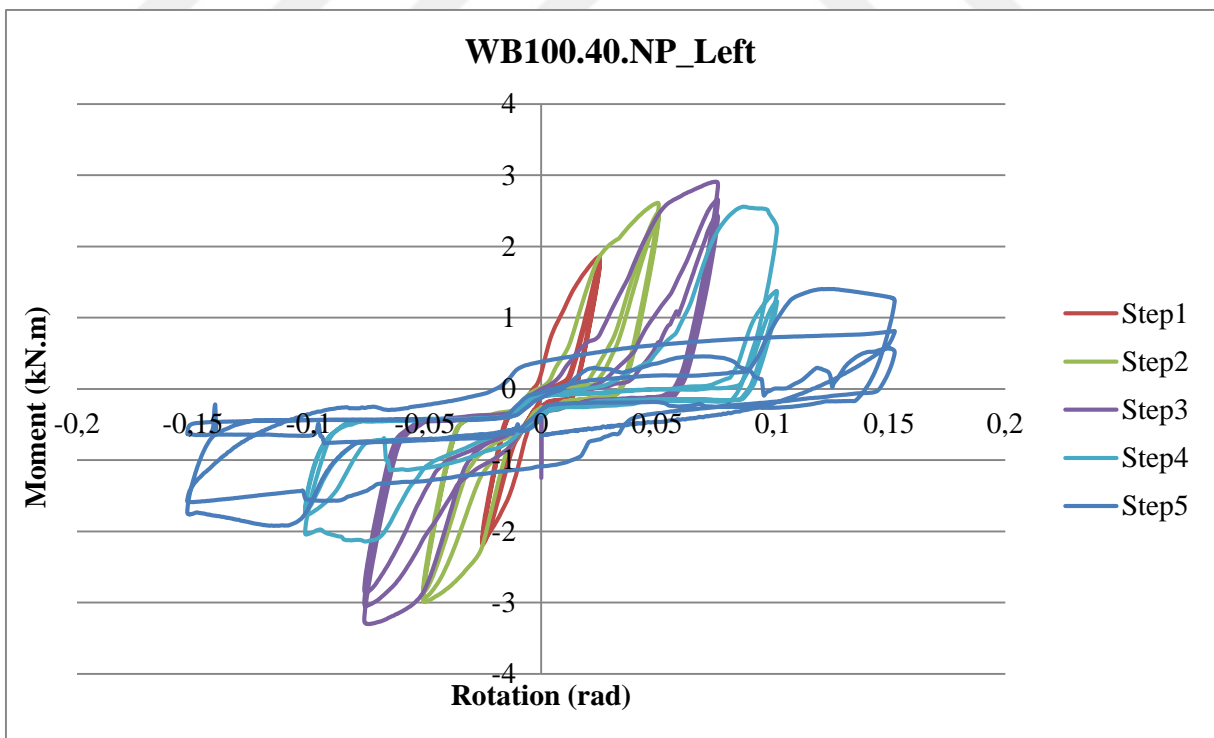
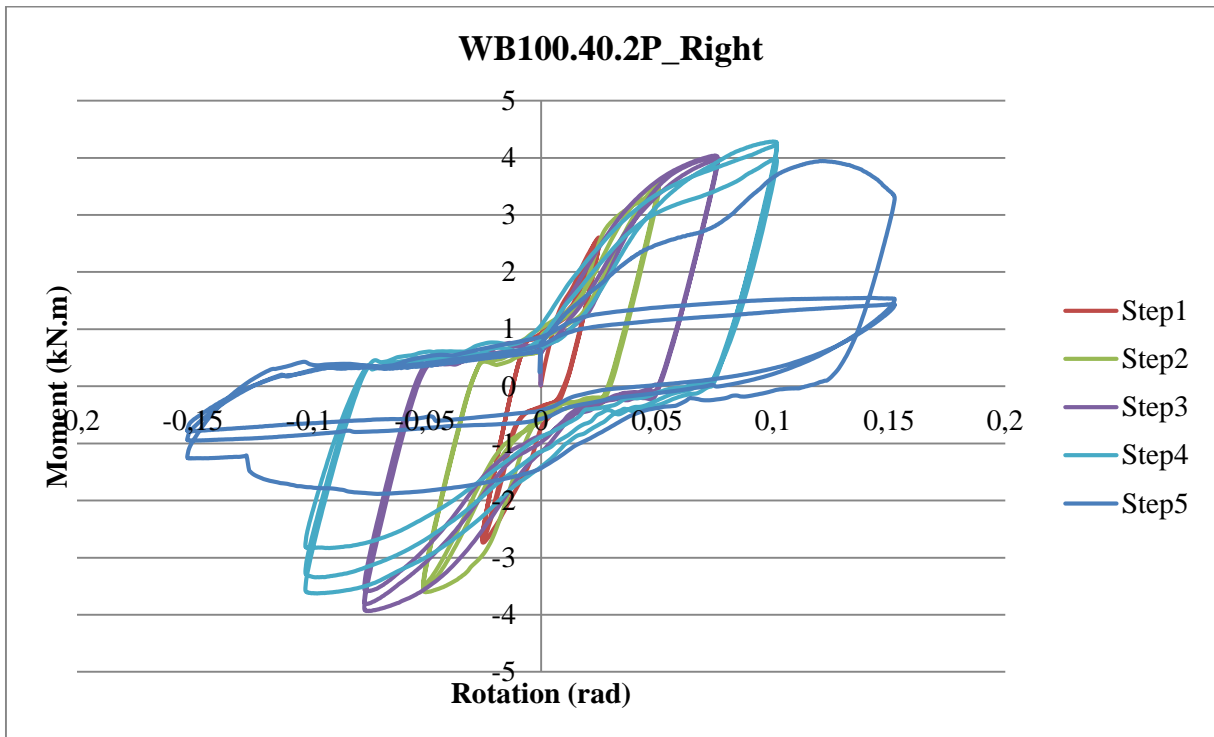
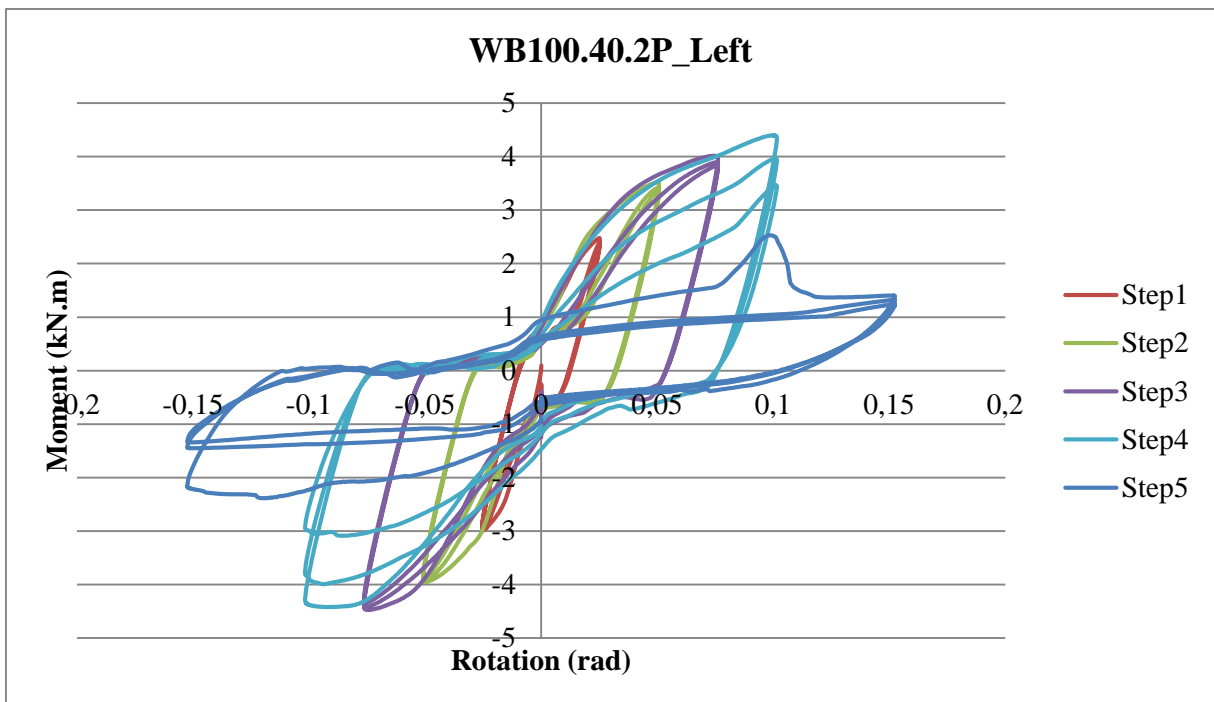


Figure 2.10: Moment rotation results for the right side connection of the beam (WB100.40.NP).



**Figure 2.11:** Moment rotation results for the left side connection of the beam (WB100.40.2P).



**Figure 2.12:** Moment rotation results for the right side connection of the beam (WB100.40.2P).

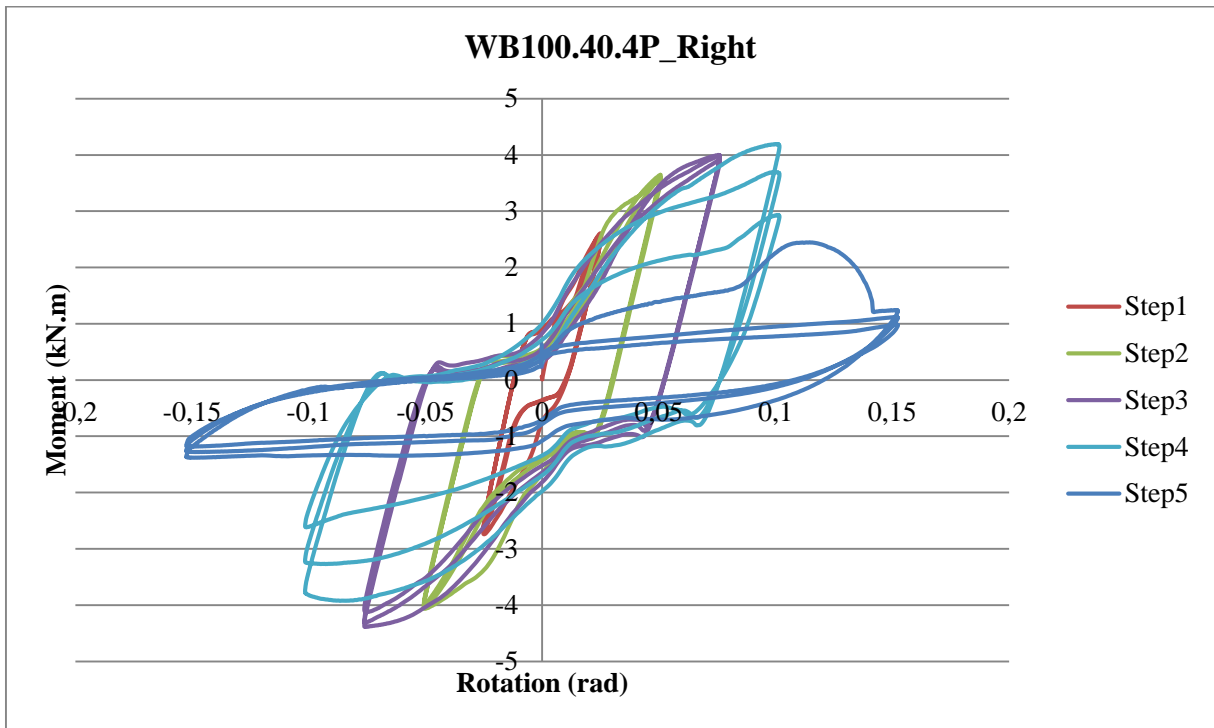


Figure 2.13: Moment rotation results for the left side connection of the beam (WB100.40.4P).

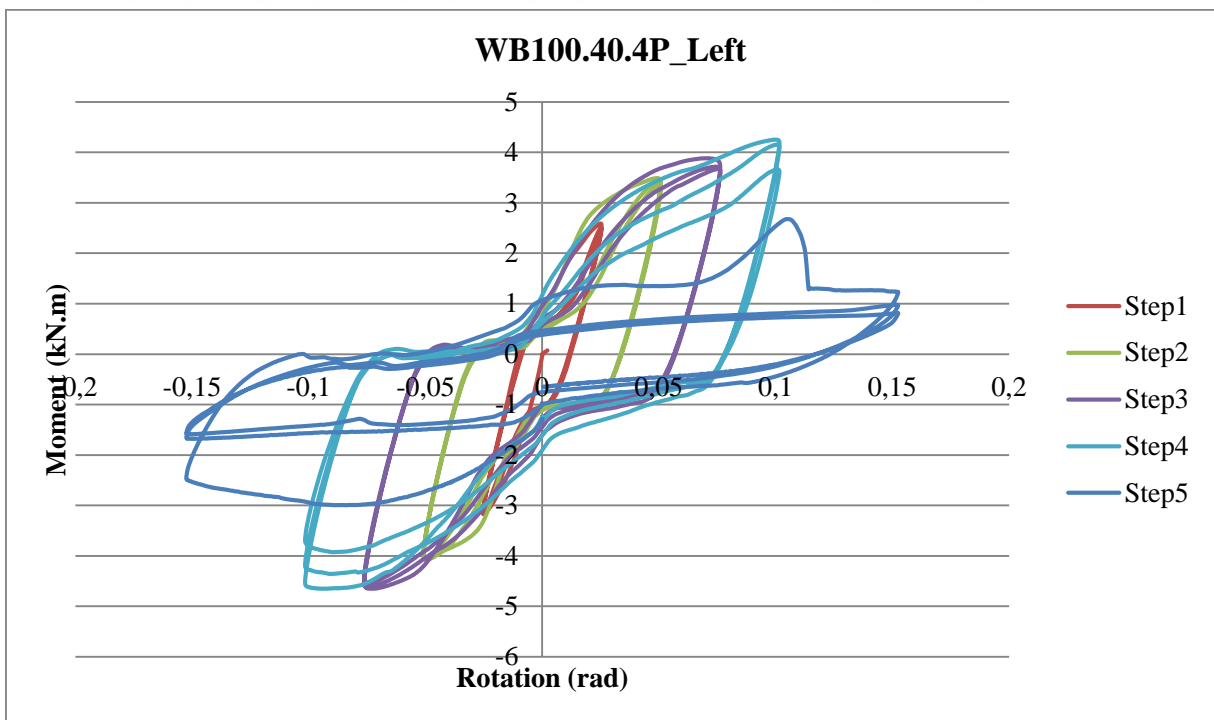


Figure 2.14: Moment rotation results for the right side connection of the beam (WB100.40.4P).

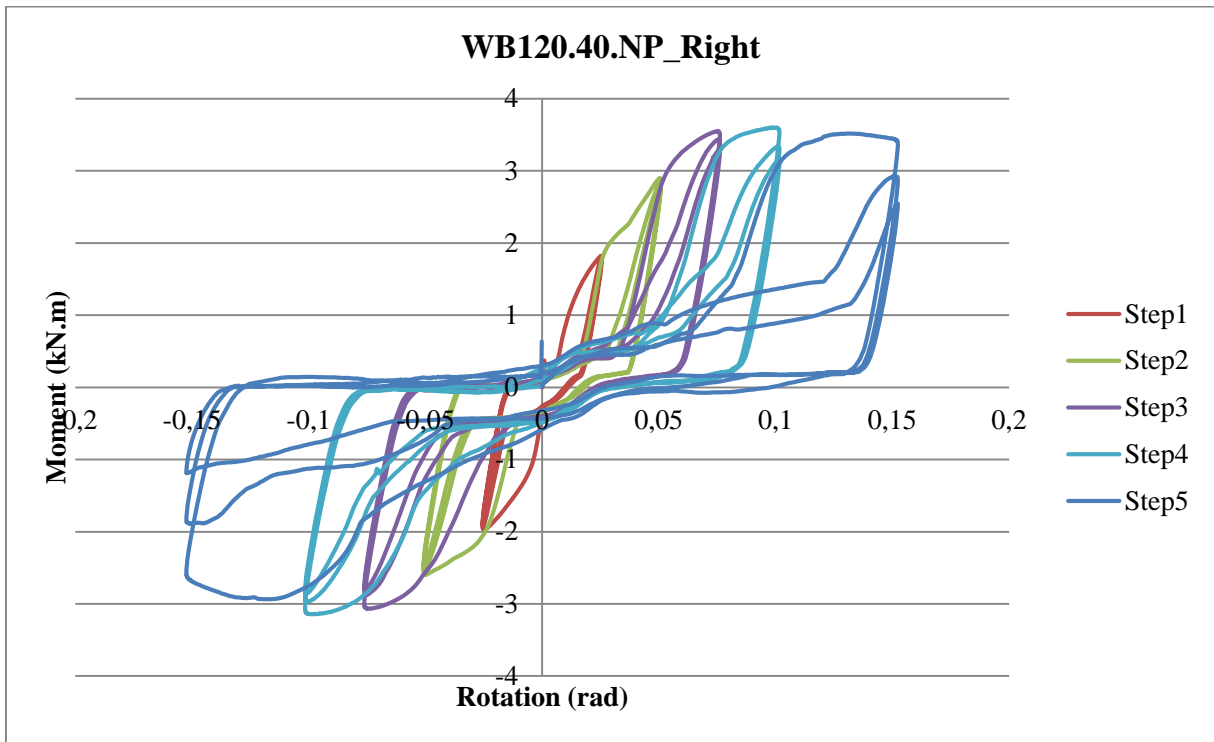


Figure 2.15: Moment rotation results for the left side connection of the beam (WB120.40.NP).

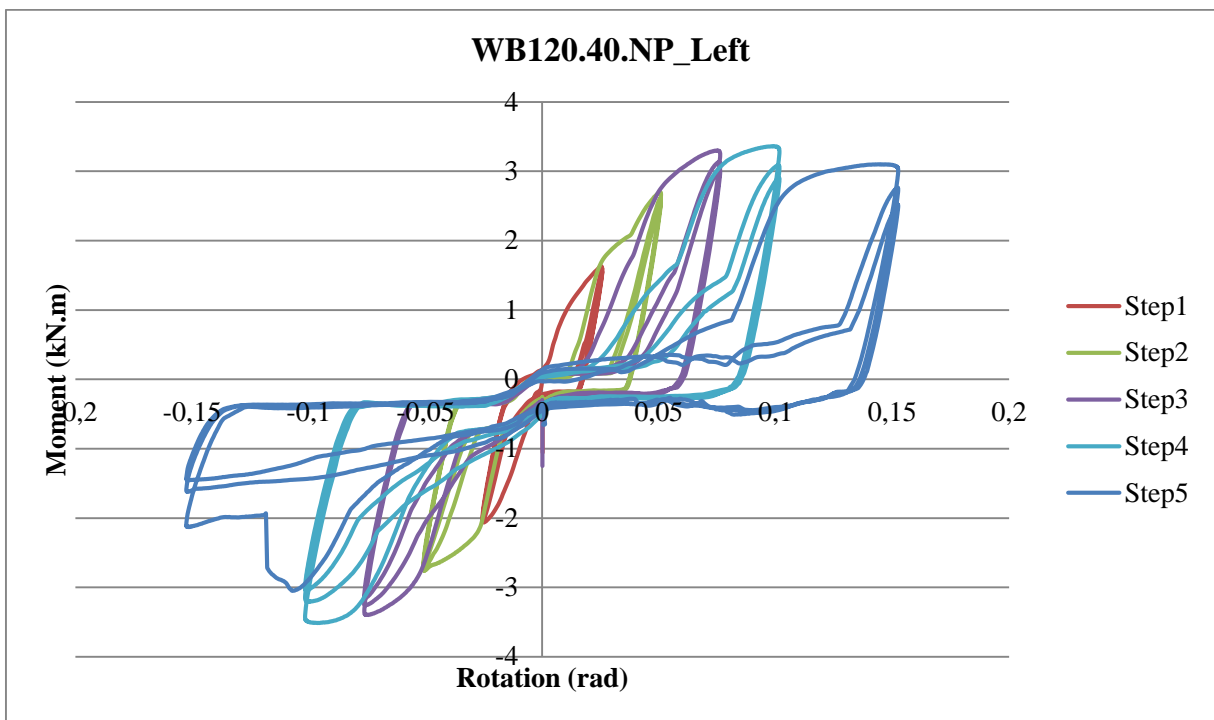
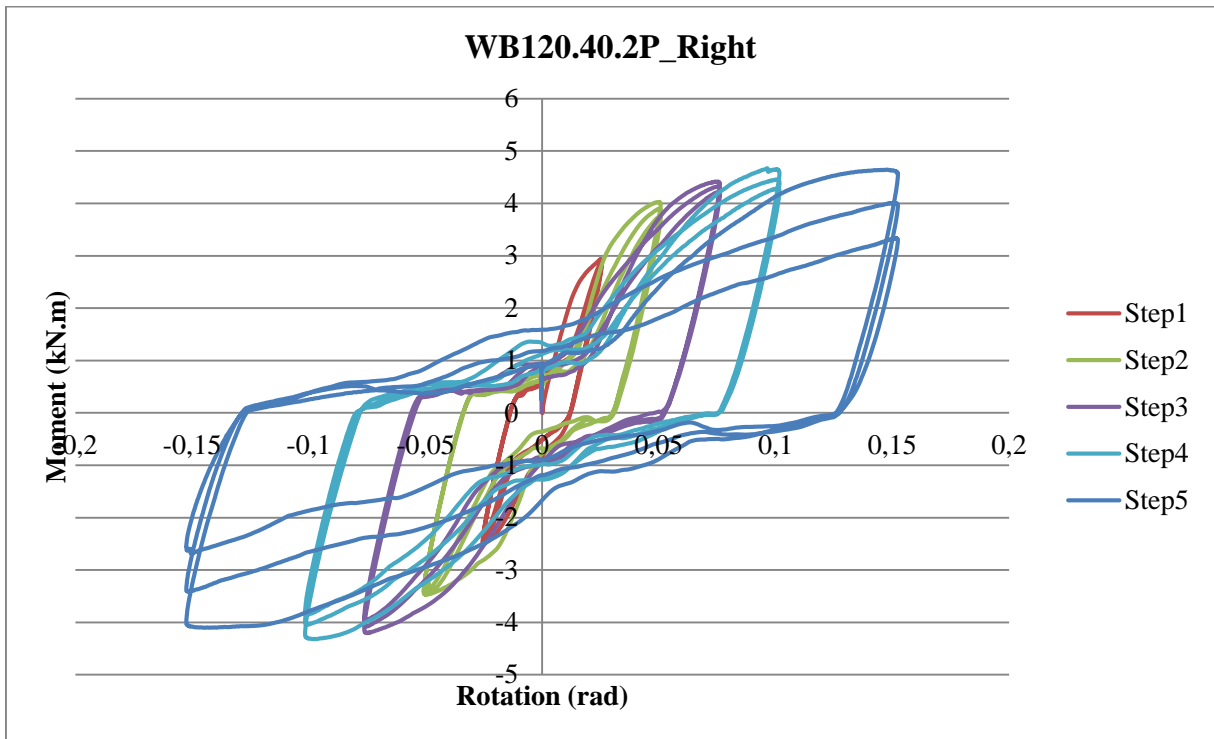
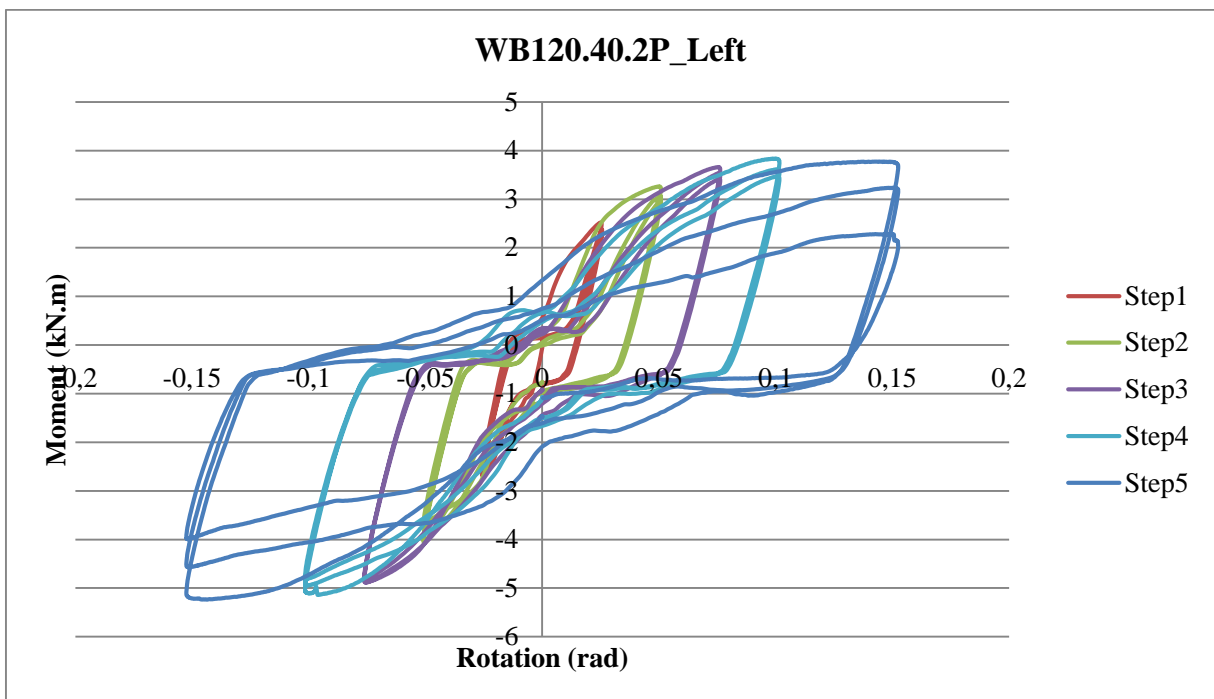


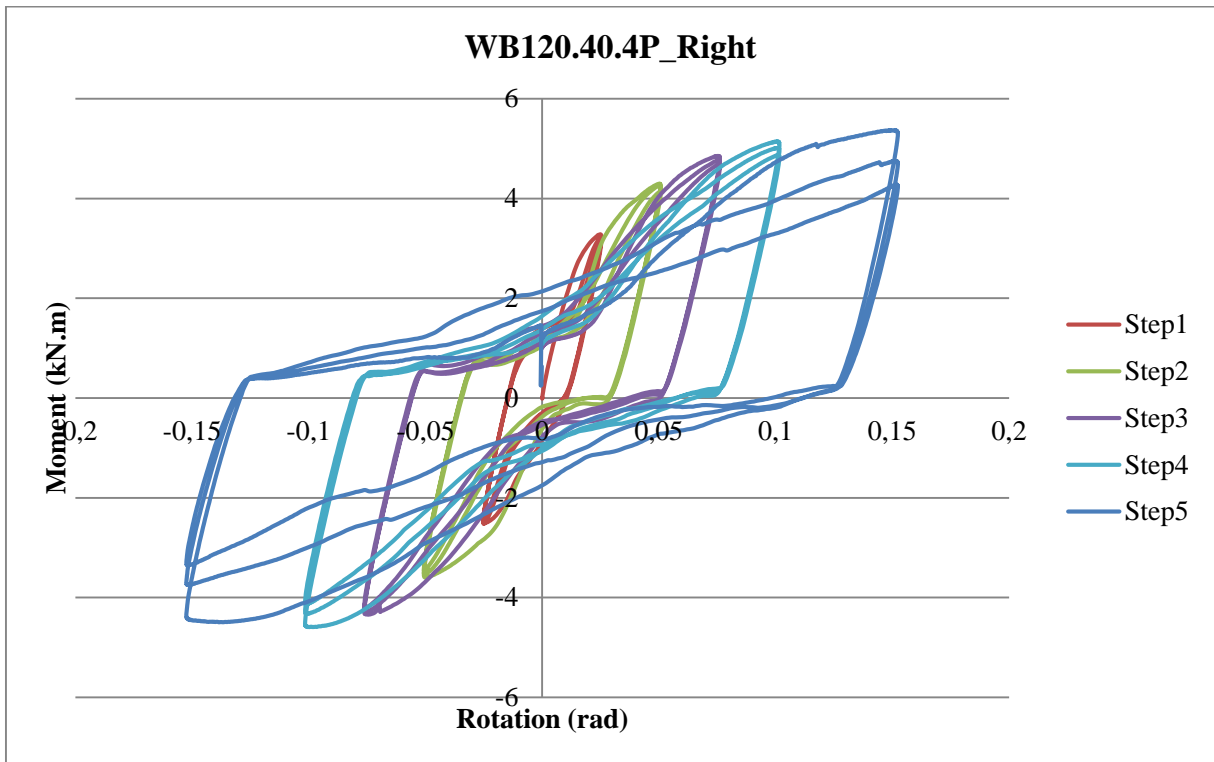
Figure 2.16: Moment rotation results for the right side connection of the beam (WB120.40.NP).



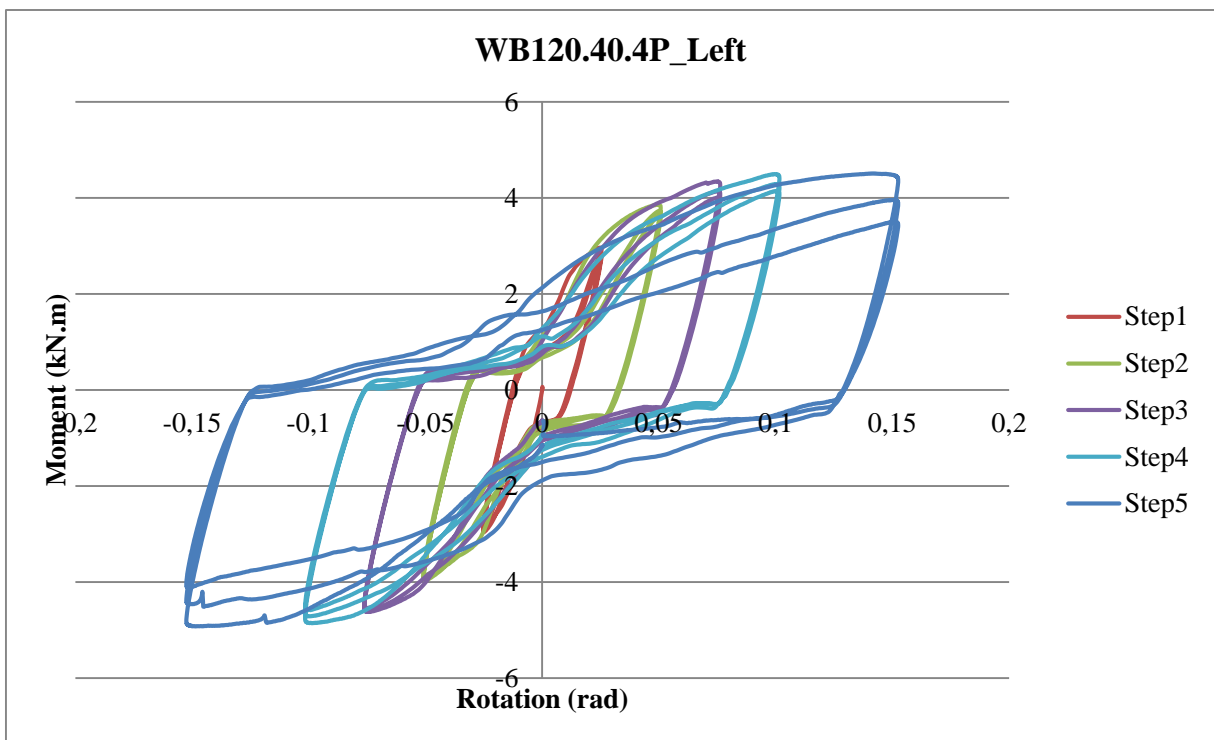
**Figure 2.17:** Moment rotation results for the left side connection of the beam (WB120.40.2P).



**Figure 2.18:** Moment rotation results for the right side connection of the beam (WB120.40.2P).

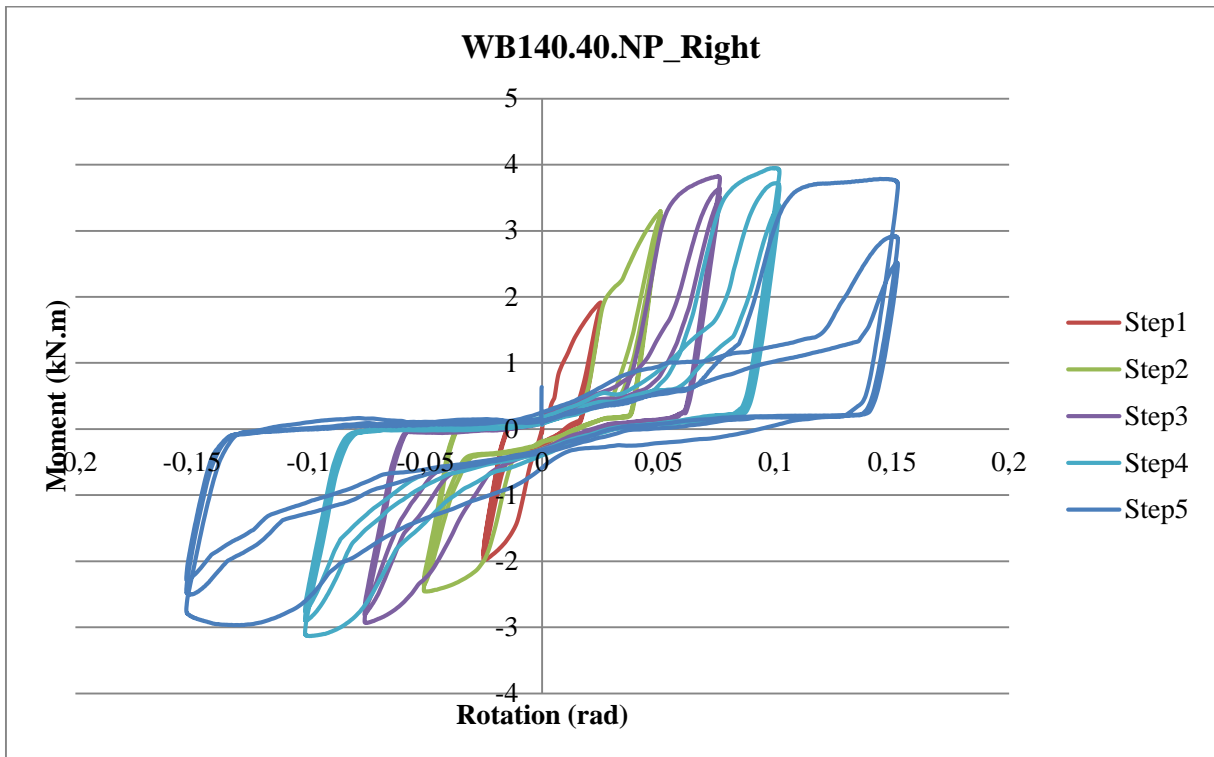


**Figure 2.19:** Moment rotation results for the left side connection of the beam (WB120.40.4P).

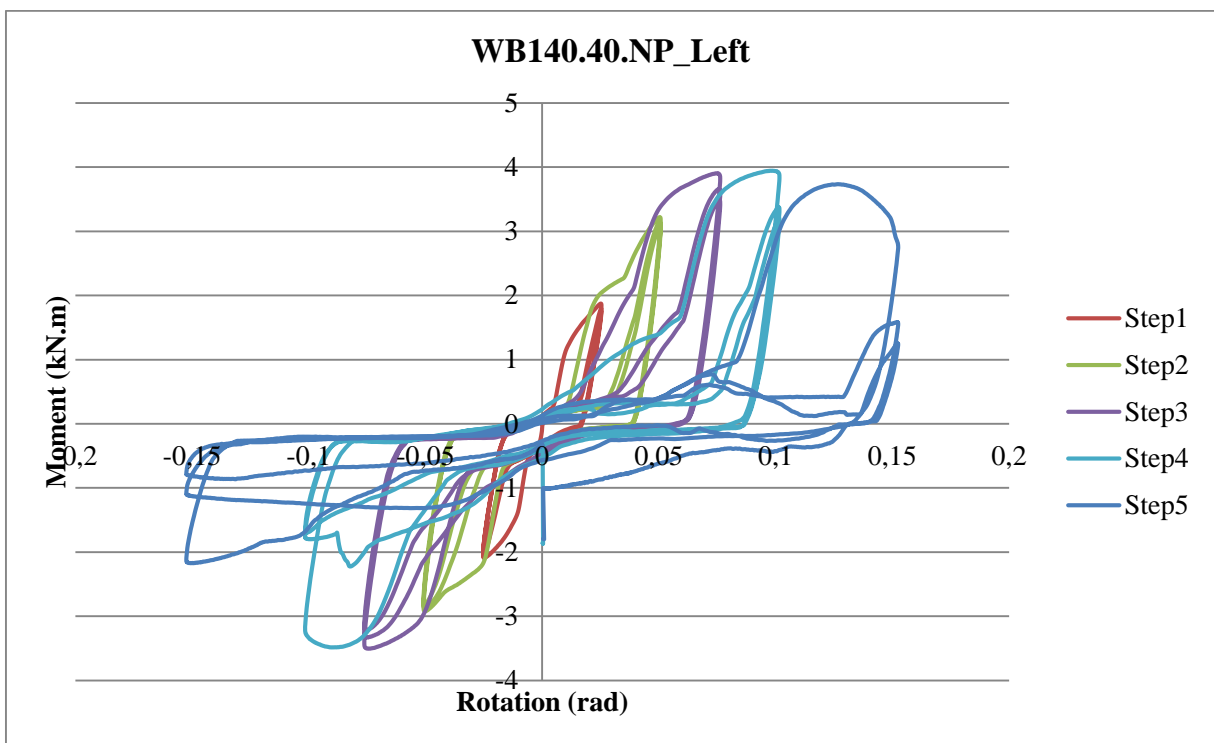


**Figure 2.20:** Moment rotation results for the right side connection of the beam (WB120.40.4P).

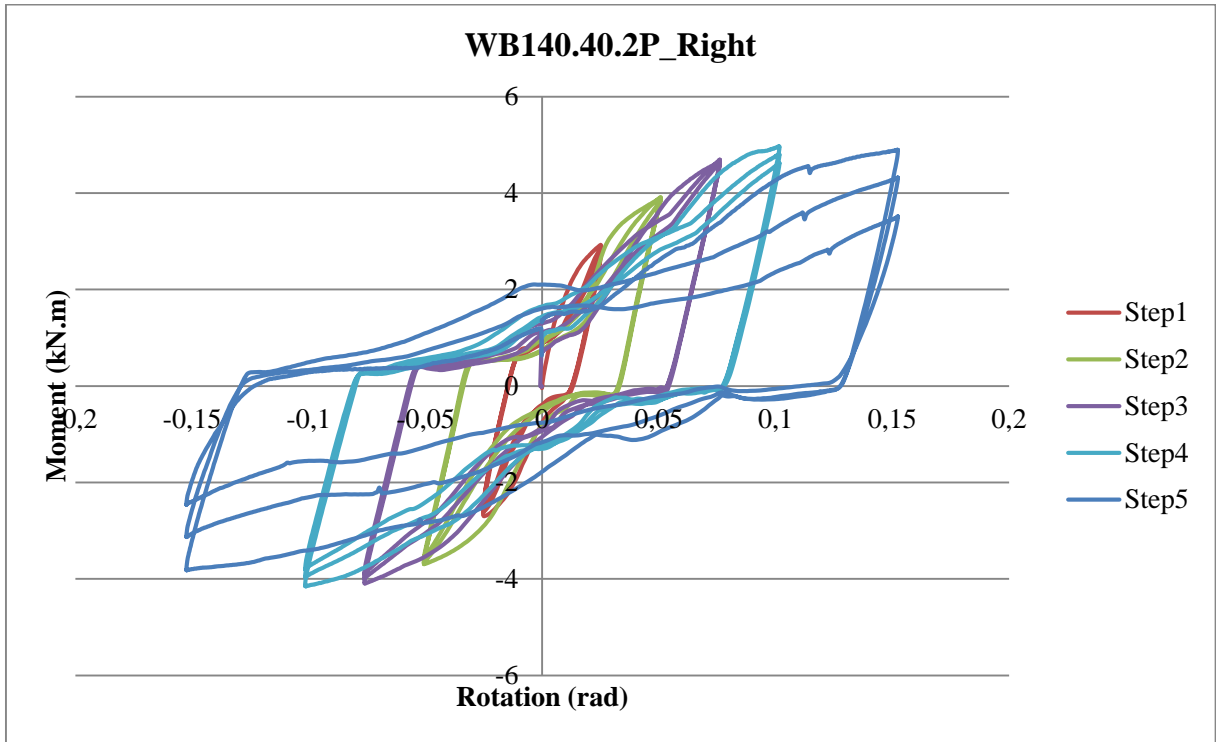




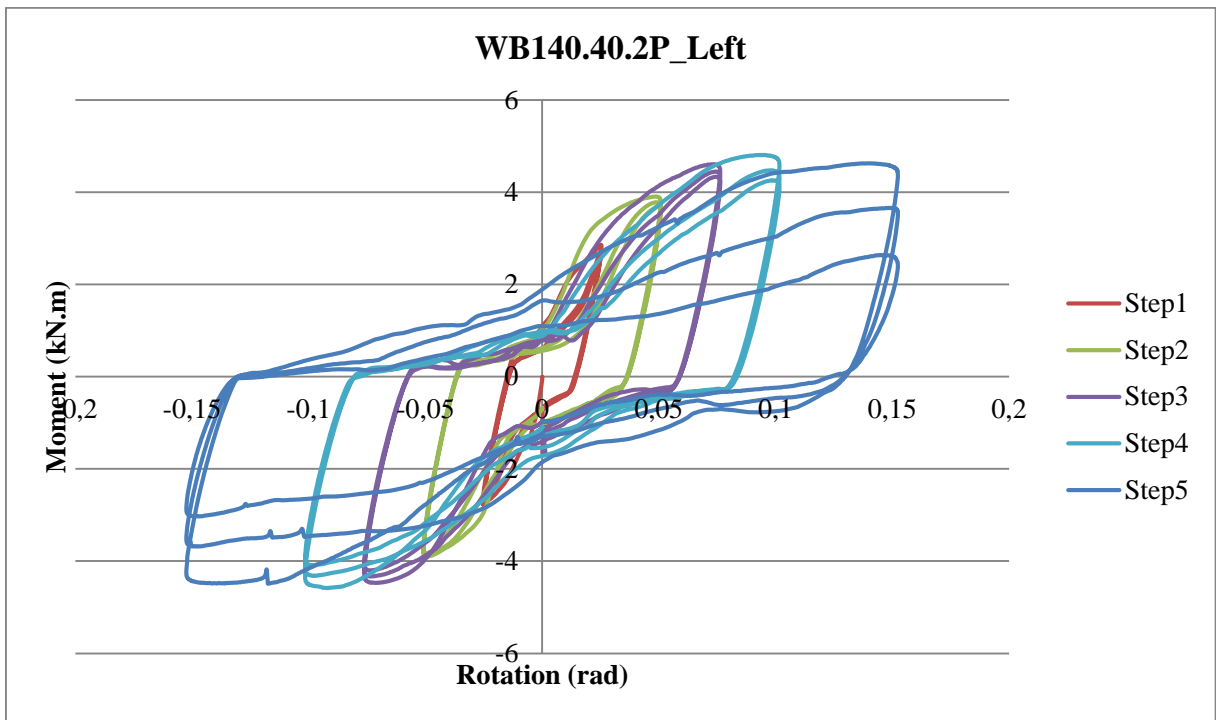
**Figure 2.21:** Moment rotation results for the left side connection of the beam (WB140.40.NP).



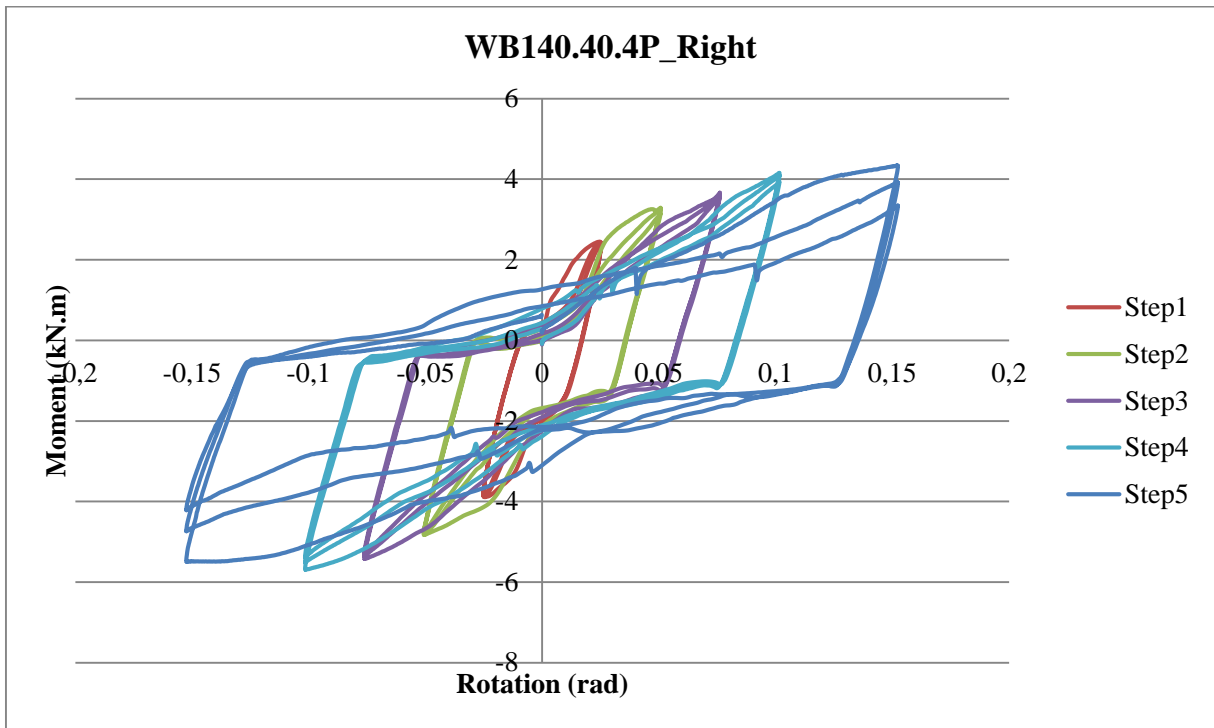
**Figure 2.22:** Moment rotation results for the right side connection of the beam (WB140.40.NP).



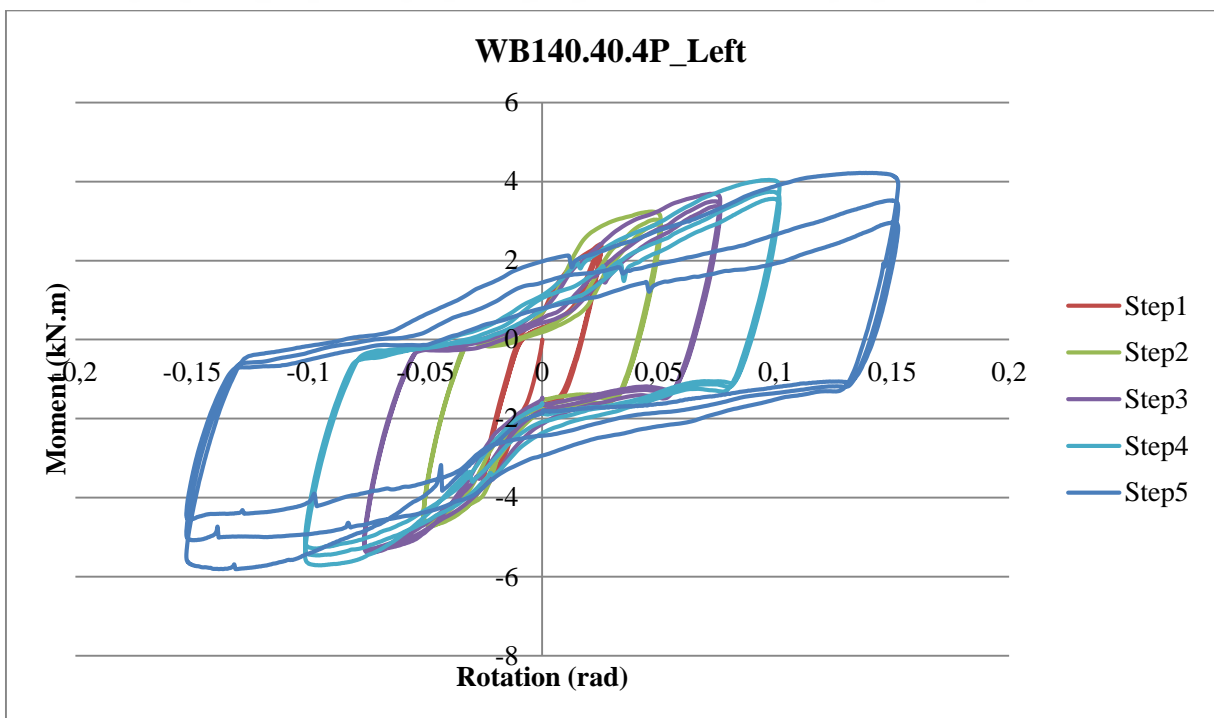
**Figure 2.23:** Moment rotation results for the left side connection of the beam (WB140.40.2P).



**Figure 2.24:** Moment rotation results for the right side connection of the beam (WB140.40.2P).

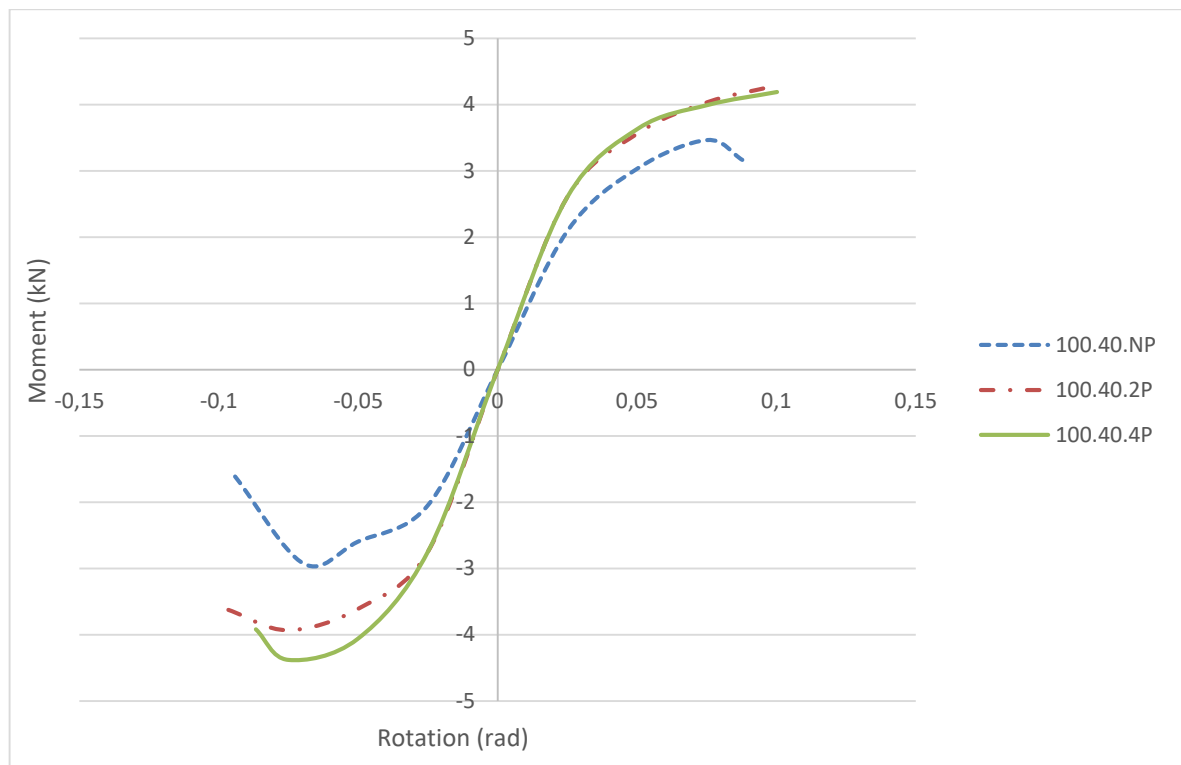


**Figure 2.25:** Moment rotation results for the left side connection of the beam (WB140.40.4P).

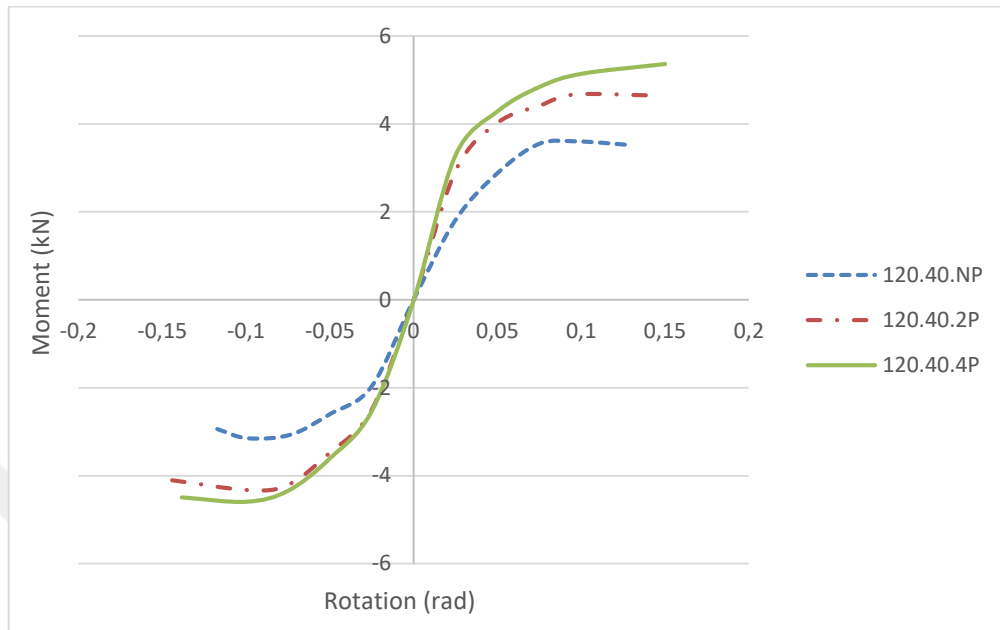


**Figure 2.26:** Moment rotation results for the right side connection of the beam (WB140.40.4P).

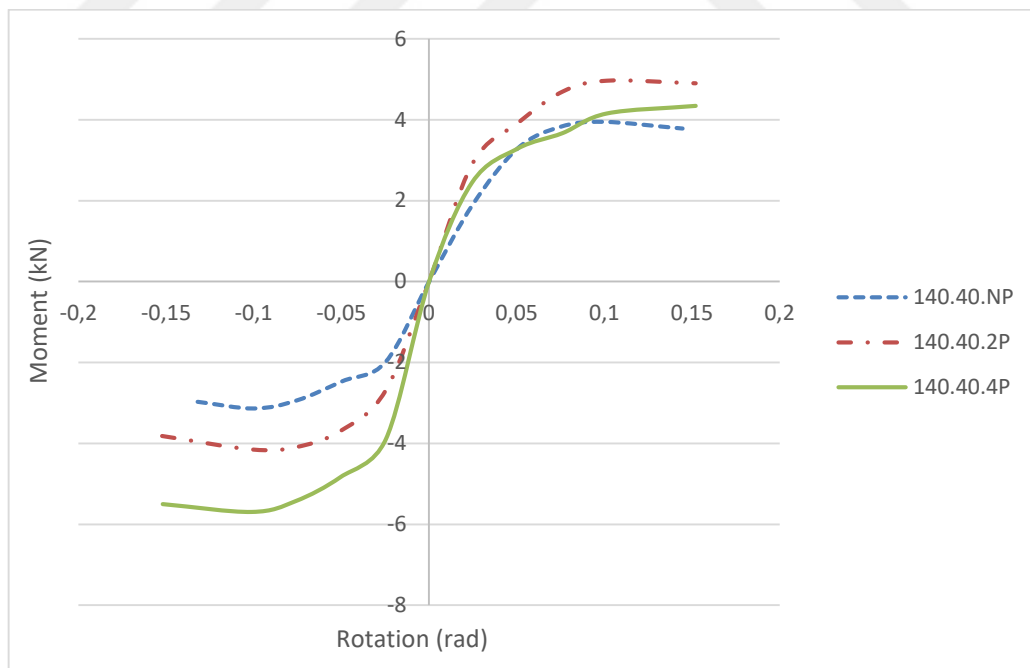
In order to compare the behavior of the three different type of connections. The peak moment-rotation curves of the beams with same depths but with different connection types were plotted in Figure 2.27, Figure 2.28 and Figure 2.29. It's clear from the figures the big difference between the NP curve and the 2P and 4P curves, which shows that using the pinned connections improves the behavior in an effective way, while it can be noticed that the 2P and 4P curves are so similar, this shows that using 2 pins only is enough, and it will be saving for time and material.



**Figure 2.27:** Peak moment-rotation curves of the connections NP, 2P, and 4P for the beam with the depth of 100 mm.

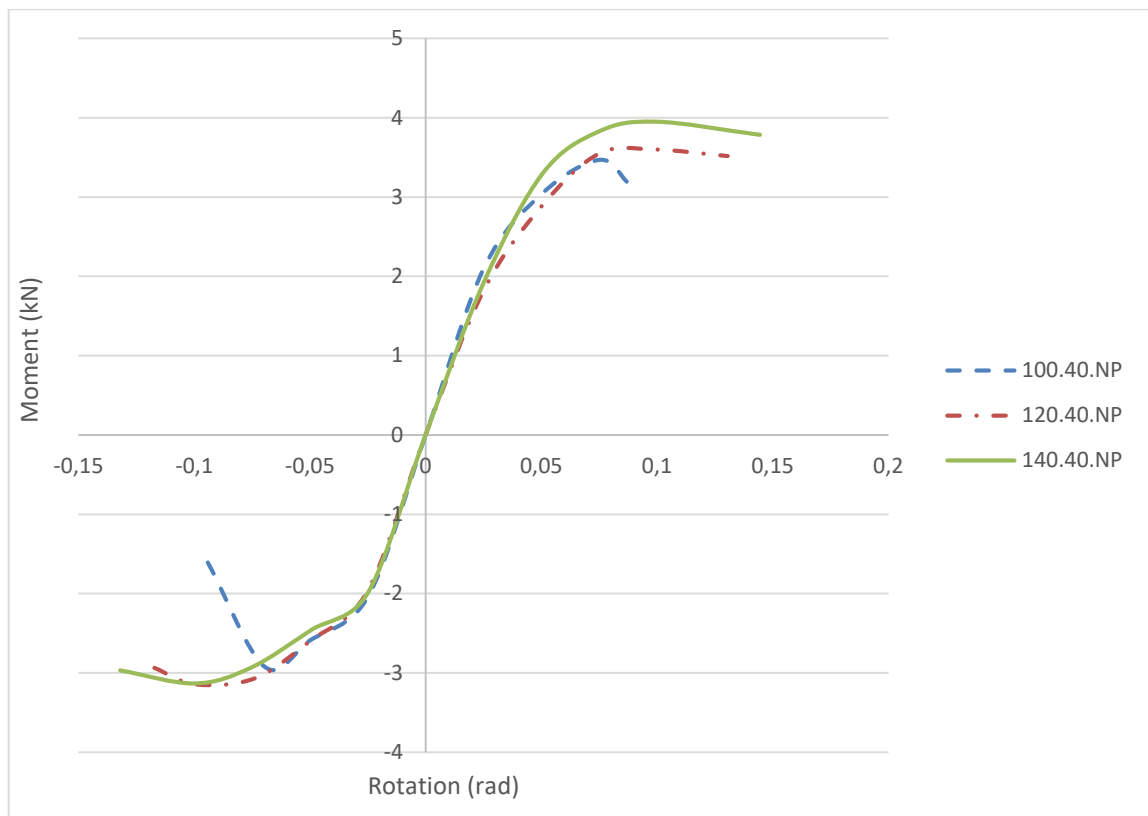


**Figure 2.28:** Peak moment-rotation curves of the connections NP, 2P, and 4P for the beam with the depth of 120 mm.

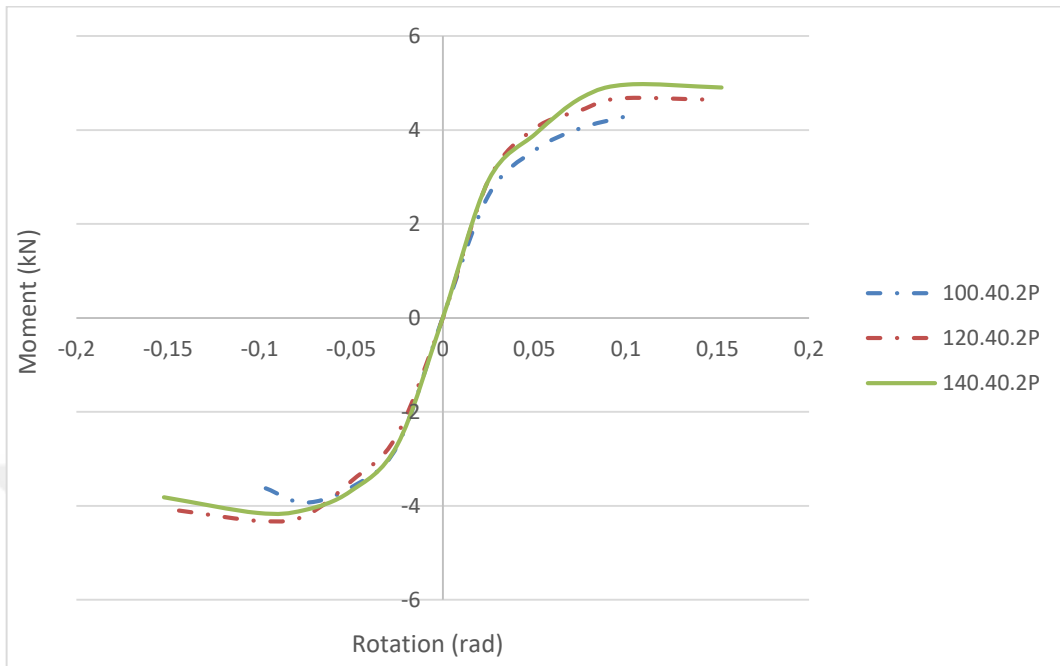


**Figure 2.29:** Peak moment-rotation curves of the connections NP, 2P, and 4P for the beam with the depth of 140 mm.

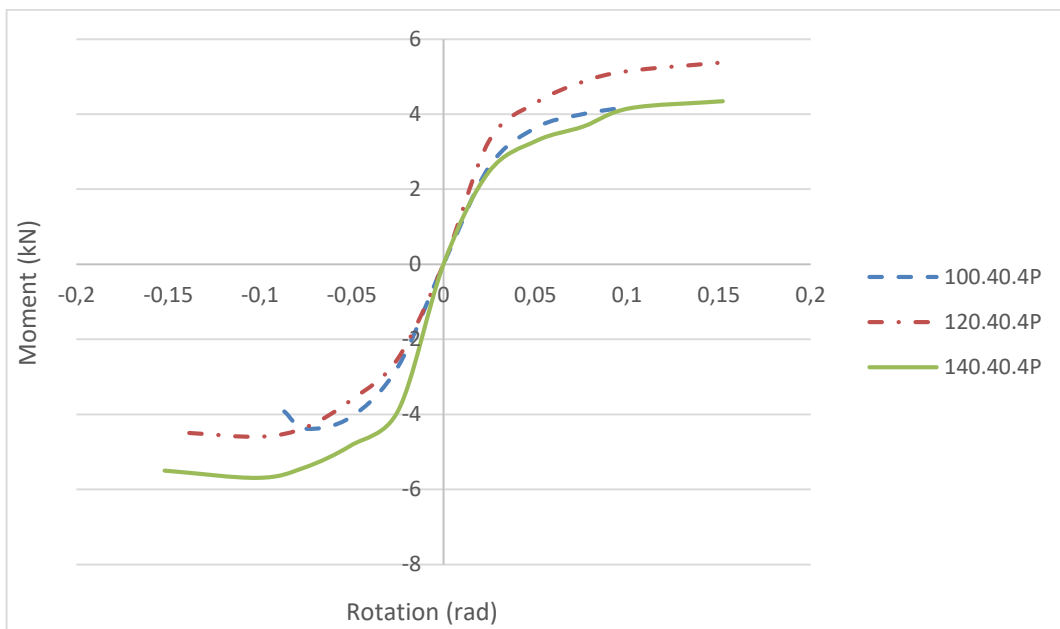
The peak moment rotation curves of the beams with same connection types but with different beam depths were compared in Figure 2.30, Figure 2.31 and Figure 2.32, and it was found that the curves are almost similar. This shows that the depth of the beam does not affect the peak moment-rotation results of the connection, but for sure it is important for the capacity of the cross-section in order to carry the vertical loads applied on it without any mode of failure. From the experimental results, it was clear the significant enhancement in the behavior of the beam-to-column connection using the newly proposed pinned hooked connection.



**Figure 2.30:** The peak moment-rotation curves of the NP connection for the different depths of the beams (100,120 and 140).



**Figure 2.31:** The peak moment-rotation curves of the 2P connection for the different depths of the beams (100,120 and 140).



**Figure 2.32:** The peak moment-rotation curves of the 4P connection for the different depths of the beams (100,120 and 140).

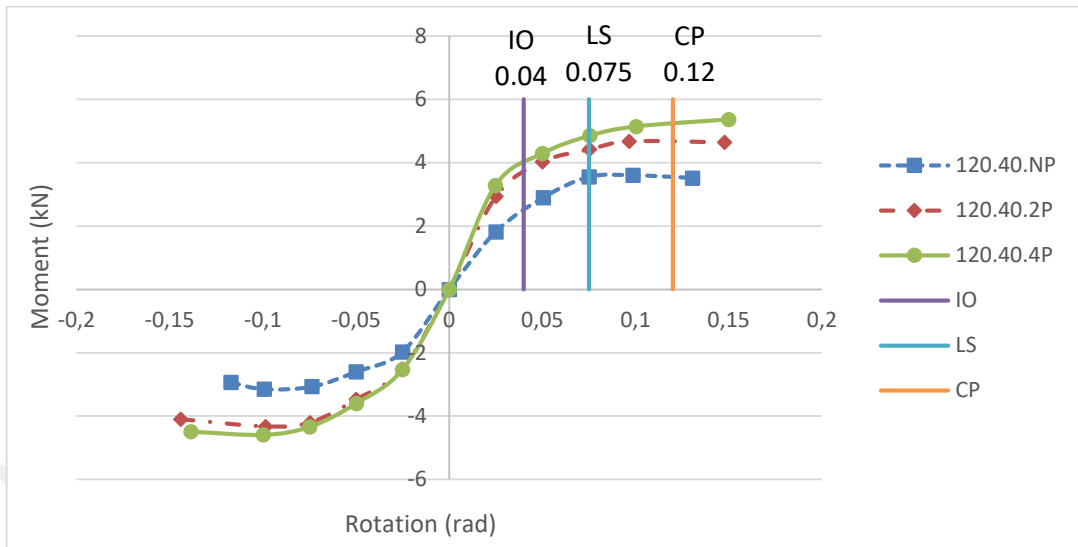
### 2.3. PERFORMANCE LEVELS OF RACK FRAMES

In most of the design codes and literature finding the performance levels of the structure was not based on mathematical formulas but it was based on observations from experimental results. Based on the observations of the experimental results stated in the table below and the moment rotation curves from the tests, the performance levels were obtained.

**Table 2.7:** Observations and results obtained from the experimental study.

	<b>Hooked connection (NP)</b>	<b>Pinned connection (2P.4P)</b>	<b>Max rotation (rad)</b>	<b>Performance level</b>
<b>step 1</b>	the test was running smoothly without any sign of a failure.	the test was running smoothly without any sign of a failure.	0.025	IO by maximum rotation 0.04 radians
<b>step 2</b>	the test was running smoothly without any sign of a failure but a slight degradation in stiffness in the moment rotation curve was noticed.	the test was running smoothly without any sign of a failure but a slight degradation in stiffness in the moment rotation curve was noticed.	0.05	LS by maximum rotation 0.075 radians
<b>step 3</b>	sounds start to be heard specially at the hooks with high reduction in the stiffness of the beam to column connection.	sounds start to be heard with high reduction in the stiffness of the beam to column connection.	0.075	
<b>step 4</b>	1 or 2 hooks could be totally damaged and are cut off the bracket of the beam.	failure in the weld between the beam and the bracket occurs in the beam of 100 mm depth while slight local buckling in the column starts to appear for the beams with depth of 120 mm and 140 mm depth.	0.1	CP by maximum rotation 0.12 radians
<b>step 5</b>	total failure of the connection occurs, by tearing of the perforations in the column and failure of the hooks.	total failure of the weld for the beam of the 100 mm depth, and total local buckling of the column for the connection with 120 mm and 140 mm depth.	0.15	





**Figure 2.33:** Performance levels of the rack structures.

Based on the observations and the results mentioned in Table 2.7, the different performance levels of immediate occupancy, life safety and collapse prevention were plotted over the moment rotation curves obtained from the experimental study as shown in Figure 2.33.

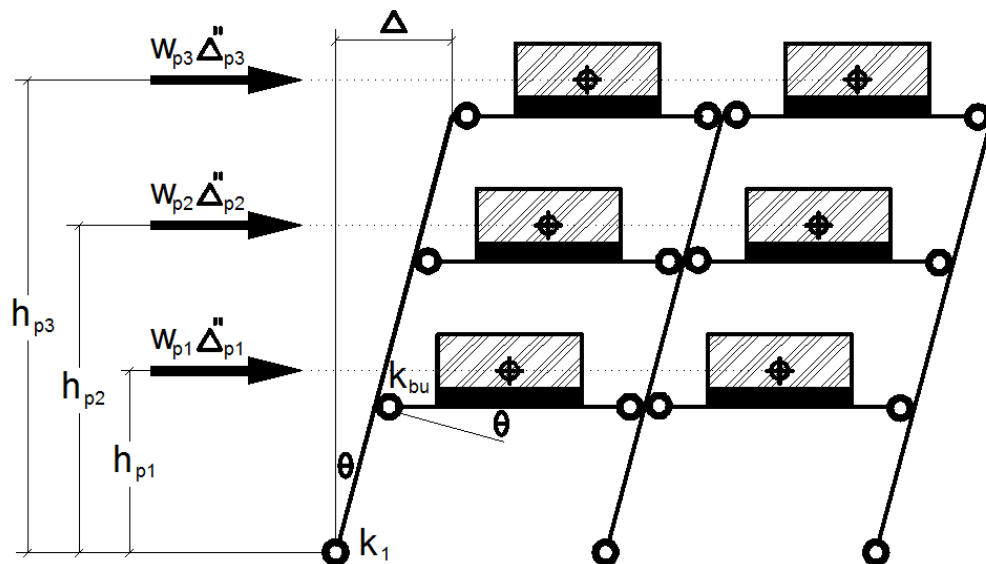
The initial behavior of the connection is a linear behavior without any sign of failure, although a reduction in the stiffness of the beam to column connection starts to occur right before the 0.04 rad rotation. Because of that, the connection is stated to reach the immediate occupancy performance point at a rotation of 0.04 rad.

Higher degradation in the stiffness occurs in the region between 0.04 rad and 0.075 rad rotations. In this region there was no any type of failure observed as it is stated in Table 2.7. As a result of that, it is stated that the connection reaches the life safety performance point at a rotation of 0.075 rad.

In the region between 0.075 rad and 0.12 rad rotations, minimal failure could be observed, such as; failure of one of the hook or slight local buckling of the column, but the connection could still resist some load after wards this region. Because of that, it is stated that the connection reaches the collapse prevention point at a rotation of 0.12 rad. The connection is considered to be failed after this point due to failure of the weld, failure in the hooks, total tearing or buckling of the column.

### 3. SEISMIC PERFORMANCE ASSESMENT

Seismic performance assessment of typical rack frames was carried out for frames composed of connections tested within this study. The assessment mainly focuses on determining the efficiency of the proposed structural upgrading method. For this purpose, a simple displacement-based seismic design procedure proposed by Filiatrault et. al. (2006) was used. The procedure mainly aims to verify the collapse prevention of storage racks in their down-aisle direction under MCE (Maximum Credible Earthquake) ground motions. The seismic performance of the racks in the down-aisle direction is captured using a simple analytical model. The model assumes that all the non-linear behavior occurs in the beam-to-column connections and the moment-resisting connections between the concrete slab and the base columns, while it assumes that the columns and beams remain elastic in the down-aisle direction. Therefore, the behavior of the cold-formed rack structures in the down aisle direction depends on the effective rotational stiffness of the beam-to-column connection and column-to-slab connections that vary significantly with the connection rotation (Filiatrault et. al. 2006).



**Figure 3.1:** Analytical model used for the seismic performance assessment of down-aisle frame behavior (Filiatrault et al., 2006).

A summary of the steps involved in the assessment method is given below. The description of the parameters involved is given separately in Table 3.1.

The fundamental period ( $T_1$ ) is calculated according to Equation (3.1) as a function of the experimentally obtained connection stiffness,  $k_c = \frac{M_{max}}{\theta_{max}}$ , where  $M_{max}$  and  $\theta_{max}$  are experimental maximum values for connection moment and rotation, respectively (Filiatrault, 2006).

$$T_1 = 2\pi \sqrt{\frac{\sum_{i=1}^{N_L} W_{pi} h_{pi}^2}{g \left( N_c \left( \frac{k_c k_{be}}{k_c + k_{be}} \right) + N_b \left( \frac{k_b k_{ce}}{k_b + k_{ce}} \right) \right)}} \quad (3.1)$$

The maximum displacement demand  $D_{max}$  by adjusting the first-order displacement demand  $D$  to account for second-order P-delta effects is calculated using Equations (3.2), (3.3) and (3.4) (Filiatrault, 2006).

$$D_{max} = D(1 + \alpha) \quad (3.2)$$

$$D = \frac{g S_{M1} T_1}{4\pi^2 B} \quad (3.3)$$

$$1 + \alpha = 1 + \frac{\sum_{i=1}^{N_L} W_{pi} h_{pi} \left( \frac{k_c + k_{be}}{k_c k_{be}} \right)}{\left( N_c + N_b \left( \frac{k_b k_{ce}}{k_c k_{be}} \right) \left( \frac{k_c + k_{be}}{k_b + k_{ce}} \right) \right)} \quad (3.4)$$

The rotational demand in the connectors ( $\theta_{demand}$ ) is calculated using Equation (3.5) (Filiatrault, 2006).

$$\theta_{demand} = \frac{D_{max}}{0.72 h_{tot}} \quad (3.5)$$

If the rotational demand ( $\theta_{demand}$ ) is less than maximum rotational capacity, ( $\theta_{max}$ ) the connection design is adequate to prevent the collapse of the rack under the MCE.

A case study problem was solved using the above equations for a four bay, three story rack frame. Table 3.1 presents the descriptions, input and calculated values for the parameters involved in this example frame including 140.40.4P type connections.

Four bay-three story rack frames with constant width and height dimensions (as given in Table 3.1), constant pallet weight value but with different connection types were analyzed in this fashion to evaluate collapse prevention in the down-aisle direction under the MCE ground motions. Using the Equations (3.1)-(3.5), rotational demand,  $\theta_{demand}$ , values were calculated and compared with the experimentally achieved rotation capacity,  $\theta_{max}$ , values for the above described rack frames.

**Table 3.1:** Input and calculated values for a four bay, three story rack frame (140.40.NP).

Pallet Weight	$W_{pi} =$	15	(kN)
Pallet Height	$P_h =$	0	(m)
Clear Span of Beams	$L =$	2.67	(m)
Clear Height of Upright	$H =$	1.52	(m)
Number of Bays	$N_{bay} =$	4	
Number of Levels	$N_L =$	3	
Number of Beam to Upright Connection	$N_c =$	48	
Number of Base Plate Connections	$N_b =$	10	
Youngs Modulus	$E =$	200000000	(kN/m <sup>2</sup> )
Beam Inertia	$I_b =$	0.0000016	(m <sup>4</sup> )
Upright Inertia	$I_c =$	3.2441E-07	(m <sup>4</sup> )
Beam End Rotational Stiffness	$k_{be} =$	719.1011236	(kN.m/rad)
Upright End Rotational Stiffness	$k_{ce} =$	170.7421053	(kN.m/rad)
One-second MCE accelartion	$S_{MI} =$	1	(g)
Damping Coefficient	$B =$	1.7	

Minimum Permitted Connection Stiffness	$k_c =$	59.63	(kN.m/rad)
Minimum Permitted Base Plate Stiffness	$k_b =$	59.63	(kN.m/rad)
Maximum Rotation Capacity	$\theta_{max} =$	0.15	(radians)

**Table 3.2:** Seismic performance assesment of rack frames with different connection configurations.

Connection type	$T_1$ (Sec)	$D$ (m)	$D_{max}$ (m)	$\theta_{demand}$ (rad)		$\theta_{max}$ (rad)	Assessment Result
<b>100.40.NP</b>	1.982	0.289	0.369	0.112	>	0.071	<i>Frame inadequate</i>
<b>100.40.2P</b>	1.773	0.259	0.316	0.096	>	0.085	<i>Frame inadequate</i>
<b>100.40.4P</b>	1.686	0.246	0.295	0.092	>	0.088	<i>Frame inadequate</i>
<b>120.40.NP</b>	1.951	0.299	0.388	0.118	>	0.089	<i>Frame inadequate</i>
<b>120.40.2P</b>	1.884	0.270	0.334	0.102	>	0.099	<i>Frame inadequate</i>
<b>120.40.4P</b>	1.847	0.254	0.325	0.100	<	0.120	<i>Frame adequate</i>
<b>140.40.NP</b>	1.908	0.279	0.350	0.107	>	0.089	<i>Frame inadequate</i>
<b>140.40.2P</b>	1.716	0.251	0.303	0.092	<	0.132	<i>Frame adequate</i>
<b>140.40.4P</b>	1.591	0.233	0.274	0.083	<	0.150	<i>Frame adequate</i>

Table 3.2 presents the results for the seismic performance assessment of the frames with different connection configurations as described in Table 1. In line with the procedure described above, experimentally obtained connection stiffness values were used to calculate the fundamental period ( $T_1$ ) of the frames. The greatest period value was calculated for the frame with 100.40.NP connections and the smallest value for the frame with 140.40.4P connections which, in this study, represent the weakest and strongest connections, respectively.

As expected, for a constant beam depth (100 mm, 120 mm or 140 mm) introduction of additional bolts (2P and 4P) leads to reductions in the fundamental period of the frames. Based on the  $T_1$  values maximum frame displacement demand values ( $D_{max}$ ) were calculated for all the frames for constant ground acceleration and damping coefficient. And finally connection rotational demand ( $\theta_{demand}$ ) values were compared with experimentally obtained maximum rotational capacity ( $\theta_{max}$ ) values for all the frames with different connection configurations. For the 100 mm depth beam connections the assessment results show that in all three cases of connections with hooks and with additional bolts, maximum connection rotational capacities are all smaller than the rotational demand resulting in collapse of the rack frames under the MCE. On the other hand, for the 120 mm and 140 mm depth connections, the frames with hooked-only connections are found to be inadequate whereas with the introduction of the bolts (both 2 and 4 bolts) collapse was prevented under the MCE.

Collapse prevention was not possible for the 100 mm depth beam connections even with the introduction of additional bolts. This is mainly due to the fact that, as observed in the test and also shown in Table 2.3, welds between the beam and the connector angle failed before the bolts could be activated. Hence the contribution of the additional bolts to the maximum rotational capacity was limited. On the other hand, no weld failures were observed for the 120 and 140 mm depth beams and additional bolts in both 2P and 4P connections were significantly contributing to the connection rotational capacity leading to collapse prevention of the rack frames incorporating such upgraded connections.

From the experimental and analytical results, it was clear that the traditional hooked connection is not sufficient to resist the seismic loads on a rack storage system.

Seismic performance assessment shows how it is so much preferred to use the pins beside the hooked connections, as the pinned connections with the 120 and 140 beams were found adequate to prevent the collapse of the frame under MCE.

## **4. FINITE ELEMENT ANALYSIS**

Finite element analysis using ANSYS software is used to be compared to the experimental results obtained for the tests.

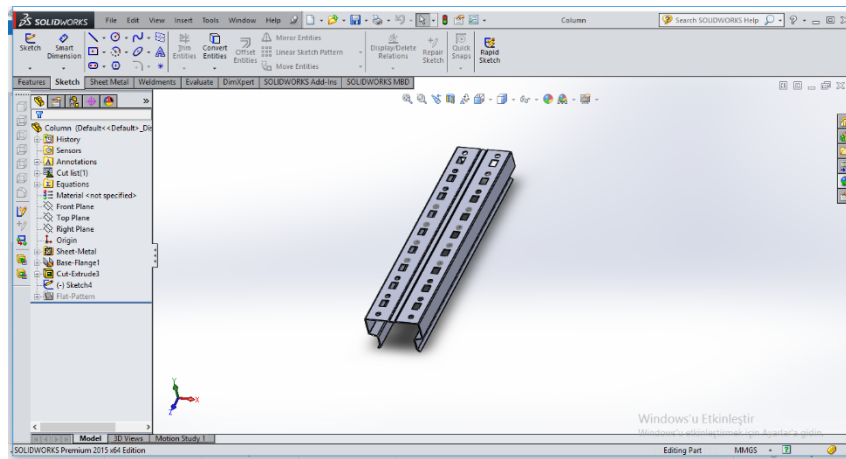
Two different models were performed to simulate the tests performed during the experimental study, the first model was the boltless hooked (no pin) model, in which the connection depends only on the hooks that exists in the beam end connector bracket that connect the beam to the column.

The second model was to simulate the pinned connection, in which the same assembly of the first model was used, but the only difference was that pins were modeled between the perforations of the beam end connector bracket and the perforations of the column.

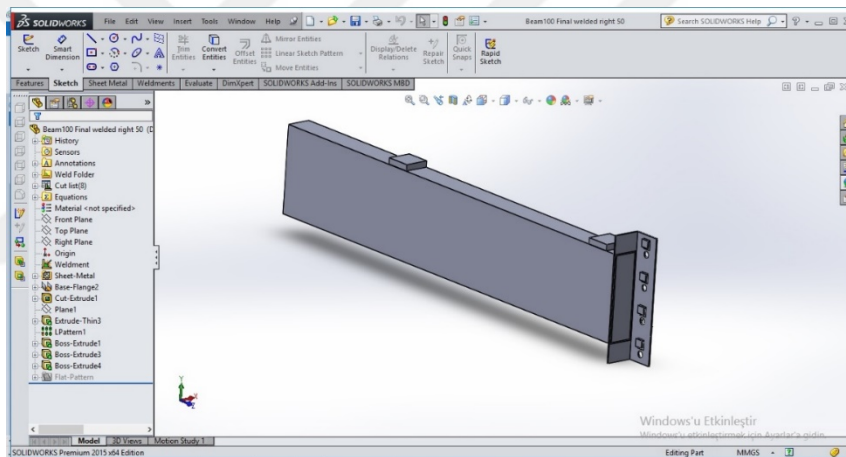
67 trails were done, each trial takes approximately 2 days to get the results and finally promising results were obtained.

### **4.1. CONNECTION MODELLING**

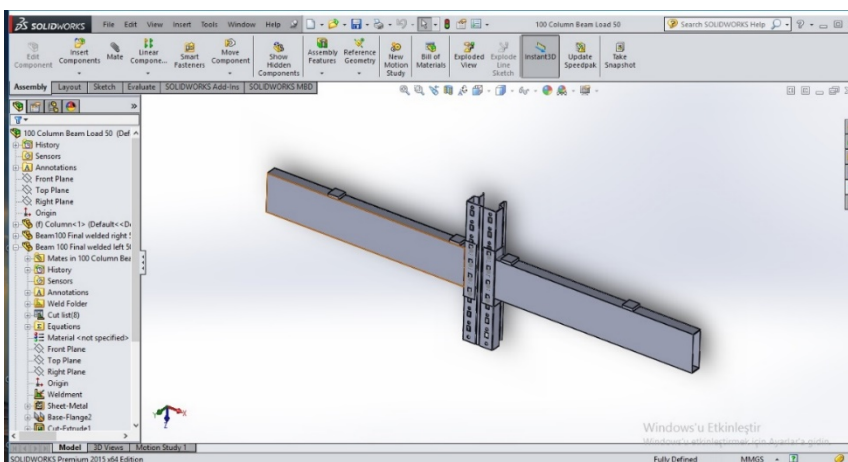
The model was divided into two parts that were modeled separately using Solidworks software. The column was modeled with the exact dimensions of the specimens used in the experimental study and with the same exact perforations along its length as shown in Figure 4.1. The beam was modeled as a simple box section with the same exact geometry like in the test specimens. The beam end connector bracket was modeled very carefully by taking into consideration a structural solid element design for the hooks in the bracket as shown in Figure 4.2. Considering the hooks as a structural solid element makes the finite element model to be more complicated, but using this approach makes it so close to the actual system that was used in the experimental study, which will help in simulating the actual behavior of the hooks during the cyclic load. The two structural parts were connected together in Solidworks software program to form one assembly of the beam to column connection as shown in Figure 4.3.



**Figure 4.1:** The column designed in Solidworks.



**Figure 4.2:** The hooked beam designed in Solidworks.



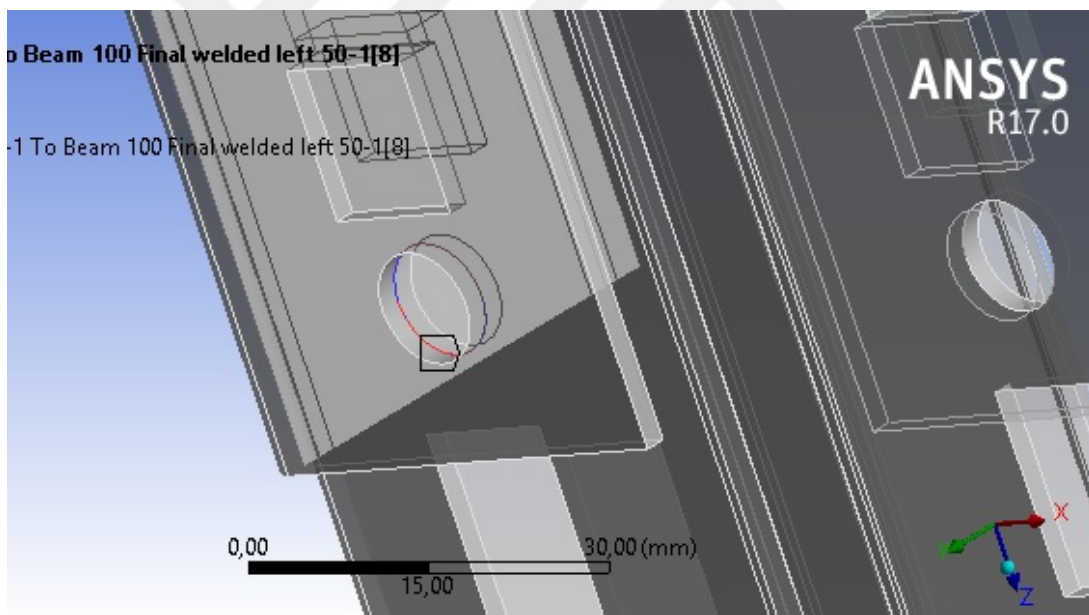
**Figure 4.3:** The beam-to-column connection designed in Solidworks.



The beam to column connection that was modeled in Solidworks are imported to ANSYS finite element software. A bilinear isotropic elasto-plastic material model was defined to the members of the beam to column connections.

#### 4.2. PINS MODELLING AND CONTACT SURFACES

The outer circumference of the perforation existing at both the beam end connector bracket and the column, through which the bolt is going to be inserted, were connected to each other. The edges of the perforations existing on both the column and the bracket were selected and bonded to each other's using a (bonded) contact surface as shown in Figure 4.4. Using this simple simulation to the existence of the bolts was a reason to keep the model less complicated and helped in obtaining good results.

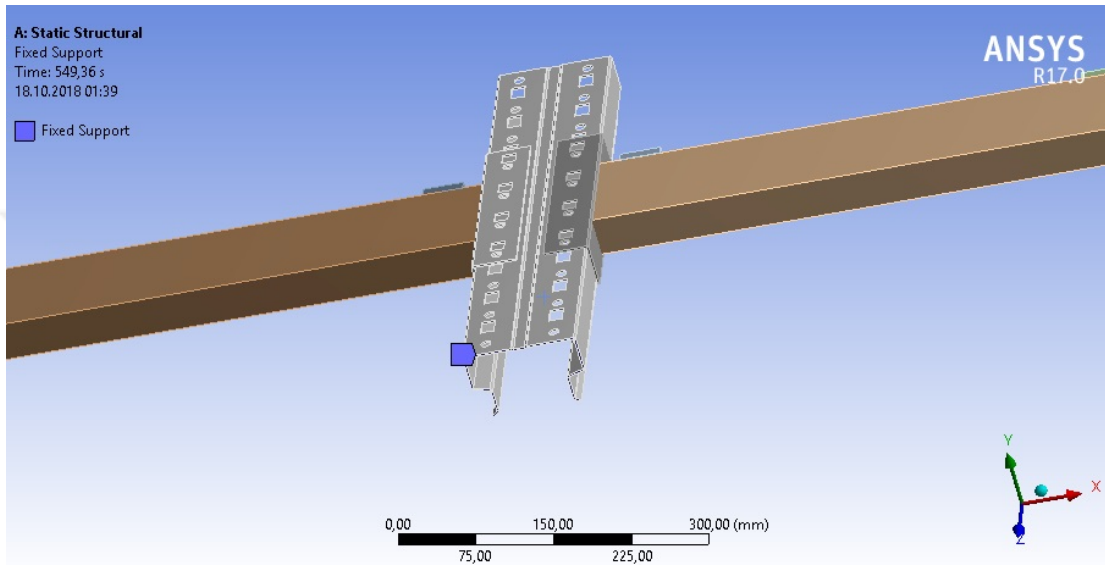


**Figure 4.4:** Pins Modeling using the bonded contact surface between the edges of the perforations of both the bracket and the column.

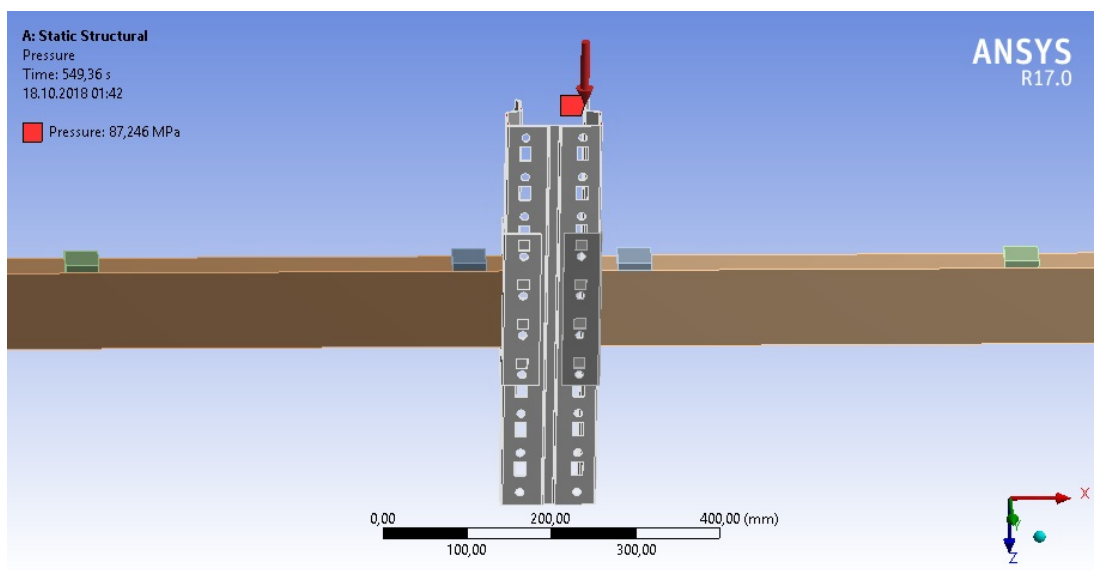
#### 4.3. BOUNDARY CONDITIONS AND ASSIGNING OF LOADS

In the experimental study the column was clamped in the lower part to form a fixed support and a constant value of 50 kN axial compression load was applied to it by a hydraulic cylinder at the top of it. In the finite element model, a fixed support was defined for the lower face of the

column with a value of 0 for the three x, y and z components as shown in Figure 4.5, while a 50 kN compression load was applied to the upper face to imply the same loading and boundary condition of the column as shown in Figure 4.6. A support was added to the upper face with 0 value for the x and y component, while leaving the z component to be set to (free).

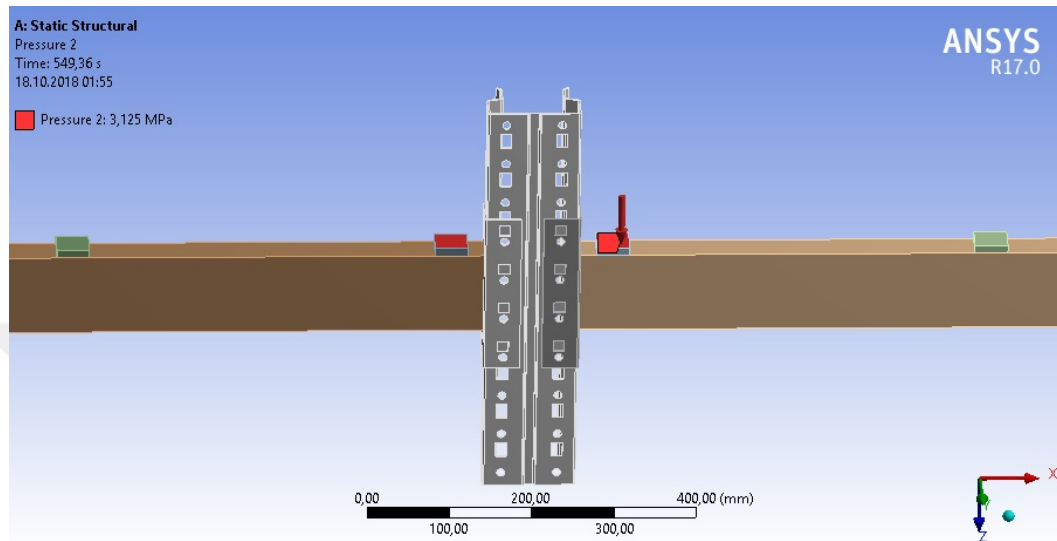


**Figure 4.5:** Fixed support applied to the lower face of the column.



**Figure 4.6:** Constant 50 kN axial load applied to the top of the column.

At each inner side of the two beams, a 5 kN load were applied to simulate the pallet loads similar to the test setup, as shown in Figure 4.7.



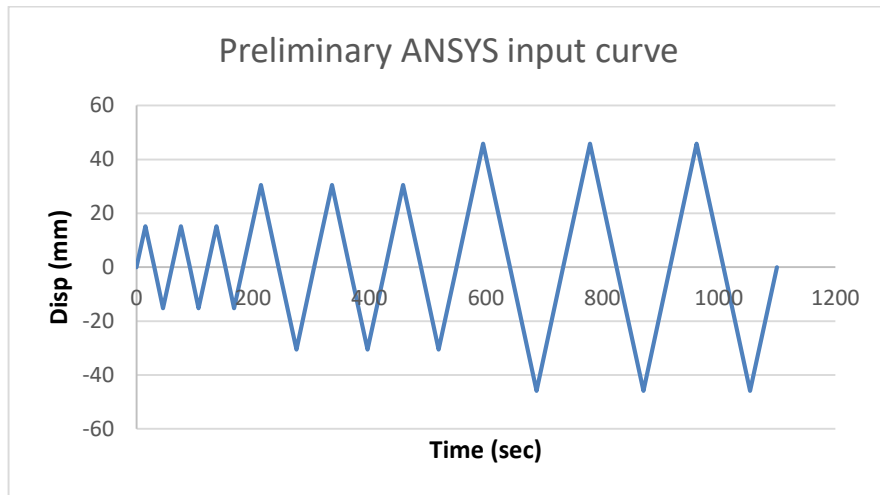
**Figure 4.7:** 5 kN pallet loads applied to the left and right beams.

In order to simulate displacement based cyclic test on the beam to column connection two displacements were applied in the opposite directions for the two beam on a 600 mm distance from the column as shown in Figure 4.11. The displacements values inserted was a simplification for the sine wave that was carried out during the test.

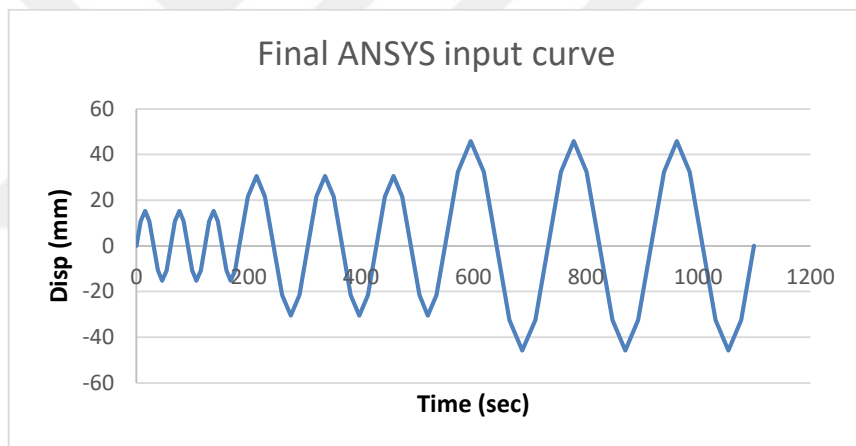
For the first few trails the sine wave was simplified into straight lines connecting the positive and peak points as shown in Figure 4.8 in order to develop a less complicated ANSYS model and to decrease the duration of the analysis. Good results were obtained from this model.

Another more detailed curve was used in which the 1 cycle of sine wave was simplified into seven straight lines using the equal area method, in order to simulate the actual behavior of the connection as much as possible as shown in Figure 4.9, specially to model the actual energy dissipation like what was occurring during the test.

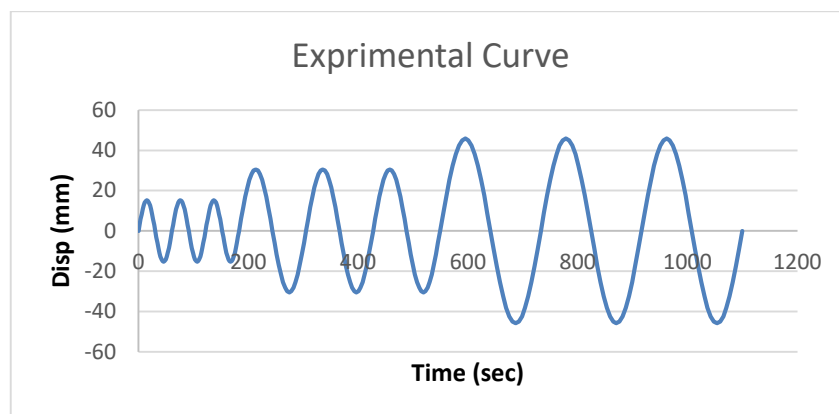
It was determined that the seven straight line simulation is better to be used for the finite element analysis, due to the high accuracy of its results, although the longer duration of analysis required compared to the first simulation.



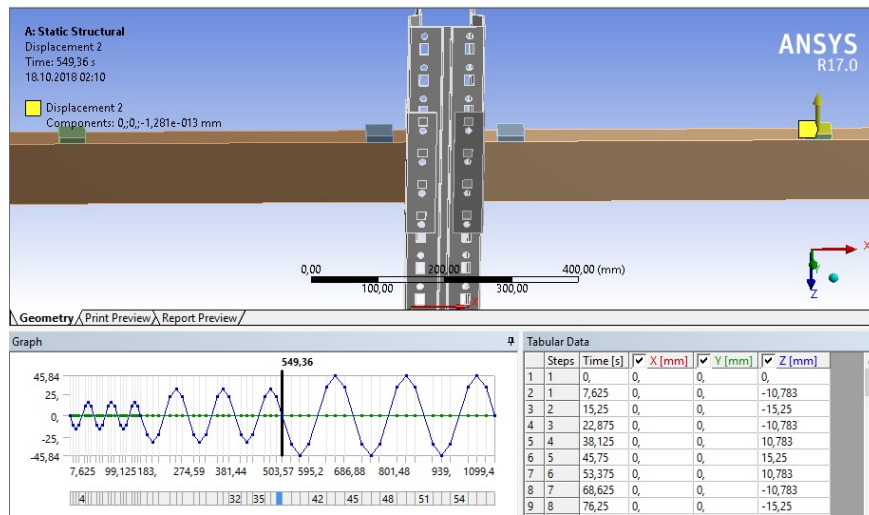
**Figure 4.8:** Simplified displacement curve to be used in ANSYS model.



**Figure 4.9:** The displacement curve that was used in the final ANSYS model.



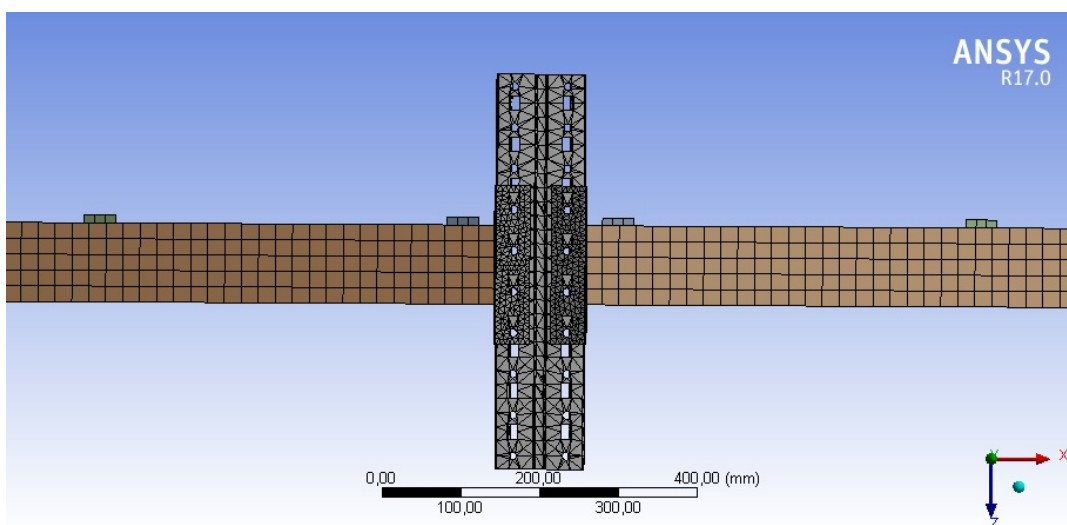
**Figure 4.10:** The displacement curve that was used in the experimental study.



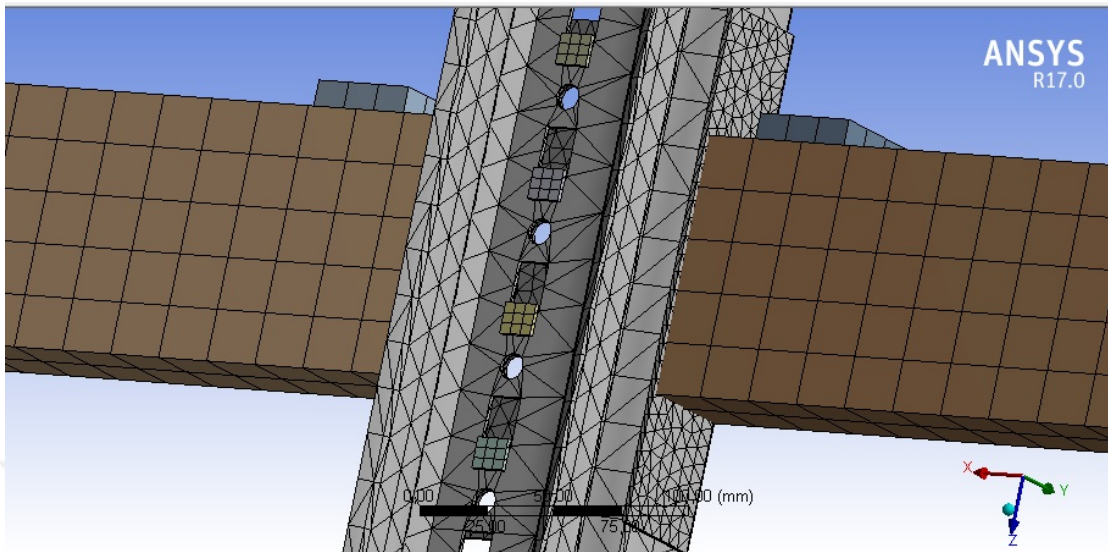
**Figure 4.11:** Displacement applied on the right beam.

#### 4.4. MODEL MESHING

All the components of the finite element model for the beam to column connection were meshed using body meshing. In the results obtained from the experimental study, high deformations were noticed in the regions connecting the hooks and the beam end connector bracket, because of that high meshes were used in this regions in order to capture the deformation behavior precisely. The meshes are shown in Figure 4.12 and Figure 4.13.



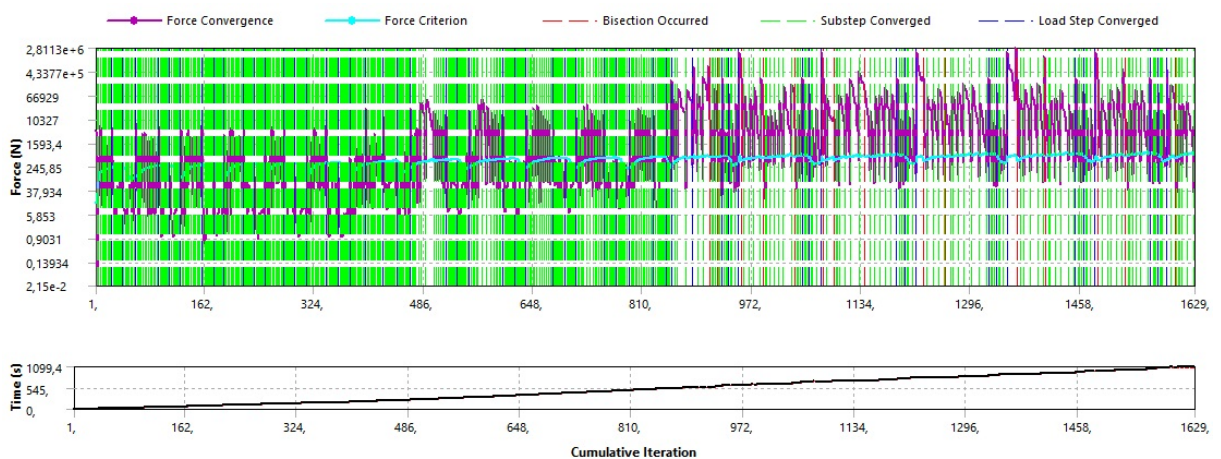
**Figure 4.12:** Body meshing of the column, beam and beam end connector bracket.



**Figure 4.13:** Body meshing of the hooks of the bracket.

#### 4.5. SUBSTEPS

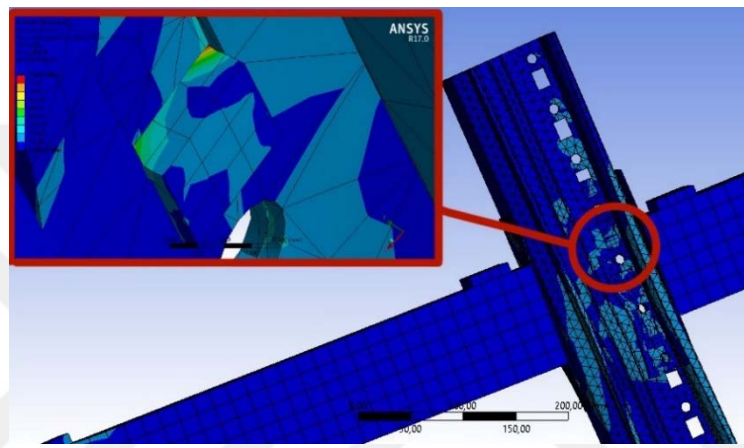
Increasing the number of substeps for the ANSYS finite element model increases the time of running of the model, because of that automatic time stepping was used in order to balance between the accuracy of the results and the required time for the running of the model. Figure 4.14 shows the convergence results of the beam to column connection model.



**Figure 4.14:** The convergence results of the beam to column connection model.

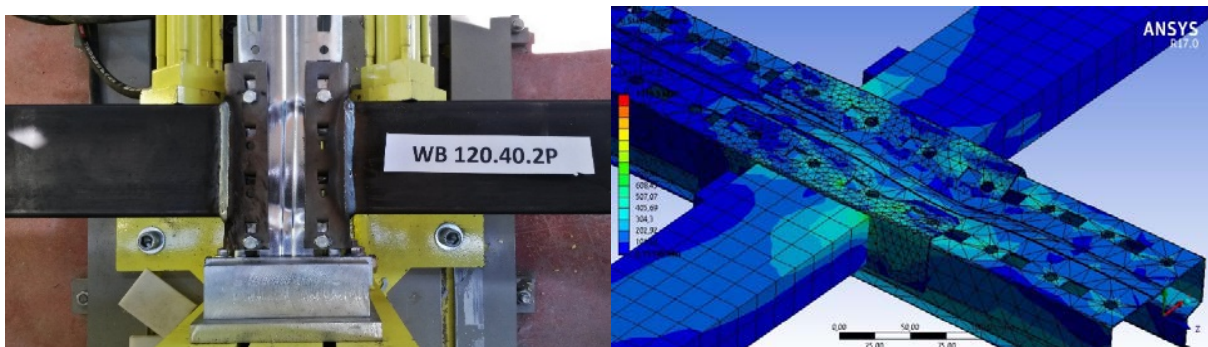
#### 4.6. FAILURE MODES

Two failure modes were obtained for the two finite element models that were performed. For the hooked boltless connection, the finite element model showed very high stress concentrations at the edge between the hook and the column as shown in Figure 4.15, which reflects the rupture that occurs in the experimental study.



**Figure 4.15:** The failure mode of the hooked connection that shows high stress concentrations at the hook.

In the pinned beam to column connection finite element model, the failure mode obtained was so similar to the failure mode obtained from the experimental study, which is the buckling that occurs at the column which appears more at the lower region of the connection beside the lower bolts as shown in Figure 4.16.



**Figure 4.16:** The column buckling failure mode obtained from the pinned connection.

## 4.7. MOMENT ROTATION RESULTS

The Moment-displacement curve obtained from ANSYS in Figure 4.17 and Figure 4.18 is converted into Moment-rotation curve, to be compared to the Moment-rotation curves obtained from experimental test results as shown in Figure 4.19 and Figure 4.20.

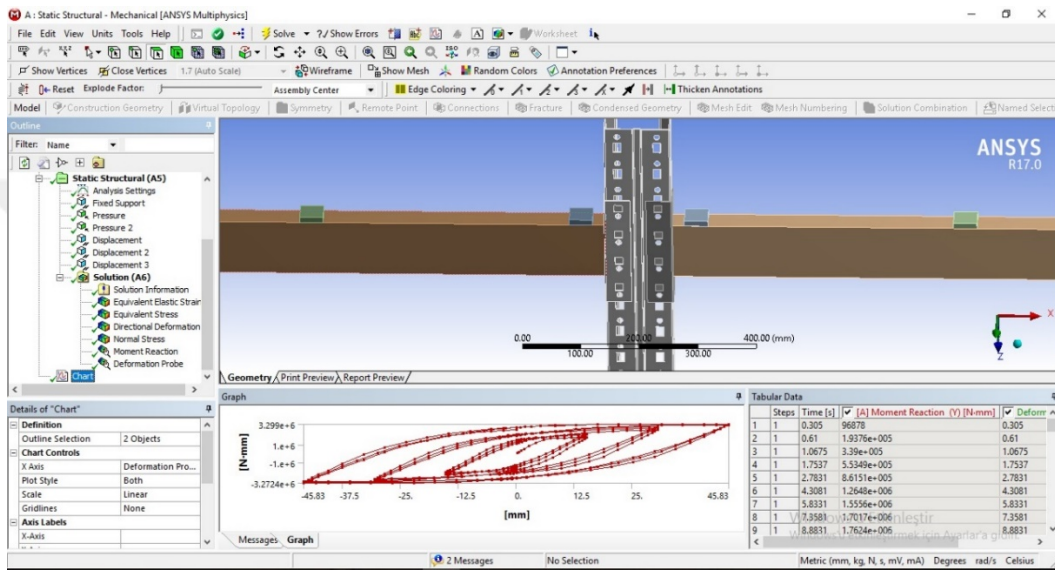


Figure 4.17: Moment-displacement curves of the no-pin beam-to-column connection in ANSYS.

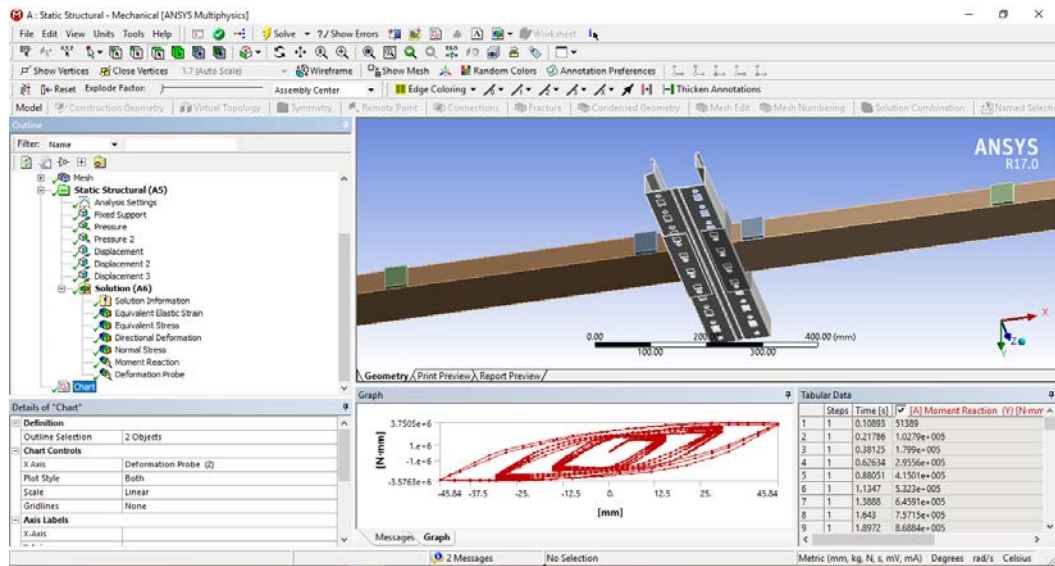


Figure 4.18: Moment-displacement curves of the pinned beam-to-column connection in ANSYS.

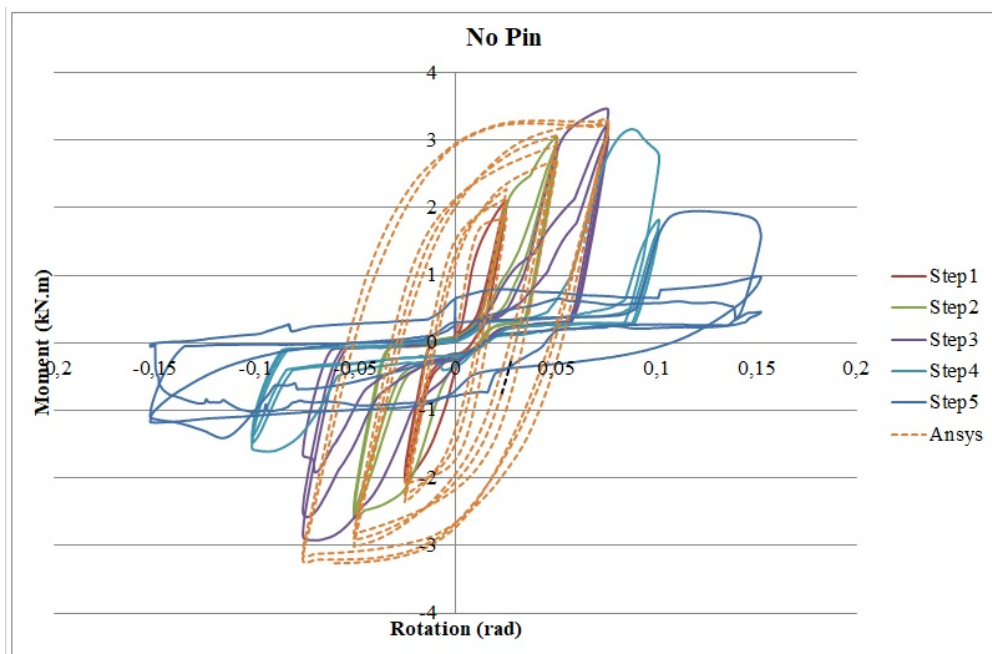


In Figure 4.19 and Figure 4.20 it can be noticed the difference in the shape of the curves obtained from ANSYS and the curves obtained from the experimental test. This difference in behavior is due to the imperfections and the gaps that exist in the experiments, while the curves from ANSYS are a total perfect loading and unloading curves as it is based on mathematical functions.

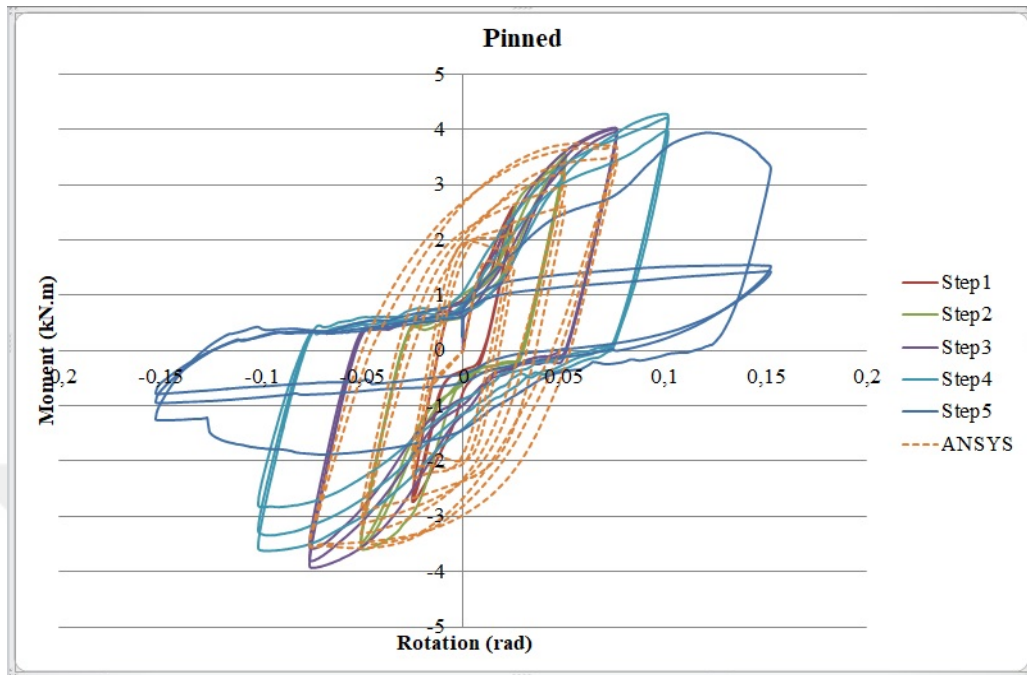
The most important results for us to compare are the peak moment and rotation points of each step, as they are the most critical points that will be used in the design in the further work.

Figure 4.21 and Figure 4.22 shows a comparison between the peak moment-rotation points of each loading step in ANSYS and the experimental test results.

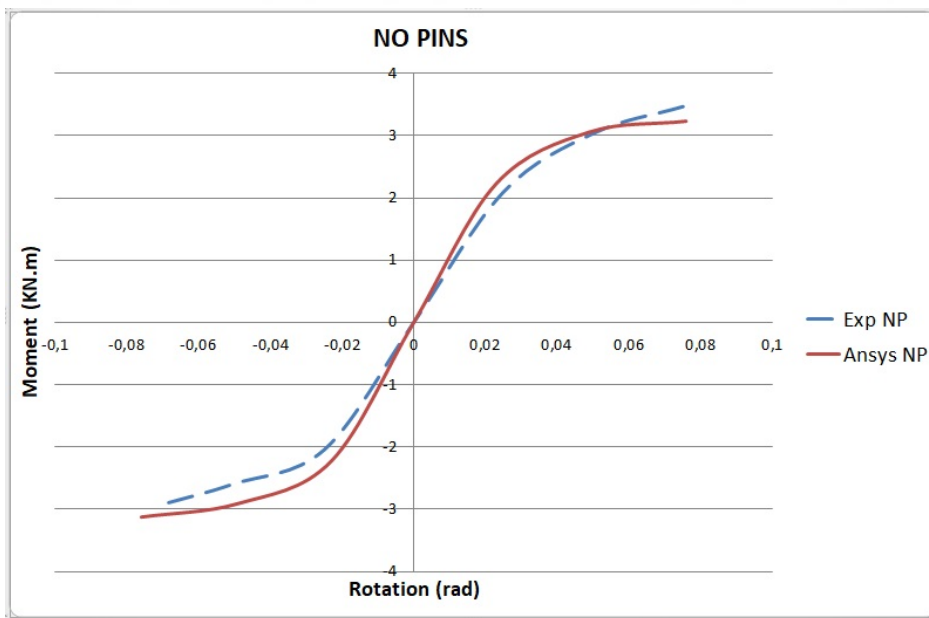
From Figure 4.21 Figure 4.21 and Figure 4.22 it is clear that the results obtained from ANSYS are very promising results which matches with the experimental results, by taking the average of the errors of each step for the two models it was found that error percentage is 5.9% for the no pin model and 10.5% error for the pinned model.



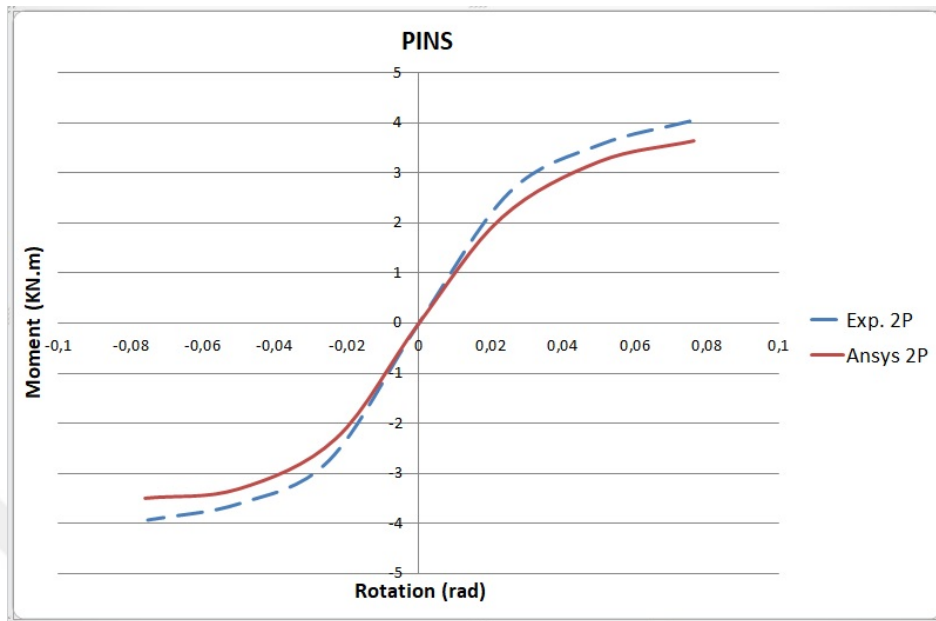
**Figure 4.19:** The moment-rotation curves of the beam-to-column connection from ANSYS and experimental test results of the no pin model.



**Figure 4.20:** The moment-rotation curves of the beam-to-column connection from ANSYS and experimental test results of the pinned model.

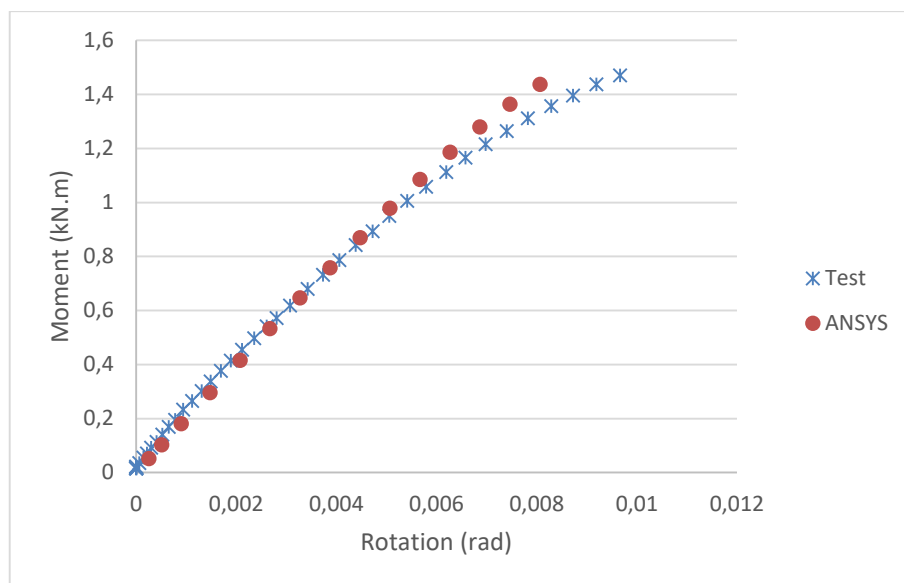


**Figure 4.21:** Comparison between the peak moment-rotation points of each loading step in ANSYS and the experimental test results for the no-pin connection.



**Figure 4.22:** Comparison between the peak moment-rotation points of each loading step in ANSYS and the experimental test results for the pinned connection.

The initial stiffness of both the test and the ANSYS model were compared in Figure 4.23, and it can be seen how the initial stiffness is almost the same.

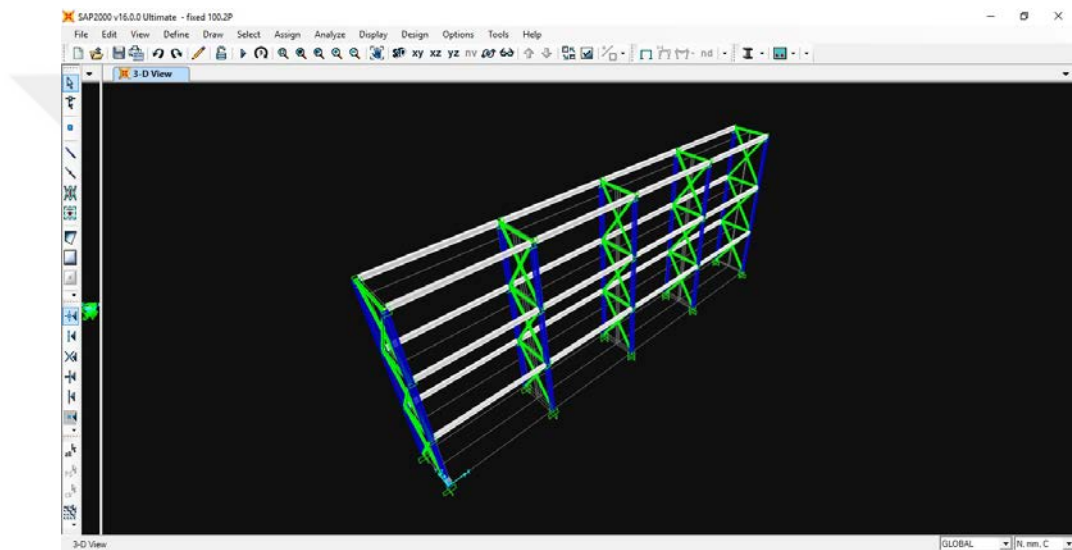


**Figure 4.23:** Comparison between the initial stiffness of both the test and ANSYS results.

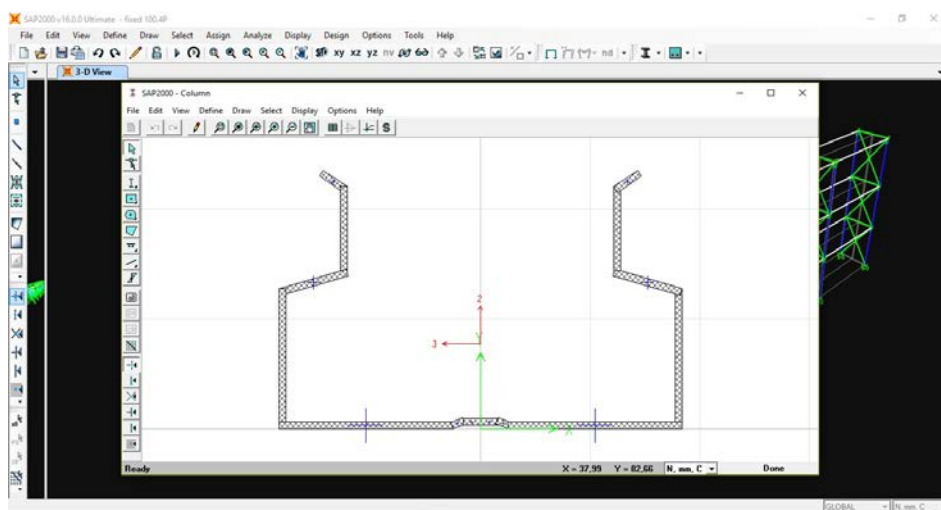
## 5. NON-LINEAR STATIC ANALYSIS OF RACK STRUCTURES

### 5.1. PUSHOVER ANALYSIS USING SAP2000

Using the results obtained from the experimental and the finite element studies, an analytical study was carried out using SAP2000 software as shown in Figure 5.1 in order to see the effect of the different types of beam-to-column connections on the behavior of the rack structure.



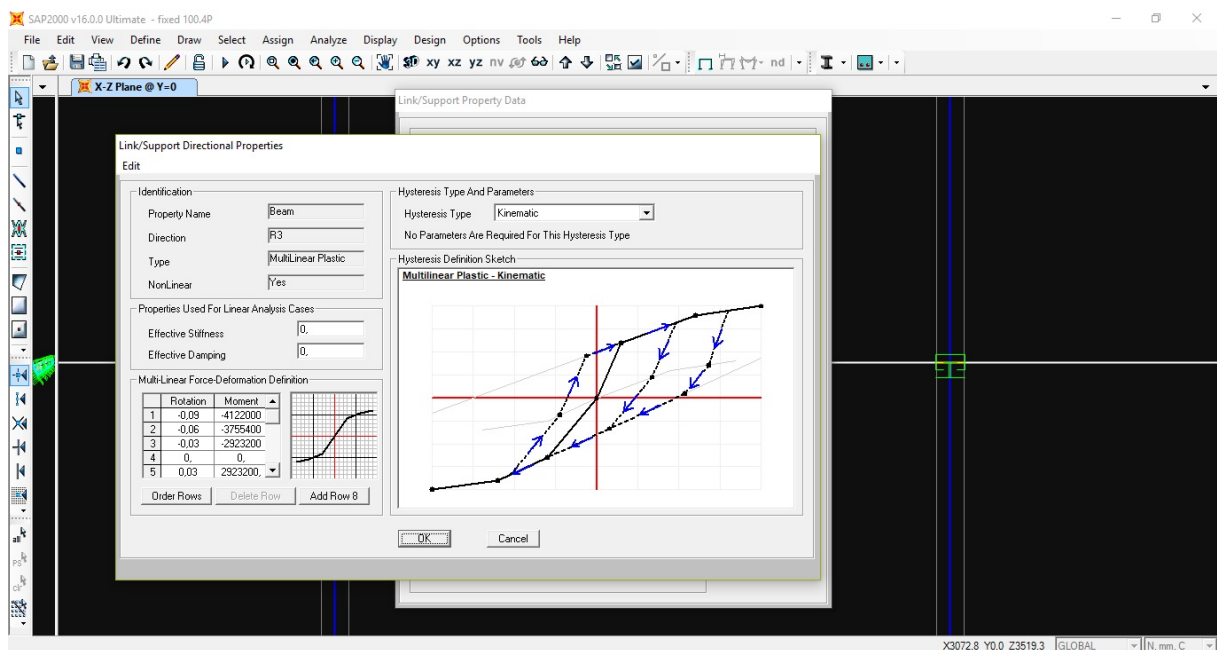
**Figure 5.1:** SAP2000 model of the rack system.



**Figure 5.2:** Defining the column in SAP2000 using section designer menu.

The exact dimensions for the columns and the beams were inserted into SAP2000 using the section designer menu as show in Figure 5.2.

moment rotation results of the beam-to-column connections that were obtained from the experiments and ANSYS were inserted to the model as links between the columns and the beams as shown in Figure 5.3.

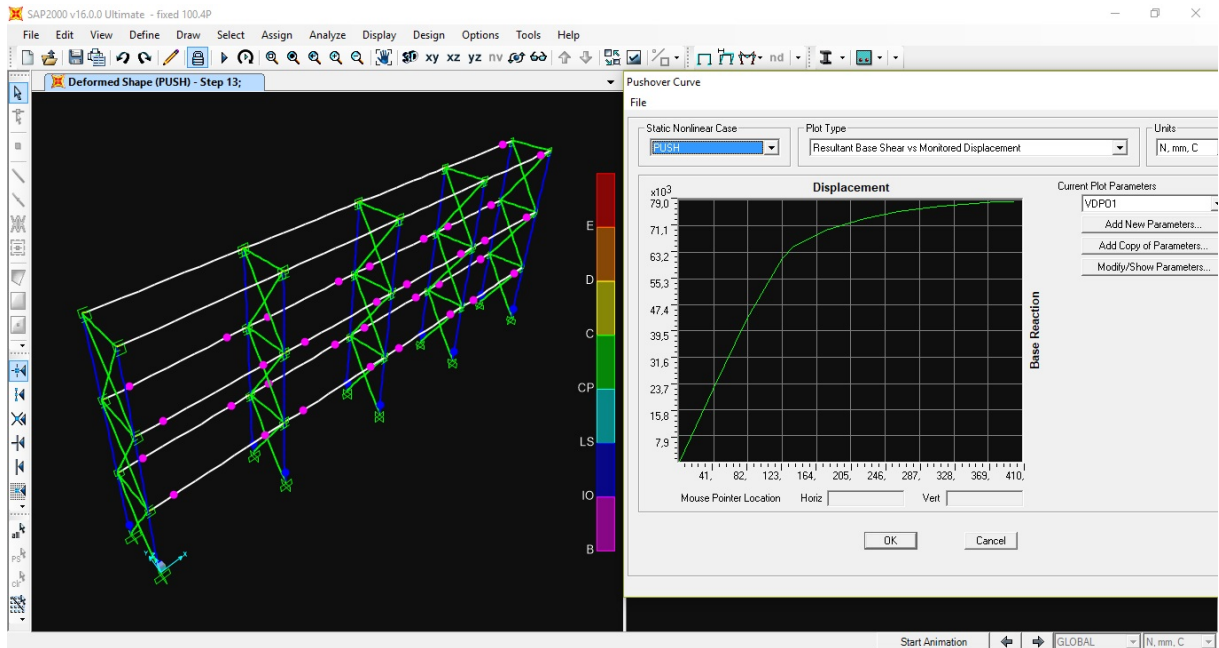


**Figure 5.3:** Defining the link element to the beam-to-column connection.

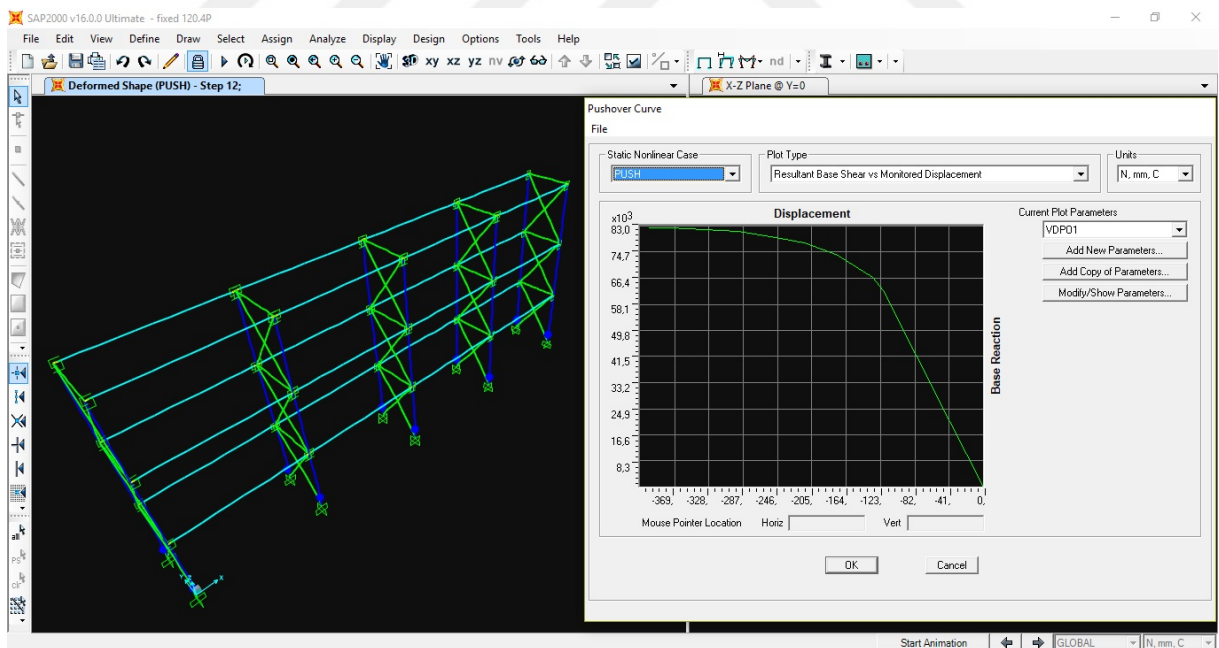
Pushover analysis were carried out and the pushover capacity curves were obtained from SAP2000 as shown in Figure 5.4 and Figure 5.5.

In Figure 5.4. we can see that plastic hinges were formed in the beam-to-column connection, this case occurred only in two cases which are for the beam 100.40.2P and 100.40.4P, which are the only two cases that failure in the weld occurs during the experimental tests.

In Figure 5.5. no plastic hinges were formed in the beam-to-column connection, this was the case for all the other connections, as these connections did not reach the plastic regions, and by checking the experimental results we could see that the failure mode of these connections was one of the following cases; rapture of the hooks, tearing in the column's perforations or buckling of the column.



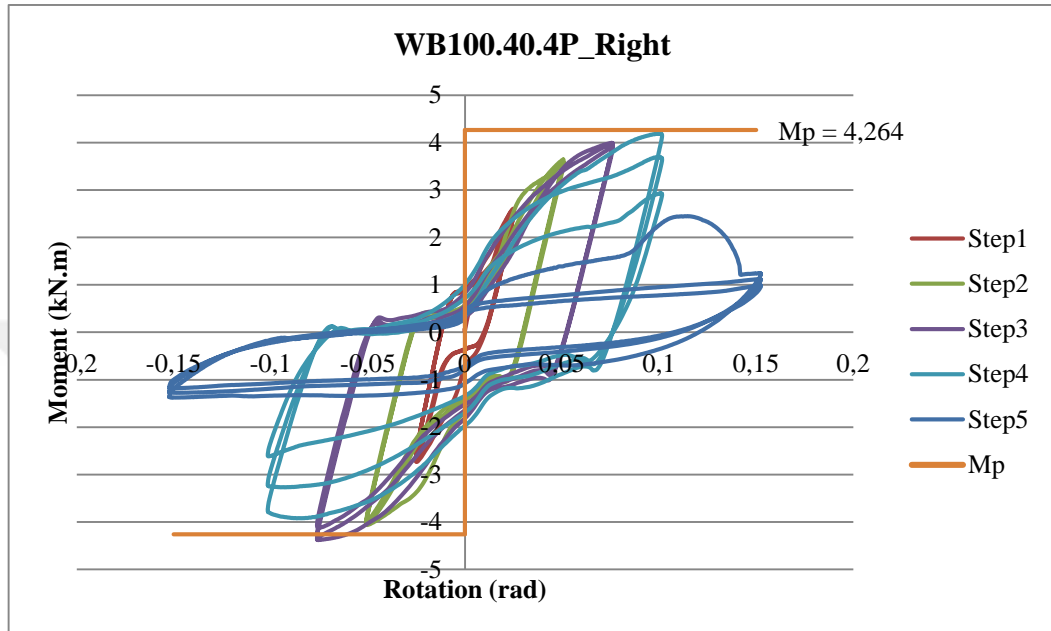
**Figure 5.4:** Pushover analysis result for the rack with the connection of 100.40.4P.



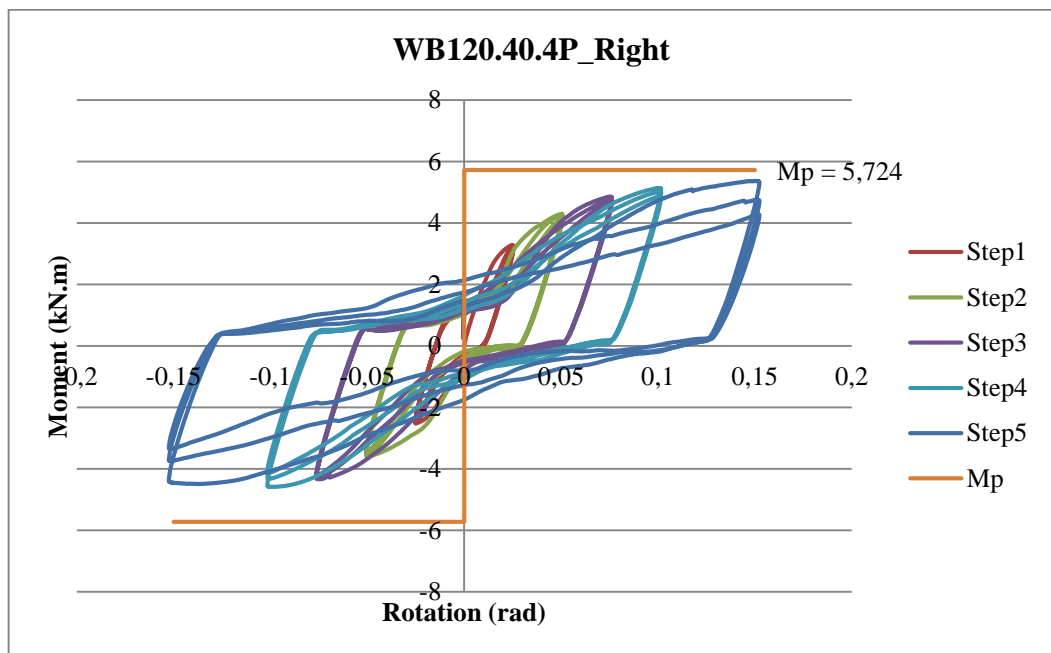
**Figure 5.5:** Pushover analysis result for the rack with the connection of 120.40.4P.

The plastic yield moments of the cross-sections were calculated and compared to the experimental results in Figure 5.6, Figure 5.7 and Figure 5.8, which shows that the connections

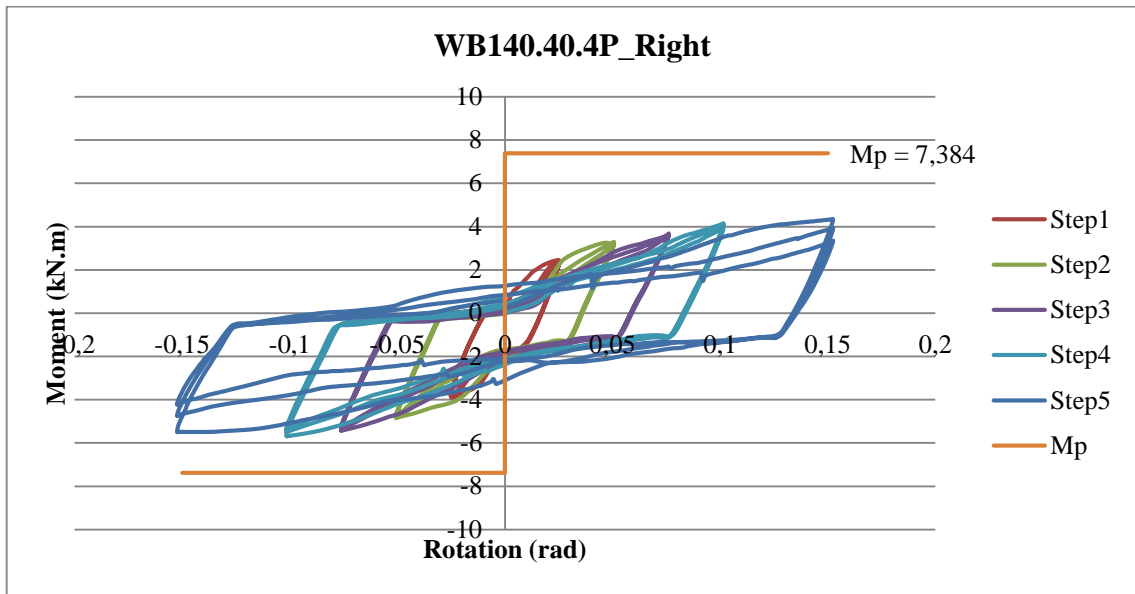
fail before it reaches the plastic yielding moment, which is the general case for the cold formed members as they always fail by buckling before yielding.



**Figure 5.6:** Plastic yield moment compared to the test result for the 100 mm depth beam.

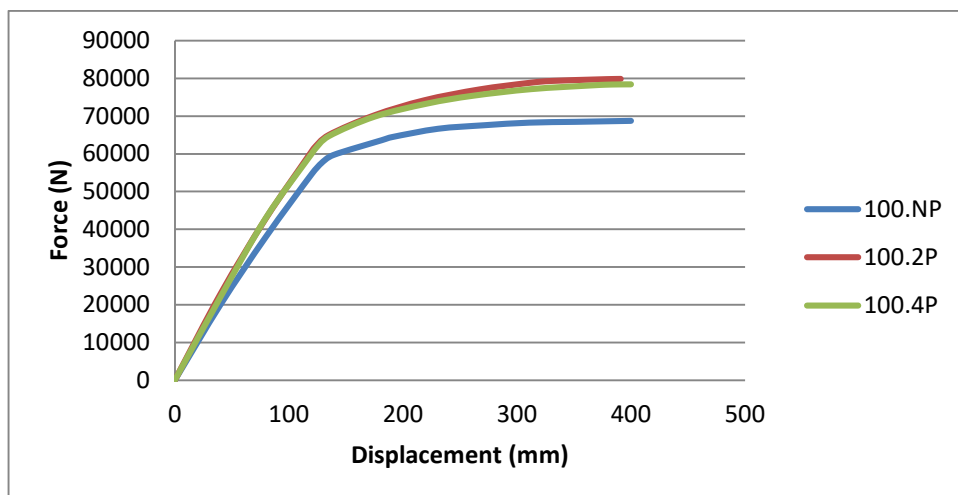


**Figure 5.7:** Plastic yield moment compared to the test result for the 120 mm depth beam.



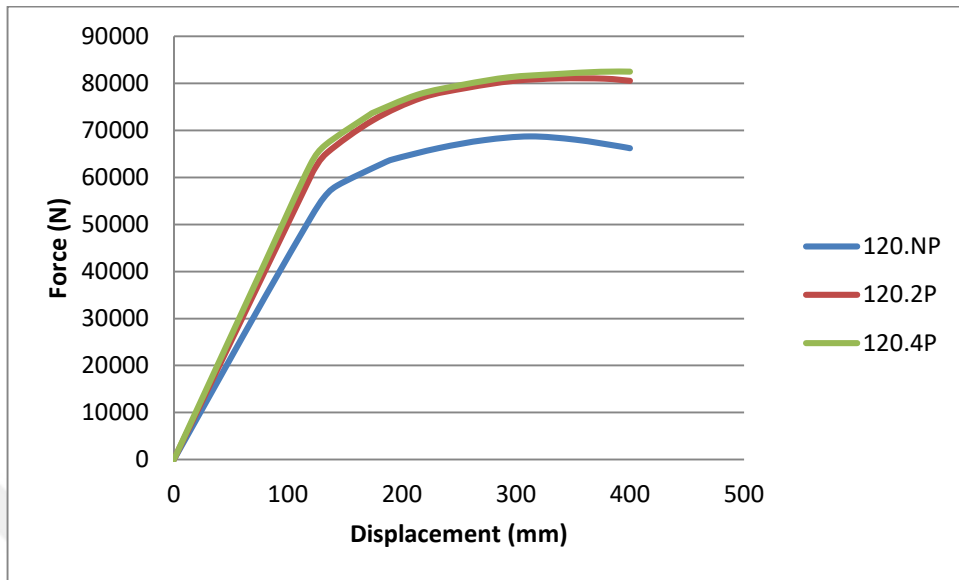
**Figure 5.8:** Plastic yield moment compared to the test result for the 140 mm depth beam.

All the pushover curves from the 9 different connections are compared in the following figures, and it is clear how the capacity curve enhanced from the NP connection compared to the 2P and 4P connection. Although, the capacity curves obtained from the rack frames using the 2P and 4P were not having a significant difference between them. Therefore, adding two pins only can be economically favored, as it will be saving both of time and materials.

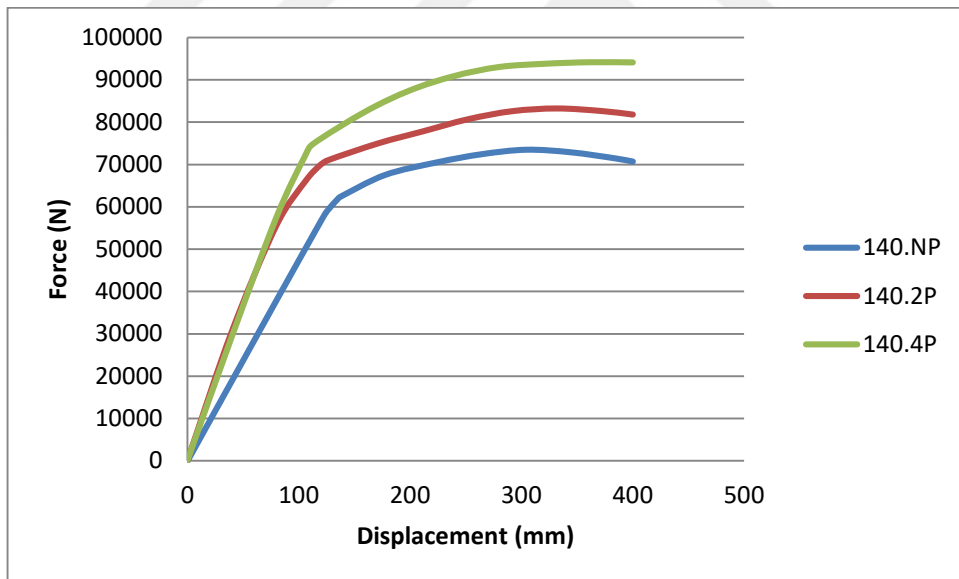


**Figure 5.9:** Pushover curves of the racks with beam of 100 mm depth.





**Figure 5.10:** Pushover curves of the racks with beam of 120 mm depth.



**Figure 5.11:** Pushover curves of the racks with beam of 140 mm depth.

## 5.2. EQUIVALENT LATERAL FORCE CALCULATION

According to FEMA 460 (Seismic Consideration for Steel Storage Rack Column) calculations for the equivalent lateral force of the racks with the different connections and beam depths are obtained to be compared to the results from the pushover analysis.

The seismic design requirements are presented in Sec. 2.6 of the RMI (2012) standard. The equivalent lateral seismic force  $V$  was calculated based on Equation (5.1), where  $C_s$  is the seismic response coefficient that was calculated according to Equation (5.2) in which  $SD_1$  is the Design earthquake spectral response acceleration at a 1 second period as described in Section 2.6.3.1 in RMI (2012).  $T_1$  is the fundamental period of the rack structure in the direction under consideration which was obtained using SAP2000 and  $R$  is 4 for the braced direction and 6 for the unbraced direction and it was taken as 6 as the calculation was done for the down-aisle unbraced direction.

$$V = C_s I_p W_s \quad (5.1)$$

$$C_s = \frac{SD_1}{TR} \quad (5.2)$$

In Equation (5.1)  $I_p$  is the system importance factor as stated in Table 5.1, while  $W_s$  is the effective seismic weight of the structure that was obtained from SAP2000.

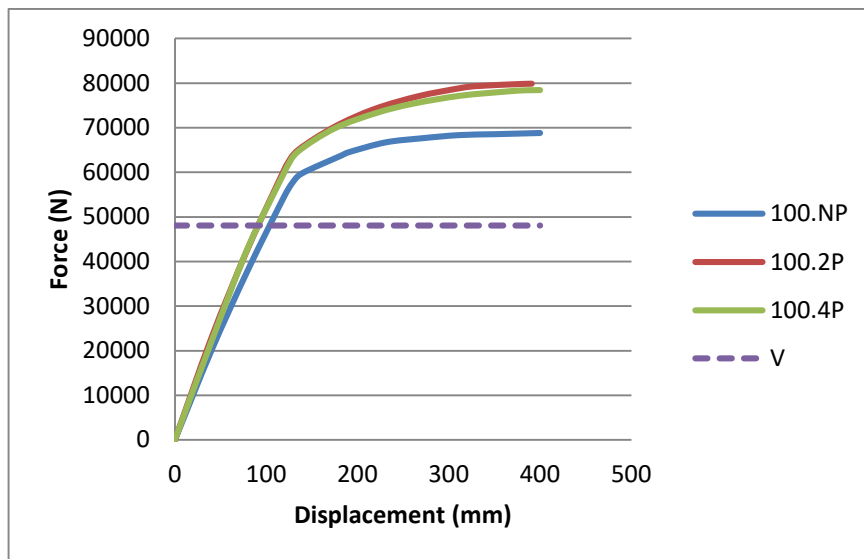
**Table 5.1:** Importance factors according to RMI (2012).

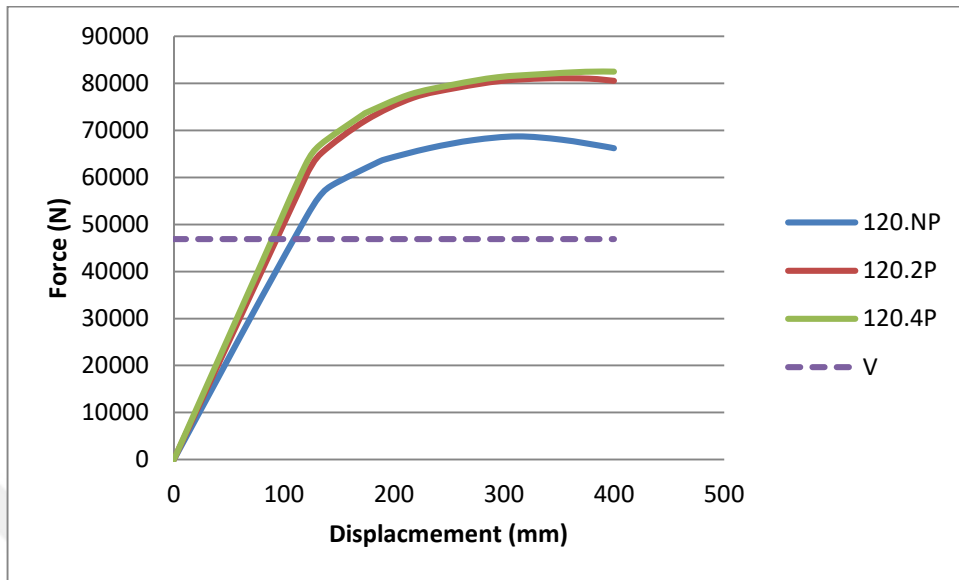
Importance factor	Type of structures
1.5	for essential facilities or hazardous material storage
1.5	for storage racks in areas open to the public
1	for all other structures

**Table 5.2:** Equivalent lateral force calculated for the different connections.

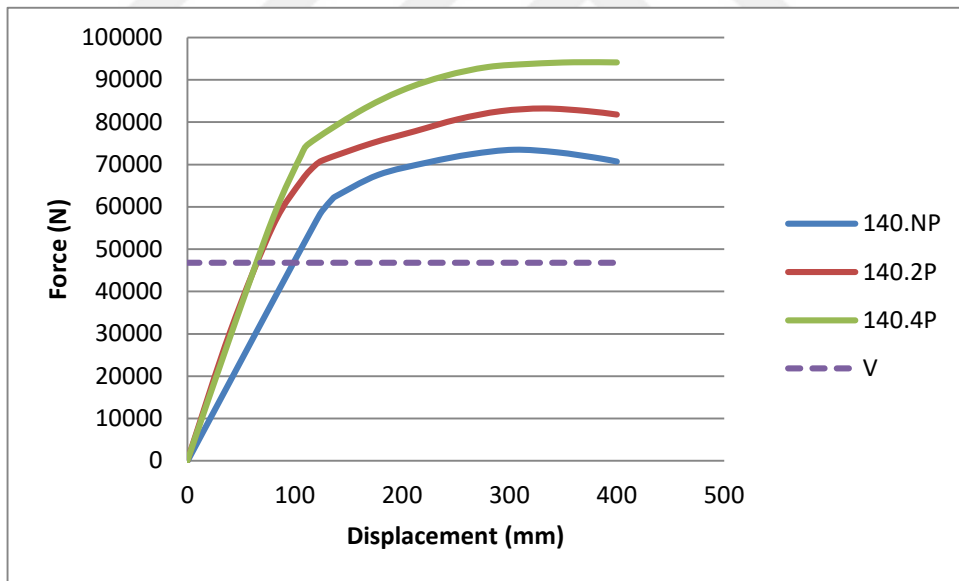
Connection	$T_I$ (sec)	$W_s$ (N)	$C_s$	$V$ (N)
100.40.NP	0.34795	185707,6	0,172494	48050,18
100.40.2P	0.34795	185707,6	0,172494	48050,18
100.40.4P	0.34795	185707,6	0,172494	48050,18
120.40.NP	0.36189	186084,4	0,168035	46903,18
120.40.2P	0.36189	186084,4	0,168035	46903,18
120.40.4P	0.36189	186084,4	0,168035	46903,18
140.40.NP	0.37533	186461,3	0,164	45869,41
140.40.2P	0.37533	186461,3	0,164	45869,41
140.40.4P	0.37533	186461,3	0,164	45869,41

The equivalent lateral force values were compared to the pushover curves in Figure 5.12, Figure 5.13 and Figure 5.14.

**Figure 5.12:** Equivalent lateral force compared to pushover curves of the 100 mm beam racks.



**Figure 5.13:** Equivalent lateral force compared to pushover curves of the 120 mm beam racks.



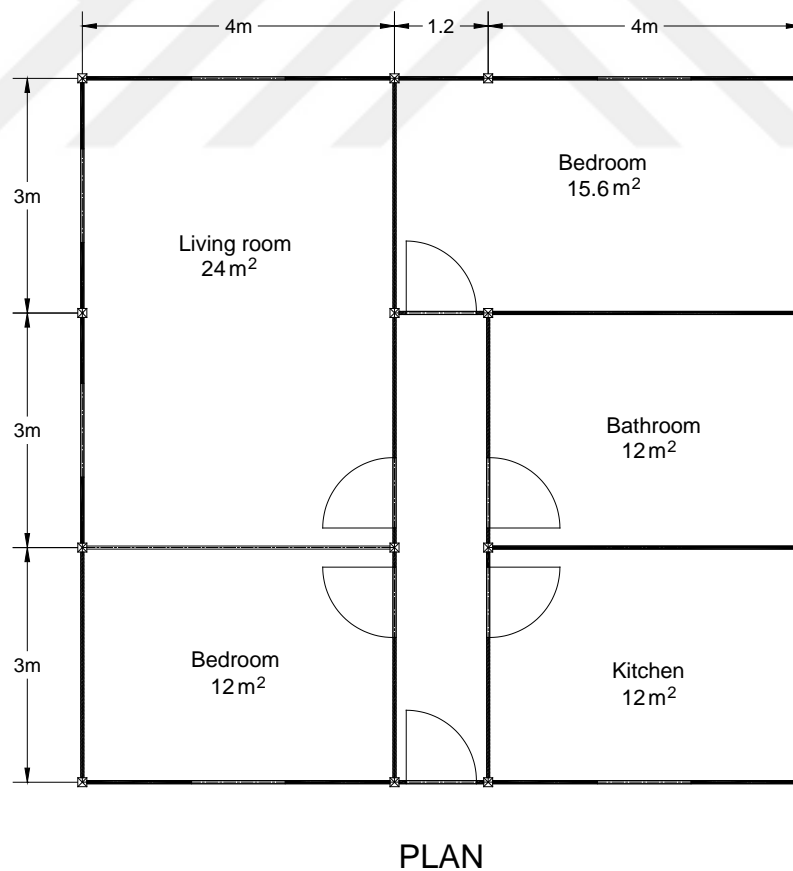
**Figure 5.14:** Equivalent lateral force compared to pushover curves of the 140 mm beam racks.

Figure 5.12, Figure 5.13 and Figure 5.14 show that the equivalent lateral force didn't exceed the ultimate or yielding force of the pushover curves.

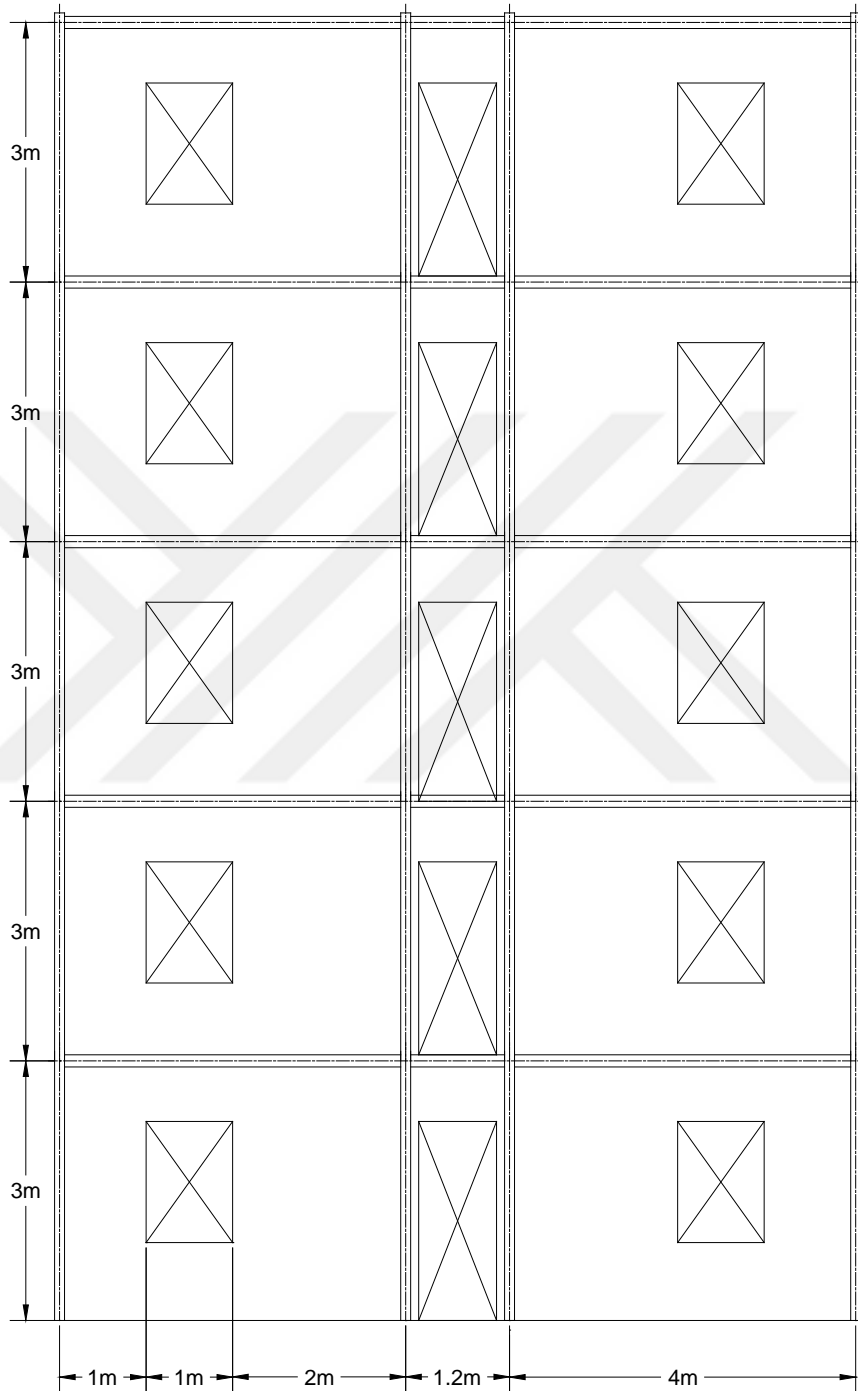
## 6. USAGE OF RACK MEMBERS IN RESIDENTIAL STRUCTURES

Rack members have a lot of advantages, such as their light weight, their fast construction duration and their ability to carry high loads compared to their weight. In this chapter, the rack cross-sections used in the experimental study will be checked if they can be used in constructing a residential structure.

SAP2000 was used to model a 5 story residential building on a base area of  $82.8 \text{ m}^2$  with the dimensions given in Figure 6.1. Beside using the rack members for the columns and the beams, plywood was used for the slabs and the walls of the building. The architectural and the structural plan and elevation for the residential building are shown in Figure 6.1, Figure 6.2, Figure 6.3 and Figure 6.4, while the details of the beam-column connection is shown in Figure 6.5.

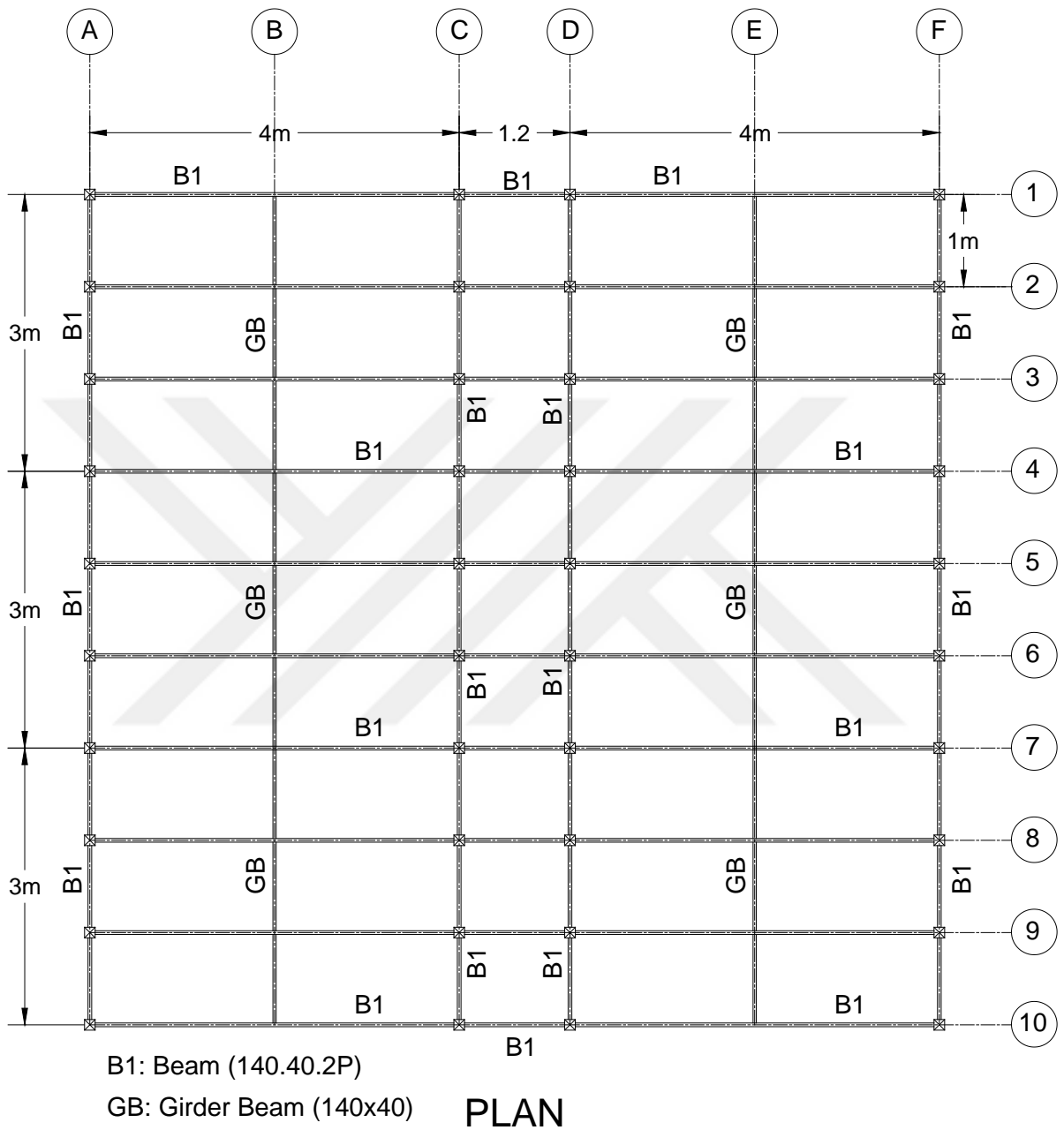


**Figure 6.1:** The architectural plan of the residential structure.

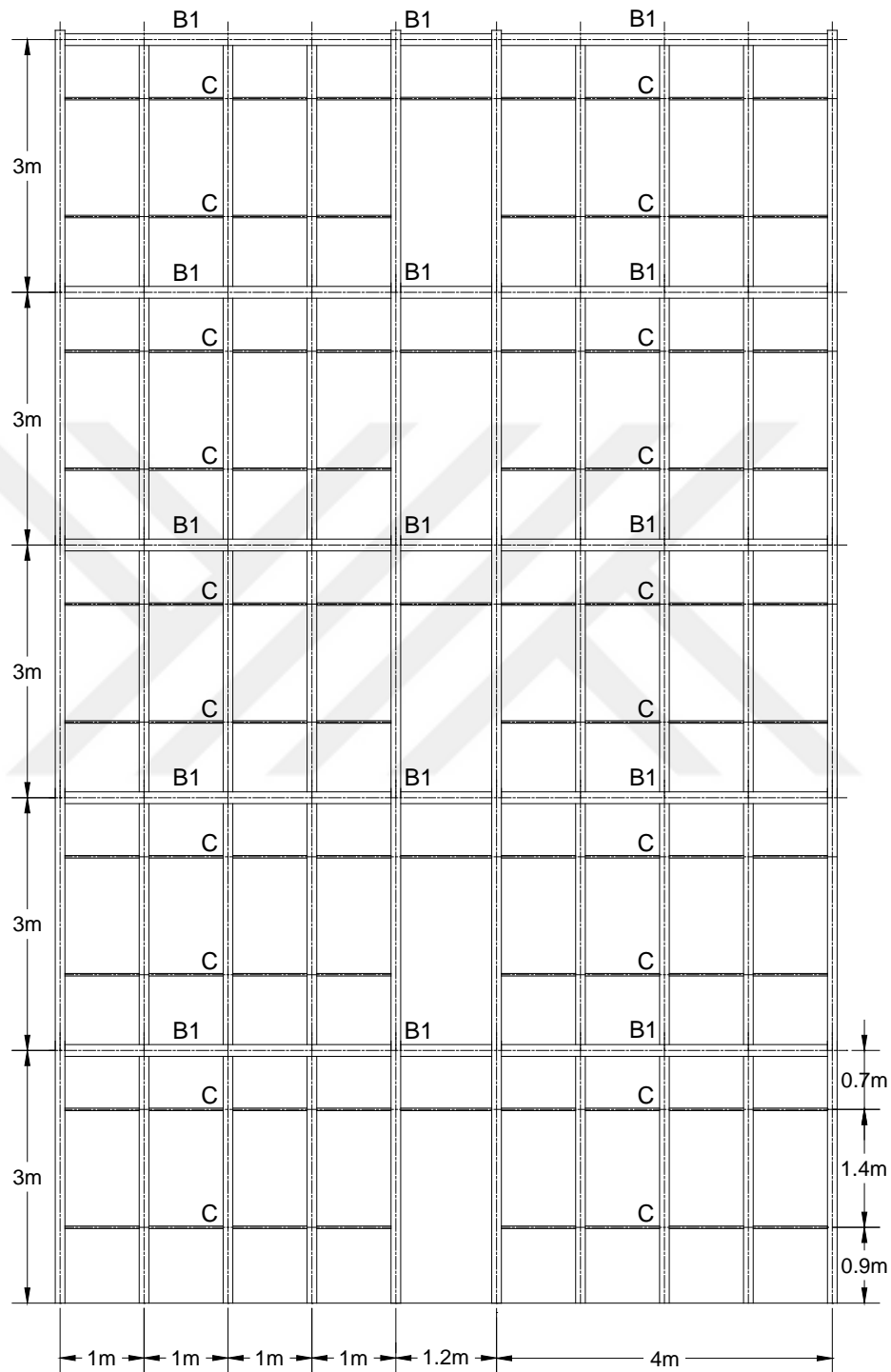


## ELEVATION

**Figure 6.2:** The architectural elevation of the residential structure.



**Figure 6.3:** The structural plan of the residential structure.



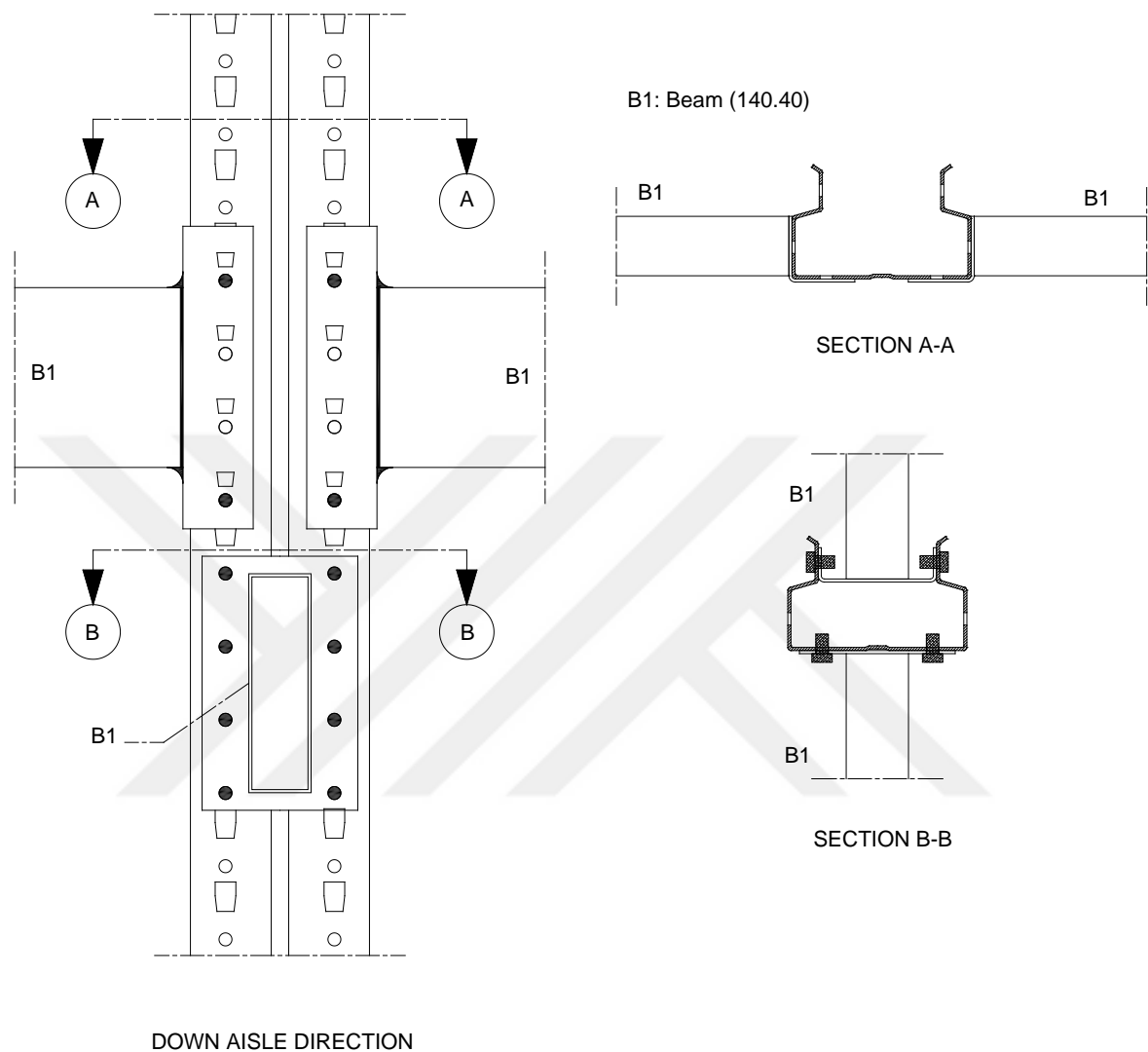
B1: Beam (140.40.2P)

C: C-section Bracing (35x35)

## ELEVATION

**Figure 6.4:** The structural plan and elevation of the residential structure.





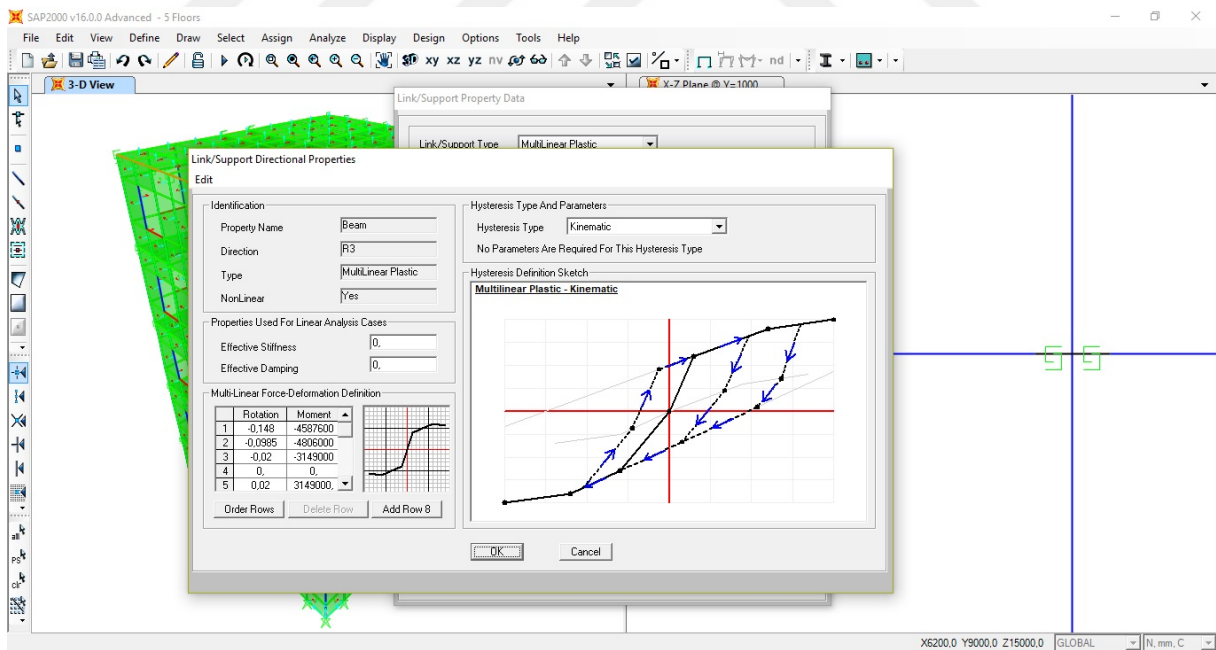
**Figure 6.5:** Details of the beam-to column direction in the down-aisle direction.

The exact dimensions of the rack column are defined to the SAP2000 model using the section designer menu as shown in Figure 6.6.

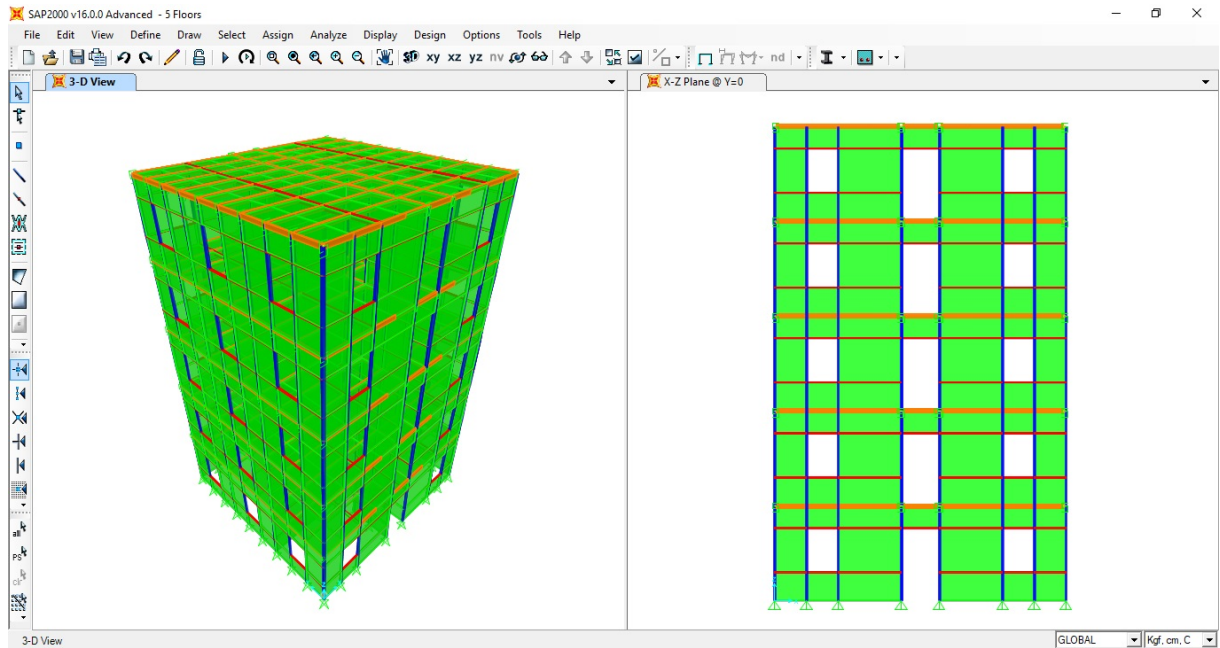
The behavior of the beam-to-column connections used in the rack members are defined to SAP2000 model by defining links between the beam and the columns and by inserting the moment rotation results obtained from experimental study performed on the rack beam-to-column connection as shown in Figure 6.7.



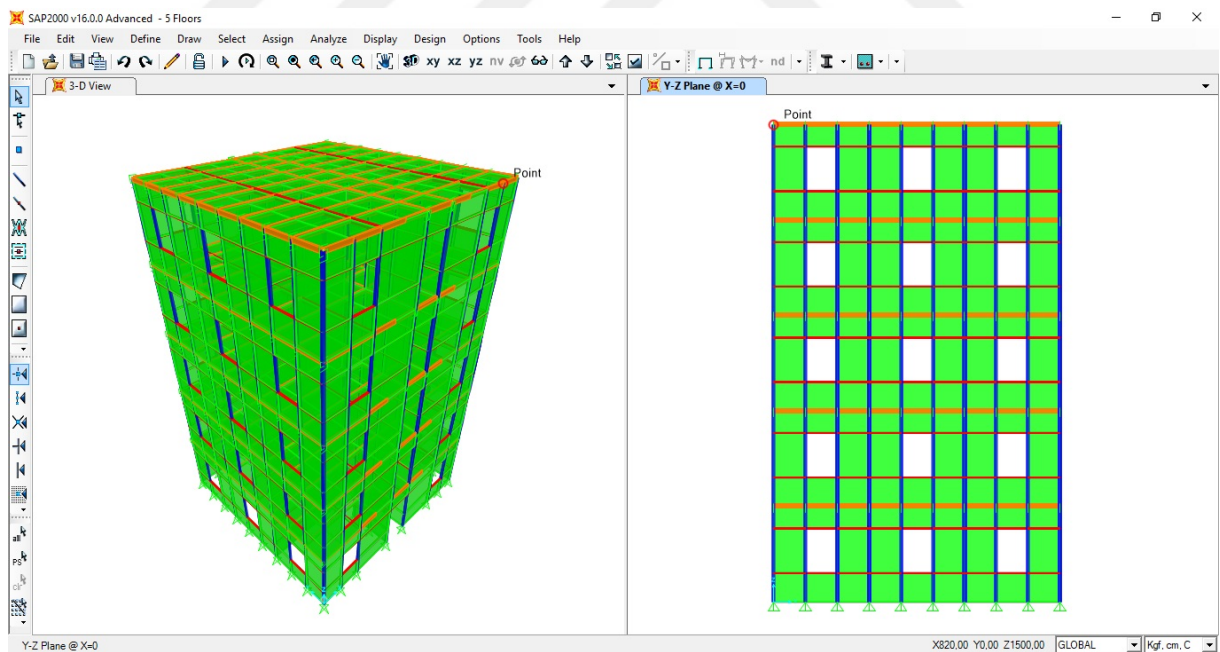
**Figure 6.6:** Defining the dimensions of the column using the section designer menu in SAP2000.



**Figure 6.7:** Defining the moment rotation experimental results to the beam-to-column connection in SAP2000.



**Figure 6.8:** SAP2000 model for 5 stories residential building using rack members (3D and X-Z view).



**Figure 6.9:** SAP2000 model for 5 stories residential building using rack members. (3D and Y-Z view).

Before assessing the performance of the beam-to-column connection under the effect of seismic loads, it is a must to assess the stability of the structure under the vertical loads too.

In order to check the stability of the columns, it is necessary to obtain the axial load capacity of the columns, which will be described in details in the following section.

### 6.1. CALCULATIONS OF THE AXIAL LOAD CAPACITY OF THE COLUMN

The calculation in this section are done according to the equations stated in the north American specification for the design of cold-formed steel structural members by the American iron and steel institute AISI.

The nominal axial strength ( $P_n$ ) shall be the minimum of the nominal axial strength for flexural, torsional or flexural-torsional buckling ( $P_{ne}$ ), the nominal axial strength for local buckling ( $P_{nl}$ ) and the nominal axial strength for distortional buckling ( $P_{nd}$ ).

In order to calculate the nominal axial strength for flexural, torsional or flexural-torsional buckling ( $P_{ne}$ ), the nominal axial strength for local buckling ( $P_{nl}$ ) and the nominal axial strength for distortional buckling ( $P_{nd}$ ), it is necessary to find the critical elastic column buckling load in flexural, torsional or flexural-torsional buckling ( $P_{cre}$ ), the critical elastic local column buckling load ( $P_{crl}$ ), and the critical elastic distortional column buckling load ( $P_{crd}$ ).

CUFSM software program was developed by Ben Schafer's thin-walled structures research group in Johns Hopkins university and its used to determine both, the critical elastic local column buckling load ( $P_{crl}$ ), and the critical elastic distortional column buckling load ( $P_{crd}$ ).

CUFSM is a software program that uses the finite strip method in its calculations. The exact column dimensions and material were inserted to the program as a series of longitudinal strips or elements, and based on these strips elastic and geometric stiffness matrices can be formulated. CUFSM helps to obtain a signature curve for the cross sections from which the critical buckling loads can be obtained, and it plots the estimated buckling shape. Figure 6.10 shows the input page of CUFSM program, while Figure 6.11 shows the signature curve for the column and a plot for the local buckling failure mode. The distortional buckling failure mode is shown in Figure 6.12.

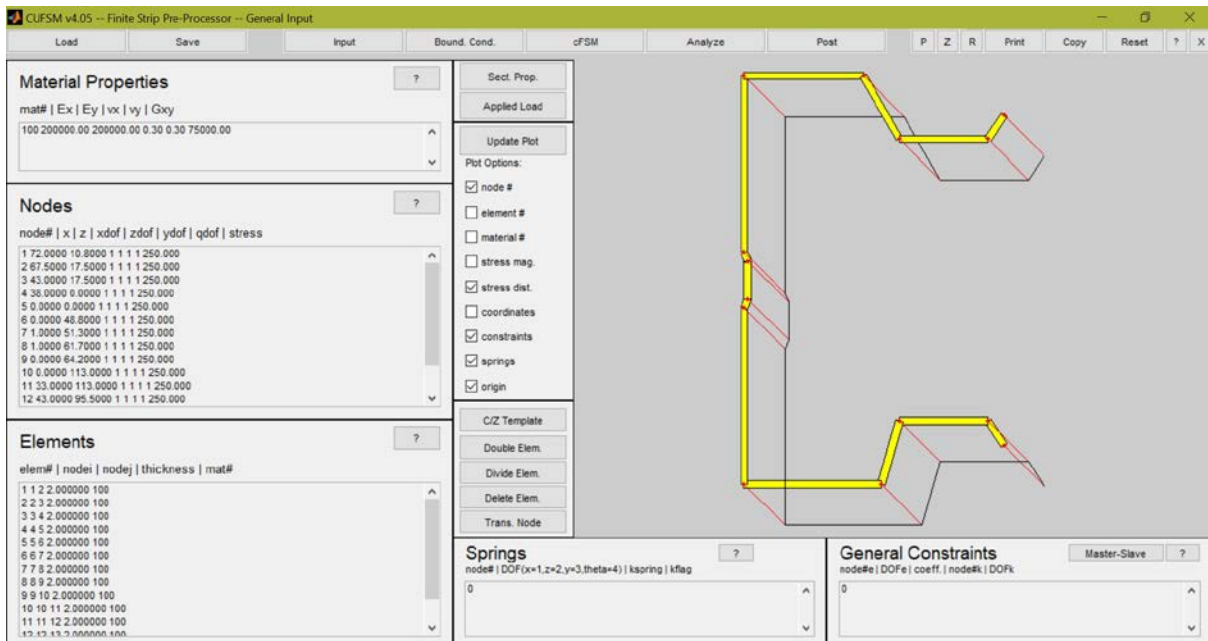


Figure 6.10: Input page on CUFSM program.

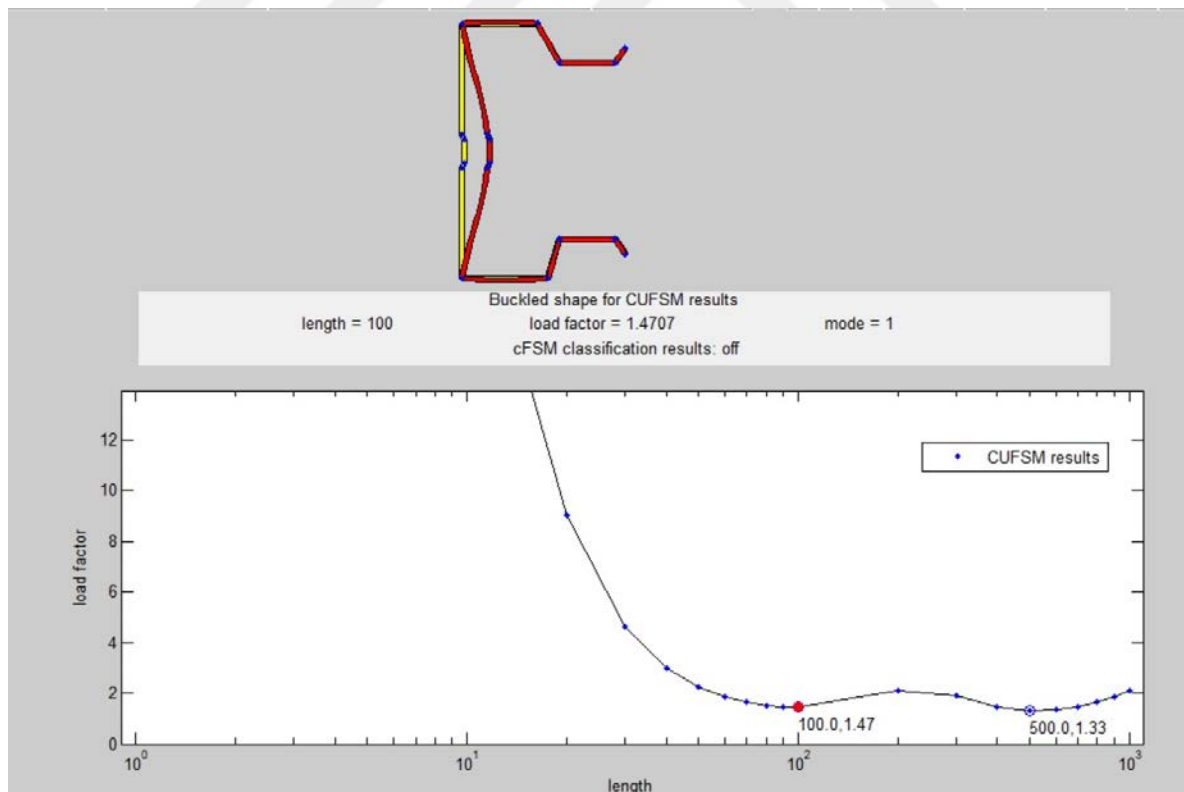
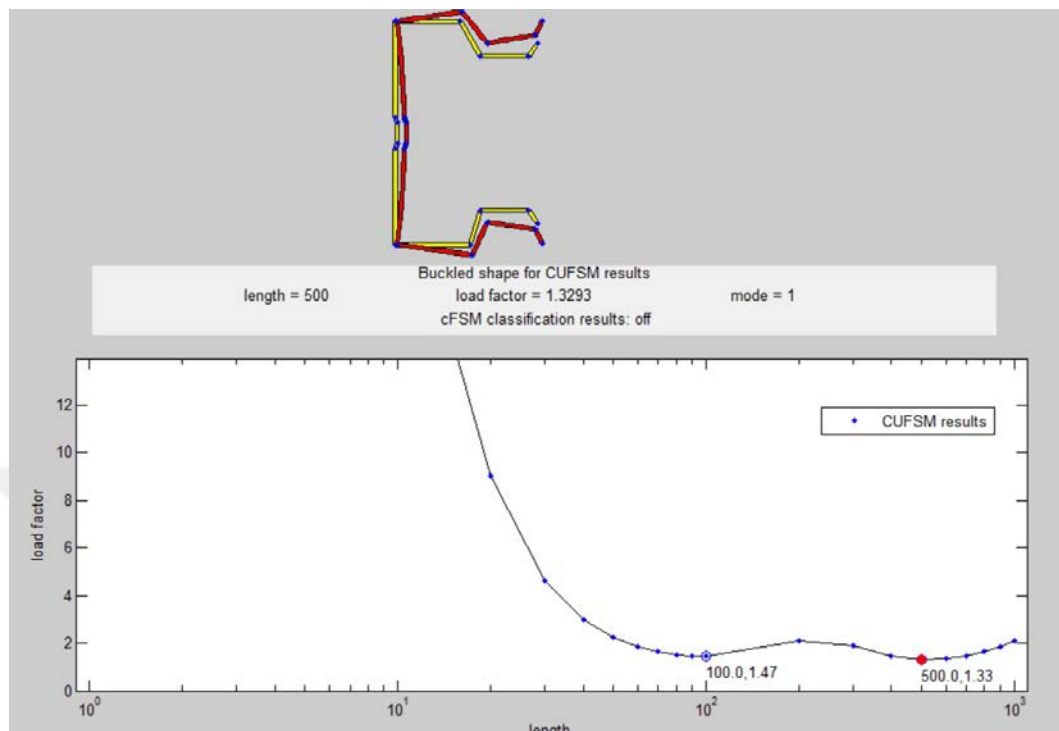


Figure 6.11: The signature curve and the plot for the local buckling failure mode in CUFSM.



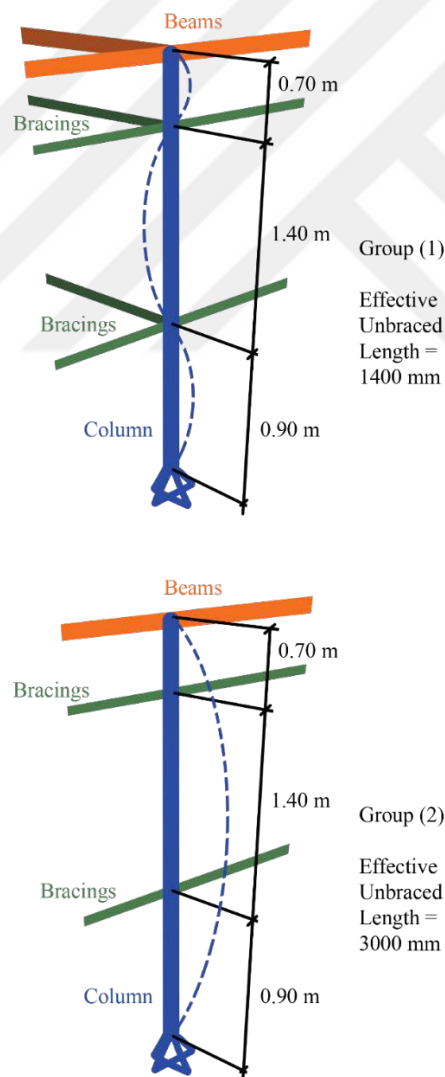
**Figure 6.12:** The signature curve and the plot for the distortional buckling failure mode in CUFSM.

From CUFSM results, it was obtained that the critical elastic local column buckling load ( $P_{cri}$ ) = 211.7 kN, and the critical elastic distortional column buckling load ( $P_{crd}$ ) = 191.3 kN.

On the other hand, another program was developed by Ben Schafer's thin-walled structures research group in Johns Hopkins university which is called CUTWP, and it is used for the global buckling analysis (flexural-torsional, lateral-torsional, etc.). CUTWP software is the method used in this thesis in order to find the critical elastic column buckling load in flexural, torsional or flexural-torsional buckling ( $P_{cre}$ ), and the results are accompanied by a plot for the buckling shape as shown in Figure 6.14 and Figure 6.15.

The calculation of the critical elastic column buckling load in flexural, torsional or flexural-torsional buckling depends on the effective unbraced length of the column. The columns were divide into two groups. The first group is the for the columns in the corners of the rooms, in which the effective unbraced length was taken as 1400 mm in both of the in-plan and out-plan representing the height of the window, due to the existence of bracings in both of the out-plan

and in-plan directions as shown in Figure 6.13. The second column group has braces in one direction only, as a result of that, the effective unbraced length was considered as 1400 mm in the in-plan direction and 3000 mm in the out-plan direction, which is the length of the entire column as shown in Figure 6.13. The exact column dimensions and material were inserted to the CUTWP program as shown in Figure 6.14 and Figure 6.15. The critical elastic column buckling load in flexural, torsional or flexural-torsional buckling was calculated as  $(P_{cre}) = 200.49 \text{ kN}$  for the first group of columns as shown in Figure 6.14, and as  $(P_{cre}) = 132.1 \text{ kN}$  for the second group of columns as shown in Figure 6.15.



**Figure 6.13:** The effective unbraced length of the columns in both of group (1) and (2).

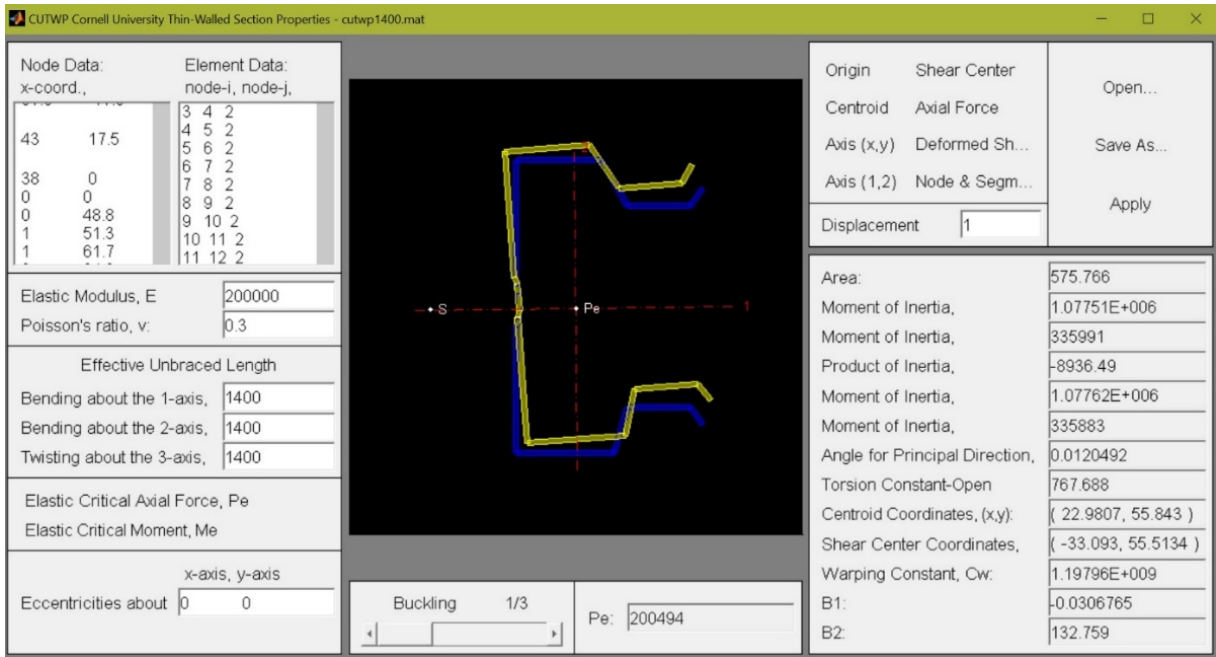


Figure 6.14: CUTWP input and result page with a plot for the flexural-torsional buckling failure mode of the first group of columns.

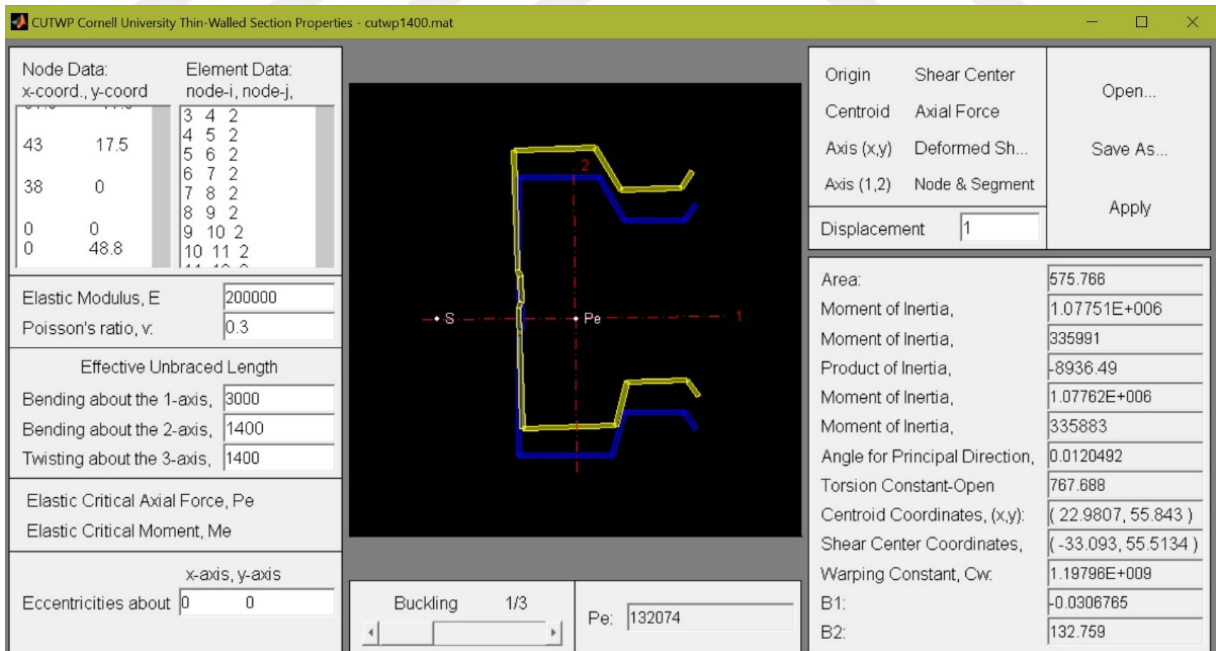


Figure 6.15: CUTWP input and result page with a plot for the flexural-torsional buckling failure mode of the second group of columns.



### 6.1.1 Flexural, Torsional, or Flexural-Torsional Buckling

The nominal axial strength for flexural, torsional or flexural-torsional buckling ( $P_{ne}$ ), is calculated in accordance with Equations (6-1)-(6-4) given in American Iron Steel Institute standard AISI (2007). In these equations  $\lambda_c$  represents the slenderness factor,  $P_{cre}$  is the minimum of the critical elastic column buckling load in flexural, torsional, or flexural-torsional buckling obtained from CUTWP software and  $P_y$  represents the member yield strength calculated according to Eq. (6-4) where  $A_g$  is the gross area of the section and  $F_y$  is the yield stress of the column material.

(a) For  $\lambda_c \leq 1.5$

$$P_{ne} = (0.658^{\lambda_c^2})P_y \quad (6.1)$$

(b) For  $\lambda_c > 1.5$

$$P_{ne} = \left( \frac{0.877}{\lambda_c^2} \right) P_y \quad (6.2)$$

$$\lambda_c = \sqrt{P_y/P_{cre}} \quad (6.3)$$

$$P_y = A_g F_y \quad (6.4)$$

### 6.1.2 Local Buckling

The nominal axial strength for local buckling ( $P_{nl}$ ), is calculated in accordance with Equations (6.5)-(6.7) from the American Iron Steel Institute standard AISI (2007), In these equations  $\lambda_l$  represents the slenderness factor,  $P_{crl}$  is the critical local column buckling load obtained from CUFSM software while  $P_{ne}$  is obtained from Section 6.1.1.

(a) For  $\lambda_l \leq 0.776$

$$P_{nl} = P_{ne} \quad (6.5)$$

(b) For  $\lambda_l > 0.776$

$$P_{nl} = \left[ 1 - 0.15 \left( \frac{P_{crl}}{P_{ne}} \right)^{0.4} \right] \left( \frac{P_{crl}}{P_{ne}} \right)^{0.4} P_{ne} \quad (6.6)$$

where

$$\lambda_l = \sqrt{P_{ne}/P_{crl}} \quad (6.7)$$

### 6.1.3 Distortional Buckling

The nominal axial strength for distortional buckling ( $P_{nd}$ ), is calculated in accordance with Equations (6.8)-(6.10) from the American Iron Steel Institute standard AISI (2007), In these equations  $\lambda_d$  represents the slenderness factor,  $P_{crd}$  is the critical distortional column buckling load obtained from CUFSM software while  $P_y$  is calculated using Equation (6.4).

(a) For  $\lambda_d \leq 0.561$

$$P_{nd} = P_y \quad (6.8)$$

(b) For  $\lambda_d > 0.561$

$$P_{nd} = \left[ 1 - 0.25 \left( \frac{P_{crd}}{P_y} \right)^{0.6} \right] \left( \frac{P_{crd}}{P_y} \right)^{0.6} P_y \quad (6.9)$$

where

$$\lambda_d = \sqrt{P_y/P_{crd}} \quad (6.10)$$

According to the Equations (6.1)-(6.10), the results for the first group of columns were

$$P_{ne1} = 106.58 \text{ kN}, P_{nl1} = 106.58 \text{ kN} \text{ and } P_{nd1} = 120.1 \text{ kN}$$

While the results for the second group of columns were,

$$P_{ne2} = 91.22 \text{ kN}, P_{nl2} = 91.22 \text{ kN} \text{ and } P_{nd2} = 120.1 \text{ kN}$$

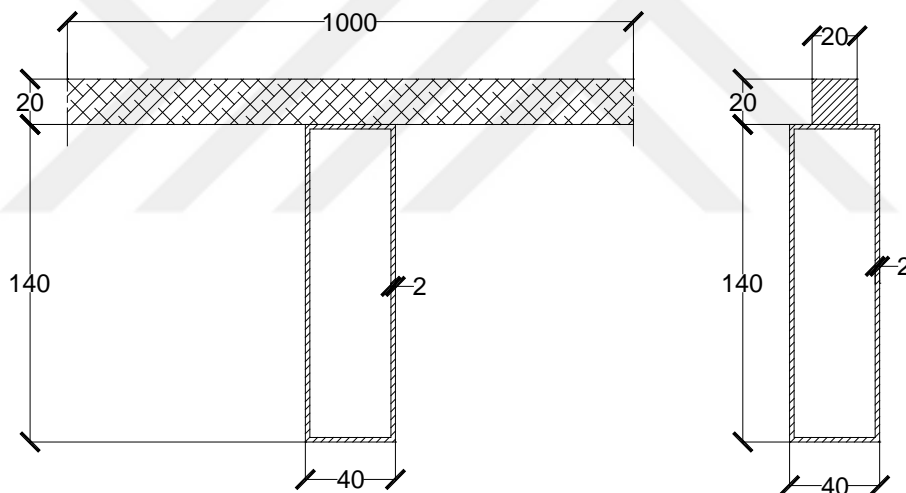
While the nominal axial strength ( $P_n$ ) shall be the minimum of the nominal axial strength for flexural, torsional or flexural-torsional buckling ( $P_{ne}$ ), the nominal axial strength for local buckling ( $P_{nl}$ ) and the nominal axial strength for distortional buckling ( $P_{nd}$ ).

From the previous results it was obtained the nominal axial strength ( $P_{n1}$ ) of the first group of columns that are located at the corners of the rooms is  $P_{n1} = 106.58 \text{ kN}$  while the nominal axial strength ( $P_{n2}$ ) of the second group of columns  $P_{n2} = 91.22 \text{ kN}$

## 6.2. CALCULATIONS OF THE MOMENT CAPACITY OF THE BEAMS

In order to model the beams to behave as similar as possible to the reality, calculations for the moment of inertia of the composite section of both the 140.40 beam and the 1 m slab of plywood over it was carried out as shown in the steps below:

### 6.2.1 Moment Capacity Calculations of the Roof Slab Beams



**Figure 6.16:** Cross-section of the beam and the roof slab (dimensions in mm).

2 cm of plywood slab was used for the roofing, while the modulus of elasticity of plywood was taken as  $E_p = 4000 \text{ MP}_a$ , while the modulus of elasticity of steel  $E_s = 200000 \text{ MP}_a$ , and the modular ratio  $n$  was calculated as 0.02.

The width of the equivalent steel section to replace the plywood  $b = 1000 \times 0.02 = 20 \text{ mm}$ .

The moment of inertia of the steel beam  $I_b = 1600298.7 \text{ mm}^4$ .

The area of the steel beam  $A_b = 704 \text{ mm}^2$ .

The center of gravity of the built-up cross-section was calculated as follow,

$$y_1 = 99 \text{ mm}$$

The moment of inertia of the built-up cross-section was calculated as follow,

$$\begin{aligned} I_x &= 1600298.7 + (704)(99 - 70)^2 + \frac{1}{12}(20)(20)^3 + (20)(20)(150 - 99)^2 \\ &= 3246096 \text{ mm}^4 \end{aligned}$$

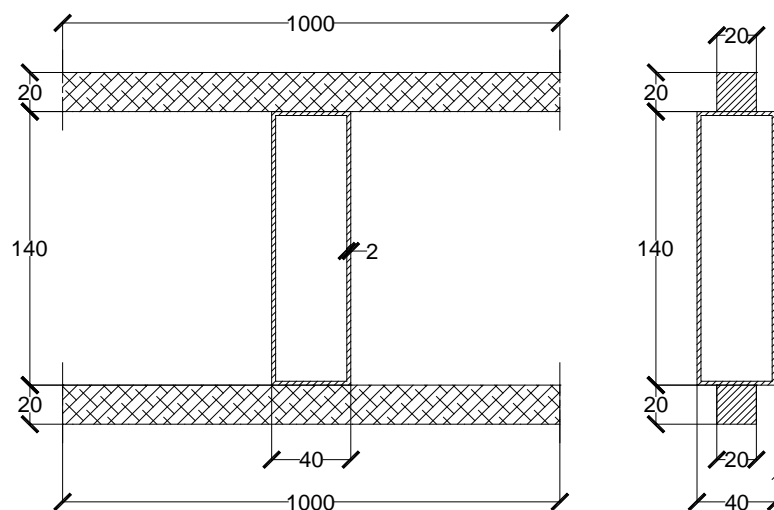
The property modifier that is used in SAP2000 model for the beams equals to  $\frac{I_x}{I_b} = 2.03$

The section modulus of the cross-section ( $S_x$ ) was calculated too in order to calculate the yielding moment ( $M_y$ ) of the cross-section.

$$S_x = \frac{I_x}{y_1} = 32788.85 \text{ mm}^3$$

$$M_y = F_y S_x = 8197212.5 \text{ N.mm} = 8.19 \text{ kN.m}$$

### 6.2.2 Moment Capacity Calculations of the Floor Slab Beams



**Figure 6.17:** Cross-section of the beam and the floor slabs (dimensions in mm).

4 cm of plywood slab was used for the roofing, while the modulus of elasticity of plywood was taken as  $E_p = 4000 MP_a$ , while the modulus of elasticity of steel  $E_s = 200000 MP_a$ , and the modular ratio  $n$  was calculated as 0.02.

The width of the equivalent steel section to replace the plywood.

$$b = 1000 \times 0.02 = 20 \text{ mm.}$$

The moment of inertia of the steel beam  $I_b = 1600298.7 \text{ mm}^4$ .

The area of the steel beam  $A_b = 704 \text{ mm}^2$ .

Determination of the center of gravity of the composite cross-section was calculated as follow,

$$y_1 = 90 \text{ mm.}$$

The moment of inertia of the built-up cross-section was calculated as follow,

$$I_x = 1600298.7 + 2 \left[ \frac{1}{12} (20)(20)^3 + (20)(20)(80)^2 \right] = 6746965.4 \text{ mm}^4$$

The property modifier that will be used in SAP2000 model for the beams equals to  $\frac{I_x}{I_b} = 4.21$

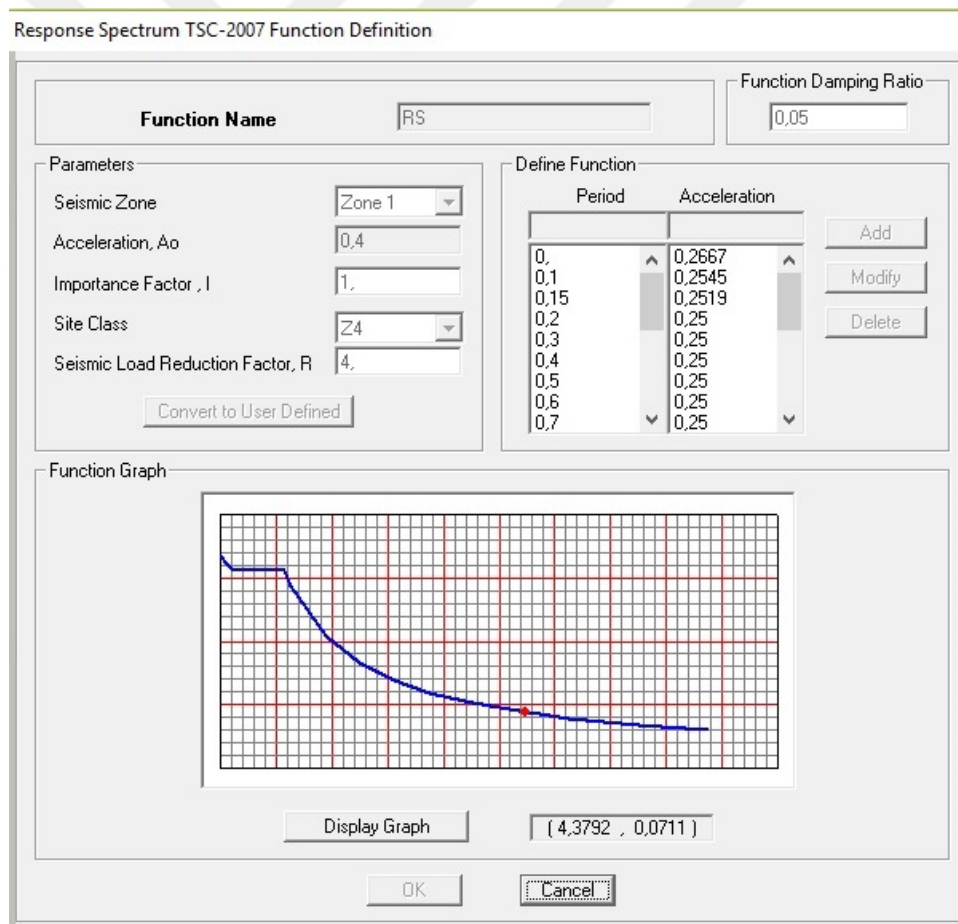
The section modulus of the cross-section ( $S_x$ ) was calculated too in order to calculate the yielding moment ( $M_y$ ) of the cross-section.

$$S_x = \frac{I_x}{y_1} = 74966.3 \text{ mm}^3$$

$$M_y = F_y S_x = 18741575 \text{ N.mm} = 18.74 \text{ kN.m}$$

### 6.3. SAP2000 INPUTS AND RESULTS

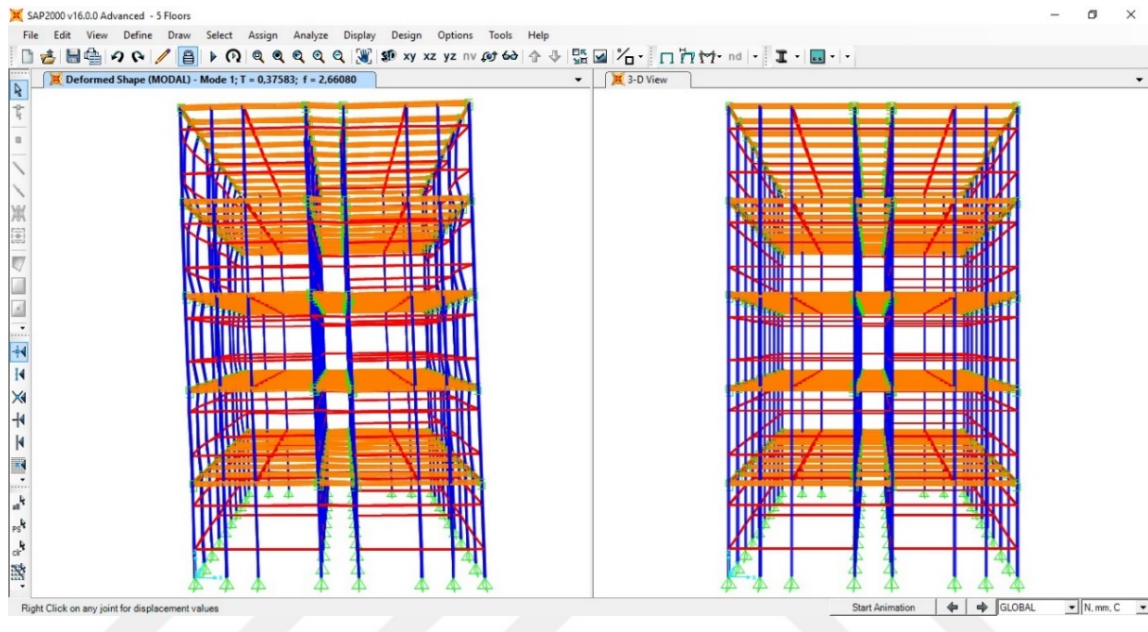
Several critical load cases were defined to the SAP2000 model such as Dead load, live load and snow load in order to check the safety of the structure under the effect of these load cases and the combinations of them. Beside the previously mention load cases, response spectrum earthquake analysis was carried out to check the effect of seismic loads on the residential building. The response spectrum parameters were inserted into SAP2000 according to the Turkish seismic code (TSC, 2007) as shown in Figure 6.18. The seismic zone was taken as Zone 1 with an acceleration of 0.4, the site class was taken as Z4 while the seismic load reduction factor R, was considered as 4 with an importance factor I=1.



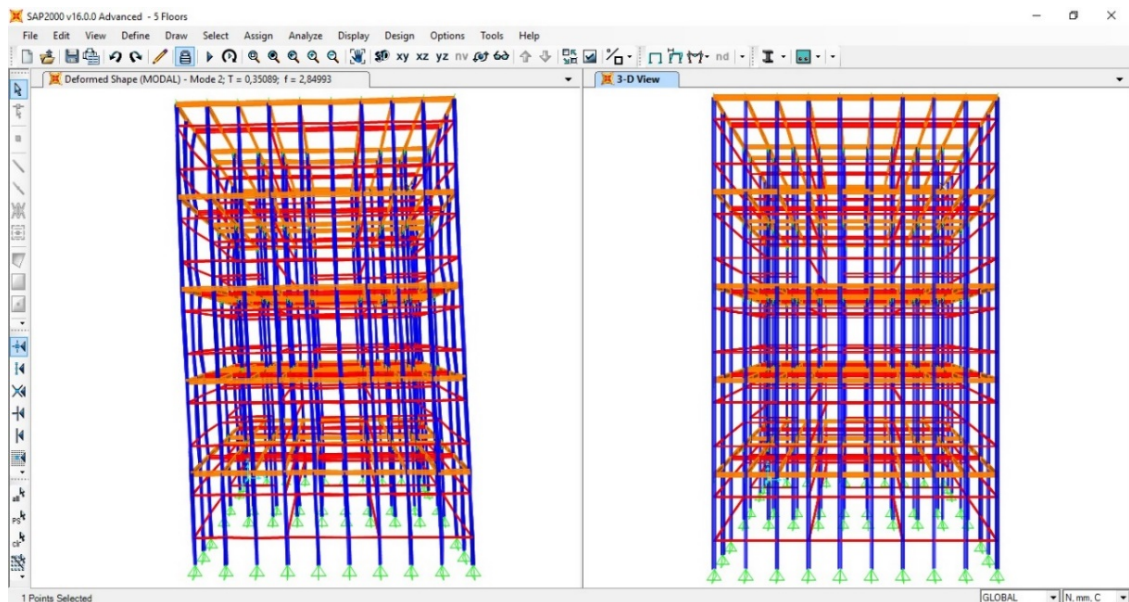
**Figure 6.18:** Response spectrum function definition into SAP2000 model.

The SAP2000 model analysis was performed and the three first modal shapes of the building were checked. It was found that the first modal shape was having a pure displacement in the X

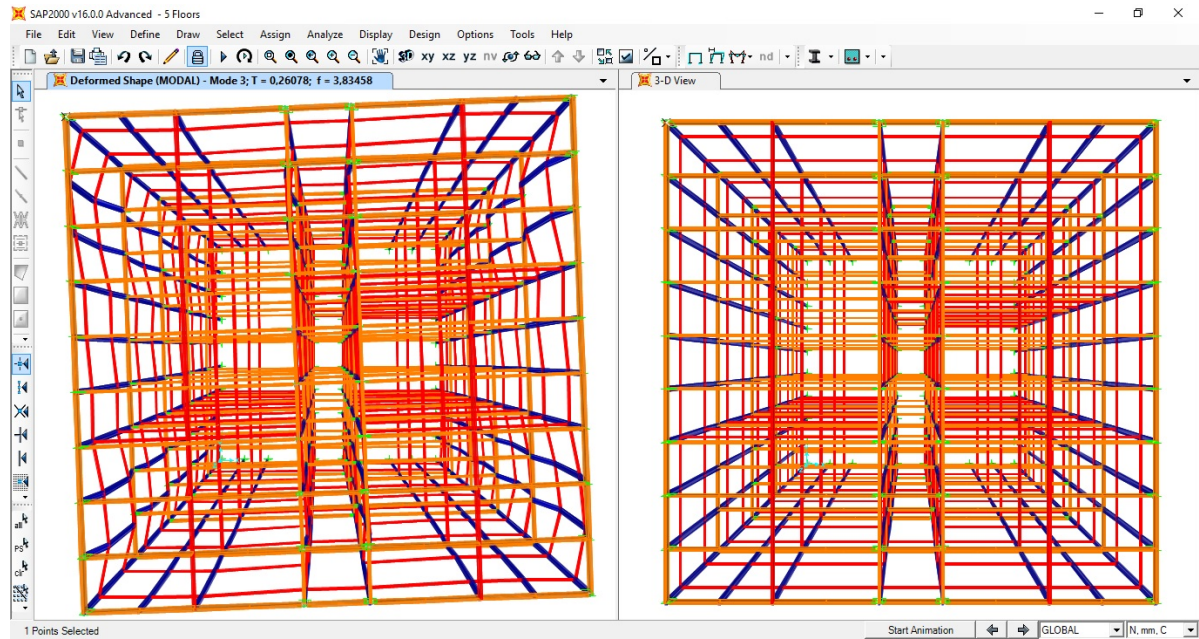
axis direction as shown in Figure 6.19, while the second modal shape was a pure displacement in the Y axis direction as shown in Figure 6.20, and the third modal shape was a torsional behavior around the Z axis as shown in Figure 6.21.



**Figure 6.19:** The first modal shape of the structure obtained from SAP2000 for the X-Z plan.



**Figure 6.20:** The second modal shape of the structure obtained from SAP2000 for the Y-Z plan.

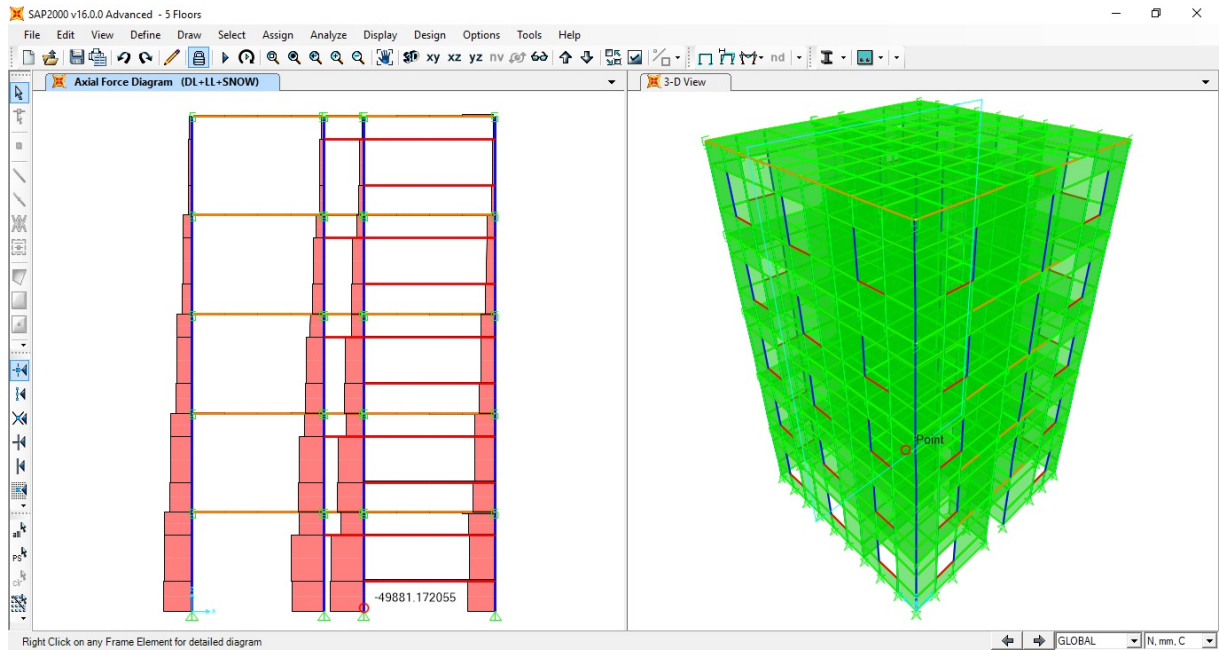


**Figure 6.21:** The third modal shape of the structure obtained from SAP2000 for the X-Y plan.

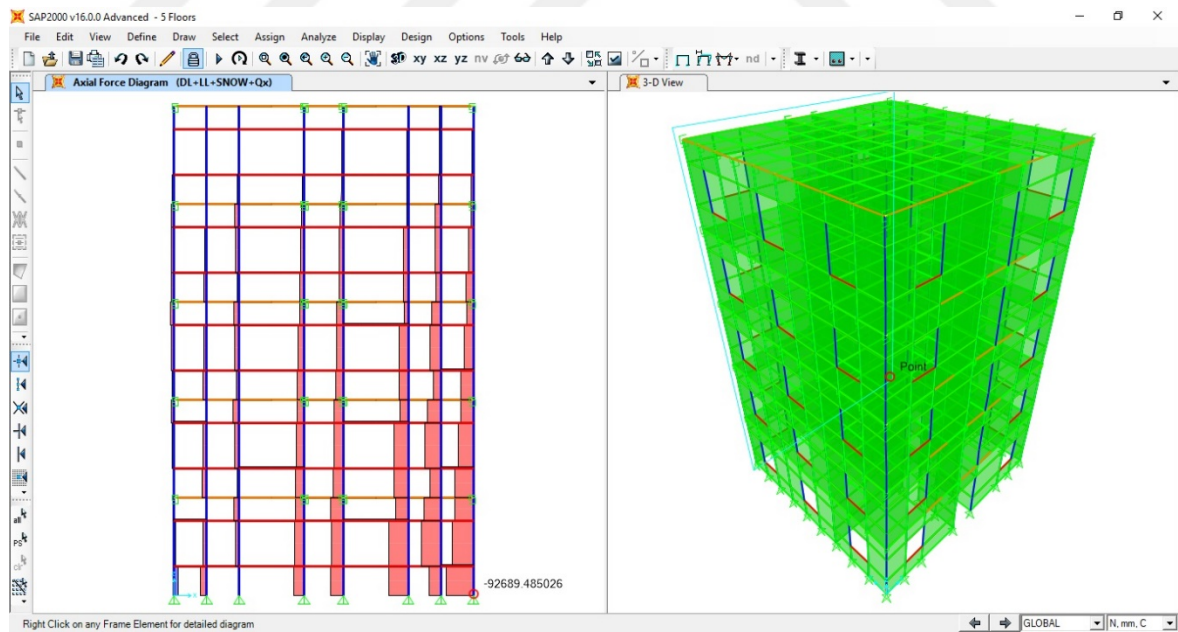
The axial load results on the columns were obtained to be compared to the nominal axial load that was calculated before. It was found that the maximum axial load on the column under the load combination of the dead load, live load and snow load occurs at column D-4 with a  $P_{max} = 49.89 \text{ kN}$  as shown in Figure 6.22, The maximum axial load for the first group of columns under the load combination of the dead load, live load, snow load and earthquake load occurs at column F-1 with a  $P_{max1} = 92.69 \text{ kN}$  as shown in

Figure 6.23, while the nominal axial load for the first group of columns,  $P_{n1} = 106.58 \text{ kN}$ . The maximum axial load for the second group of columns under the load combination of the dead load, live load, snow load and earthquake load occurs at column F-3 with a  $P_{max2} = 84.24 \text{ kN}$  as shown in Figure 6.24 while the nominal axial load for the second group of columns,  $P_{n2} = 91.2 \text{ kN}$ . The effect of the clamping of the column due to the existence of the wall was not taken into consideration while calculating the nominal axial load of the columns. By comparing the maximum axial load results obtained from SAP2000 and the nominal axial load of the column, the column is considered to be safe.

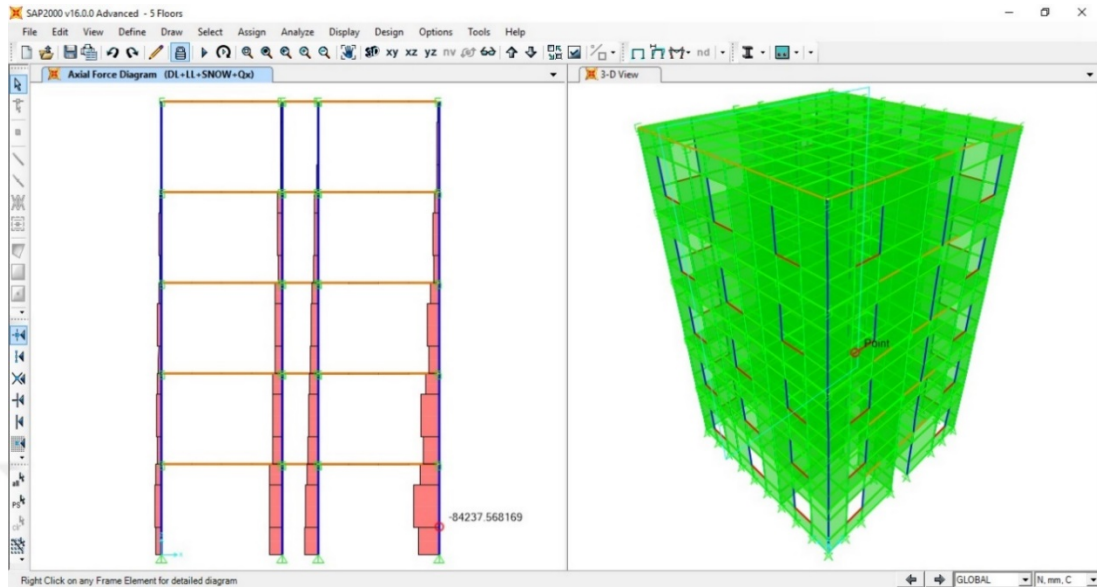




**Figure 6.22:** Maximum Axial load results for the columns from SAP2000 model under dead load, live load and snow load combination.

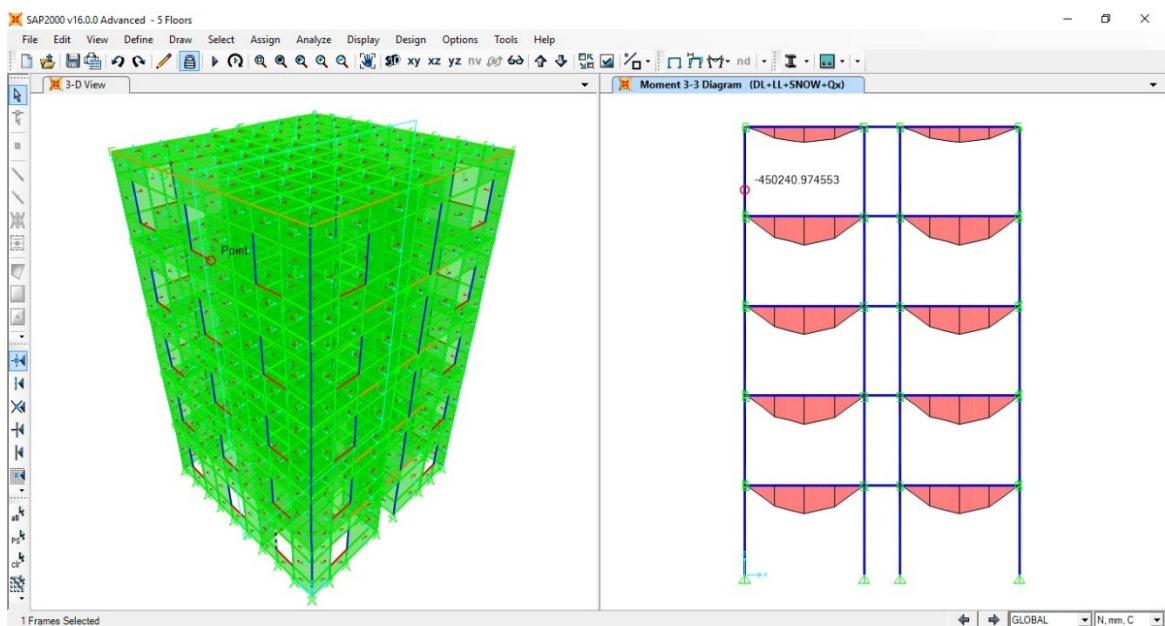


**Figure 6.23:** Maximum Axial load result for the columns from SAP2000 model under earthquake load, dead load, live load and snow load combination for the group (1) of columns.

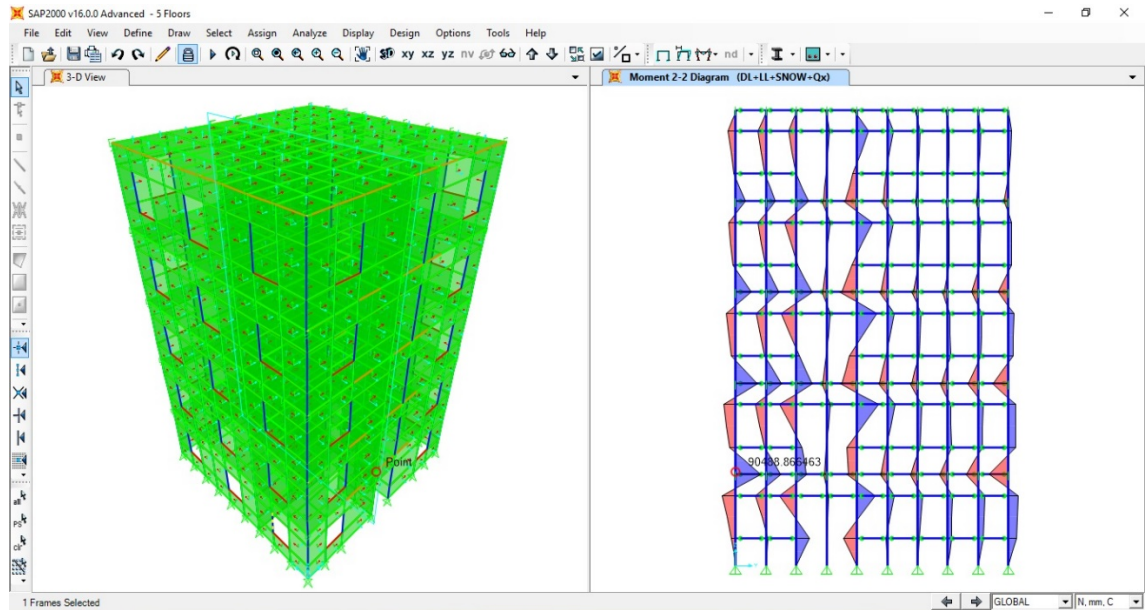


**Figure 6.24:** Maximum Axial load result for the columns from SAP2000 model under earthquake load, dead load, live load and snow load combination for group (2) of columns.

the maximum moments occurred during the seismic loads on the columns were checked. It was found that the maximum moments  $M_{3-3\ max} = 0.45\ kN.m$  at column A-6 and  $M_{2-2\ max} = 0.09\ kN.m$  at column C-10, while the maximum moment capacity of the column  $M_y = 4.69\ kN.m$ . as shown in Figure 6.25 and Figure 6.26.

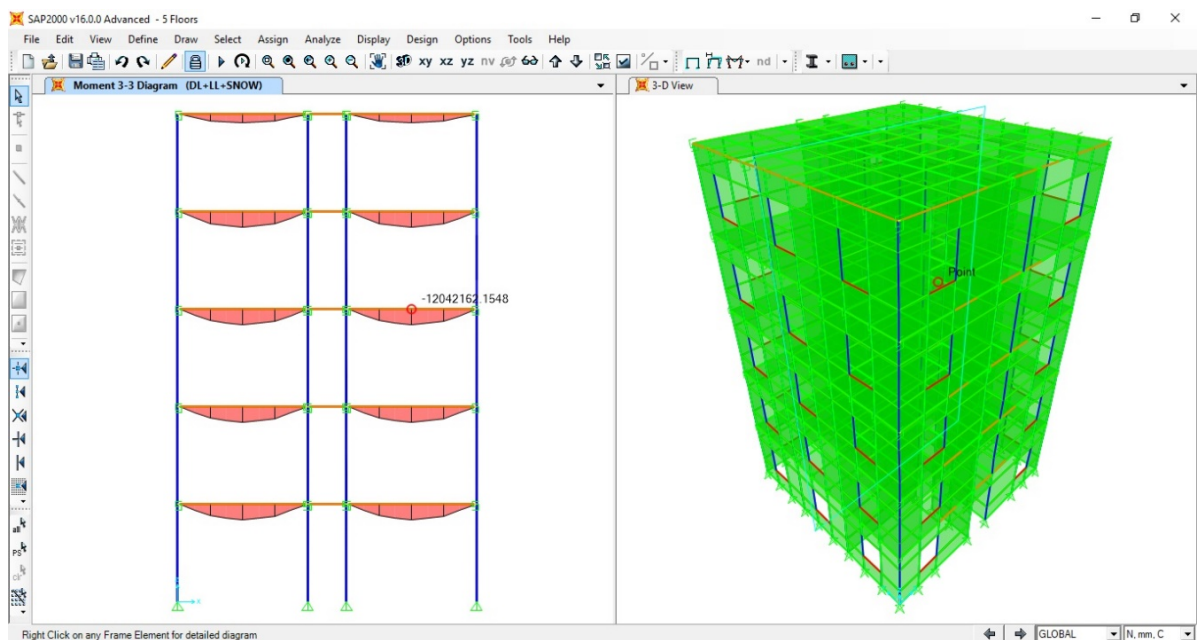


**Figure 6.25:** Maximum M 3-3 moment result for the columns from SAP2000 model.



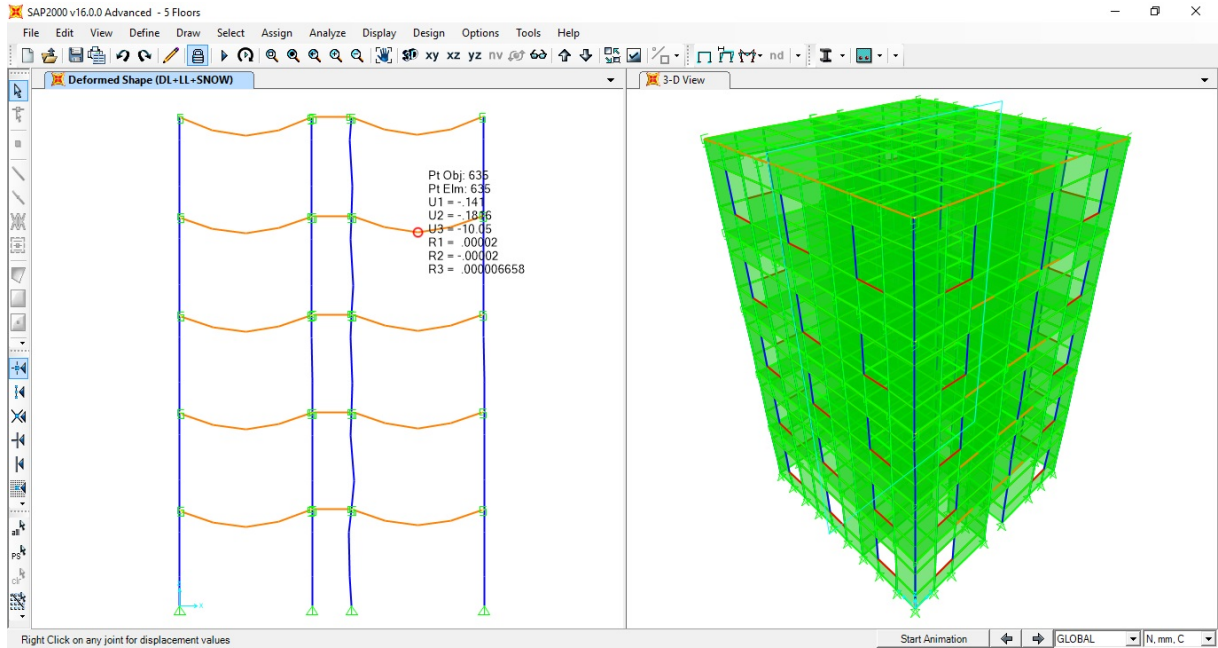
**Figure 6.26:** Maximum M 2-2 moment result for the columns from SAP2000 model.

The maximum moments of the beams were obtained, and it was found that the maximum moment,  $M_{max} = 12.04 \text{ kN.m}$  as shown in Figure 6.27, while the yield moment capacity of the beam cross-section was calculated before as  $M_y = 18.74 \text{ kN.m}$ , this shows that the beams are safe.



**Figure 6.27:** Moment results for the beams from SAP2000 model.

Additionally, the maximum deflection of the beams were checked from SAP2000 and it was found that the maximum deflection,  $\delta_{max} = 10.05 \text{ mm}$  as shown in Figure 6.28, while the allowable deflection of the beam  $\delta_{allow} = 13.33 \text{ mm}$ , this means that the beams are safe.

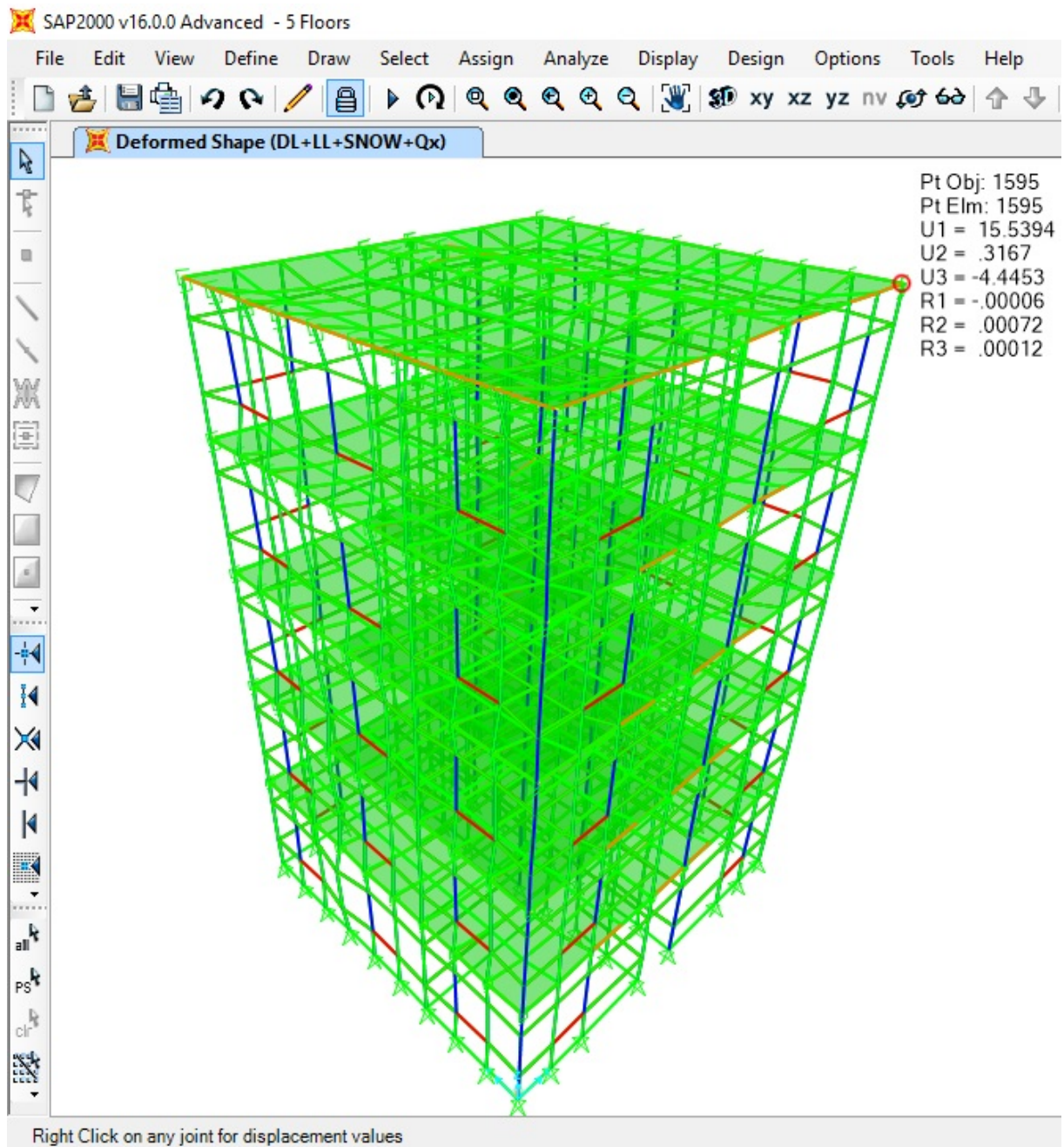


**Figure 6.28:** Maximum deflection of the beams from SAP2000 model.

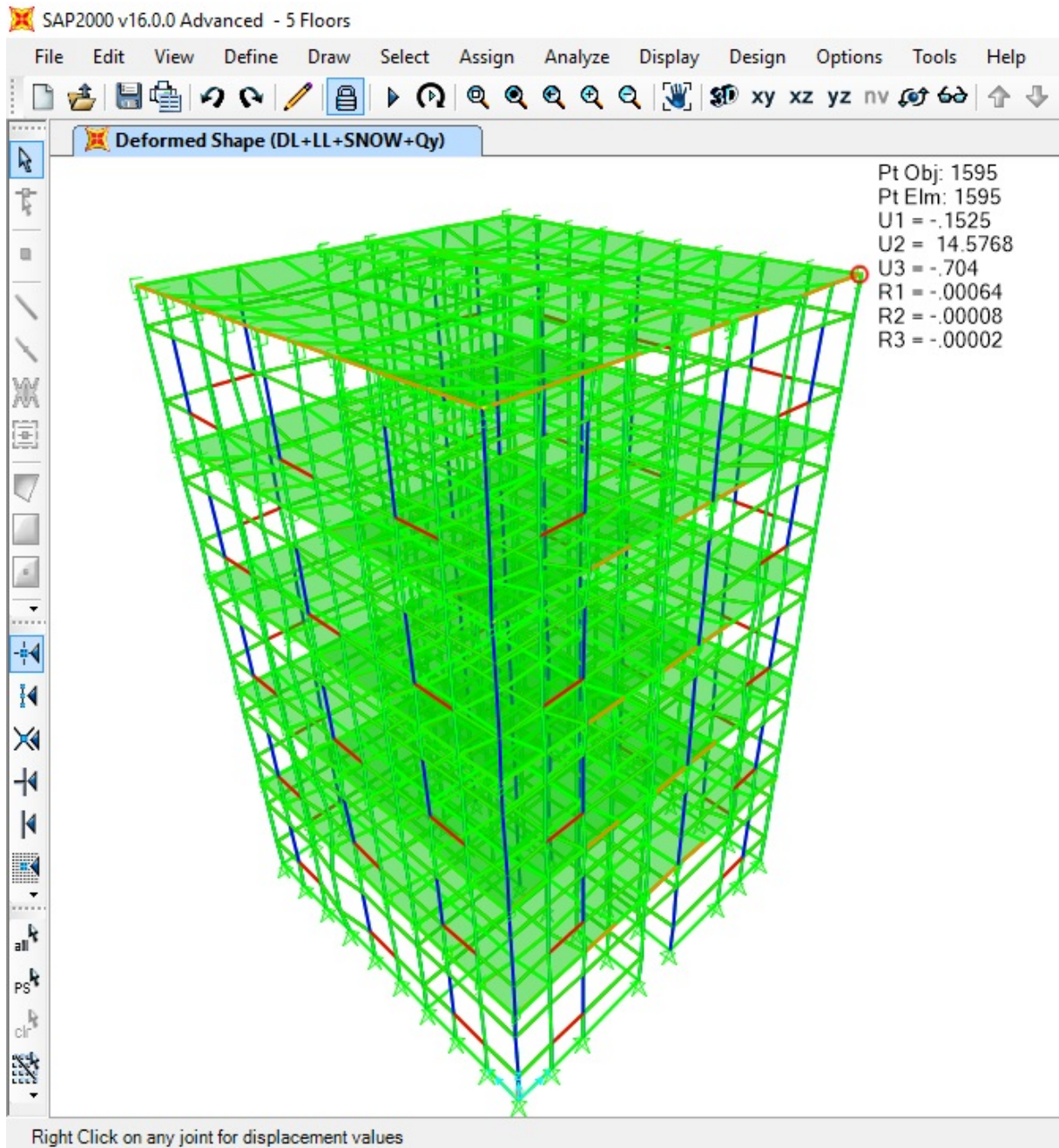
The deformed shape under the combination of dead loads, live loads, snow loads and earthquake loads was checked, and it was found that the maximum displacement occurred at the roof in X direction,  $D_x = 15.54 \text{ mm}$  as shown in Figure 6.29, while the maximum displacement occurred at the roof in Y direction,  $D_y = 14.58 \text{ mm}$ , as shown in Figure 6.30.

$$\delta_i = R\Delta_i / h_i \quad (6.11)$$

It is found that the maximum drift ratio  $\delta_i$  of the building equals to 0.004 calculated according to Equation (6.11) given in Turkish seismic code (TSC, 2007) which is smaller than the ultimate value 0.02, in which  $R$  is the reduction factor and taken as 4 while  $\Delta_i$ ,  $h_i$  are the maximum lateral displacement at top floor and the height of the building, respectively. Therefore, the building is considered safe according to the allowable drift ratio value.



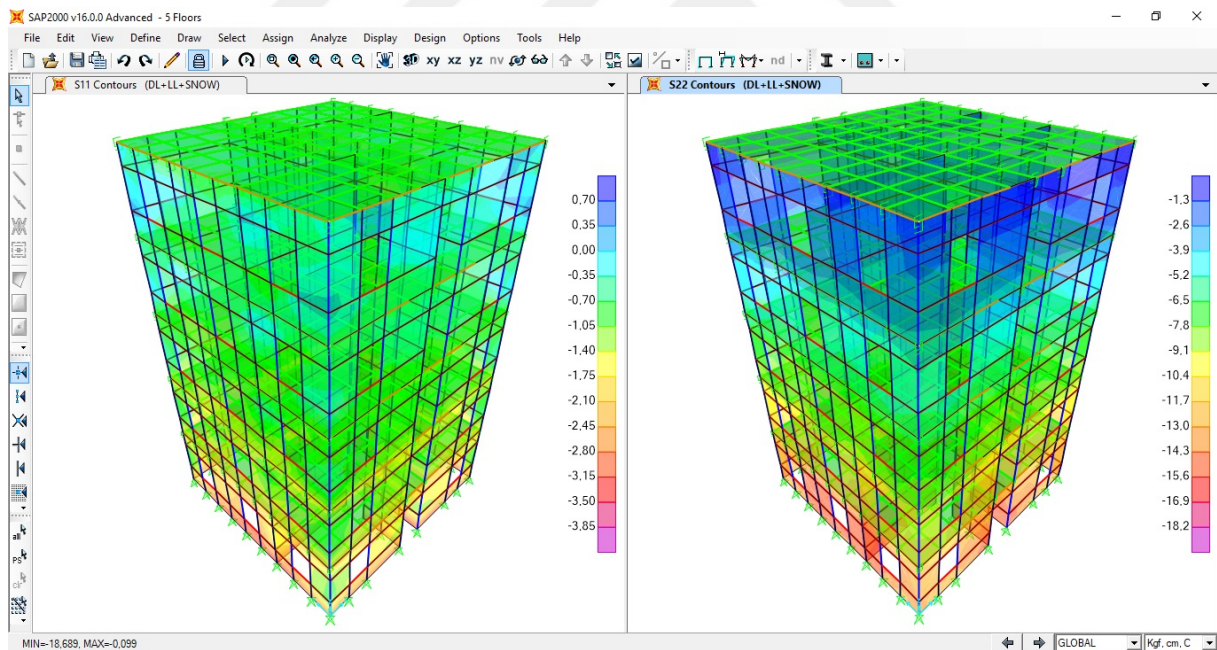
**Figure 6.29:** Maximum roof displacements due to seismic loads for the 5 stories building in the X direction.



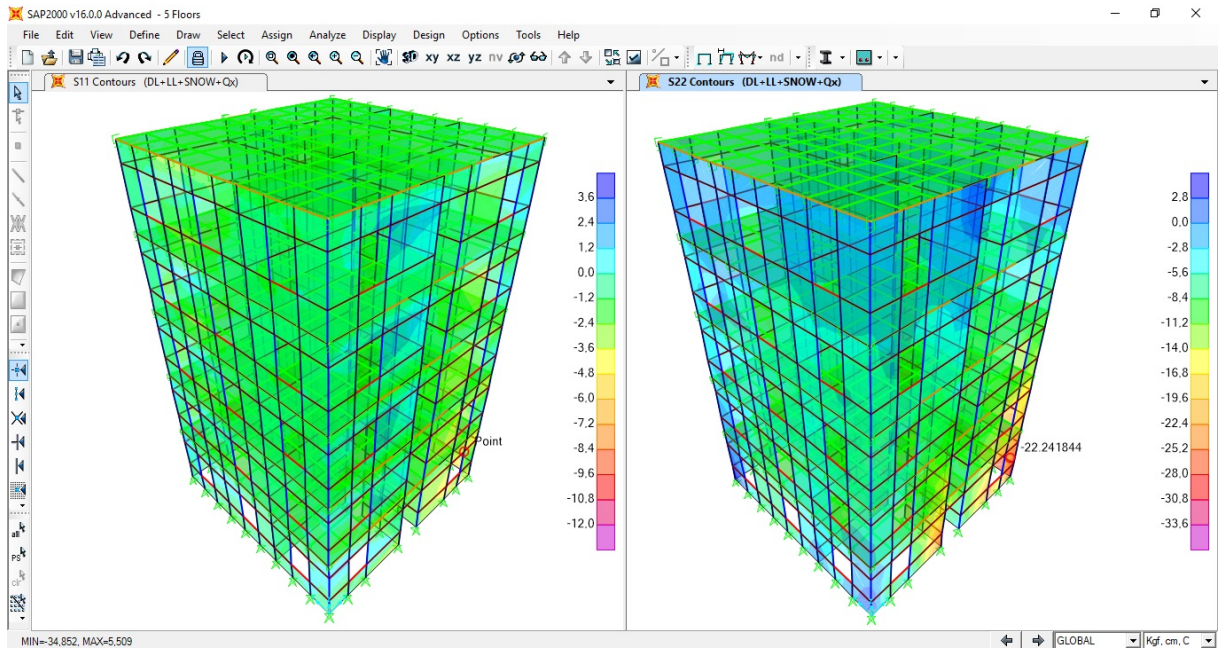
**Figure 6.30:** Maximum roof displacements due to seismic loads for the 5 stories building in the Y direction.

The plywood walls were defined in SAP2000 model using the area section defining menu as plane stress sections. In the figures below the horizontal S11 and vertical S22 stress distributions are shown under the different load combinations including the dead, live, snow and earthquake load cases in the both of the X and Y directions separately. It is clear from the

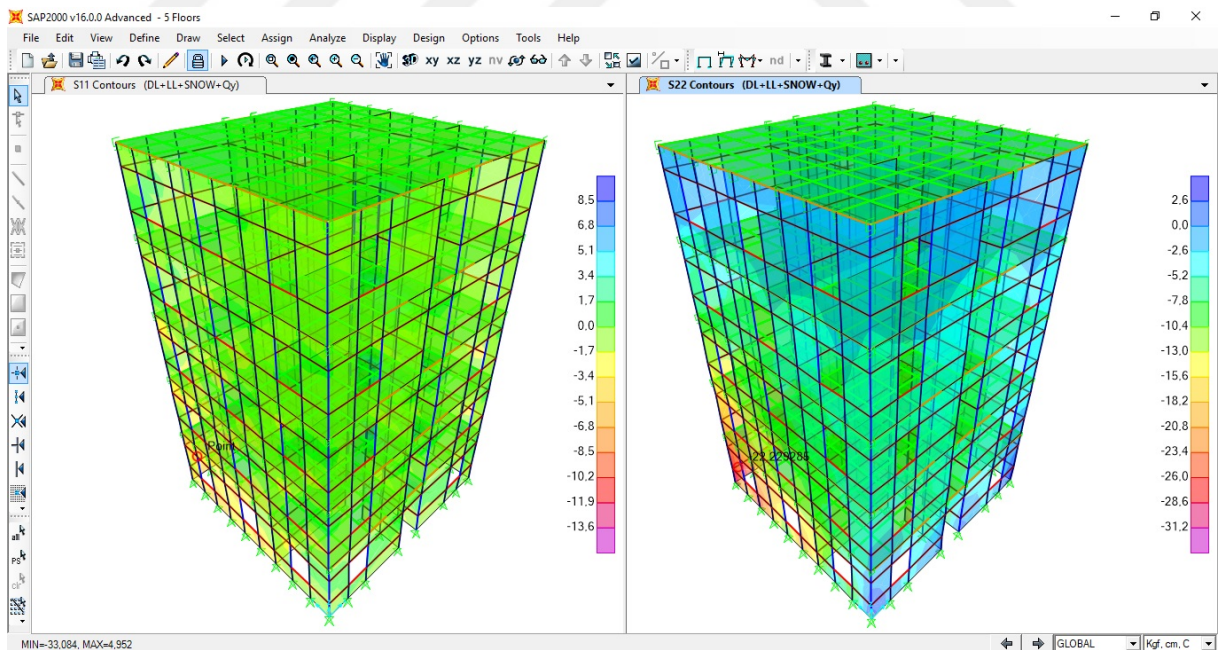
results that the S22 stress are higher than the S11 stresses in the three different load combinations. Under the dead, live and snow load combination the maximum achieved S22 stress is 1.82 MPa (18.2 kgf/cm<sup>2</sup>) as shown in figure 6.31, while under the dead, live, snow and earthquake in Y direction load combination the maximum achieved S22 stress is 3.12 MPa (31.2 kgf/cm<sup>2</sup>) as shown in figure 6.32, and under the dead, live, snow and earthquake in X direction load combination the maximum achieved S22 stress is 3.36 MPa (33.6 kgf/cm<sup>2</sup>) as shown in figure 6.33 which is the critical case. The plywood panels stress capacities are 8 MPa (80 kgf/cm<sup>2</sup>) in one direction and 4 MPa (40 kgf/cm<sup>2</sup>) in the other direction according to the Turkish Standard TS-647. According to that, the plywood panels are considered safe. But it is still preferable to install the panels while caring that the outer fiber direction of the panels be placed vertically, by that it will be guaranteed that the powerful direction of the panel will resist the higher S22 stresses.



**Figure 6.31:** The S11 and S22 stress distributions on the walls under the dead load, live load and snow load combination.

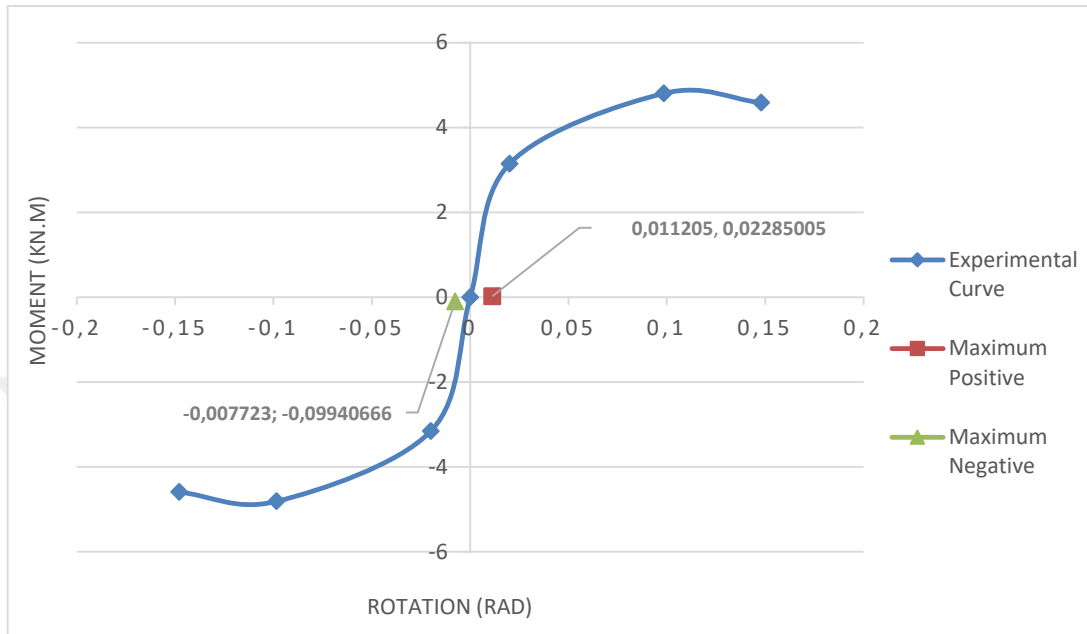


**Figure 6.32:** The S11 and S22 stress distributions on the walls under the earthquake load in X direction, dead load, live load and snow load combination.



**Figure 6.33:** The S11 and S22 stress distributions on the walls under the earthquake load in Y direction, dead load, live load and snow load combination.





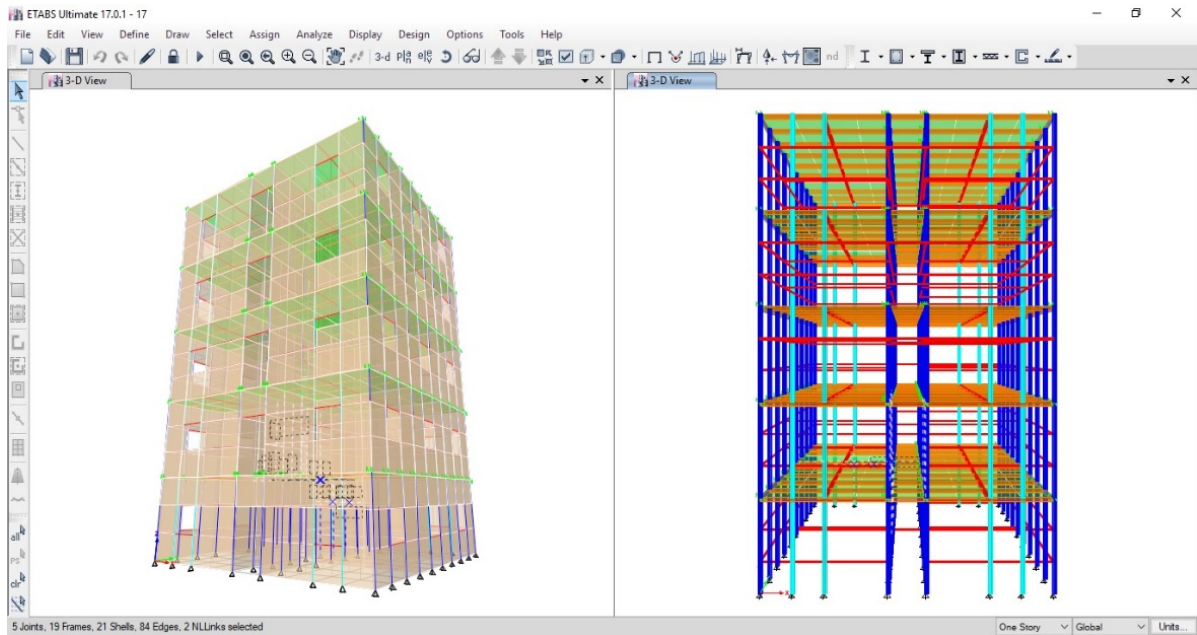
**Figure 6.34:** The maximum positive and negative moment rotation values obtained from SAP2000 results due to the earthquake loads compared to the experimental moment rotation results.

Non-linear analysis was performed using SAP2000 in order to obtain the moment rotation results from the defined link elements, that were used to simulate the actual beam-to-column connection behavior. The maximum positive and negative moment rotation values were obtained from SAP2000 due to the dead, live, snow and earthquake load combination and is compared to the moment rotation results obtained from the experimental results as shown in Figure 6.34. The moment rotation results from SAP2000 did not exceed the moment rotation results from the experimental study.

#### 6.4. PERFORMANCE BASED DESIGN USING ETABS

ETABS was used to carry out performance based design pushover analysis on the residential building that was designed in the previous sections using rack members. Trials were done in order to perform the pushover analysis using SAP2000 but a lot of hardships were faced. The main problem that did not allow SAP2000 to perform the pushover analysis correctly is modelling the non-linear behavior of the walls of the residential structure. So in order to get more precise results for the pushover analysis, ETABS software was used.

The columns were defined to ETABS using the section designer method, while all the other members of the residential building were defined using the normal steel member's menu in the software.



**Figure 6.35:** 3D views for the residential building modeled in ETABS.

Link elements were used to define the properties of the beam-to-column connections as the moment rotation results obtained from the experimental tests were inserted to the link properties menu as shown in Figure 6.36.

Column plastic hinges were defined at the two ends of the column members. Additionally, automatic fiber hinges were defined to the plywood wall panels. A load combination of dead load and 0.3 of the live load was applied to the building. After this load combination, a horizontal force was implied to the building in order to obtain the pushover curve of the structure in both the X and Y directions. The nonlinear material properties of plywood were inserted to ETABS using the stress-strain curve shown in Figure 6.37.

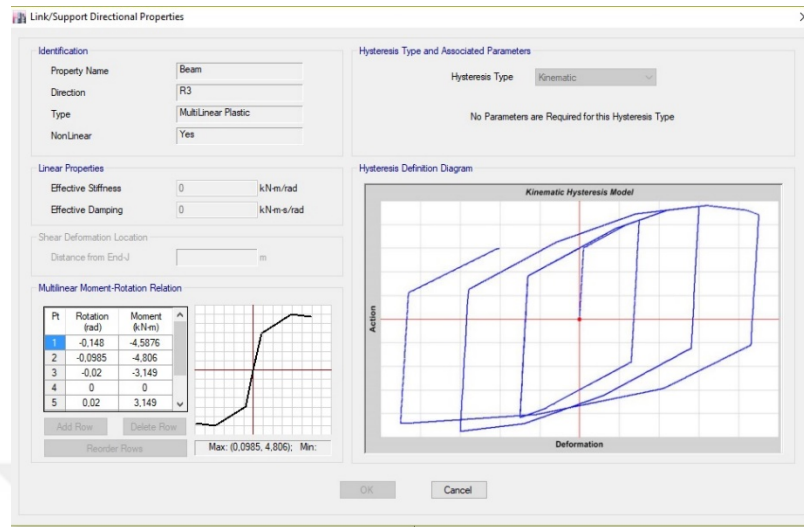


Figure 6.36: Defining the experimental moment rotation results to the link properties in ETABS.

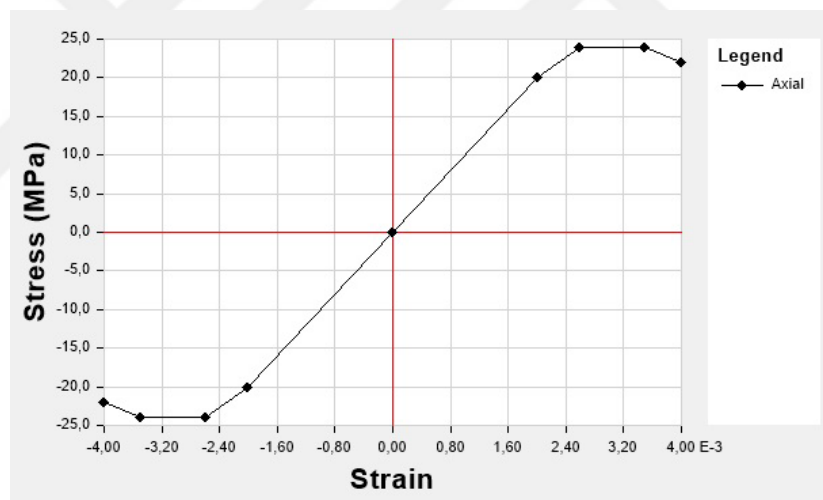


Figure 6.37: Stress-strain curve of plywood inserted to ETABS (Yoshihara, 2010).

#### 6.4.1 Pushover Analysis in the X Direction

The pushover curve in the X direction is shown in Figure 6.38. The X direction is considered to be the critical direction, as it consists of the rack beam-to-column semi rigid connections and less number of walls compared to the Y direction.

The plastic and fiber hinges formed during the pushover analysis in the X direction at the last step of loading is shown in Figure 6.39. Plastic and fiber hinges were formed at the columns and the walls in the direction of the pushing. Most of the fiber hinges formed in the walls were in immediate occupancy

performance level, while all the plastic hinges formed in the columns were in the collapse prevention performance limit. Detailed information about the plastic and fiber hinges formed in the structure due to the pushover load in the X direction is given in Table 6.1.

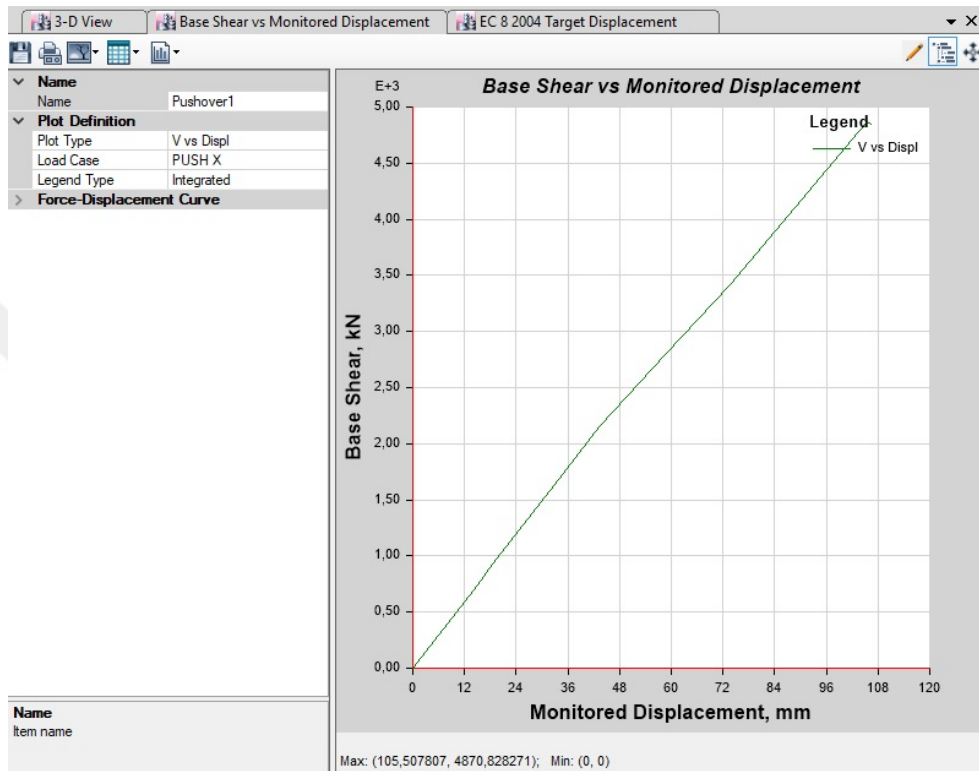


Figure 6.38: Pushover curve obtain from ETABS in X direction.

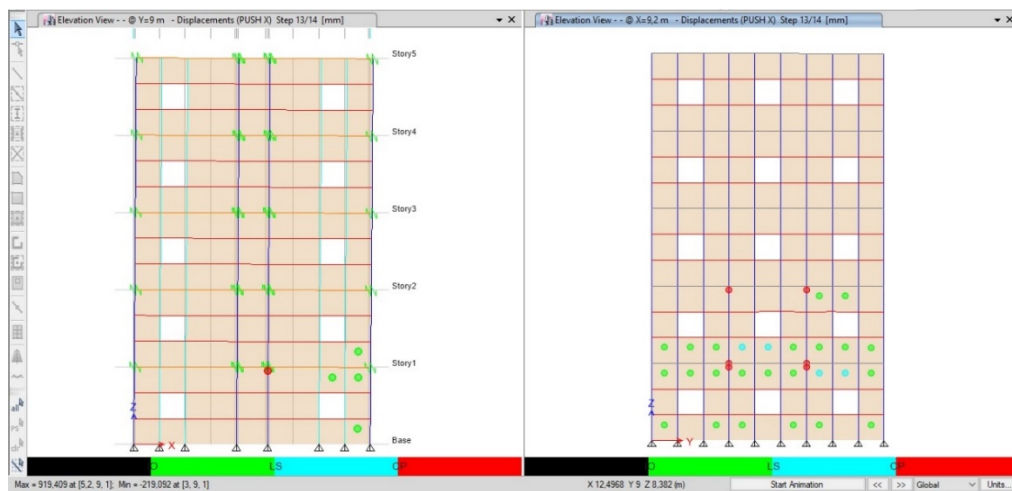
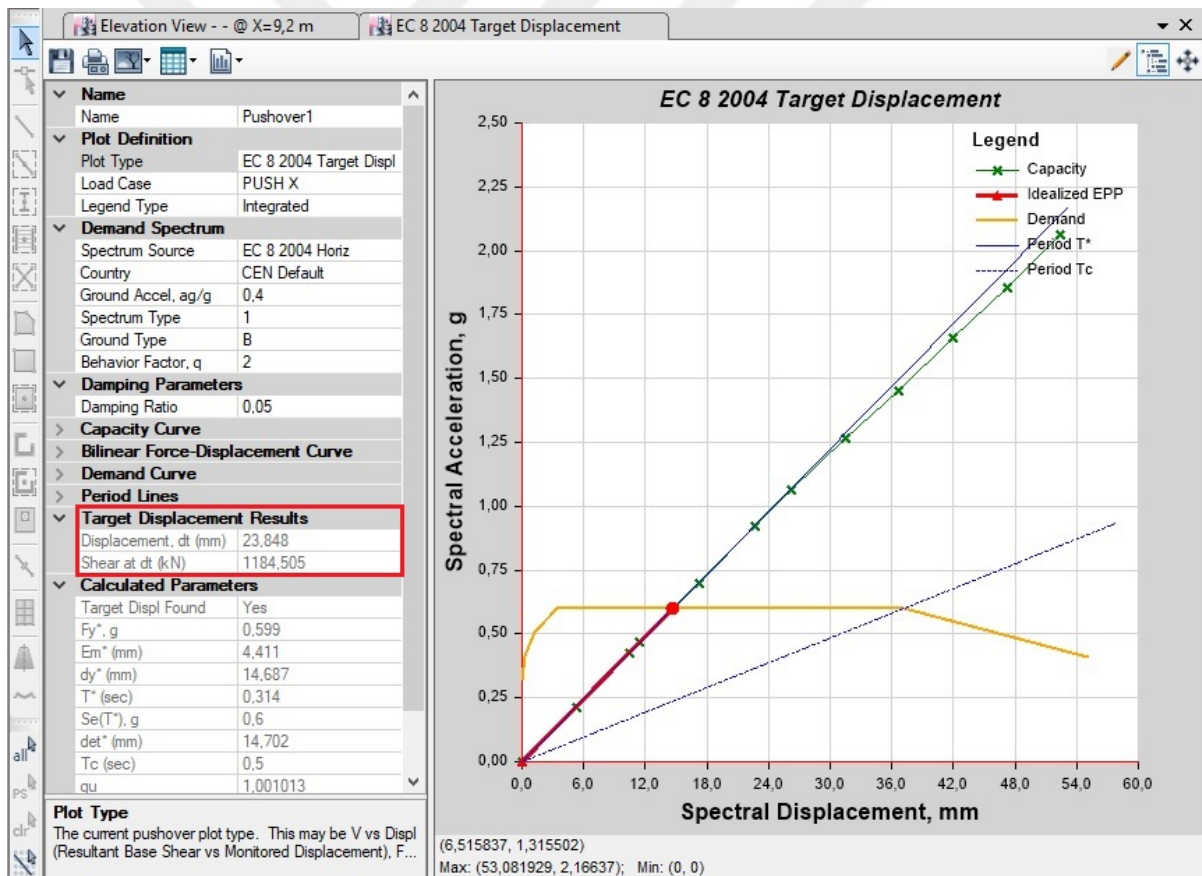


Figure 6.39: Plastic and fiber hinges formed during the pushover analysis in the X direction at the last step of loading.

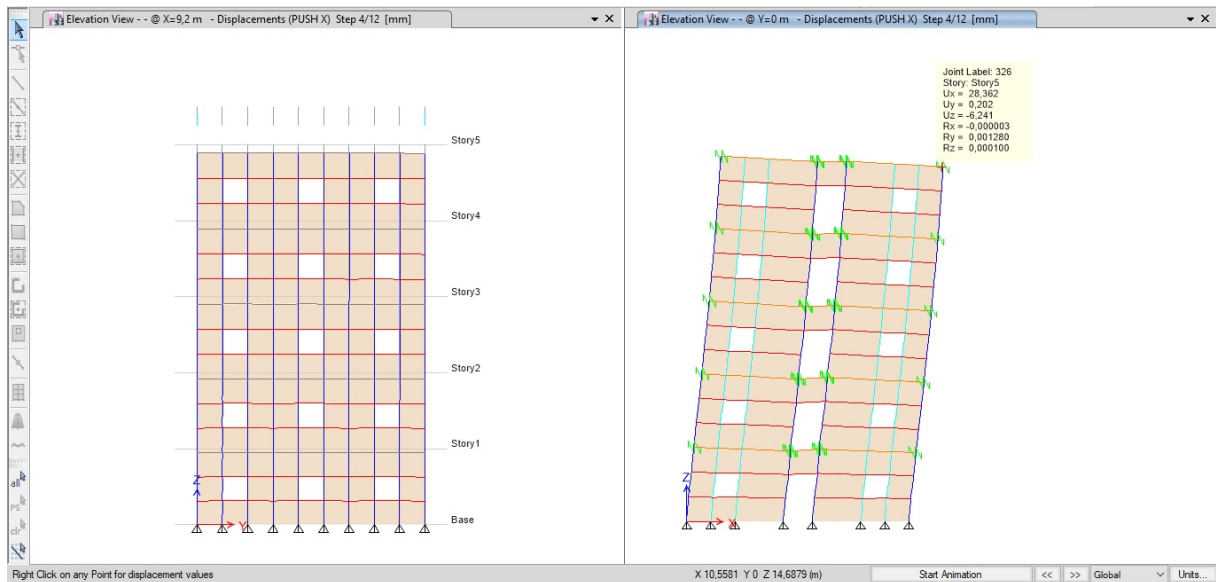
**Table 6.1:** Plastic and fiber hinges results due to pushover load in X direction at the last loading step.

Element Type	Number of elements	Number of defined hinges	Push (X) IO hinges	Push (X) LS hinges	Push (X) CP hinges	Push (X) IO hinges %	Push (X) LS hinges %	Push (X) CP hinges %
Columns	200	400	0	0	7	0.00	0.00	1.75
Walls	715	715	34	4	0	4.75	0.56	0.00

In order to obtain the target displacement of the structure in the X direction. The capacity curve was compared to the demand spectrum as shown in Figure 6.40. The target displacement value was obtained as 23.848 mm at a base shear force of 1185 kN for the X direction.

**Figure 6.40:** Target displacement values and the capacity curve in the X direction.

The plastic and fiber hinges results at the point of target displacement in the X direction were checked, it was found that the structure did not have any plastic or fiber hinges formed in any of its elements as shown in Figure 6.41



**Figure 6.41:** No plastic or fiber hinges were formed at the target displacement in X direction.

#### 6.4.2 Pushover Analysis in the Y Direction

The pushover curve in the Y direction is shown in Figure 6.42. It is known that the Y direction is a little bit stiffer than the X direction as it does not have any semi rigid beam to column connection and it has more number of columns compared to the X direction.

The plastic and fiber hinges formed during the last step of pushover analysis in the Y direction are shown in Figure 6.43. Most of the fiber hinges formed in the walls were in the immediate occupancy performance level, while two plastic hinges only were formed in the column one of them was in the life safety performance level while the other was in the collapse prevention performance level. Detailed information about the plastic and fiber hinges formed in the structure due to the pushover load in the Y direction is given in Table 6.2.

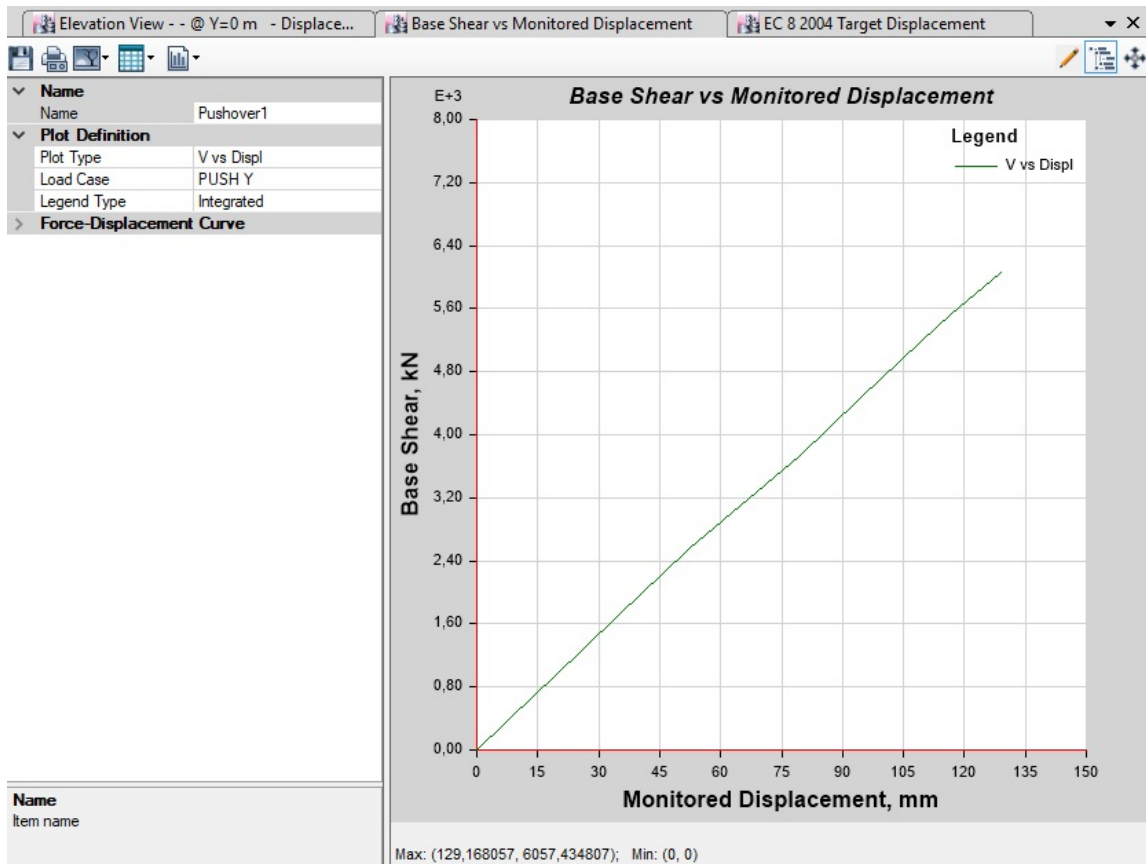


Figure 6.42: Pushover curve obtain from ETABS in Y direction.

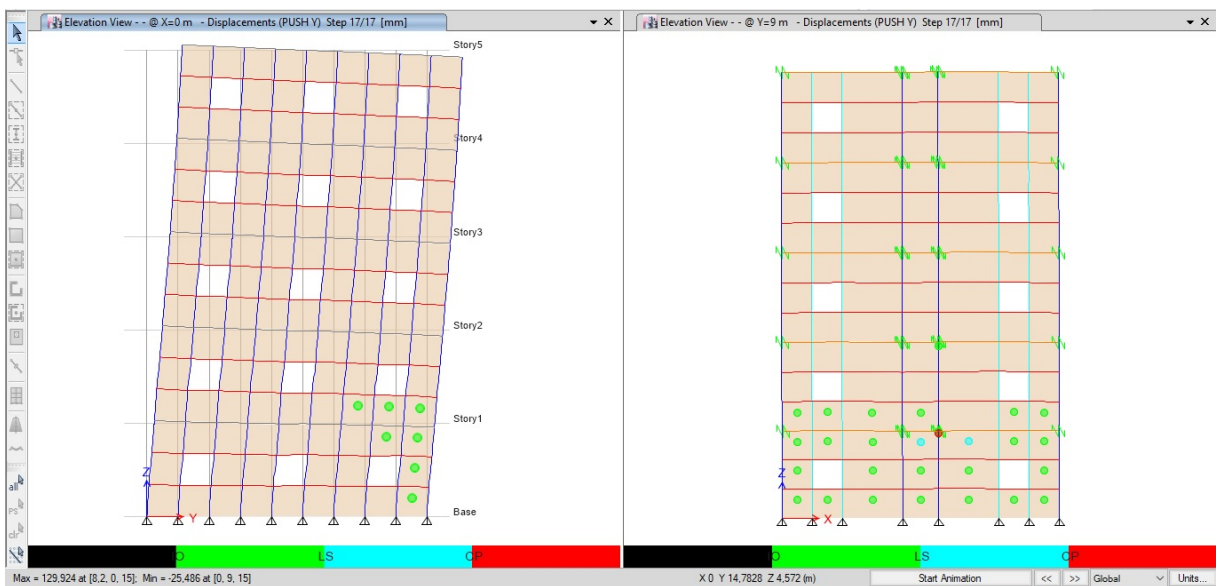
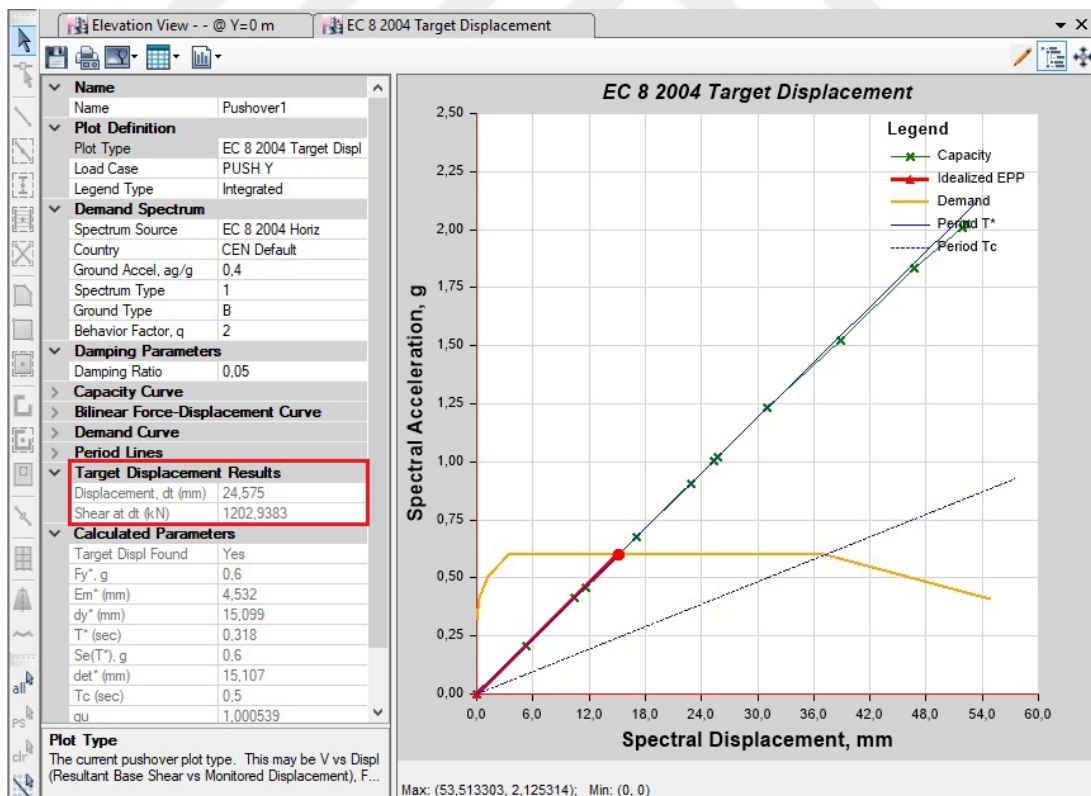


Figure 6.43: Plastic and fiber hinges formed during the pushover analysis in the Y direction at the last step of loading.

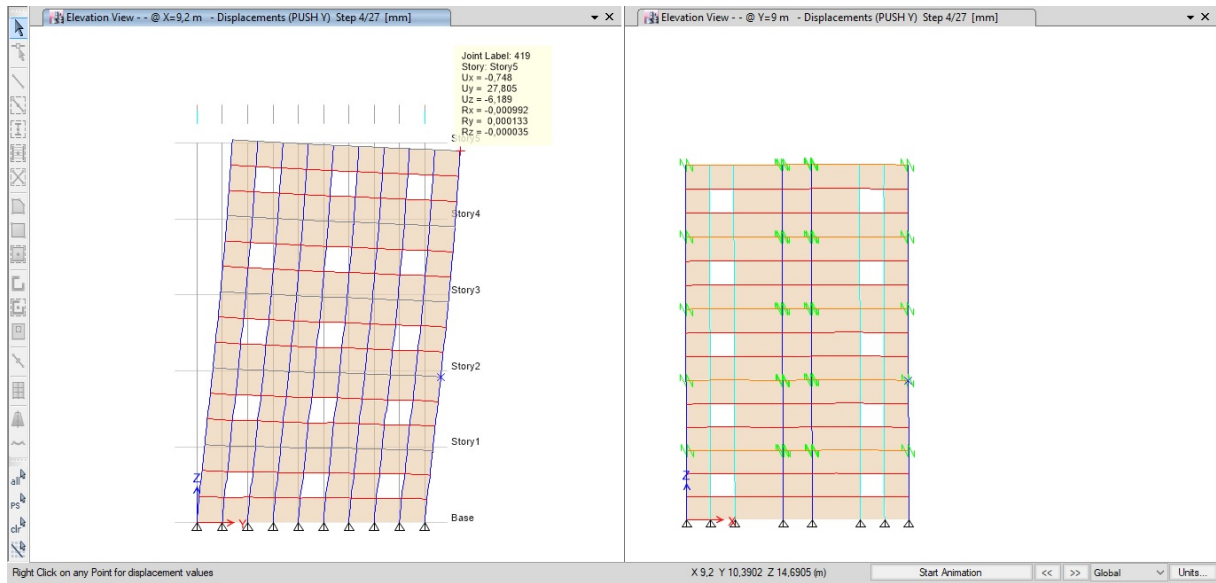
**Table 6.2:** Plastic and fiber hinges results due to pushover load in Y direction at the last loading step.

Element Type	Number of elements	Number of defined hinges	Push (X) IO hinges	Push (X) LS hinges	Push (X) CP hinges	Push (X) IO hinges %	Push (X) LS hinges %	Push (X) CP hinges %
Columns	200	400	0	1	1	0.00	0.25	0.25
Walls	715	715	42	4	0	5.87	0.56	0.00

The capacity curve was compared to the demand spectrum to obtain the target displacement. The capacity and the demand curves as well as the target displacement results are shown in Figure 6.44. The target displacement value was obtained as 24.575 mm at a base shear force of 1203 kN for the Y direction. The plastic and fiber hinge results at the point of target displacement in the Y direction were checked, it was found that the structure did not have any plastic or fiber hinges formed in any of its elements as shown in Figure 6.45.

**Figure 6.44:** Target displacement values and the capacity curve in the Y direction.

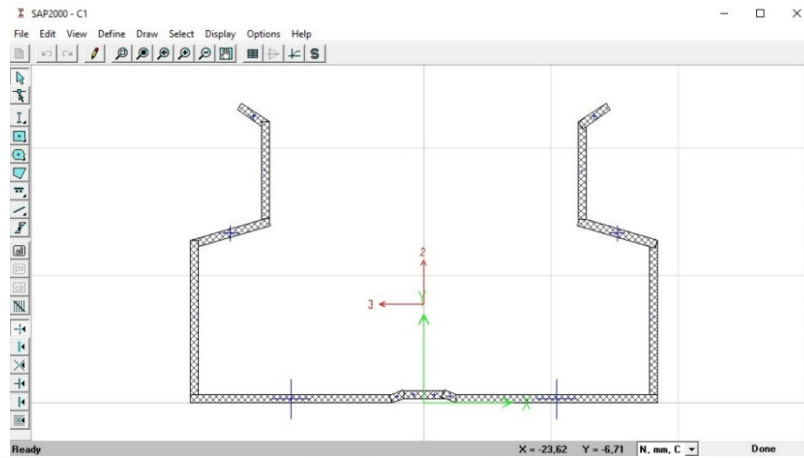




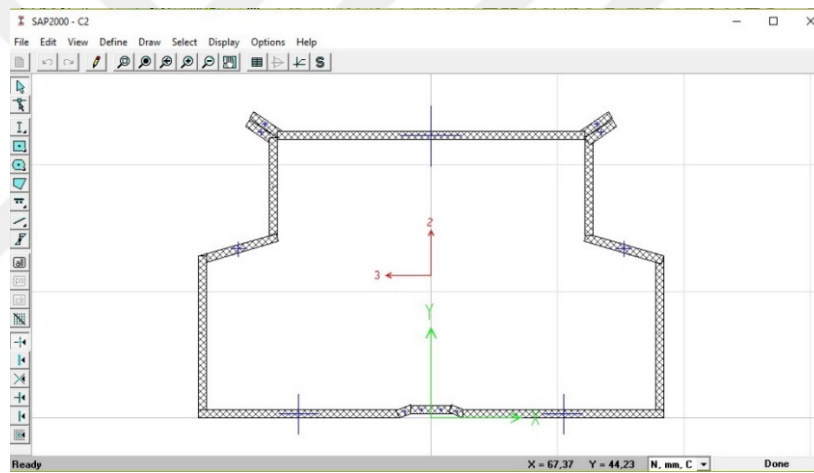
**Figure 6.45:** No plastic or fiber hinges were formed at the target displacement in Y direction.

## 6.5. DESIGN OF 8 STORY RESIDENTIAL BUILDING USING RACK MEMBERS

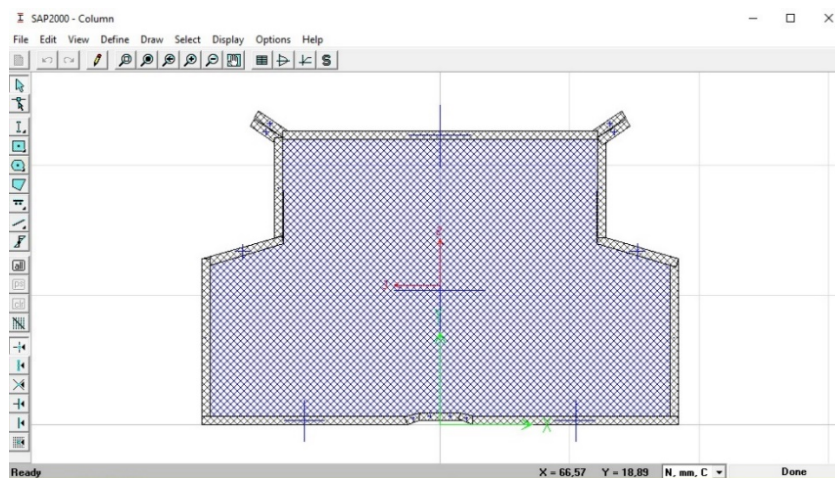
In this section, trials are going to be performed in order to increase the number of stories of the residential structure, by doing small modifications to the original cross-section (C1) of the column used in the previous studies, Figure 6.46. Two modifications were done; the first modification is to close the outer flange of the columns with a plate (C2) as shown in Figure 6.47, to limit the distortional buckling. While the second modification is to fill the column with micro self-compacting concrete (C3) as shown in Figure 6.48. The new columns were defined into SAP2000 and ETABS models. Several trials were performed in order to reach the maximum number of stories using the new cross-sections. The maximum number of stories that could be reached is 8 stories. Combination of the different cross-sections were used as follows; the column filled with grouted concrete (C3) is used for story 1 and 2, while the column with plate closing the outer flanges of the column (C2) is used for story 3 and 4, while the ordinary column without plate or concrete fill (C1) is used for the stories from 5 to 8 as shown in Figure 6.53.



**Figure 6.46:** Defining the dimensions of (C1) column using section designer in SAP2000.



**Figure 6.47:** Defining the dimensions of (C2) column using section designer in SAP2000.

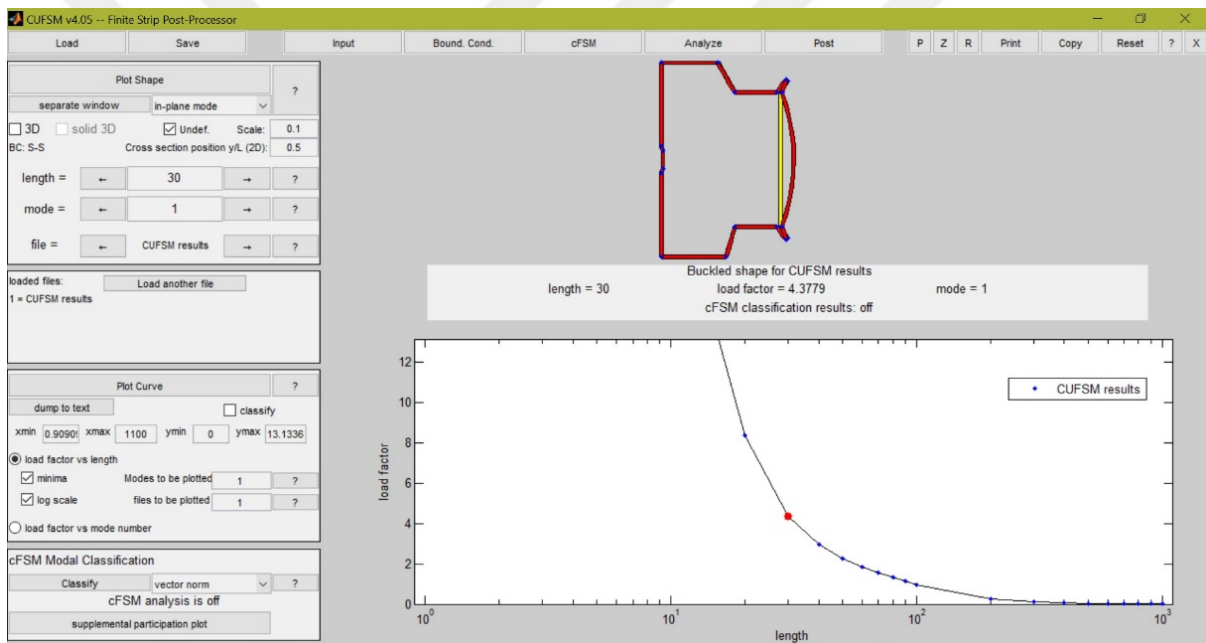


**Figure 6.48:** Defining the dimensions of (C3) column using section designer in SAP2000.

### 6.5.1 Obtaining the Axial Load Capacities of the Columns

The axial load capacity of column (C2) was checked taking into consideration the three main buckling modes, local, distortional and global buckling, using the same steps stated in Section 6.1 based on the equations stated in the AISI standard.

CUFSM software was used to obtain the critical local and distortional buckling load as shown in Figure 6.49, while CUTWP was used to obtain the critical global buckling load as shown in Figure 6.50 and Figure 6.51.



**Figure 6.49:** The signature curve for the local buckling failure mode in CUFSM for C2.

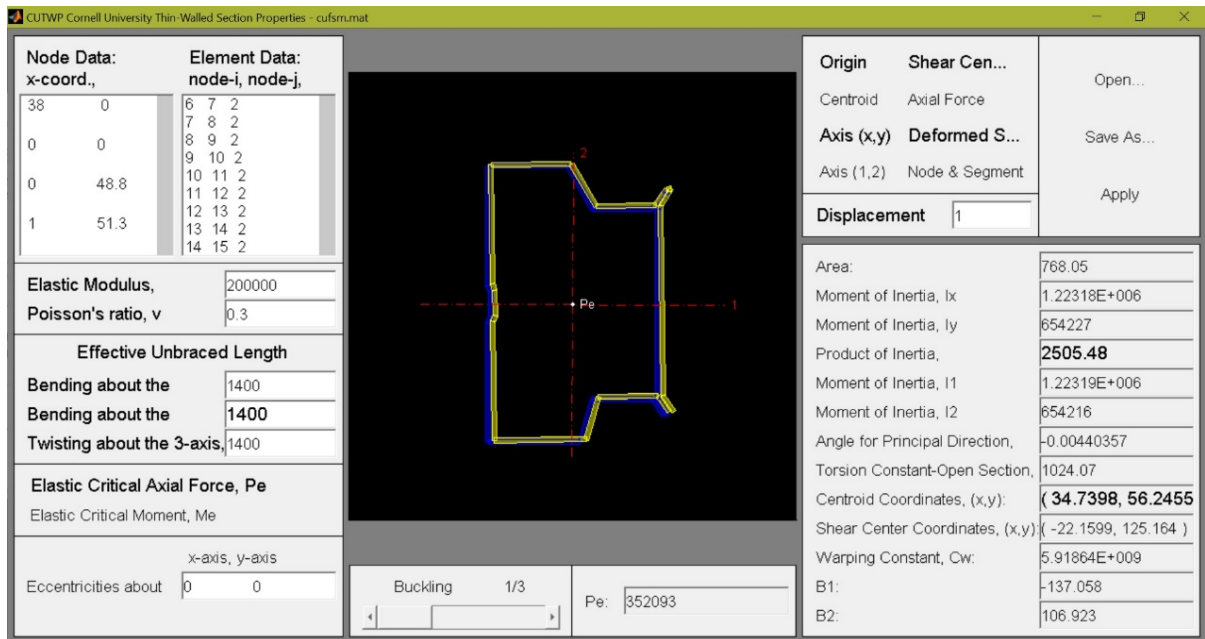


Figure 6.50: CUTWP input and result page with a plot for the flexural-torsional buckling failure mode of the first group of columns for C2 with effective buckling length of 1400 mm.

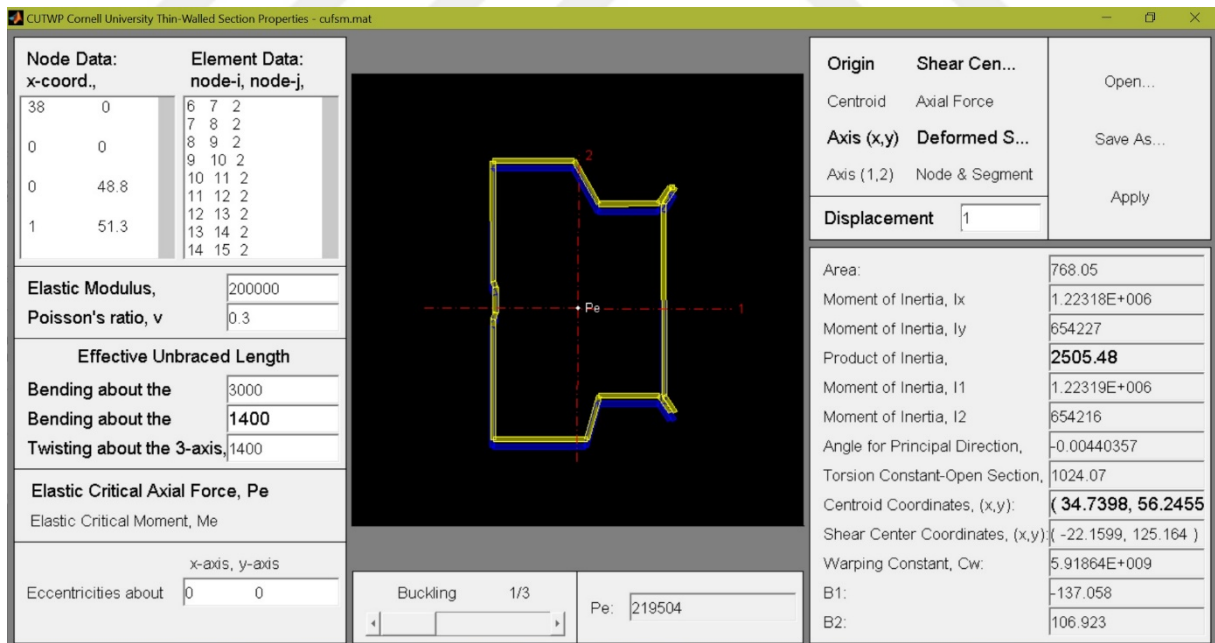


Figure 6.51: CUTWP input and result page with a plot for the flexural-torsional buckling failure mode of the second group of columns for C2 with effective buckling length of 3000 mm.

According to the equations mentioned in section 6.1., the results for the first group of columns for (C2) were

$$P_{ne1} = 152.82 \text{ kN}, P_{nl1} = 152.83 \text{ kN} \text{ and } P_{nd1} = 192 \text{ kN}.$$

While the results for the second group of columns for (C2) were,

$$P_{ne2} = 133.13 \text{ kN}, P_{nl2} = 133.13 \text{ kN} \text{ and } P_{nd2} = 192 \text{ kN}.$$

While the nominal axial strength ( $P_n$ ) shall be the minimum of the nominal axial strength for flexural, torsional or flexural-torsional buckling ( $P_{ne}$ ), the nominal axial strength for local buckling ( $P_{nl}$ ) and the nominal axial strength for distortional buckling ( $P_{nd}$ ).

From the previous results it was obtained the nominal axial strength ( $P_{n1}$ ) of the first group of columns for (C2) that are located at the corners of the rooms is  $P_{n1} = 152.82 \text{ kN}$  while the nominal axial strength ( $P_{n2}$ ) of the second group of columns for (C2)  $P_{n2} = 133.13 \text{ kN}$ .

The axial capacity of column (C3) was calculated based on the Equations (6.12)-(6.19) stated in Eurocode 4, taking into consideration the expected buckling effect of a composite cross-section. In these equations  $N_p$  and  $N_{cr}$  represents the design axial capacity and the critical axial load of the columns, respectively.  $E_s$  and  $I_s$  are the modulus of elasticity and the moment of inertia of the steel, while  $E_c$  and  $I_c$  are the modulus of elasticity and the moment of inertia of the concrete.  $\delta$  is the contribution factor,  $\lambda$  is the relative slenderness,  $\chi$  is the reduction factor and  $P_{n3}$  is the nominal axial strength of column C3.

$$N_p = A_c f_c + A_s f_y = 402.807 \text{ kN} \quad (6.12)$$

$$N_{cr} = \frac{\pi^2}{k L^2} E I_{eff} \quad (6.13)$$

$$E I_{eff} = E_s I_s + 0.6 E_c I_c = 3.5297 \times 10^{11} \quad (6.14)$$

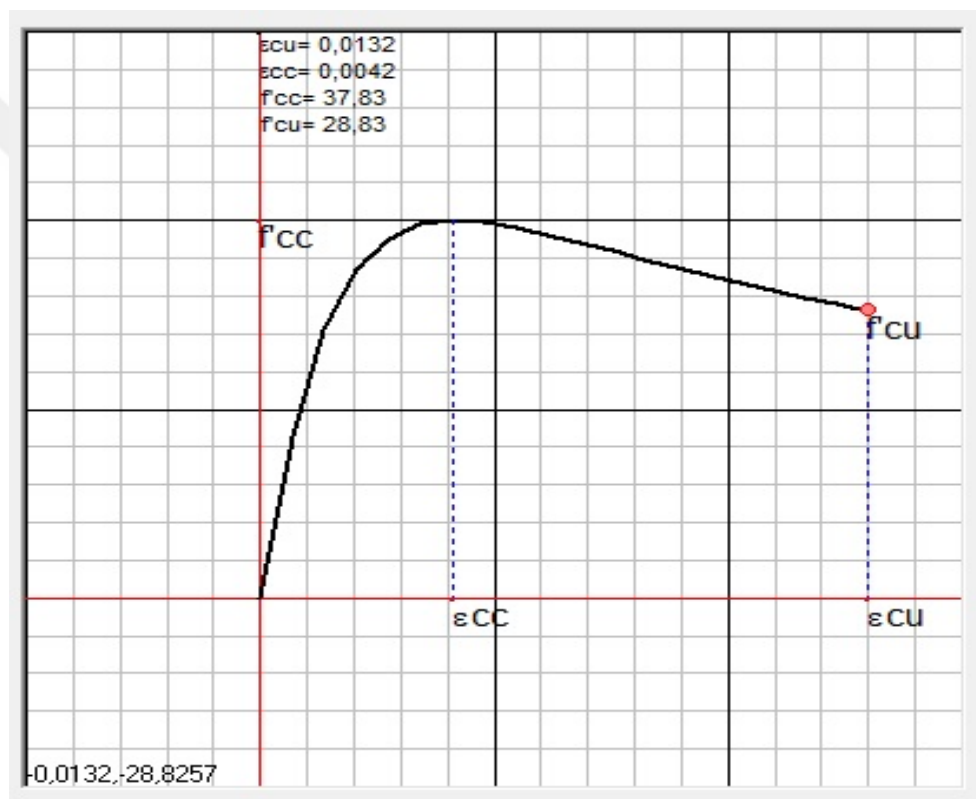
$$\delta = \frac{A_s f_y}{N_p} = 0.47 \quad (6.15)$$

$$\lambda = \sqrt{\frac{N_p}{N_{cr}}} = 1.02 \quad (6.16)$$

$$\chi = \frac{1}{\phi + \sqrt{\phi^2 - \lambda^2}} \quad (6.17)$$

$$\phi = 0.5(1 + \alpha(\lambda - 0.2) + \lambda^2) = 1.08 \quad (6.18)$$

$$P_{n3} = \chi N_p = 280.7 \text{ kN}. \quad (6.19)$$

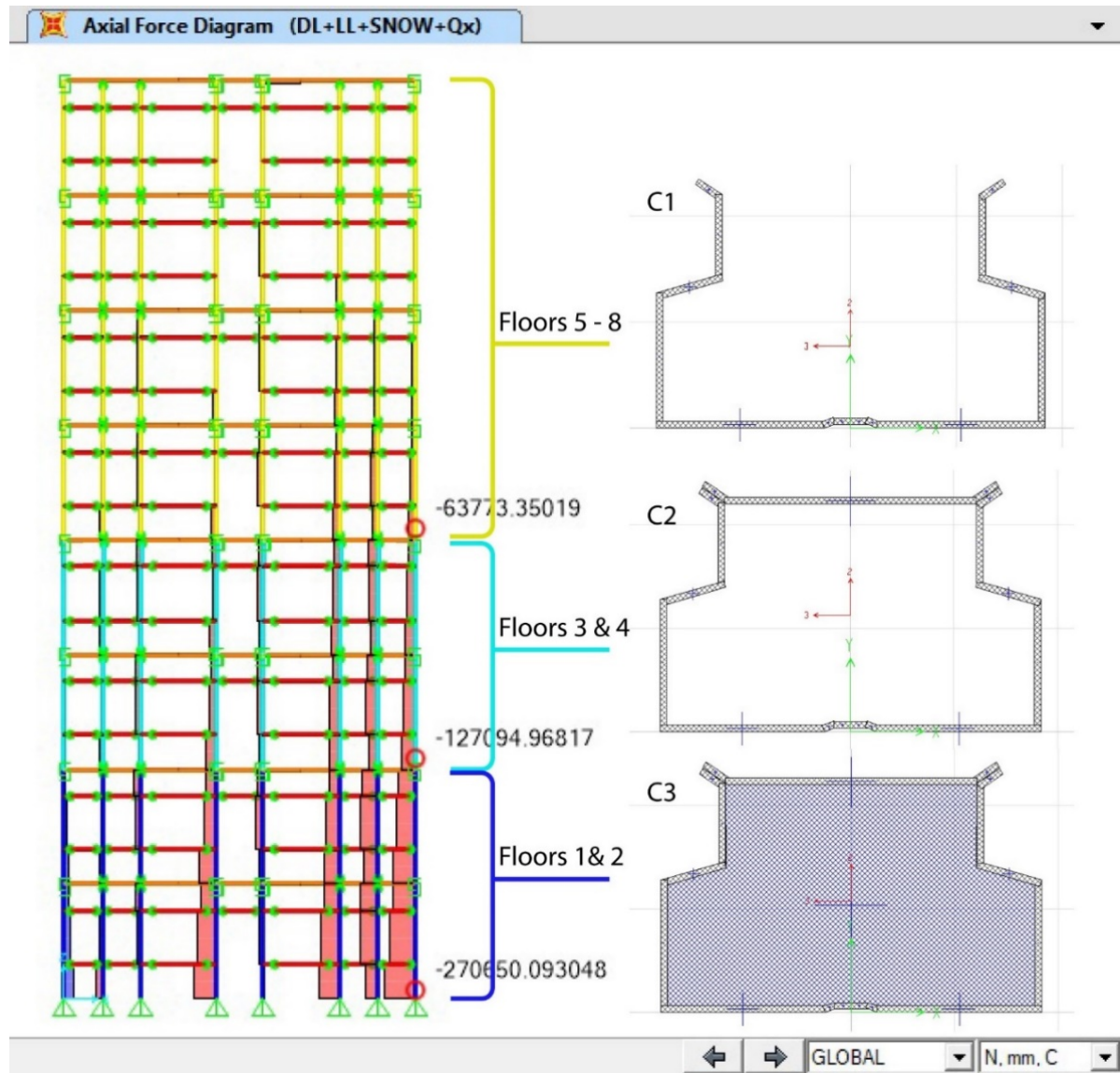


**Figure 6.52:** The stress strain curve of the micro concrete from SAP2000.

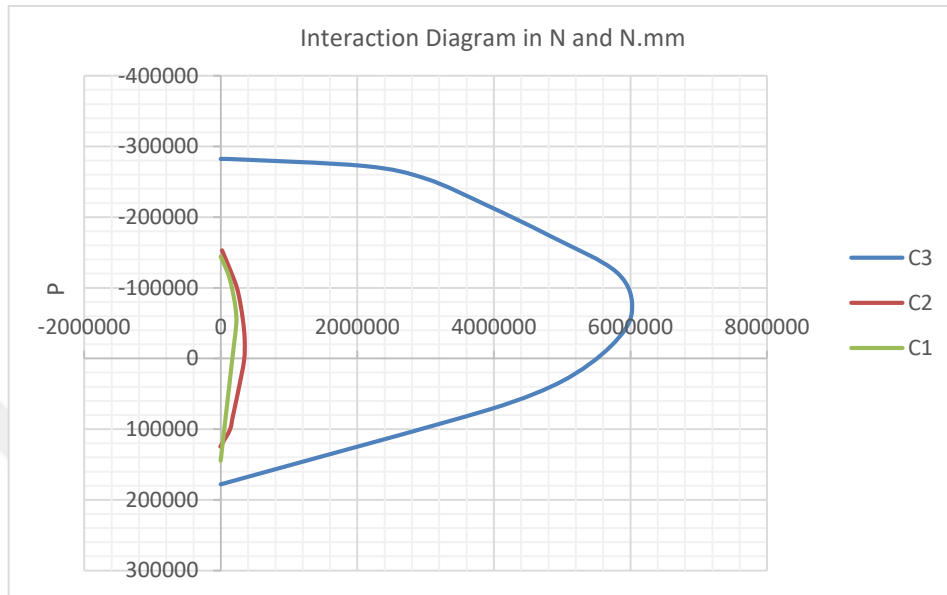
### 6.5.2 SAP2000 Results

The axial load results on the columns were obtained to be compared to the nominal axial load that was calculated before. It was found that the maximum axial load for the C1 columns under the load combination of the dead load, live load, snow load and earthquake load is  $P_{\max C1} = 63.77 \text{ kN}$ , while the nominal axial load for the first group of columns,  $P_{n C1} = 91.2 \text{ kN}$ . The maximum axial load for the C2 columns  $P_{\max C2} = 127.09 \text{ kN}$ , while the nominal axial load

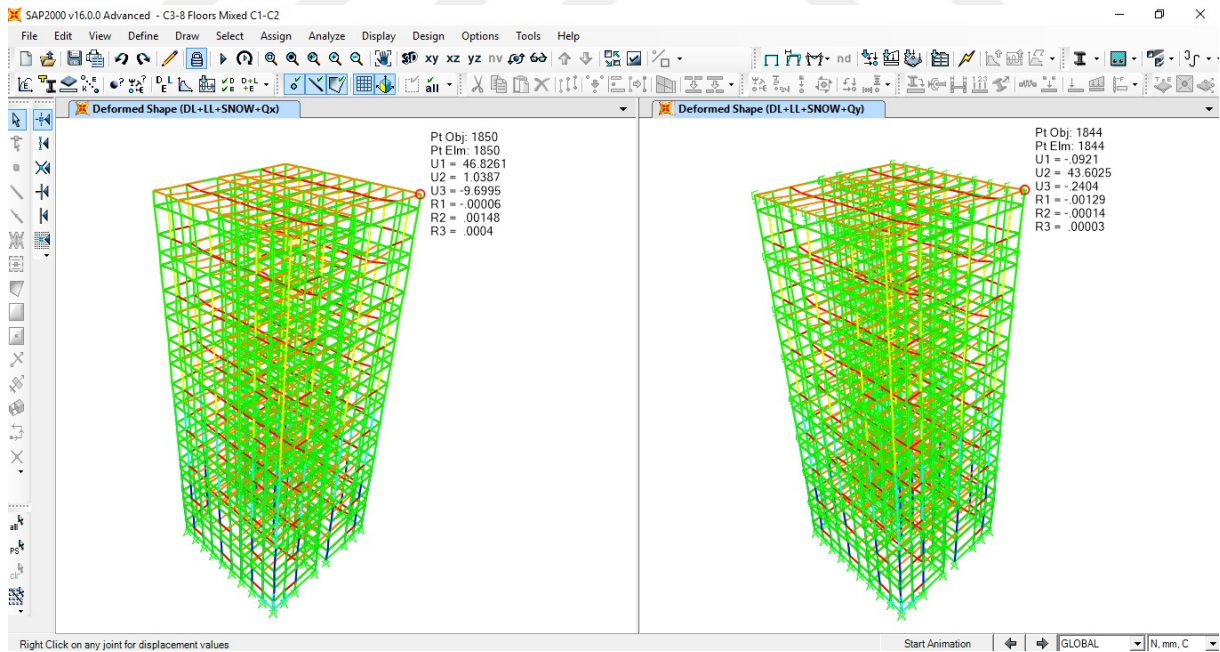
for the columns C2,  $P_{n\ C2} = 133\text{ kN}$ . The maximum axial load for the C3 columns  $P_{\max\ C3} = 270.65\text{ kN}$ , while the nominal axial load for the columns C3,  $P_{n\ C3} = 280.7\text{ kN}$ . The interaction diagram of the three column cross-sections is shown in Figure 6.54.



**Figure 6.53:** Maximum Axial load result for the columns from SAP2000 model under earthquake load, dead load, live load and snow load combination.



**Figure 6.54:** Comparison between the interaction diagrams of C1, C2 and C3.



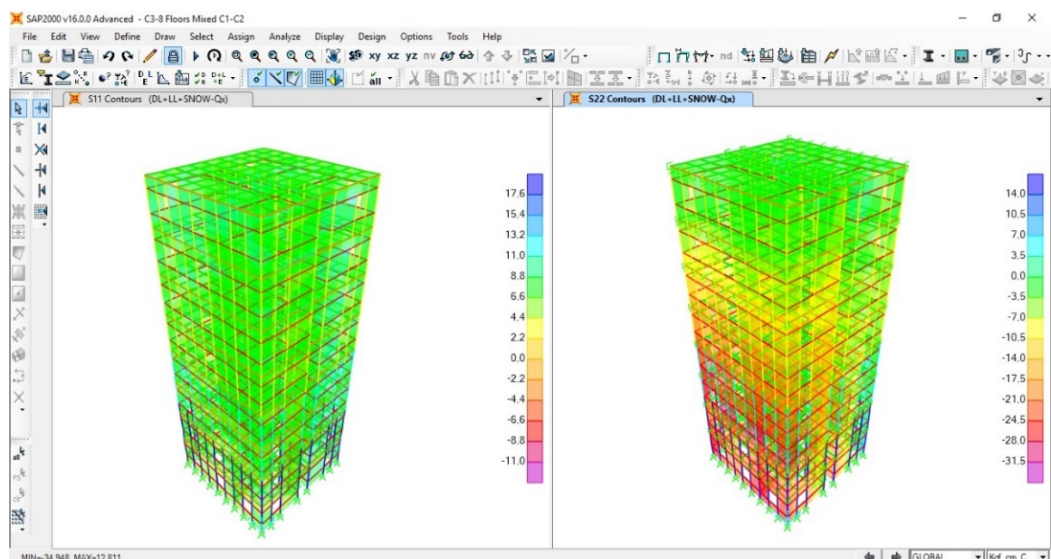
**Figure 6.55:** Maximum roof displacements due to seismic loads for the 8 stories building in the X and Y directions.

The deformed shape under the combination of dead loads, live loads, snow loads and earthquake loads was checked, and it was found that the maximum displacement occurred at the roof in X

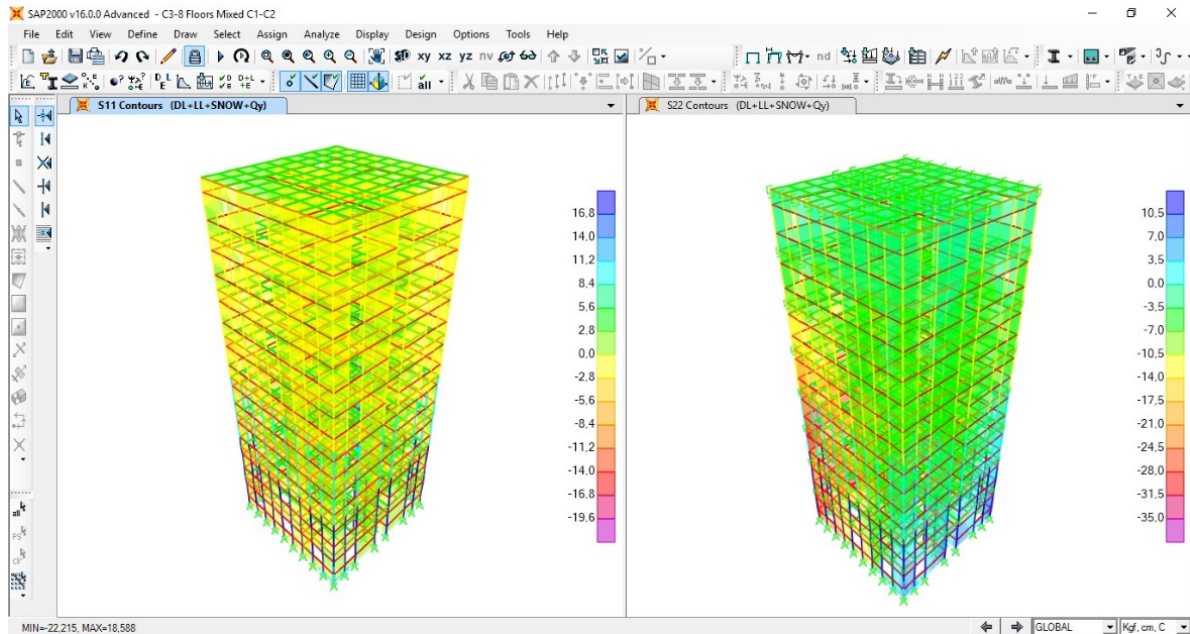


direction,  $D_x = 46.82 \text{ mm}$  as shown in Figure 6.55, while the maximum displacement occurred at the roof in Y direction,  $D_y = 43.60 \text{ mm}$ , as shown in Figure 6.55. It is found that the maximum drift ratio  $\delta_i$  of the building equals to 0.0078 calculated according to Equation (6.11) given in Turkish seismic code (TSC, 2007) which is smaller than the ultimate value 0.02, in which  $R$  is the reduction factor and taken as 4 while  $\Delta_i$ ,  $h_i$  are the maximum lateral displacement at top floor and the height of the building, respectively. Therefore, the building is considered safe according to the allowable drift ratio value.

The stresses in the plywood wall panels were obtained as follow; under the dead, live, snow and earthquake in X direction load combination the maximum achieved S22 stress is 3.1 MPa (31.5 kgf/cm<sup>2</sup>) as shown in Figure 6.56, and under the dead, live, snow and earthquake in Y direction load combination the maximum achieved S22 stress is 3.5 MPa (35 kgf/cm<sup>2</sup>) as shown in Figure 6.57 which is the critical case. The plywood panels stress capacities are 8 MPa (80 kgf/cm<sup>2</sup>) in one direction and 4 MPa (40 kgf/cm<sup>2</sup>) in the other direction according to the Turkish Standard TS-647. According to that, the plywood panels are considered safe. It is preferable to install the panels while caring that the outer fiber direction is placed vertically, by that it will be guaranteed that the powerful direction of the panel will resist the higher S22 stresses.



**Figure 6.56:** The S11 and S22 stress distributions on the walls under the earthquake load in X direction, dead load, live load and snow load combination.



**Figure 6.57:** The S11 and S22 stress distributions on the walls under the earthquake load in Y direction, dead load, live load and snow load combination.

### 6.5.3 Non-Linear Pushover Analysis in the X Direction Using ETABS

ETABS was used to carry out performance based design pushover analysis on the 8 story residential building. The pushover curve obtained from the pushover analysis in the X direction is shown in Figure 6.58. The building could be pushed till a displacement of 137 mm and base shear force of 2948 kN.

The plastic and fiber hinges formed during the pushover analysis in the X direction at the last step of loading is shown in Figure 6.59. Plastic and fiber hinges were formed at the columns and the walls in the first 3 stories only in the direction of the pushing. Most of the fiber hinges formed in the walls were in immediate occupancy performance level, while the other fiber hinges formed in the walls were in life safety performance level. Most of the plastic hinges formed in the columns were in the life safety performance level, while the rest of the plastic hinges formed in the columns were in the immediate occupancy performance level. Detailed information about the plastic and fiber hinges formed in the structure due to the pushover load in the X direction is given in Table 6.3.

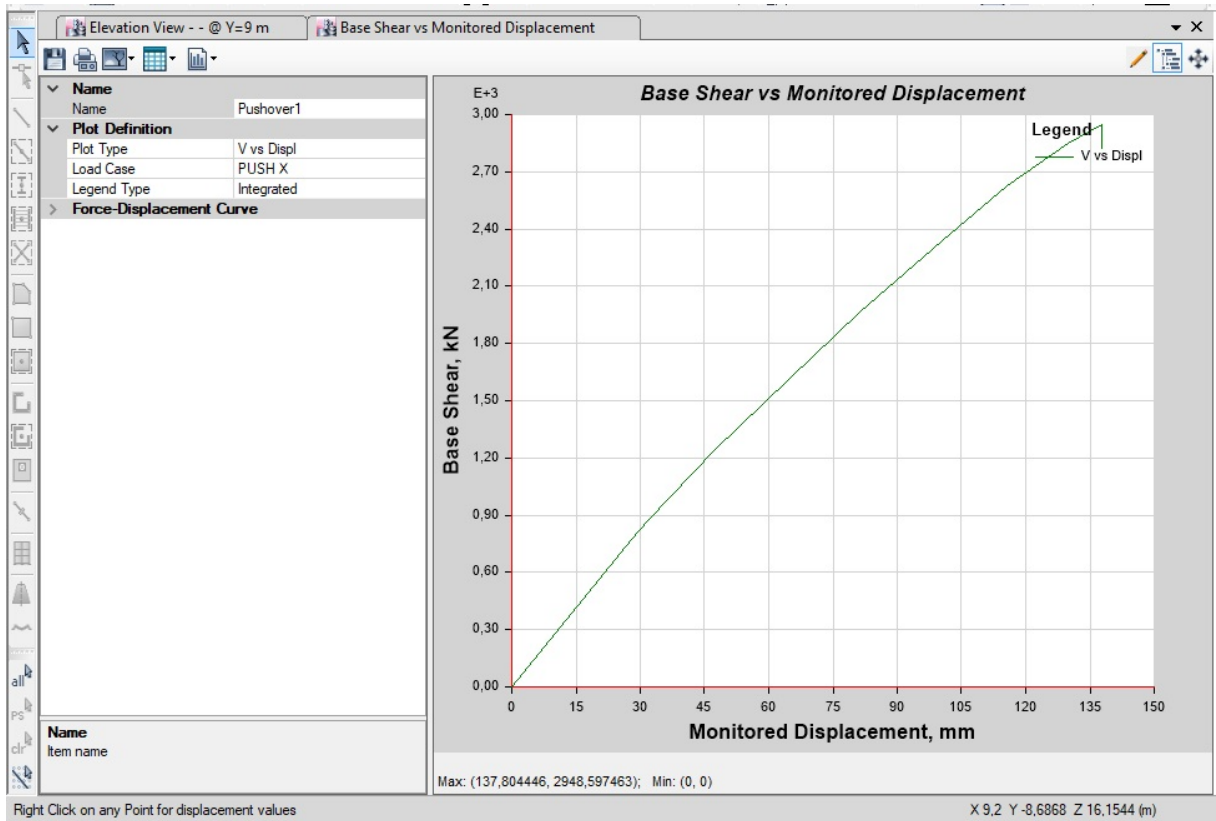


Figure 6.58: Pushover curve obtain from ETABS in X direction.

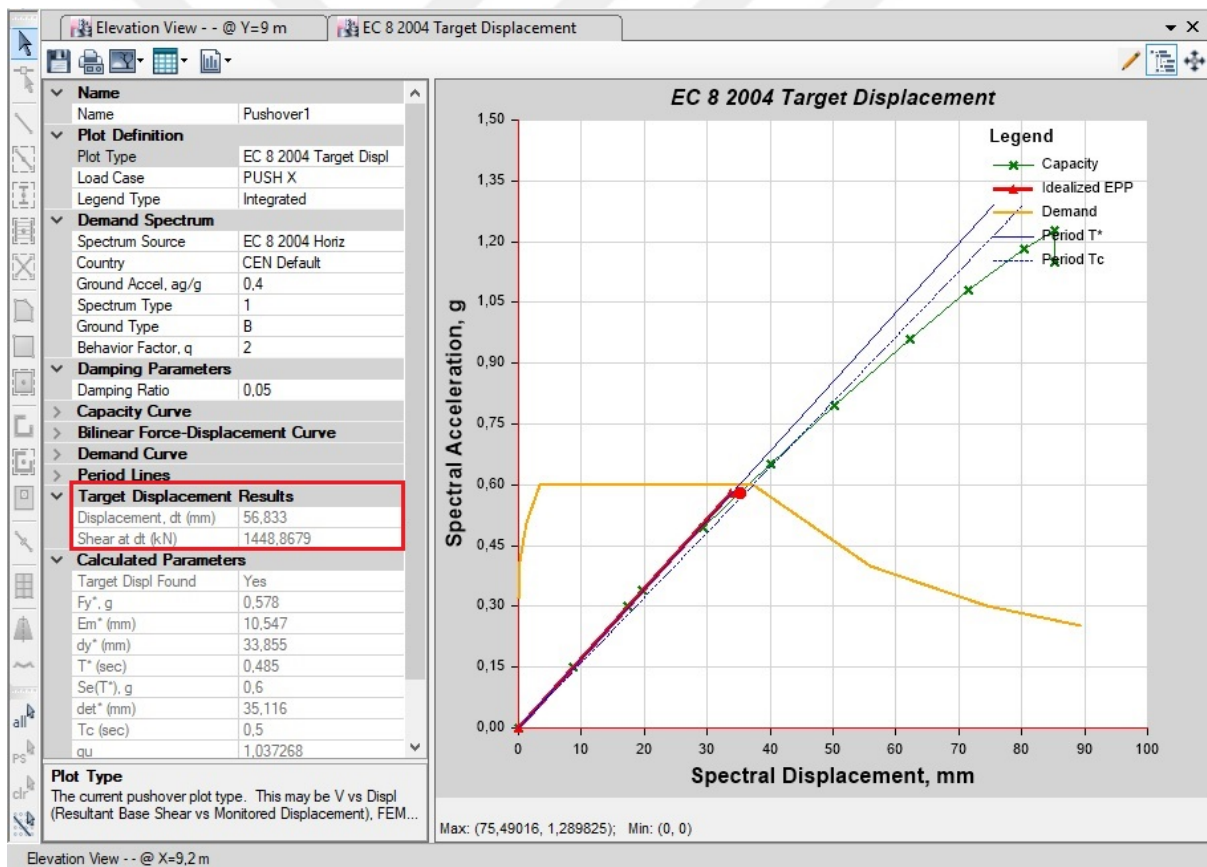


Figure 6.59: Plastic or fiber hinges formed during the pushover analysis in the X direction at the last step of loading.

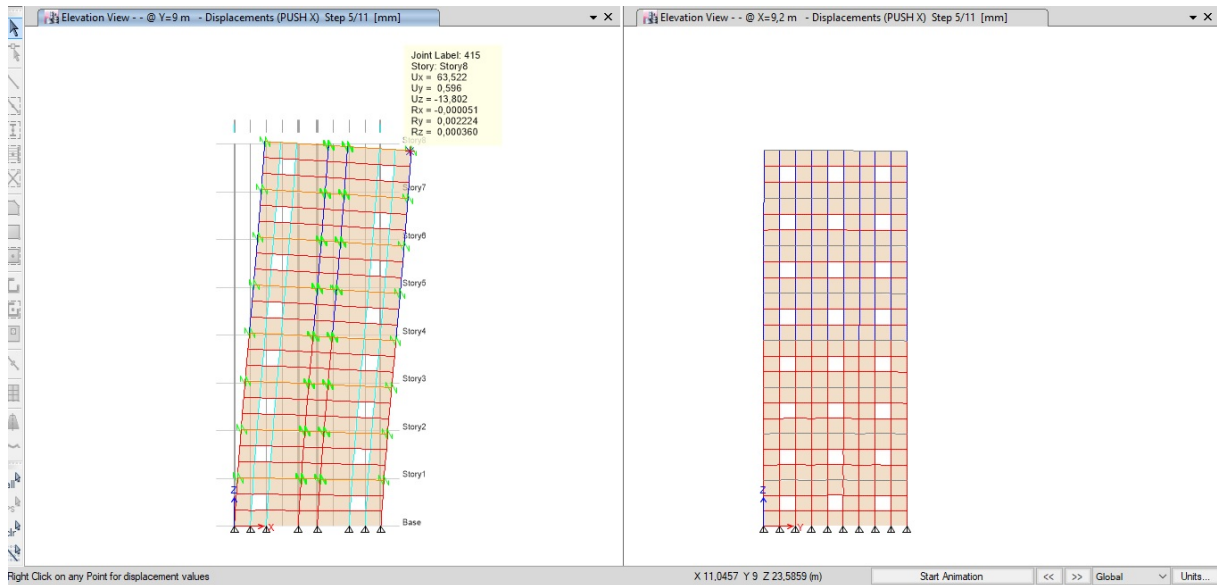
**Table 6.3:** Plastic and fiber hinges results due to pushover load in X direction at the last loading step.

Element Type	Number of elements	Number of defined hinges	Push (Y) IO hinges	Push (Y) LS hinges	Push (Y) IO hinges %	Push (Y) LS hinges %
Columns	320	640	2	10	0.31	1.56
Walls	1144	1144	24	11	2.10	0.96

The capacity curve is compared to the demand curve in Figure 6.60. The target displacement in the X direction is obtained as 56.83 mm at a base shear of 1449 kN.

**Figure 6.60:** Target displacement values and the capacity curve in the X direction.

The plastic and fiber hinge results at the point of target displacement in the X direction were checked, it was found that the structure did not have any plastic or fiber hinges formed in any of its elements as shown in Figure 6.61.



**Figure 6.61:** No plastic or fiber hinges were formed at the target displacement in X direction.

#### 6.5.4 Non-Linear Pushover Analysis in the Y Direction Using ETABS

The pushover curve obtained from the pushover analysis in the Y direction is shown in Figure 6.62. The building could be pushed till a displacement of 175 mm and base shear force of 3720 kN. The plastic and fiber hinges formed during the pushover analysis in the Y direction at the last step of loading is shown in Figure 6.63. Plastic and fiber hinges were formed at the columns and the walls in the first 3 stories only in the direction of the pushing. Most of the fiber hinges formed in the walls were in immediate occupancy performance level, while the other fiber hinges formed in the wall were in life safety performance level. Most of the plastic hinges formed in the columns were in the immediate occupancy performance level, while the rest of the plastic hinges formed in the columns were in the life safety performance level. Detailed information about the plastic and fiber hinges formed in the structure due to the pushover load in the Y direction is given in Table 6.4.

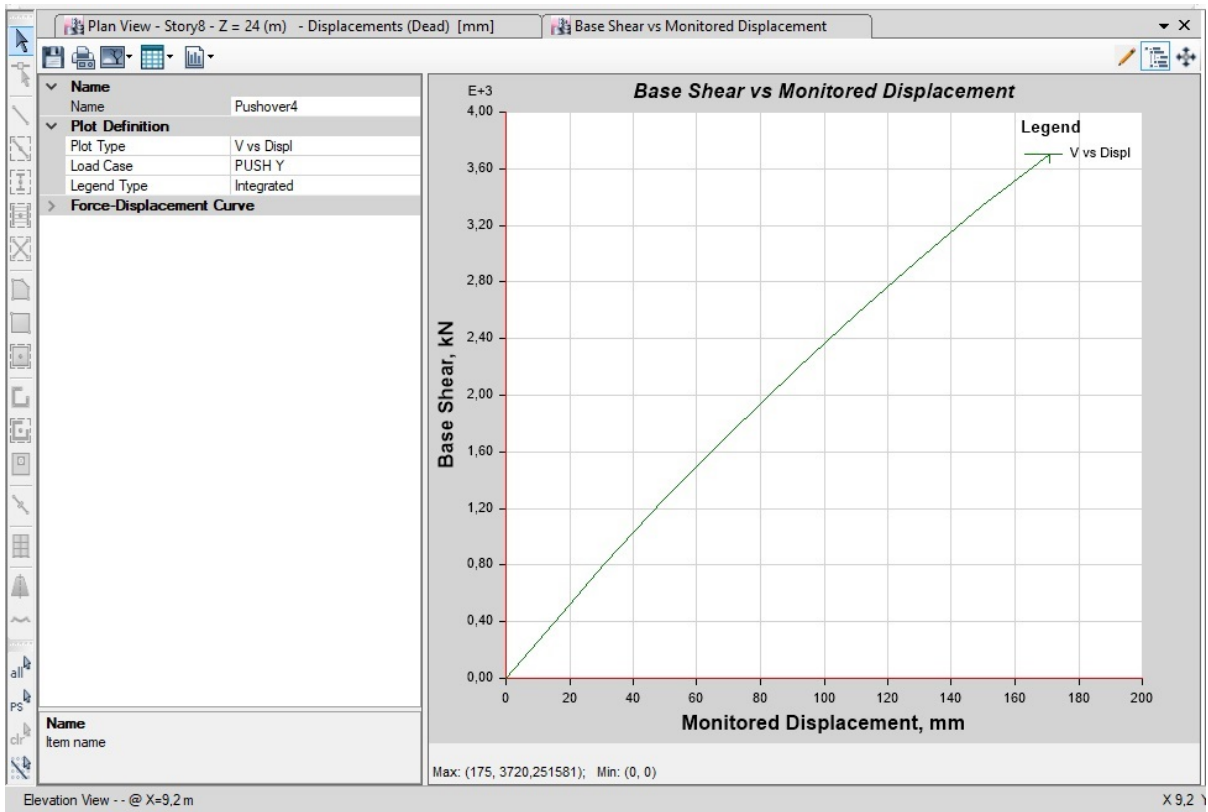


Figure 6.62: Pushover curve obtain from ETABS in Y direction.

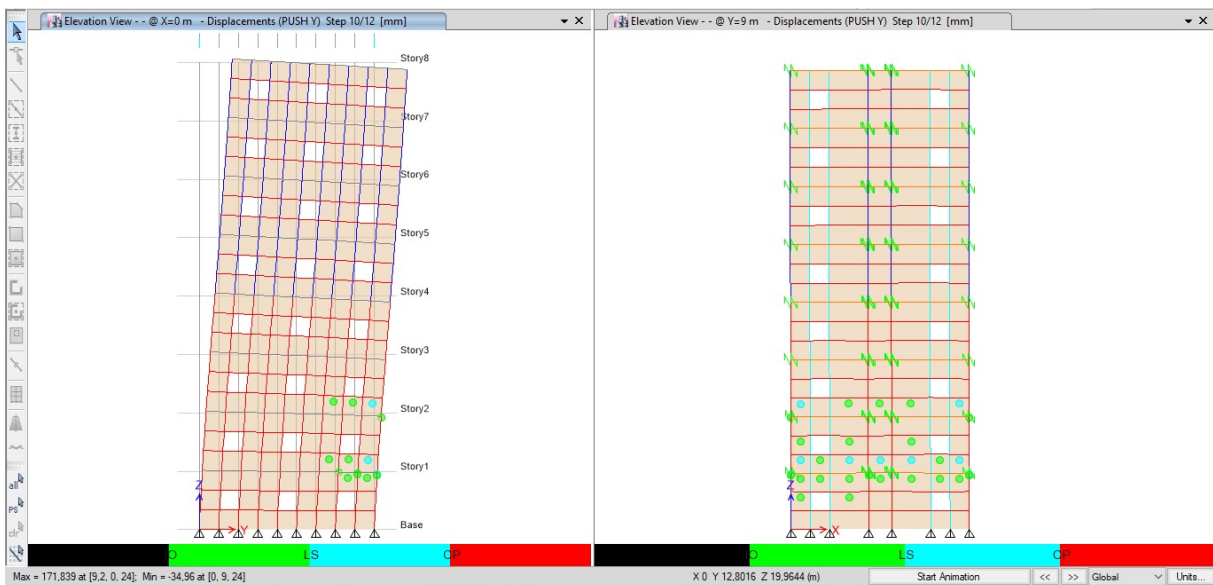
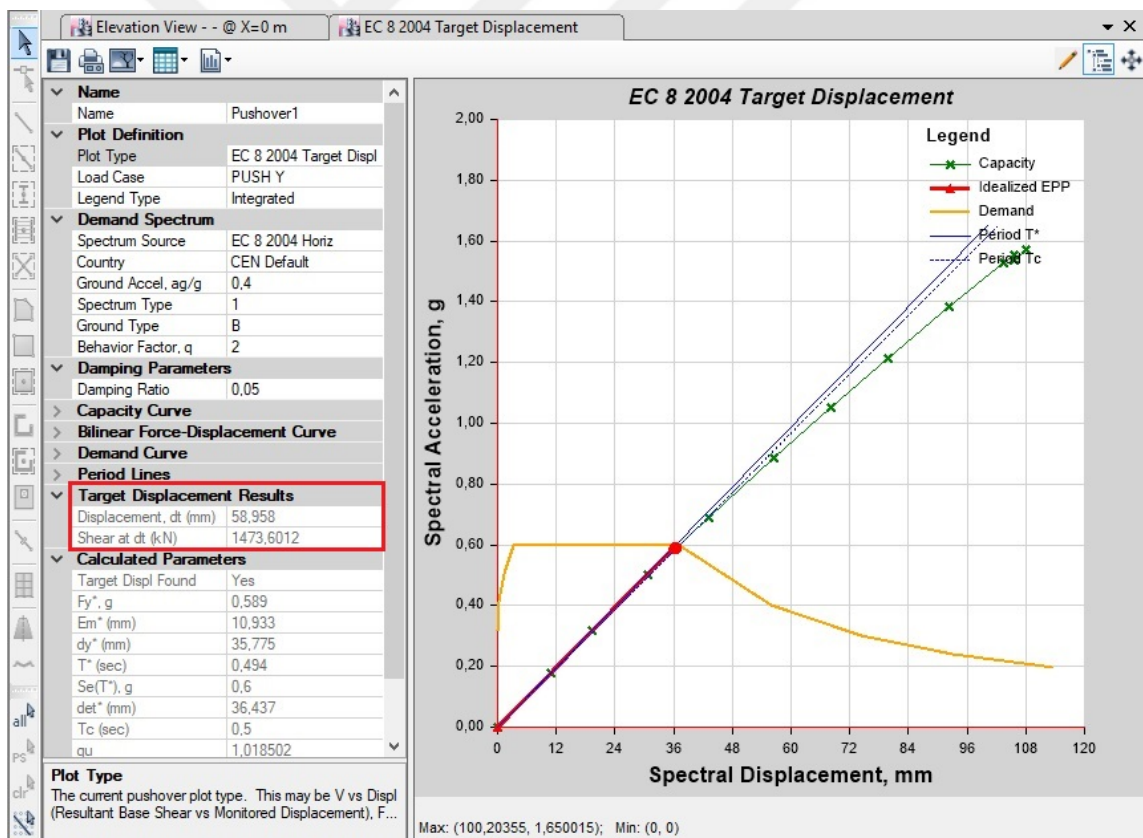


Figure 6.63: Plastic or fiber hinges formed during the pushover analysis in the Y direction at the last step of loading.

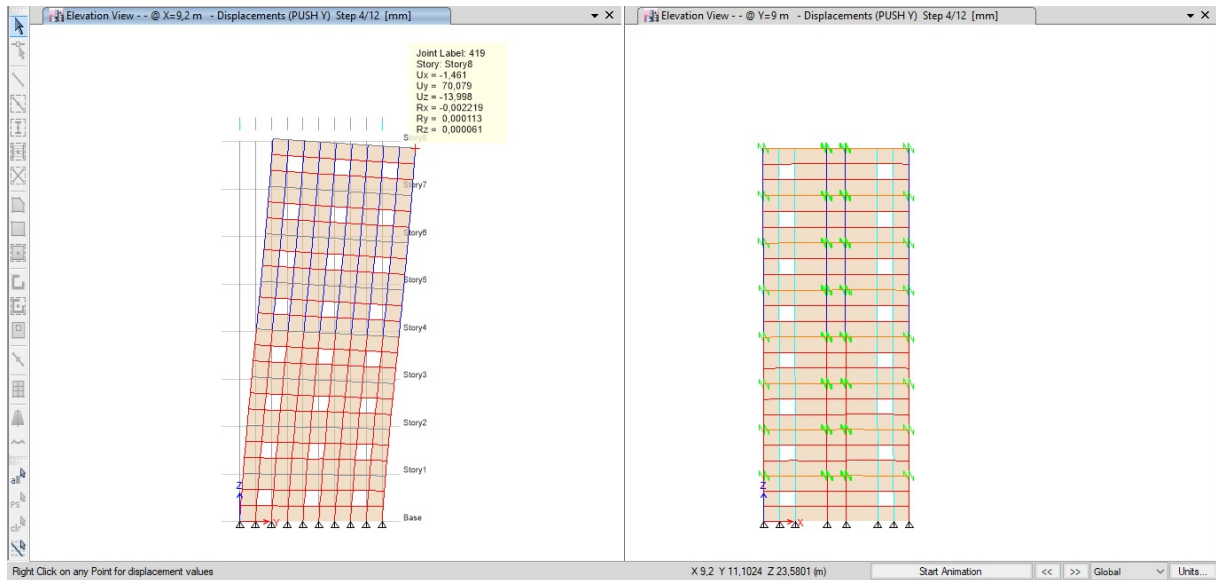
**Table 6.4:** Plastic and fiber hinges results due to pushover load in Y direction at the last loading step.

Element Type	Number of elements	Number of defined hinges	Push (Y) IO hinges	Push (Y) LS hinges	Push (Y) IO hinges %	Push (Y) LS hinges %
Columns	320	640	12	3	1.88	0.46
Walls	1144	1144	34	13	2.97	1.13

The capacity curve is compared to the demand curve in Figure 6.64 based on EC 8 2004. The target displacement in the X direction is obtained as 58.958 mm at a base shear of 1474 kN.

**Figure 6.64:** Target displacement values and the capacity curve in the Y direction.

The plastic and fiber hinge results at the point of target displacement in the Y direction were checked, it was found that the structure did not have any plastic or fiber hinges formed in any of its elements as shown in Figure 6.65.



**Figure 6.65:** No plastic or fiber hinges were formed at the target displacement in Y direction.

The newly proposed bolted beam-to-column connection of the rack members enhances the performance of the connection significantly, which leads to a new design for residential buildings that can be constructed using rack members and the newly proposed bolted connection. From the former study it is proved that a 5 story residential building may be constructed using the rack members that provides many advantages such as:

- Light weight economical building.
- Considered as a rapid structure because the time required for installing it will be relatively small as it is formed only from cold formed steel rack members and plywood panels.
- Beside its usage as a permanent residential building it can be used as temporary residential structure after enormous natural disasters.
- Mobility, because it can be moved from one place to another without economical losses as the building can be easily installed and uninstalled.
- Recyclable, as both of cold formed steel and plywood are easily recyclable materials.

The number of stories can be maximized to 8 stories by small modifications to the column cross-section that was used in the 5 story building, such as closing the cross-section with an additional cold formed steel plate, and injecting the cross-section with a self-compacting micro concrete, in order to overcome the buckling problems of the column.



## 7. CONCLUSIONS AND FUTURE WORK

Storage rack systems are of vital importance in our modern industrial world. They play a key role in the logistics supply chain of products. Considering the possible economic and human life losses, the seismic safety of these systems is critical. Particularly rack systems directly accessible to public and used in big box stores should not pose any risk during a strong ground shaking.

Rack systems are structural load carrying systems typically made up of cold formed steel elements assembled in a similar way conventional steel framed structures are assembled. Nevertheless, columns, beams, braces and connections with characteristics peculiar to these systems necessitate a different treatment in their structural design. For example, the hooked beam-to-column connections results in a markedly semi-rigid behavior. On the other hand, under strong ground motions, storage rack frames have their inelastic behavior occur directly in the semi- rigid beam-to-column connections and hence the connection behavior plays a significant role in the frame behavior.

In this thesis, the cyclic behavior of such connections was experimentally investigated and further tests were carried on the connections structurally upgraded by simple introduction of bolts. Tests were carried out on connections formed by three different beam sections and three different connection methods.

- The hooked connections, that are widely used in practice, were essentially benchmarked against a proposed connection method involving the introduction of extra bolts. The proposed method can be considered as a practical way of structurally upgrading an existing hooked beam-to-column connection.
- The test results revealed the improvement in cyclic behavior for the upgraded specimens. Peak moments achieved for the upgraded connections were in a range between 26% to 47% greater.
- The difference between the peak moments achieved from the connection with two pins and the connection with four pins is so small (between 1% and 9% for the different beam depths) this shows that using the two pins connection can be enough to enhance the

behavior of the connections. Additionally, it will save material and time during construction.

- By comparing the results obtained from identical connection types for different beam depths, it was found that increasing the depth of the beam doesn't have a great contribution in increasing the peak moment-rotation results. Increasing the depth of the beam will help to increase the capacity of the beam itself and enhancing the energy dissipation of the beam to column connection.

The performance levels of a structure in most of the design standards were not based on mathematical formulas but it was based on observations from experimental results. The 9 different tests on different rack beam to column connections were used in order to find the performance levels of rack structures.

- The immediate occupancy performance level is stated when the connection reaches a rotation of 0.04 rad. Before the connection reaches 0.04 rad rotation it behaves normally without any sign of failure, just when the curves come closer to the rotation of 0.04 rad, a very slight degradation in the stiffness of the connection starts to occur.
- The life safety performance level is stated when the connection reaches a rotation of 0.075 rad. Higher degradation in stiffness is observed in this region.
- The collapse prevention performance level is stated when the connection reaches a rotation of 0.12 rad. In this state very minimal failures occurs, like a failure of one of the hooks in the hooked connections or slight local buckling takes place in the pinned connections.
- If the rotation exceeds 0.12 rad, the connection is considered to be in the collapse zone. Total failure occurs by tearing of the perforations of the column, failure in the hooks, failure in the weld or total local buckling of the column.

These performance limits were proposed based on limited experimental and numerical studies, further studies are required in order to reach more precise and firm conclusions regarding the performance limits of rack structures.

To evaluate whether a rack frame will likely not collapse in the down-aisle direction under the maximum credible earthquake a simple displacement based procedure was used for frames incorporating the tested beam-to-column connections.

- Promising results were obtained for frames with upgraded connections and beam depths of 120 mm and 140 mm. Collapse prevention under the maximum credible earthquake was achieved for these frames which would otherwise collapse under the same ground motion if no structural upgrading was provided.
- It was indicated that the proposed method of upgrading appears to be a practical and effective way of increasing the seismic performance of existing hooked connections and hence the existing rack frames in their down-aisle direction.

Finite element analysis using ANSYS software was carried out to model both of the hooked and pinned beam-column connections of the rack members.

- The moment-rotation curves obtained from ANSYS have an initial stiffness that is almost identical to the initial stiffness obtained from the experimental results.
- The failure mode obtained from ANSYS model for the hooked connection was due to the high stresses formed in the hooks, which is the same failure reason for the connection during the experimental study.
- During the experimental tests that were carried out on the pinned connection, local buckling of the column was occurred. That was the same failure mode that was obtained from the ANSYS model for the pinned connection.
- By comparing the moment-rotation results obtained from the ANSYS models to the moment-rotation curves obtained from the experimental results, it was found that the average error percentage of each step for the hooked and pinned connection models were 5.9% and 10.5% successively.

Non-linear static pushover analysis was performed using SAP2000 software. 9 different models were done for the 9 different connections that were tested in the experimental study. The moment-rotation curves obtained from the experimental results were inserted to the SAP2000 models as links between the beams and the columns in order to observe the effect of the 9 different connections on the behavior of the rack frame.

- From the pushover curves obtained for the 9 different models it was noticed that using the pinned connections has 20% enhancing in the behavior of the whole structure compared to the traditional hooked beam to column connections.
- The pushover curves obtained from the rack frames with the four pin connection was almost similar to the pushover curves obtained from the rack frames with the two pin connection for the beams of 100 mm and 120 mm depths. Because of that using the two pinned connection can be enough to enhance the performance of the traditional hooked connection.
- The equivalent lateral forces of the 9 different frames were calculated according to FEMA 460 to compare it to the results obtained from the pushover analysis. It was found that the equivalent lateral forces for the 9 different frames did not exceed the ultimate or yielding points of pushover curves of the frames.

The enhancement in the beam to column connection of the rack members due to the newly bolted connection was a motivation to use the rack members in designing structures that can be used residentially. SAP2000 and ETABS software were used to model residential buildings using the rack members and plywood walls and slabs.

The results obtained regarding the design of residential buildings using rack members should be verified by experimental studies. Additionally, during the last phases of this study a new Turkish seismic code was developed (TSC, 2019). However, the structural checks that were done in the study were based on the old Turkish seismic code (TSC, 2007).

- 5 story residential building could be designed using the rack members that were tested in the experimental study. Using rack members in construction provides many advantages as the building can be constructed in a very short time compared to other ordinary residential structures, having a lighter residential buildings compared to concrete and hot rolled steel buildings, the members can be easy recycled and it provides high economic efficiency. This type of buildings will be a great solution for rapid housing, especially after natural disasters. The number of stories could not exceed 5 stories using the ordinary rack members due to expected column failure due to local, distortional and global buckling modes.

- The number of stories of the building was maximized to 8 story building using small modifications to the column cross-section that was used in the 5 story residential building. For the first two stories of the 8 story residential building, self-compacting micro concrete was injected to the column after closing the cross-section with an additional cold formed steel plate, this helped to overcome the local and distortional buckling problems. For the third and fourth stories the closed cross-section was used to protect the cross-section from the formation of distortional buckling. For the fifth to the eighth floor the ordinary opened cross-section was used as the axial loads in this story was relatively small compared to the first four stories.

The newly proposed bolted rack beam to column connection appears to be a practical and effective way to increase the seismic performance of existing hooked connection and hence the existing rack frames in their down-aisle direction. Additionally, the bolted rack beam to column connection has opened the door to the usage of rack members in residential buildings, which can be an effective solution for fast constructions after natural or man-made disasters.

## REFERENCES

American Institute of Steel Construction, 2010, Specification for Structural Steel Buildings, ANSI/AISC 360-10 an American National Standard, American Institute of Steel Construction, Chicago.

American Iron and Steel Institute, 2007, North American Specification for the Design of Cold-Formed Steel Structural Members, American Iron and Steel Institute, Washington, DC 2007 Edition.

American Society of Civil Engineers, 2012, Minimum Design Loads for Buildings and Other Structures, American Society of Civil Engineers.

ANSI MH16.1:2012. Specification for the Design, Testing and Utilization of Industrial Steel Storage Racks, Rack Manufacturers Institute (RMI).

ANSYS® Academic Research, Release 17.

ASCE (2000). FEMA 356 Prestandard and Commentary for the Seismic Rehabilitation of Buildings, *ASCE for the Federal Emergency Management Agency*, Washington, D.C., November 2000.

Bajoria, M.K., Sangle K.K., Talicotti, S.R., 2010, Modal analysis of cold-formed pallet rack structures with semi-rigid connections, *Journal of Constructional Steel Research*, 66 (3),428–441.

Bernuzzi C. and Castiglioni C.A. 2001, Experimental analysis on the cyclic behaviour of beam-to-column joints in steel storage pallet racks, *Thin-Walled Structures*, 39,841-859.

British Standards, EN 15512, 2009, Steel Static Storage Systems - Adjustable Pallet Racking Systems - Principles for Structural Design, Brussels Studies Institute, Brussels.

Carlos, A., 2005, Seismic behavior of rack structures, *Journal of Constructional Steel Research*, 61, 607-624.

Carr, A., 1996, Inelastic Dynamic Analysis, Computer Program Library, Department of Civil Engineering, University of Canterbury.

Castiglioni, C.A., Panzeri, N., Brescianini, J.C., and Carydis, P., Shaking table tests on steel pallet racks, *Proceedings of the Conference on Behaviour of Steel Structures in Seismic Areas*, Stessa, 2003, Naples, Italy, 775-781.

Chen, C.K., Scholl, R.E. and Blume, J.A., 1980, Seismic study of industrial storage racks, *Report prepared for the National Science Foundation and for the Rack Manufacturers Institute and Automated Storage and Retrieval Systems (sections of the Material Handling Institute)*, San Francisco, CA.

Chen, C.K., Scholl, R.E., and Blume, J.A., Seismic-resistant design of industrial storage racks, *Proceedings of the Second Specialty Conference on Dynamic Response of Structures: Experimentation, Observation and Control*, 1981, Atlanta, GA, 745-759.

Clifton, C., Bruneau, M., MacRae, G., Leon, R. and Fussell, A., 2011, Steel structures damage from the Christchurch earthquake series of 2010 and 2011, *Bulletin of The New Zealand Society for Earthquake Engineering*, 44 (4), 297-318.

Computers and Structures inc., CSI Analysis Reference Manual for SAP2000, ETABS, and SAFE, Berkeley, California, USA, 2010.

Elkadi, B., 2014, *Behavior and design of perforated steel storage rack columns under axial compression*, Thesis (MSc), Fatih University.

Elkadi, B., Cosgun, C., Mangir, A., Kiyamaz, G., 2017, Strength Upgrading of Steel Storage Rack Frames in the Downaisle Direction, *Steel and composite structures journal*, 23 (2), 143-152.

Elkadi, B., Kiyamaz, G., 2015, Behavior and Design of Perforated Steel Storage Rack Columns Under Axial Compression, *Steel and composite structures journal*, 18 (5), 1259-1277.

Eurocode 3, *Design of steel structures*, EN 1993-1-1, Part 1-1, General rules and rules of buildings.

Eurocode 4, *Design of composite steel and concrete structures*, EN 1994-1-1, Part 1-1, General rules and rules for buildings.

Federal Emergency Management Agency, 460, 2005, *Seismic Considerations for Steel Storage Racks Located in Areas Accessible to the Public*, Building Seismic Safety Council.

FEMA 460, *Seismic Considerations for Steel Storage Racks Located in Areas Accessible to the Public*, 2005, Building Seismic Safety Council for the Federal Emergency Management Agency, National Institute of Building Sciences Washington, D.C., USA.

Filiatrault, A., and Wanitkorkul, A., 2004, Shake-table testing of Frazier Industrial Storage Racks, *Report No. CSEE-SEESL-2005-02, Structural Engineering and Earthquake Simulation Laboratory, Departmental of Civil Structural and Environmental Engineering, SUNYBuffalo*.

Filiatrault, A., Bachman, R.E., and Mahoney, M.G., 2006, Performance-based seismic design of pallet-type steel storage racks, *Earthquake Spectra*, 22,1,47–64.

Filiatrault, A., Wanitkorkul, A., and Higgins, P., 2006, Experimental stiffness and seismic response of pallet-type steel storage rack connectors, *ASCE Practice Periodical on Structural Design and Construction*, 11 (3),161-170.

Jaspart, J.P., 1999, *Semi-Rigid Behavior of Civil Engineering Structural Connections, Recent Advances in the field of Structural Steel Joints and their Representation in the Building Frames Analysis and Design Process*, COST C1 European Commission, University of Liege, Brussels Luxembourg.

Kalavagunta, S., Naganathan, S. and Mustapha, K.N., 2012, Pushover Analysis for Cold Formed Storage Rack Structures, *Jordan Journal of Civil Engineering*, 6 (4),489-500

Li, Z., Schafer, B.W., Buckling analysis of cold-formed steel members with general boundary conditions using CUFSM: conventional and constrained finite strip methods, 2010, <http://www.ce.jhu.edu/bschafer/cufsm/>

Markazi, F. D., Beale, R. G., and Godley, M. H. R., 1997, Experimental Analysis of Semi-Rigid Boltless Connectors, *Thin-Walled Structures*, 28, 57-87.



Markazi, F. D., Beale, R. G., and Godley, M. H. R., 2001, Numerical modelling of semi-rigid boltless connectors, *Computers & Structures*, 79, 2391-2402.

National Earthquake Hazards Reduction Program, 2003, Recommended Provisions for the Development of Seismic Regulations for New Buildings, Building Seismic Safety Council, Federal Emergency Management Agency, Washington DC.

Petrovic, S. and Kilar, V., 2012, Effects of Horizontal and Vertical Mass-Asymmetric Distributions on the Seismic Response of a High-Rack Steel Structure, *Advances in Structural Engineering*, 15 (11), 1977-88.

Prabha, P., Marimuthu, V., Saravanan, M. and Jayachandran, S.A., 2010, Evaluation of connection flexibility in cold formed steel racks, *Journal of Constructional Steel Research*, 66, 863–872.

Rack Manufacturers Institute (RMI), 2008, Specification for the Design, Testing and Utilization of Industrial Steel Storage Racks, ANSI MH16.1: 2008.

Rack Manufacturers Institute (RMI), 2012, Specification for the Design, Testing and Utilization of Industrial Steel Storage Racks, ANSI MH16.1: 2012.

Saravanan, M., Marimuthu, V., Prabha, P., Surendran, M., and Palani, G.S., 2014, Seismic characterization of cold formed steel pallet racks, *Earthquakes and Structures*, 7(6).

Sarawit, A. CUTWP Thin-walled section properties, December 2006, [www.ce.jhu.edu/bschafer/cutwp](http://www.ce.jhu.edu/bschafer/cutwp).

Schafer, B., Direct Strength Method (DSM) Design Guide, Committee on Specifications for the Design of Cold-Formed Steel Structural Members, *American Iron and Steel Institute*, January 2006.

Shah, S.N.R, Ramli Sulong, N.H., Khan, R., Jumaat, M.Z., Shariati, M., 2016, Behavior of Industrial Steel Rack Connections, *Mechanical Systems and Signal Processing*, 70-71, 725-740.

Shahshenas, R., 2015, *Experimental and numerical study on the cyclic behavior of connections in storage rack structures*, Thesis (PhD), Boğaziçi University.

Sideris, P., Filiatrault, A., Leclerc, M., and Tremblay, R., 2010, Experimental Investigation on the Seismic Behavior of Palletized Merchandise in Steel Storage Racks, *Earthquake Spectra*, 26 (1), 209- 233.

SolidWorks 2016, Dassault Systèmes SolidWorks Corporation, 2016.

The Federation Europeenne de la Manutention, 2001, Guidelines for the safe use of static steel racking and shelving, Federation Europeen de la Manutention.

The Federation Europeenne de la Manutention, 2001, The design of static steel pallet racks, Federation Europeenne de la Manutention.

The Federation Europeenne de la Manutention, 2005, The seismic design of static steel pallet racks, Federation Europeenne de la Manutention, Final Draft.

Turkish Seismic Code 2007, *Regulations for the construction of buildings in earthquake regions*, TSC 2007, Ministry of Public Works and Settlement, Ankara, Turkey.

Turkish Seismic Code 2019, *Turkish building seismic code*, TSC 2019, Disaster and Emergency Management Presidency, Ankara, Turkey.

Turkish Seismic Code 2019, *Turkish building seismic code*, TSC 2019, Disaster and Emergency Management Presidency, Ankara, Turkey.

Turkish Standard Institute 1979, *Building code for timber structures*, TS 647:1979, Turkish Standard Institute, Ankara, Turkey.

URGO racking, 1998, *Nanjing URGO Logistics Equipment Co.*, <https://urgorack.en.made-in-china.com/product-group/ybjEseRJrrWZ/Heavy-Duty-Rack-1.html>.

Yoshihara, H., 2010, Characterization of in-plane compressive properties of plywood by IITRI and end-loading compression tests, *Department of Natural Products Resource Engineering, Shimane University, Matsue, Japan, February 2010.*

Zhao, X., Dai L., Rasmussen, J.R., 2018, Hysteretic behavior of steel storage rack beam-to-upright boltless connections, *Journal of Constructional Steel Research*, 144, 81-105.

Zhao, X., Wang, T., Chen, Y., Sivakumaran, K.S., 2014, Flexural behavior of steel storage rack beam-to-upright connections, *Journal of Constructional Steel Research*, 99, 161-175.



## CURRICULUM VITAE

Personal Information	
Name Surname	Bassel ELKADI
Place of Birth	Manama, BAHRAIN
Date of Birth	15.07 1990
Nationality	<input type="checkbox"/> T.C. <input checked="" type="checkbox"/> Other: Egyptian
Phone Number	+90 540 532 3880
Email	bassel_elkadi@hotmail.com
Web Page	



Educational Information	
B. Sc.	
University	Ain Shams University
Faculty	Faculty of Engineering
Department	Civil Engineering Department
Graduation Year	17.09.2012

M. Sc.	
University	Fatih University
Institute	Institute of Sciences and Engineering
Department	Department of Civil Engineering
Programme	Masters of Science in Civil Structure and Infrastructure Engineering

Ph. D.	
University	Istanbul University
Institute	Institute of Graduate Studies
Department	Department of Civil Engineering
Programme	Civil Engineering Programme

Publications
Elkadi, B., Cosgun, C., Mangir, A., Kiymaz, G., 2017, Strength Upgrading of Steel Storage Rack Frames in the Downaisle Direction, <i>Steel and composite structures journal</i> , 23 (2), 143-152.
Elkadi, B., Kiymaz, G., 2015, Behavior and Design of Perforated Steel Storage Rack Columns Under Axial Compression, <i>Steel and composite structures journal</i> , 18 (5), 1259-1277.

Elkadi, B., Kiyamaz, G., Experimental Investigation on the Behavior of Perforated Steel Storage Rack Columns Under Axial Compression, *13th Nordic Steel Construction Conference, NSCC*, 23-25 September 2015, Tampere, Finland,

Kiyamaz, G., Cosgun, C., Mangir, A., Elkadi, B., Strength Upgrading of Existing Steel Storage Rack Beam-to-Column Connections, *3rd Conference on Smart Monitoring, Assessment and Rehabilitation of Structures, SMAR*, 2015, Antalya, Turkey.

